# Hydrometallurgical processes applied to the demanganization of water and the decadmiation of industrial phosphoric acid

Sanaa Kouzbour

Clermont-Auvergne University
Doctoral College of Engineering Sciences of Clermont-Ferrand

**THESIS**

Defended by

**Sanaa KOUZBOUR**

To obtain the degree of

**Doctor of Philosophy**

Speciality: Process Engineering

# Hydrometallurgical processes applied to the demanganization of water and the decadmiation of industrial phosphoric acid

Defended on 10 december 2022 in the presence of the jury members:

| | | |
|---|---|---|
| **Mr. Abdelmajid BADRI** | University professor, Hassan II University of Casablanca | **President** |
| **Mr. Jamal CHAOUKI** | University professor, Polytechnic School of Montreal | **Reviewer** |
| **Mr. Rachid BRAHMI** | University professor, Chouaib Doukkali University | **Reviewer** |
| **Mrs. Alina Violeta URSU** | Associate professor, Clermont-Auvergne University | **Examiner** |
| **Mrs. Bouchra BELAISSAOUI** | Associate professor, Lorraine University | **Examiner** |
| **Mr. Abderrahman NOUNAH** | University professor, Mohammed V University | **Examiner** |
| **Mr. Adil DANI** | Professor, Hassan II University of Casablanca | **Guest** |
| **Mr. Christophe VIAL** | University professor, Clermont-Auvergne University | **Thesis supervisor** |
| **Mr. Bouchaib GOURICH** | University professor, Hassan II University of Casablanca | **Thesis supervisor** |
| **Mr. Fabrice GROS** | University professor, Clermont-Auvergne University | **Thesis co-supervisor** |

*Year 2022*

# Hydrometallurgical processes applied to the demanganization of water and the decadmiation of industrial phosphoric acid

Sanaa KOUZBOUR [a,b]

*Supervised by:*

Bouchaib GOURICH [a], Christophe VIAL [b], and Fabrice GROS [b]

This work was funded by the Office Chérifien des Phosphates (OCP, Morocco) and the OCP Foundation within the framework of the R&D Initiative - Call for Projects around Phosphates APPHOS (project ID: ACD GOU-01/2017) and by CAMPUS FRANCE (PHC TOUBKAL/16/37 (France – Morocco bilateral program) Grant Number: 34726PM).

[a] Laboratoire d'Ingénierie des Procédés et d'Environnement, Ecole Supérieure de Technologie, Université Hassan II de Casablanca, Casablanca, Morocco

[b] Clermont Auvergne University, Clermont Auvergne INP, CNRS, Institut Pascal, F-63000, Clermont–Ferrand, France

Université Clermont-Auvergne
École Doctorale Sciences pour l'Ingénieur de Clermont-Ferrand

**THÈSE**

Présentée par

**Sanaa KOUZBOUR**

En vue d'obtenir le grade de

**Doctorat d'Université**

Spécialité : Génie des Procédés

# Génie des procédés hydrométallurgiques appliqués à la démanganisation des eaux et à la décadmiation de l'acide phosphorique industriel

Soutenue le 10 décembre 2022 devant le jury :

| | | |
|---|---|---|
| **M. Abdelmajid BADRI** | Professeur des universités, Université Hassan II de Casablanca | **Président** |
| **M. Jamal CHAOUKI** | Professeur des universités, Polytechnique Montréal | **Rapporteur** |
| **M. Rachid BRAHMI** | Professeur des universités, Université Chouaib Doukkali | **Rapporteur** |
| **Mme Alina Violeta URSU** | Maître de conférences, Université Clermont-Auvergne | **Examinatrice** |
| **Mme Bouchra BELAISSAOUI** | Maître de conférences, Université de Lorraine | **Examinatrice** |
| **M. Abderrahman NOUNAH** | Professeur des universités, Université Mohammed V | **Examinateur** |
| **M. Adil DANI** | Professeur habilité, Université Hassan II de Casablanca | **Invité** |
| **M. Christophe VIAL** | Professeur des universités, Université Clermont-Auvergne | **Directeur de thèse** |
| **M. Bouchaib GOURICH** | Professeur des universités, Université Hassan II de Casablanca | **Directeur de thèse** |
| **M. Fabrice GROS** | Professeur des universités, Université Clermont-Auvergne | **Co-directeur de thèse** |

*Année 2022*

# Génie des procédés hydrométallurgiques appliqués à la démanganisation des eaux et à la décadmiation de l'acide phosphorique industriel

Sanaa KOUZBOUR [a,b]

*Sous l'encadrement de :*

Bouchaib GOURICH [a], Christophe VIAL [b] et Fabrice GROS [b]

Ce travail a bénéficié du financement de l'Office Chérifien des Phosphates (OCP, Maroc) et de la Fondation OCP dans le cadre du programme R&D Initiative – Appel à Projets autour des Phosphates APPHOS (l'ID du projet : ACD GOU-01/2017) et par CAMPUS FRANCE (PHC TOUBKAL/16/37 (programme bilatéral France - Maroc) Numéro de subvention : 34726PM).

[a] Laboratoire d'Ingénierie des Procédés et d'Environnement, Ecole Supérieure de Technologie, Université Hassan II de Casablanca, Casablanca, Morocco

[b] Université Clermont Auvergne, Clermont Auvergne INP, CNRS, Institut Pascal, F-63000, Clermont–Ferrand, France

*To my dear grandfather,*

# ACKNOWLEDGMENTS

I would like to acknowledge all those who have participated in bringing this work to fruition. Firstly, I would like to express my deepest gratitude to my thesis advisors, Prof. Bouchaib GOURICH, Prof. Christophe VIAL, and Prof. Fabrice GROS, for their patience, motivation, and guidance particularly during the tough moments of the doctoral journey. For providing me with a suitable working environment to carry out my research, and for sharing their knowledge and their experience. I truly appreciate working with you professors and you have imparted valuable lessons to me that will be useful in every phase of my life.

I sincerely thank the members of the committee, Prof. Abdelmajid BADRI, Prof. Jamal CHAOUKI, Prof. Adil DANI, Prof. Rachid BRAHMI, Prof. Alina Violeta URSU, Prof Bouchra BELAISSAOUI, and Prof. Abderrahman NOUNAH for the interest they showed in my work, for evaluating my thesis, and for giving judicious comments.

During my research work, I had to encounter some issues that required some help. My deepest gratitude goes to the technicians of the different departments (Mechanical, Electrical, and Chemical Engineering Departments), and in particular to Mr. Driss DRISSI and Mr. Mohamed Bachir Boutakaoua. In addition, I wish to thank the Department of Chemical Engineering at the High School of Technology, notably Prof. Fouad ALLAM, for the appropriate atmosphere they provide to help us to conduct our research work.

One of the most beautiful outputs of a Ph.D. project is the number of people and new friends that we met during this journey. This thesis would not have been completed without the continuous support of my amazing friends Noura, Assia, Noufissa, Fathia, Simoti, Majid, Mehdi, Hamza, and all those whose company ensured that my stay in Clermont-Ferrand was a pleasant and unforgettable one.

I also wish to acknowledge the OCP group, OCP Foundation, and Campus France (PHC TOUBKAL/16/37 (France – Morocco bilateral program) for the financial support which made this Ph.D. work achievable.

Finally, I would like to extend my profound gratitude to my mother, father, my brother for the support they provided me throughout this journey, and without whose encouragement I would not have finished this Ph.D. I just don't have the right words to express what I really feel in my heart for you.

# RESUME

La pollution par les métaux et les métaux lourds a des répercussions néfastes considérables sur l'environnement écologique et la santé humaine en raison de leur toxicité, de leur persistance et de leur caractère non biodégradable, et ce même à l'état de traces. Il est ainsi devenu nécessaire afin de préserver l'environnement tout en maintenant les équilibres naturel, sanitaire et économique (dans une démarche de développement durable) d'adapter et de mettre en œuvre des techniques de traitement et d'épuration disponibles et adaptées du génie des procédés. A cet effet, les procédés hydrométallurgiques se présentent comme une technologie prometteuse pour la récupération et l'élimination des métaux et des métaux lourds contenus dans des solutions aqueuses telles que l'eau et l'acide phosphorique. A cet égard, ce travail est consacré :

- D'une part à l'étude de l'élimination des ions manganèse de l'eau potable par un procédé d'aération dans des réacteurs à agitation pneumatique tels que les colonnes à bulles et les airlifts. L'objectif final est également de comparer leurs performances en fonction de l'énergie consommée pour mener à bien cette réaction.
- D'autre part à la séparation du cadmium des solutions d'acide phosphorique produit par voie humide (synthétique et industriel) par la précipitation par des sulfures, en mode discontinu et continu, dans une unité conçue et fabriquée pour le traitement des effluents acides.

Cette étude peut donc être perçue selon trois axes :

Ainsi, avant de procéder à la démanganisation des eaux dans des contacteurs à agitation pneumatique, il a été nécessaire de réaliser un recensement des travaux de recherche afin d'exposer les diverses applications de ces réacteurs, ainsi que les études réalisées sur l'hydrodynamique et le transfert de matière dans les colonnes à bulles et les réacteurs à base d'airlift, car ces caractéristiques influent sur les performances de ces réacteurs. Cette revue bibliographique a été complétée par une étude expérimentale qui a consisté à étudier les caractéristiques hydrodynamiques et de transfert de matière d'une colonne à bulles carrée en présence de liquides de différentes tensions de surface. En guise de phases liquides, nous avons utilisé l'eau du réseau et des solutions aqueuses contenant deux types de surfactants (collecteurs cationique et anionique) qui sont largement utilisés dans la flottation des phosphates. En effet, ces tensioactifs sont des

collecteurs organiques constitués d'amine et d'ester. Les impacts de la concentration en tensioactifs et de la vitesse superficielle du gaz sur le coefficient de transfert de matière volumétrique et la rétention de gaz ont été mises en évidence.

Dans la deuxième partie de cette étude, l'élimination du manganèse soluble Mn (II) de l'eau potable par un procédé d'aération utilisant des réacteurs à agitation pneumatique à base d'une colonne à bulles carrée et d'un réacteur airlift fonctionnant en mode discontinu a été réalisée. Les effets des paramètres opératoires telles que le débit d'aération, le pH initial, les concentrations en Mn(II) en $MnO_2$ sur l'efficacité de l'élimination ont été étudiés. Afin de choisir le réacteur adéquat pour la démanganisation des eaux potables par l'oxydation en utilisant l'oxygène atmosphérique, une comparaison des performances des deux réacteurs en termes d'élimination des ions Mn(II) en fonction de l'énergie consommée a été menée.

Partant d'une revue exhaustive de la littérature dans laquelle les différents procédés de purification d'acide phosphorique ont été analysés pour déterminer leurs performances ainsi que leurs limites, nous avons pu identifier les aspects et points essentiels à prendre en compte pour le développement d'une technique de purification de l'acide phosphoriques. Ainsi, La troisième partie est consacrée au développement d'une approche pour améliorer les performances du procédé de précipitation par les sulfures en tant que technique de purification. Cette approche est basée sur l'utilisation du NaHS plutôt que celle du $Na_2S$ comme agent de précipitation, en modes batch et continu, pour l'élimination du cadmium de l'acide phosphorique produit par voie humide (synthétique et industriel). En effet, les performances du $Na_2S$ et du NaHS ont été comparées en mode batch. Les résultats expérimentaux obtenus montrent que le NaHS améliore la décadmiation de l'acide phosphorique synthétique par rapport au $Na_2S$. De plus, un modèle cinétique apparent a été développé en prenant en compte les mécanismes de réaction et la sursaturation pour prédire la concentration résiduelle de cadmium dans les solutions d'acide phosphorique. Finalement, les résultats de ce travail ont fourni des indications pertinentes sur la faisabilité de la précipitation chimique utilisant NaHS comme technique de décadmiation de l'acide phosphorique au sein de l'industrie.

**Mots-clés :** Réacteurs à agitation pneumatique ; Eaux potables ; Acide phosphorique ; Précipitation ; Démanganisation ; Décadmiation.

# ABSTRACT

Metal and heavy metal pollution has a detrimental impact on the ecological environment and human health due to their toxicity, persistence, and non-biodegradability, even in trace amounts. Therefore, it has become necessary in order to preserve the environment while maintaining natural, health, and economic balances (within a sustainable development approach) to adapt and implement treatment and purification techniques available from process engineering. To this end, hydrometallurgical processes constitute a promising technology for the recovery and removal of metals and potentially toxic heavy metals from aqueous solutions such as water and phosphoric acid solutions. In this context, this work was devoted:

- On the one hand, the study of the manganese ions removal from drinking water by aeration process in pneumatically agitated reactors such as bubble columns and airlifts. The objective was also to compare their performances according to the specific energy consumed to carry out this reaction. However, the study of the hydrodynamic and mass transfer characteristics of these reactors is essential before proceeding to the manganese removal.
- On the other hand, to the investigation of the cadmium elimination from synthetic and industrial wet phosphoric acid solutions using batch and continuous sulfide precipitation in a conceived and manufactured unit for acidic effluent treatment.

This study can thus be perceived in three axes:

Before proceeding with the demanganization of waters in pneumatically agitated contactors, it was deemed necessary to conduct a comprehensive literature review to outline the various applications of these reactors, and the studies carried out on the hydrodynamics and mass transfer in bubble column and airlift reactors as these variables influence the performance of these reactors. This review was thereafter supplemented by an experimental study which consisted in investigating the hydrodynamic and mass transfer characteristics of a square bubble column in the presence of liquid phases with varying surface tension. As liquid phases, we used tap water and aqueous solutions containing two types of surfactants (cationic and anionic). Indeed, these surfactants are organic collectors made of amine and ester which are widely used in phosphate flotation. The

impacts of surfactant type and concentration, and gas superficial velocity on the volumetric mass transfer coefficient and gas holdup have been discussed.

In the second part of this study, the mitigation of soluble manganese Mn(II) from drinking water by aeration process using pneumatic reactors including square bubble column and split airlift reactor operating in semi-batch conditions was investigated. The effects of operating conditions such as aeration flow rate, initial pH, Mn(II) concentrations, and amount of $MnO_2$ particles on the Mn(II) removal efficiency were analyzed. Meanwhile, to determine the appropriate reactor for the demanganization of drinking water by oxidation using atmospheric oxygen, a comparison of the performance of the two reactors in terms of Mn(II) ion removal as a function of the energy consumed was performed.

Starting from an exhaustive literature review in which different phosphoric acid purification processes have been analyzed to determine their performances as well as their limitations, it was possible to identify the fundamental aspects and points to be considered for the development of a phosphoric acid purification technique. The third part was dedicated to developing a novel approach to improve the performance of the sulfide precipitation process as a purification technique. This approach is based on NaHS rather than $Na_2S$ as a precipitating agent in both batch and continuous modes for cadmium removal from synthetic and industrial wet phosphoric acid. First, the respective performance of $Na_2S$ and NaHS was compared in the batch mode. NaHS was shown to improve the decadmiation of synthetic phosphoric acid in comparison to $Na_2S$. An apparent kinetic model was developed taking into consideration the reaction mechanisms and supersaturation to predict the residual cadmium concentration in phosphoric acid solutions. Eventually, the findings obtained through this work provide useful insights into the feasibility of chemical precipitation using NaHS as a technology of phosphoric acid decadmiation in the industry.

**Keywords:** Pneumatically agitated reactors; Drinking water; Phosphoric acid; Precipitation; Demanganization; Decadmiation.

# TABLE OF CONTENTS

# LIST OF TABLES

# LIST OF FIGURES

# LIST OF SYMBOLS AND ABBREVIATIONS

**Abbreviation**

| | |
|---|---|
| AG | Annular gap |
| ARL | Airlift |
| ARPL | Packed airlift |
| BC | Bubble column |
| BSD | Bubble size distribution |
| CMC | Carboxymethylcellulose |
| DO | Dissolved oxygen |
| HRT | Hydraulic residence time |
| IPA | Industrial phosphoric acid |
| NaDBDTC | Sodium dibutyldithiocarbamate |
| NaEPDTC | Sodium ethylphenyldithiocarbamate |
| OT | Open tube |
| OTR | Oxygen transfer rate |
| OUR | Oxygen uptake rate |
| PA | Phosphoric acid |
| SCX | Sodium cellulose xanthate |
| SLS | Sodium lauryl sulfate |
| SSTP | Sodium tripolyphosphate |
| SSE | Sum of square error |
| TBP | Tributyl phosphate |
| ZnEPDTC | Zinc ethylphenyldithiocarbamate |

**Nomenclature**

Roman letters

| | |
|---|---|
| $a_L$ | Interfacial area (per volume of liquid) [$m^{-1}$] |
| $A_d/A_r$ | Downcomer/riser cross sectional area [dimensionless] |
| $C_0$ | Initial dissolved oxygen concentration [$mg.L^{-1}$] |

| | |
|---|---|
| $C_t$ | Instantaneous dissolved oxygen concentration [$mg.L^{-1}$] |
| $C_s$ | Dissolved oxygen concentration at saturation [$mg.L^{-1}$] |
| $C_1$ | Parameter in Akita and Yoshida (1973) correlation [dimensionless] |
| $d_c$ | Column diameter [m] |
| $d_0$ | Sparger hole diameter [m] |
| $d_B$ | Bubble diameter [m] |
| $D_{50}$ | Median diameter [m] |
| $f_m$ | Average frequency [Hz] |
| $g$ | Gravity constant [$m.s^{-2}$] |
| $H$ | Height [m] |
| $H_c$ | Column height [m] |
| $H_0$ | Clear liquid height [m] |
| $j_{gl}$ | Drift flux [$m.s^{-1}$] |
| $K$ | Consistency index [$Pa.s^n$] |
| $k_L$ | Liquid mass transfer coefficient [$m.s^{-1}$] |
| $k_L a_L$ | Volumetric liquid mass transfer coefficient [$s^{-1}$] |
| $L$ | Length [m] |
| $P$ | Pressure [Pa] |
| $P_{xx}(f)$ | Average power spectral density [$Pa^2.s$] |
| $U_g$ | Superficial gas velocity [$m.s^{-1}$] |
| $U_{swarm}$ | Superficial gas velocity [$m.s^{-1}$] |
| $V_R$ | Reactor volume [$m^3$] |
| $V_w$ | Working volume [$m^3$] |
| $w$ | Width [m] |

*Greek letters*

| | |
|---|---|
| $\Delta P$ | Differential pressure [Pa] |
| $\Delta H$ | Height difference [m] |
| $\varepsilon_g$ | Gas hold-up [dimensionless] |
| $\rho_L$ | Liquid density [$kg.m^{-3}$] |

| | |
|---|---|
| $\nu_L$ | Bubble terminal velocity [$m^2.s^{-1}$] |
| $\rho_g$ | Gas density [$kg.m^{-3}$] |
| $\mu_L$ | Liquid viscosity [Pa.s] |
| $\sigma_L$ | Liquid surface tension [$N.m^{-1}$] |

*Subscripts*

| | |
|---|---|
| d | Downcomer |
| g | Gas phase |
| L | Liquid phase |
| r | Riser |

# INTRODUCTION

Nowadays, with a current population of 7.4 billion people, the planet should host nearly 8 billion people in 2030 and experts predict population growth of between 9 and 10 billion in 2050, which corresponds to a demographic growth of 80 million people per year. Therefore, the need for water will necessarily be rising. Knowing that in 2050, about 2/3 of the world's population will live in large cities, mainly in developing countries, where access to water is likely to be made even more difficult than at present because these geographical areas are already in a situation of water scarcity and are also suffering from pollution. Indeed, groundwater is the most available source of drinking water production, accounting for more than 90 % of the world's readily accessible freshwater. Approximately 1.5 billion people rely on groundwater for their drinking water supply. Yet, groundwater commonly contains some contaminants such as dissolved manganese, which should be reduced for health and aesthetic purposes. Combined with dissolved iron, manganese (II) can flocculate and form sediment in distribution pipes. With increased flow in distribution lines, the sediment can be re-suspended and lead to customer claims of black or brown water incidents. These black water incidents can be encountered when the concentration of manganese in the treated water is even lower than 0.02 $mg.L^{-1}$. In an attempt to prevent health risks from chronic exposure to manganese, the World Health Organization has recommended a limit value of 0.1 $mg.L^{-1}$ for manganese in drinking water. To meet the required guideline, several techniques are used to remove manganese, such as hydroxide precipitation, ion exchange, coagulation/flocculation, oxidation using strong oxidation agents, electrocoagulation, adsorption, and membrane processes. Nevertheless, they pose some shortcomings: namely, high energy consumption and operating cost, and the formation of by-products.

Meanwhile, the demographic growth will also lead to exploding the needs linked to the agriculture and food sector, and thereafter the demand for phosphate fertilizers will drastically increase. Actually, phosphate fertilizers play a tremendous role in agriculture as they are used to supply agricultural fields with nutrients for plant growth, constituents in animal feedstocks, and the food industry. Phosphate fertilizer production goes essentially through an intermediate stage which is the manufacturing of phosphoric acid. Therefore, phosphoric acid and its manufacturing industries play a vital role by providing phosphorus for food and nutrition needs. This acid is produced by two major processes which are the “thermal” and the “wet” route. Because of the low

energy requirements, the wet process is the most commonly used. Although the obtained product is relatively cheap compared to the thermal phosphoric acid, the wet phosphoric acid is contaminated with many ionic impurities found in minerals used as substrates in the production process, such as $F^{-}, Fe^{3+}, Al^{3+}, UO_2^{2+}, Cu^{2+}, Zn^{2+}, Cd^{2+}$ and $Pb^{2+}$, and organic matter. Recently, the focus of different institutions on the impact of heavy metals present in fertilizers has been noteworthy, especially on cadmium (Cd) due to its toxicity and non-biodegradable property and causing renal dysfunction, hypertension, hepatic injury, lung damage, anemia, and teratogenic effects. Moreover, repeated exposure to cadmium exhibits many harmful effects on growth, reproduction, immune and endocrine systems, development, and behavior in addition to mortality. In fact, Cd can be brought to the soil through anthropogenic activities such as mining and smelting of zinc-bearing ores, fossil fuel combustion, waste incineration, sewage sludge, irrigation waters, manure, and fertilizers derived from phosphate rock. However, the demand for purified wet phosphoric acid has become increasingly strong in order to mitigate the serious soil pollution caused by the excessive use of phosphate fertilizers, and also to contribute to the improvement of the agricultural production yield, as well as the quality of food products and animal feed. To deal with this concern, many processes have been developed to lower the cadmium content in wet phosphoric acid, namely solvent extraction, adsorption, ion exchange, flotation, co-crystallization, and membrane processes. Nonetheless, the high operating cost, the medium alteration, by-product formation, or the inability to comply with the desired standards, remain currently a constraint to the industrial application of these processes.

Consequently, the present work proposed the oxidation by aeration and chemical precipitation processes to lower respectively the content of manganese from drinking water, and the cadmium ion from wet-process phosphoric acid, which will eventually lead to a decrease in the pollution degree shown previously. Indeed, manganese was removed by gas-liquid oxidation in bubble columns and airlift multiphase reactors, which are pneumatic reactors with several advantages, such as the high mixing degree combined with simple construction and without mechanical agitation. In parallel, the performance of both reactors in manganese removal was evaluated and compared.

Regarding phosphoric acid decadmiation, sulfide precipitation was adopted since it is among the most preferred techniques for the separation and recovery of heavy metals from effluents such

as acid wastewaters. It is commonly used in the industry owing to its multiple positive aspects, namely high removal/recovery efficiency, the low solubility of the resulting metal sulfide, and the potential for reuse of the sulfide precipitates. Hence, a new approach has been evolved to enhance the performance of the sulfide precipitation process as a purification technique by conceiving and manufacturing a unit dedicated to the treatment of acidic effluent such as phosphoric acid solutions. This approach is also based on the use of NaHS instead of $Na_2S$ as a sulfide precipitating agent in the batch and continuous modes for cadmium removal from synthetic and industrial wet phosphoric acid solutions.

The structure of this thesis report is presented as follows. The first chapter consists of a literature review of the main works on hydrodynamics, and gas-liquid mass transfer characteristics of bubble columns and airlift reactors. This chapter provides a description of bubble columns and airlift reactors, and their applications, and summarizes the main correlations from the literature that will enable a comparison between experimental data with those obtained in other similar multiphase reactors.

The second chapter is an article, published in the International Journal of Heat and Mass Transfer, that aimed at studying hydrodynamics and gas–liquid mass transfer rate in a square bubble column reactor with tap water and aqueous solution of cationic and anionic collectors (an amine and an ester). The influences of parameters, such as the collector concentration and superficial gas velocity on the overall gas hold-up, the flow regime, and the volumetric mass transfer coefficient are examined. Besides, different methods have been used to identify the prevailing flow regime in the bubble column reactor.

The third chapter describes the removal of soluble Mn(II) from drinking water using atmospheric oxygen in order to oxidize it into insoluble manganese dioxide $MnO_2$ in a split-square airlift reactor and square bubble column that was previously characterized. This article details the principles of experimental techniques employed in this work along with the experimental setup available for manganese removal. The effects of operating conditions on the kinetic of Mn(II) oxidation by aeration were evaluated, including the influence of air flow rate, pH, and initial concentrations of soluble Mn(II) and insoluble Mn(IV) manganese forms. Besides, the feasibility of the aeration process in the bubble column and the airlift reactors in terms of manganese removal was evaluated by comparing their oxidation efficiency and energy requirements. In fact, this work

centered on the removal of Mn(II) from drinking water by atmospheric oxygen in a split-airlift reactor constitute an article published in the Journal of Water Process Engineering.

The fourth chapter is a literature review on the industrial processes for cadmium removal from wet phosphoric acid published in Hydrometallurgy. This chapter focuses on the comparative analysis of different available processes that have been used for cadmium removal from WPA, with an evaluation of their respective advantages and limitations. A comprehensive approach is followed to cover all the significant works done in this field to date, including the thermodynamic modeling of the $H_3PO_4/H_2O$ system, which can provide essential information for designing and simulating different kinds of processes. In this regard, data and resources provided in this section will be used to develop an apparent kinetic model of cadmium sulfide precipitation in the ensuing two chapters. Furthermore, the cost of phosphoric acid production is discussed, while comparing the price of thermal and wet phosphoric acid and purified wet phosphoric acid. Finally, in order to obtain more insight into the environmental impacts of phosphoric acid, the harmful effect of the production and use of phosphoric acid on the environment is analyzed by evaluating available life cycle assessment studies.

The fifth chapter is an article, published in Minerals Engineering, that describes the removal of cadmium from synthetic dilute phosphoric acid using batch and continuous sulfide precipitation. In this work, $Na_2S$ and NaHS were used as sulfide precipitating agents. The influences of operating conditions, such as Sulfur/$Cd^{2+}$ molar ratio, temperature, acidity level, initial cadmium concentration, and hydraulic residence time on cadmium removal yield are investigated. An apparent kinetic model was proposed taking into consideration the reaction mechanisms and supersaturation to predict the residual cadmium concentration in phosphoric acid solutions. Eventually, the mechanisms responsible for cadmium sulfide formation are explained along with analyzing the solid phase.

The sixth chapter is an article accepted in the Journal of Cleaner Production, that investigated the mitigation of cadmium from industrial dilute wet phosphoric acid solution (25 % $P_2O_5$) by NaHS precipitation in the batch and continuous modes. In this study, the effects of operating parameters on the purification performance were evaluated, namely $\mathrm{Sulfur}/\mathrm{Cd}^{2+}$ molar ratio, the occurrence of other metallic impurities than $Cd^{2+}$, temperature, and hydraulic residence time. The

proposed kinetic model is also tested in the case of industrial phosphoric acid. Lastly, the characterization of the resulting precipitate is conducted with the help of semi-quantitative chemical and morphological analyses.

Finally, a general conclusion is presented with the main findings obtained from the experimental studies to answer the initial objectives.

# Chapter 1: Literature review of bubble columns and airlift reactors


## Abstract

Bubble column and airlift reactors are multiphase contactors based on the dispersion of a gas phase in the form of bubbles inside a cylindrical vessel where a liquid or a suspension circulates. Those reactors present many advantages such as good heat and mass transfer rates, no moving parts, compactness, easy operating, and low maintenance and operating costs. Indeed, they have served a broad range of industrial applications and gained particular attention in the field of water and wastewater treatment processes application. Indeed, hydrodynamic parameters (such as gas hold-up and backmixing) and mass transfer determine the necessary reactor design and impact reactor performance, thus, detailed knowledge of these variables is crucial for the optimal design and operation of reactors. This review is intended to cover the various applications of these reactors during the period 2018 – 2022. In addition, it is aimed at providing an overview of research studies that focus on the hydrodynamics and mass transfer of bubble columns and airlift. The main mechanisms prevailing the bubble column and airlift will be described. The influence of the different parameters on gas hold-up and mass transfer properties will be extensively discussed.



**Keywords:** Pneumatically agitated reactors; Bubble column; Airlift, Hydrodynamics; Gas−liquid mass transfer; Industrial applications

## 1.1 Introduction

Multiphase bubble columns (BC) and Airlift (ARL) reactors are commonly used in many industrial processes. The applications of these reactors are of increasing importance in the process industries. The theoretical analysis and design of multiphase systems are complicated due to various factors, such as hydrodynamic characteristics, mixing, gas-to-liquid mass transfer and kinetics, etc. In the last decades, considerable advances have been made in understanding the basic aspects of bubble columns and airlift systems and in developing rational design procedures.

This chapter presents an overview of bubble column and airlift reactors. Some of the important recent applications of these pneumatic reactors are summarized. A detailed discussion on hydrodynamics and mass transfer characteristics is presented. The major correlations for predicting the key design parameters (gas hold-up and liquid-side mass transfer) are summarized and critically compared.

### 1.1.1 Multiphase bubble column reactors

Bubble columns consist of multiphase reactors wherein the gaseous phase is dispersed as bubbles in a continuous phase that can be either a liquid phase in two-phase bubble columns or a suspension in slurry bubble columns. The simplest (basic) bubble column configuration is a vertical cylinder or rectangular without internals, into which the gas is sparged as discrete rising bubbles from the bottom through a gas distributor (Figure 1.1). In fact, considering the specific requirements of the process, various geometric forms for gas distribution can be conceivably used, including porous plates, perforated plate spargers, ring-type distributors, and needle gas sparger or spider gas sparger (Besagni et al., 2018; Gemello et al., 2018). Regarding the liquid phase, it can be supplied in batch or continuous mode. In the case of continuous operation, the liquid phase can flow co-currently or counter-currently with respect to the flow direction of the gas phase and may be recycled back to the feed vessel after leaving the column (Besagni et al., 2018).

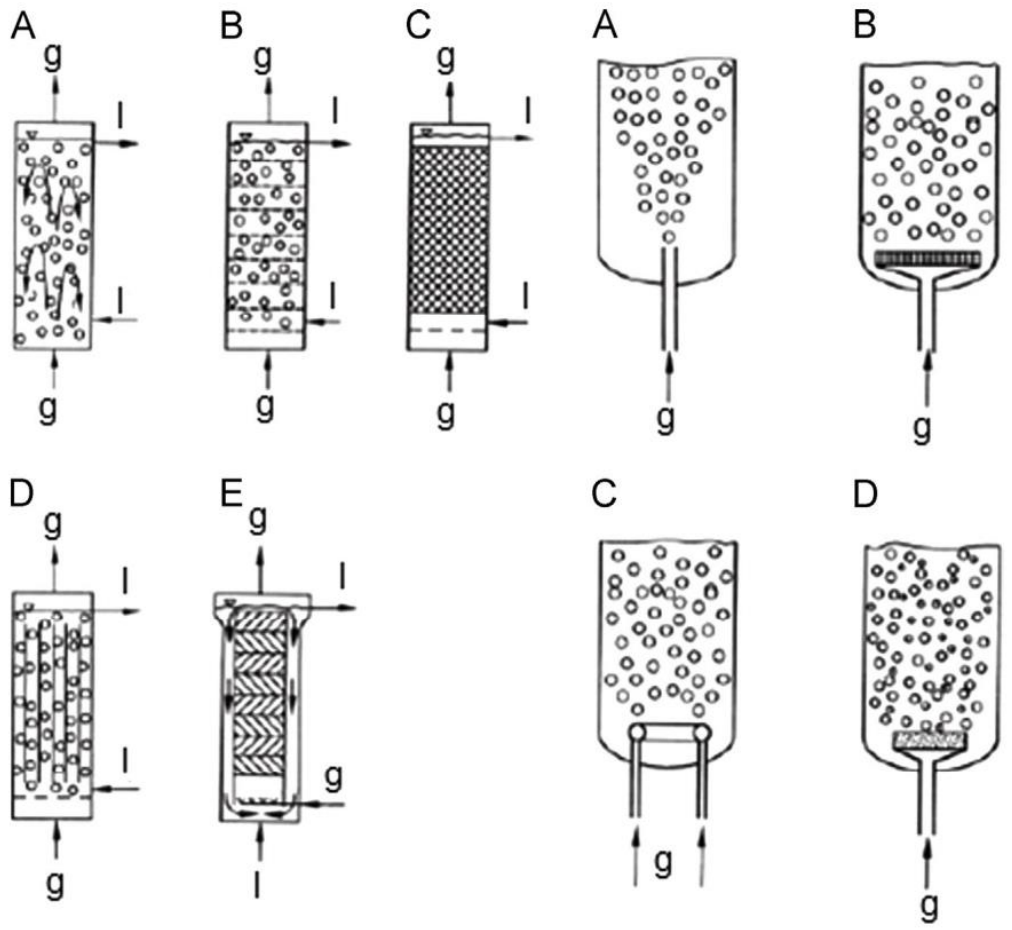


Figure 1.1 Left: examples of bubble column designs (A) empty, (B) cascaded, (C) packed, (D) multishift, and (E) equipped with static mixers. Right: example of gas distributors (A) simple tube, (B) perforated plate, (C) perforated ring, and (D) porous plate (Rollbusch et al., 2015).

Multiphase bubble columns are extensively used to conduct gas−liquid and gas−liquid-solid reactions in petrochemical, biochemical, chemical and metallurgical processes. Some very well-known chemical applications are the famous Fischer-Tropsch process which is the indirect coal liquefaction process to produce transportation fuels or methanol, and the manufacture of biomass fuels which are environmentally much more advantageous than petroleum-derived fossil fuels (Kantarci et al., 2005). They are also used especially in chemical processes involving reactions, such as oxidation, chlorination, alkylation, polymerization, and hydrogenation, and in biochemical processes such as fermentation and biological wastewater treatment (Fard, 2020; Sirohi et al., 2022). Besides, bubble columns can be used in the bioleaching of mineral ores and to carry out gas−liquid precipitation to separate heavy metals such as copper, zinc, and nickel from liquid

effluent by using hydrogen sulfide (Al-Tarazi et al., 2005, 2004). Table 1.1 summarizes the applications of bubble column reactors in the period covering 2018 – 2022.

As a matter of fact, the wide use of BCs is mainly related to the advantages they offer over other multiphase reactors. In particular, they present ease of operation, simplicity of construction, low operating and maintenance costs thanks to the absence of moving parts, high heat and gas−liquid mass transfer rates per unit volume with low energy input, high overall gas−liquid mass transfer coefficients and interfacial areas, high liquid residence time, which allows the performing of slow reactions, the temperature is easier to control and has a uniform distribution, high liquid or slurry phase fraction to enable the occurring of the reaction, and low to moderate mixing intensity induced by the gas flow. However, BCs suffer from some disadvantages that considerably impair their performance and that need to be considered to optimize their design. Indeed, the main drawbacks can be listed as follow: The high static head of the liquid which causes a high gas pressure drop, the gas−liquid interfacial area is significantly decreased by the bubble coalescence phenomenon, especially in the heterogeneous regime, the back-mixing is substantial in both the continuous liquid and dispersed gas phases and may result in unfavorable selectivity and lower conversion, the high shear in the region close to the gas distributor can cause catalyst attrition and deactivation, and scaling up constraints (Deckwer and Schumpe, 1993; Fard, 2020; Ferreira et al., 2017; Lakhdissi, 2020; Ruzicka et al., 2001).

Table 1.1 Major applications of bubble column reactors in the period covering 2018 – 2022.

| Applications | BC geometry and design | Temperature (°C) | Pressure (bar) | Study | Reference |
|---|---|---|---|---|---|
| Removal of refractory humic- and fulvic-like organics from biotreated landfill leachate by ozonation | Cylindrical glass column<br>$H_c$ = 200 cm, $d_c$ = 10 cm, and $V_w$ = 15 L<br>Porous glass plate diffuser | 20 ± 1 | 1.013 | Experimental | Yang et al. (2022) |
| Production of fucoxanthin from the golden-brown microalga "*Tisochrysis lutea"* applying mass transfer coefficient | Cylindrical glass column<br>$H_c$ = 30 cm, $d_c$ = 15 cm, and $V_w$ = 4 L<br>Ring sparger with 8 nozzles<br>Multiple orifice sparger with 12 nozzles | 24 ± 1 | - | Experimental | Mohamadnia et al. (2022) |
| Growth of *Chlorella sorokiniana* on cooking cocoon wastewater | Cylindrical glass column<br>$H_c$ = 35 cm, $d_c$ = 4.5 cm, and $V_w$ = 0.3 L<br>Gas sparger with a pore size of 0.002 Cm | 25 ± 1 | - | Experimental | Gao et al. (2022) |
| The use of a bubble column evaporator as a solvent swap device in the pharmaceutical industry | Cylindrical column<br>$H_c$ = 100 cm, $d_c$ = 3 cm | 30 – 50 | 1 | Numerical | Cappelli et al. (2022) |
| Photosynthetic (Microalgal) biogas upgrading | Clear acrylic tube<br>$H_c$ = 200 cm, $d_c$ = 2.4 cm<br>Air-stone diffuser | 20 ± 1 | 1.013 | Experimental and optimization study | Bose et al. (2022) |
| Production of $CO_2$-free hydrogen from methane with molten liquid alloy | Quartz tube contains 3 stages: Ni-Bi molten alloy catalyst layer, bed of zirconia beads, and Na-Br molten salt layer<br>$H_c$ = 65 cm, $d_c$ = 0.8 cm<br>Porous ceramic membrane | 900 – 985 | 1.013 | Experimental | Noh et al. (2022) |
| Agro-industrial wastewater-grown microalgae cultivation | Three independent acrylic cylinder tubes<br>$H_c$ = 100 cm, $d_c$ = 15 cm, and $V_w$ = 15 L<br>Cylindrical porous stone disperser (2.2 cm long and 1.2 cm inner diameter) | 30 – 42 | 1.013 | Techno-environmental assessment | Magalhães et al. (2022) |
| Carbon dioxide removal by weathering of calcite with seawater | Glass column packed with mineral particles<br>$d_c$ = 14.5 cm, $V_R$ = 18 L | 20 | 1.013 | Numerical | Xing et al. (2022) |
| Removal of dissolved oxygen from wine by desorption | Cylindrical column<br>$H_c$ = 90 cm, $d_c$ = 15 cm<br>Stone sparger with a pore size of 0.004 cm | 25 | - | Experimental | Sutton et al. (2022) |

Table 1.1 Continued.

| | | | | | |
|---|---|---|---|---|---|
| Fungal bioleaching of e-waste utilizing molasses as the carbon source (Ni and Cu recovering from mobile phone printed circuit boards waste) | Glass column<br>$H_c$ = 55 cm, $d_c$ = 7.5 cm | 30 | - | Experimental and optimization study | Nili et al. (2022) |
| Methane pyrolysis in a molten gallium bubble reactor for sustainable hydrogen production | Quartz bubble column<br>$H_0$ = 15 cm<br>Porous plate distributor with the biggest nominal pore size distribution available ($d_0$ = 0.016 – 0.025 Cm) | 1119 | 1.013 | Experimental and techno-economic assessment | Leal Pérez et al. (2021) |
| Ethylene dimerization process in the presence of titanium-based Ziegler–Natta as a homogenous catalyst | Cylindrical column<br>$H_c$ = 1110 cm, $d_c$ = 370 cm | 31.85 – 56.85 | 23.3 | Experimental and optimization study | Mohammadzade Fard et al. (2021) |
| Removal of several ozone-persistent trace organic contaminants by ozonation | Cylindrical glass column packed with stainless-steel cleaning ball, lava rock, and stainless-steel pall ring<br>$H_c$ = 200 cm, $d_c$ = 10 cm, $V_w$ = 8 – 10 L | Room temperature | - | Experimental | Liu et al. (2021) |
| Removal of diclofenac (a non-steroidal analgesic drug) from water by ozonation | Glass column<br>$V_R$ = 1 L<br>Sparger of pore size of 0.004 cm | 24.85 | - | Experimental | Patel et al. (2021) |
| Catalytic hydrocracking of a $H_2$ – vacuum residue system | Stainless-steel slurry bubble column<br>$H_c$ = 200 cm, $d_c$ = 5 cm<br>The perforated plate had three holes with an inner diameter of 0.1 cm | 425 | 160 | Experimental and numerical | Van Tran et al. (2021) |
| Humic acid removal by intensified ozonation | Cylindrical glass column packed with lava rocks and metal pall ring<br>$H_c$ = 200 cm, $d_c$ = 10 cm, $V_w$ = 15 L<br>Porous glass plate diffuser | 20 ± 1 | - | Experimental | Yang et al. (2021) |
| Phenol removal from contaminated water using ozonation | Cylindrical stainless-steel column<br>$H_c$ = 130 cm, $d_c$ = 10 cm, and $V_w$ = 18 L<br>Gas diffuser with an average 200-micron pore size | 20 | - | Experimental | Barlak et al. (2020) |
| Fermentative oxidation of butane | Glass cylinder<br>$H_c$ = 60 cm, $d_c$ = 8 cm, and $V_w$ = 2 L<br>Sinter cylinder sparger with 0.0002 cm pore size | 25 – 40 | 1.1 – 1.5 | Experimental | Sluyter et al. (2020) |

Table 1.1 Continued.

| | | | | | |
|---|---|---|---|---|---|
| Bio-oil conversion by hydrothermal liquefaction process using produced lipid-rich biomass of *"Rhodococcus opacus"* | Perspex made column<br>$H_c$ = 45 cm, $d_c$ = 8 cm, $V_R$ = 2 L, and $V_w$ = 1.8 L<br>Stainless-steel nozzle sparger | 27 ± 2 | - | Experimental | Paul et al. (2020) |
| Enhancing the removal of $H_2S$ from biogas through refluxing of the outlet gas | Glass column packed with a cylindrical plastic carrier with internal ribs<br>$H_c$ = 60 cm, $d_c$ = 4 cm | - | - | Experimental | Jiang et al. (2020) |
| Evaporation process with helium for seawater desalination | Glass column<br>$H_0$ = 9 - 11 cm, $d_c$ = 13 cm<br>Porous sinter with 0.004 – 0.01 cm pore size | 75 – 150 | - | Experimental | Wei and Pashley (2020) |
| Brine elimination by hybridization of a novel brine-recycle bubble-column humidification-dehumidification system with a multiple-effect distillation system | Cylindrical column | 45 | 15 | Thermodynamic modeling, exergy, exergo-economic and exergo-environmental analyses | Ghofrani and Moosavi (2020) |
| Thermophilic waste air treatment of an airborne ethyl acetate/toluene mixture | Glass column<br>$H_c$ = 62 cm, $d_c$ = 7.5 cm, and $V_w$ = 1.5 L<br>Glass frit sparger with 0.016 – 0.025 cm pore size | 25 – 60 | - | Experimental | Chalupa et al. (2020) |
| $H_2S$ removal from the gas phase using calcium carbonate based solid wastes | PVC made cylindrical column<br>$H_c$ = 160 cm, $d_c$ = 34 cm, and $V_R$ = 145 L | - | - | Experimental | Galera Martínez et al. (2020) |
| Biogas valorization via continuous polyhydroxybutyrate production by *"Methylocystis hirsuta"* | Cylindrical column<br>$V_w$ = 2.5 L<br>Micropore stainless-steel diffuser ($d_0$ = 0.0002 cm) | 25 | - | Experimental | Rodríguez et al. (2020) |
| CO2 capturing by *"Chlorella vulgaris"* | Glass cylindrical column<br>$H_c$ = 50 cm, $d_c$ = 3 cm, and $V_w$ = 1 L<br>- Sparger with a large aperture size (~ 0.0035 cm)<br>- Sparger with a tiny aperture size (~ 0.002 cm) | 15 – 35 | - | Experimental and optimization study | Barahoei et al. (2020) |

Table 1.1 Continued.

| | | | | | |
|---|---|---|---|---|---|
| Oxidation removal of gaseous elemental mercury ($Hg^0$) using $Cu^{2+}$ enhanced-Fenton system | Corrosion-resistant glass tube<br>$H_c$ = 30 cm and $d_c$ = 9 cm | 26.85 – 76.85 | - | Experimental | (Liu et al. (2019) |
| Enzymatic pretreatment and hydrolysis of apple pomace as a possible renewable feedstock for the production of biofuels and bio-commodities | Glass column<br>$H_c$ = 40 cm and $d_c$ = 3.4 cm<br>Stainless-steel tube gas sparger (0.1 cm inner diameter) | 28 – 50 | - | Experimental | Niglio et al. (2019) |
| Agricultural wastewater remediation with fatty acid production by two cyanobacteria (*Anabaena sphaerica* and *Anabaena variabilis*) | Glass cylindrical column<br>$H_c$ = 30 cm, $d_c$ = 5 cm, and $V_R$ = 0.5 L | - | - | Experimental | Gorain et al. (2019) |
| Bioremoval of trinitrophenol from wastewater using nanostructured zero-valent iron and graphene oxide | Corning glass column<br>$H_c$ = 35 cm, $d_c$ = 10 cm, $V_w$ = 0.2 L, and $V_R$ = 0.3 L | 30 ± 1 | - | Experimental and optimization study | Bavandi et al. (2019) |
| Pilot-scale production of phylloquinone (vitamin $K_1$) | Clear acrylic tube<br>$H_c$ = 200 cm, $d_c$ = 19 cm<br>- Perforated stainless-steel tube sparger with 3 rows of 10 holes ($d_0$ = 0.2 cm)<br>- Ceramic cylinder air-stone with a pore size less than 0.03 cm | 28 | 1.01 – 2.98 | Experimental | Tarento et al. (2019) |
| Production of precipitated calcium carbonate during carbon dioxide dissolution and ammonia losses | Polycarbonate column<br>$H_c$ = 200 cm, $d_c$ = 12.7 cm, and $V_w$ = 24.9 L<br>The gas distributor had 8 lines of 4 holes ($d_0$ = 0.05 cm) | 18.3 – 22.4 | 1.013 | Experimental | Zevenhoven et al. (2019) |
| Efficient catalytic ozonation of oxalic acid using mesoporous Ce-Ti-Zr ternary oxide millispheres | Glass cylindrical column<br>$H_c$ = 18 cm and $d_c$ = 10 cm<br>A porous plate of sand core with an average pore size of ~ 4 μm | 25 | 1.013 | Experimental | Shan et al. (2018) |
| Water sterilization using 6 different hot gases ($CO_2$, $O_2$, $N_2$, Ar, air and combustion gas) | Cylindrical column<br>Glass sinter with 0.0004 – 0.01 cm pore size | 150 – 200 | 1.013 | Experimental | Garrido et al. (2018) |

Table 1.1 Continued.

| | | | | | |
|---|---|---|---|---|---|
| Fatty acids production by marine microalgae "*Chlorella minutissima*" | - Three acrylic tubes<br>$H_c$ = 120 cm, $d_c$ = 13.5 cm, and $V_w$ = 18 L<br>- Three acrylic tubes<br>$H_c$ = 203.3 cm, $d_c$ = 18.4 cm, and $V_w$ = 44 L<br>Stone diffuser | 25 | - | Experimental and optimization study | Pereira et al. (2018) |
| Isolation, identification, and outdoor cultivation of thermophilic freshwater microalgae "*Coelastrella sp. FI69* " | Borosilicate glass column<br>$H_c$ = 1 cm, $d_c$ = 9 cm, and $V_w$ = 4.5 L<br>Sparger tube with an inner diameter of 0.8 cm | 25 – 50 | - | Experimental | Suriya Narayanan et al. (2018) |
| *p*-Nitrophenol degradation by Fenton's oxidation | Acrylic column<br>$H_c$ = 140 cm, $d_c$ = 9.8 cm, and $V_w$ = 7 L<br>Gas dispenser (acrylic dish) with 9 orifices ($d_0$ = 0.05 cm) | 22 – 24 | 1.013 | Experimental | Rodrigues et al. (2018) |
| Methane abatement and polyhydroxyalkanoate production by "*Methylocystis hirsuta*" | PVC column<br>$H_c$ = 60 cm, $d_c$ = 8 cm, and $V_w$ = 2.5 L<br>0.5 µm-pore size stainless-steel gas diffuser | 25 | - | Experimental | García-Pérez et al. (2018) |
| Industrial Fischer–Tropsch synthesis | Cylindrical column<br>$H_c$ = 3000 cm, $d_c$ = 580 cm | 230 – 280 | 20 – 40 | Numerical (modeling) | Li (2018) |

### 1.1.2 Airlift reactors

Airlift (ARL) reactors consist of a liquid vessel divided into two distinct sections, only one of which is typically sparged with gas. In fact, the part of the reactor enclosing the gas−liquid upflow stream is the riser, and the region with the downflowing fluid is called the downcomer (Chisti and Moo-Young, 1987; Talvy, 2003). The difference in gas hold-up in the gassed and non-gassed zones leads to different bulk densities of the fluid in these regions, which in turn prompts the circulation of the fluid in the reactor by a gas-lifting action. A broad variety of ARL reactor configurations have been studied and considered in the literature; however, two basic classes of airlift reactors can be distinguished: (1) internal loop ARL reactors which is a simple bubble column that is divided into a riser and a downcomer by an internal baffle; (2) external loop ARL reactors where the riser and the downcomer are two completely separate tubes connected by horizontal sections near the top and bottom (Merchuk, 2003; Zhang et al., 2019). Internal and external loop reactors can be further subdivided according to their distinctive features (Figure 1.2). Moreover, internal and external loop ARL reactors are commonly designed with circular, rectangular or square cross-sections, and each of these geometries possesses practical applications in industry and has been thoroughly investigated. Regarding gas injection, the types of gas distributors (static or dynamic), and their location in the riser and/or downcomer can be altered to achieve the desired performance for various ends.

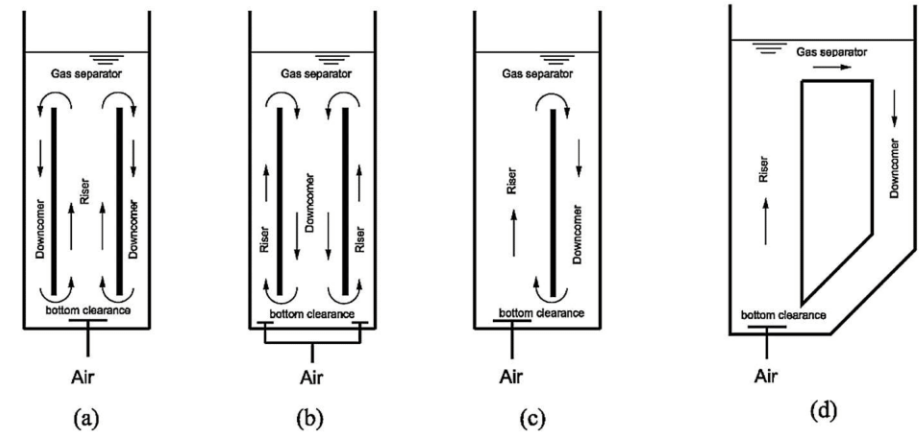


Figure 1.2 The typical configurations of the Airlift reactors (a) Center aeration ARL (b) Perimeter aeration ARL (c) Baffle-split ARL and (d) External loop ARL (Zhang et al., 2019).

Along with their simplicity of design and construction, ARL reactors exhibit advantages, such as better-defined flow patterns and relatively low power inputs for the required transport rates, low shear fields, prominent mixing and mass transfer at competitively low energy

consumption and extended aseptic operation thanks to the elimination of stirrer shafts, seals, and bearings. These properties make ARL reactors very attractive for use in a variety of applications, such as hydrogenation, desulfurization, coal liquefaction, and Fisher-Tropsch synthesis, biological processes of fermentation and cell cultivation, and environmental engineering applications, such as wastewater treatment, volatile organic compounds abatement. The various applications of ARL are reported in Table 1.2.

Table 1.2 Major applications of ARL reactors in the period covering 2018 – 2022.

| Applications | ARL geometry and design | Temperature (°C) | Pressure (bar) | Study | Reference |
|---|---|---|---|---|---|
| The degradation of organic pollutants using S-scheme ZIF-8/$Ag_2S$ heterojunction photocatalyst | External-loop ARL reactor<br>- Riser (made of graphite): $H_c$ = 55.5 cm, and $d_c$ = 6.35 cm<br>- Downcomer: $H_c$ = 40 cm, and $d_c$ = 2.45 cm | Room temperature | Room pressure | Experimental | Jabbar and Al-Farraji (2022) |
| The enhancement of gaseous o-xylene biodegradation by using an airlift microbial electrolytic cell system | Internal-loop ARL reactor<br>- Riser (made of graphite): $H_c$ = 20 cm, and $d_c$ = 3.6 cm<br>- Downcomer: $H_c$ = 30 cm, and $d_c$ = 8 cm<br>$V_w$ = 2 L | 30 | - | Experimental | Y. Li et al. (2022) |
| The reduction of reduced algal wall growth during the *"Chlorococcum humicola"* cultivation by using plastic media | Transparent acrylic ARL photobioreactor<br>Two cylindrical tubes<br>- Riser: $H_c$ = 25 cm, and $d_c$ = 4.4 cm<br>- Downcomer: $H_c$ = 50 cm, and $d_c$ = 9 cm<br>$V_w$ = 2 L | 30 - 35 | - | Experimental | Plengsakul et al. (2021) |
| Nutrients recovery from fresh liquid manure to mitigate the greenhouse gas emissions of open anaerobic lagoons | Internal-loop ARL reactor<br>Two concentric tubes made of transparent PVC<br>$A_d/A_r$ = 0.89, $H_c/d_c$ = 5.2 cm and $V_w$ = 1.8 L | 28 | - | Experimental | Sobhi et al. (2021) |
| Reduction of *p*-nitrophenol with iron electrodes | ARL electrochemical reactor made of plexiglass<br>Two cylindrical tubes<br>- Downcomer: $H_c$ = 70 cm, and $d_c$ = 15 cm<br>$V_w$ = 15 L | 19.3 ± 0.5 | - | Experimental | Pereira et al. (2021) |
| Enhanced bioenergy recovery and nutrient removal from swine wastewater | Split ARL cubic bioreactor with a baffle (8 cm in height) placed in the middle of the photobioreactor<br>$V_R$ = 0.4 L | 25 | - | Experimental | Li et al. (2021) |

Table 1.2 Continued.

| | | | | | |
|---|---|---|---|---|---|
| Photocatalytic degradation of organic pollutants (azo dye Cibacron Brilliant Yellow 3G-P) using Core/shell $Fe_3O_4@Al_2O_3-PMo$ magnetic nanocatalyst | Internal-loop ARL reactor<br>Two acrylic concentric tubes<br>- Riser: $H_c$ = 22 cm, and $d_c$ = 8 cm<br>- Downcomer: $H_c$ = 30 cm, and $d_c$ = 12 cm<br>$V_w$ = 0.816 L | Room temperature | - | Experimental | Ammar et al. (2020) |
| Simultaneous removal of carbon and nitrogen from soft drink industrial wastewater | Jet loop-ARL bioreactor<br>- Riser: $H_c$ = 53.5 cm, and $d_c$ = 10 cm<br>- Downcomer: $H_c$ = 66.5 cm, and $d_c$ = 15 cm<br>$V_w$ = 9.5 L | - | - | Experimental and optimization study | Gholami et al. (2020) |
| Removal of gaseous tetrahydrofuran with immobilized cells of GFP-tagged *Pseudomonas oleovorans* GDT4 | ARL bioreactor made of Perspex<br>- Downcomer: $H_c$ = 57 cm, and $d_c$ = 9 cm<br>$V_w$ = 2.8 L | - | - | Experimental | J. Chen et al. (2020) |
| Treatment of refined soybean oil Wastewater using a swirling demulsified airlift loop reactor | ALR made of transparent organic glass material<br>- Riser: $H_c$ = 24 cm, and $d_c$ = 12 cm<br>- Downcomer: $H_c$ = 74 cm, and $d_c$ = 19 cm | 25 | 1.013 | Numerical and optimization study | Shi et al. (2020) |
| Simultaneous removal of nitrogen and organic carbon from tannery wastewater using granulated sludge | Internal-loop ARL reactor<br>Two plexiglass concentric tubes<br>- Riser: $H_c$ = 60.5 cm<br>- Downcomer: $H_c$ = 80 cm, and $d_c$ = 10 cm<br>$V_w$ = 5 L | 29 – 31.5 | - | Experimental | Melesse et al. (2020) |
| Treatment of organic waste gases (dichloromethane and toluene) emitted from the pharmaceutical industry | Internal-loop ARL and ARPL (packed with polyurethane sponge and polypropylene Raschig) bioreactors<br>Two plexiglass concentric tubes<br>- Riser: $H_c$ = 55 cm, and $d_c$ = 5 cm<br>- Downcomer: $H_c$ = 65 cm, and $d_c$ = 10 cm<br>$V_w$ = 4.2 L | 25 – 30 | - | Experimental and statistical analysis | Xu et al. (2020) |

Table 1.2 Continued.

| | | | | | |
|---|---|---|---|---|---|
| Degradation of complex phthalocyanine dye-containing wastewater using immobilized ternary photocatalytic polymer film | Internal-loop ARL made of quartz glass<br>Two cylindrical tubes<br>- Riser: $H_c$ = 22 cm, and $d_c$ = 2,4,6 cm<br>- Downcomer: $H_c$ = 30 cm, and $d_c$ = 8 cm<br>$V_w$ = 1.2 L, and $V_R$ = 1.5 L<br>Sintered porous sparger | - | - | Experimental | Das and Mahalingam (2020) |
| Ozonation as a non-thermal option for bacterial load reduction of *Chlorella* biomass | ARL photobioreactor made of transparent plexiglass<br>$V_w$ = 3.4 L | 25 – 30 | - | Experimental | Chegukrishnamurthi et al. (2020) |
| Acidic 7-amino cephalosporanic acid (7-ACA) wastewater treatment | Multiple ARL loop draft tubes<br>Riser: $d_{c1}$ = 3 cm, $d_{c2}$ = 6 cm, and $d_{c3}$ = 9 cm<br>- Downcomer: $H_c$ = 36 cm, and $d_c$ = 12 cm<br>$V_w$ = 4 L | 25 ± 3 | - | Experimental | Hu et al. (2020) |
| Performance of a novel multiple draft tubes airlift loop membrane bioreactor to treat ampicillin pharmaceutical wastewater | Multiple ARL loop draft tubes<br>Riser: $d_{c1}$ = 3 cm, $d_{c2}$ = 6 cm, and $d_{c3}$ = 9 cm<br>- Downcomer: $H_c$ = 36 cm, and $d_c$ = 12 cm<br>$V_w$ = 4 L | 7 – 48 | | Experimental | Z. Chen et al. (2020) |
| The removal performance of dichloromethane and toluene from waste gases | Internal-loop ARL and ARPL (packed with polyurethane sponge and polypropylene Raschig) bioreactors<br>Two plexiglass concentric tubes<br>- Riser: $H_c$ = 55 cm, and $d_c$ = 5 cm<br>- Downcomer: $H_c$ = 65 cm, and $d_c$ = 10 cm | 30 | - | Experimental | Xu et al. (2019) |
| Electrocoagulation technique for refinery wastewater treatment | Internal-loop ARL made of Perspex<br>- Riser (rectangular split-plates): w = 8 cm, and L = 20 cm<br>- Downcomer (cylinder): $H_c$ = 35 cm, and $d_c$ = 10 cm<br>$V_w$ = 2 L | 30 | - | Experimental | Ammar et al. (2019) |

Table 1.2 Continued.

| | | | | | |
|---|---|---|---|---|---|
| Enhancement of $CO_2$ biofixation and bioenergy generation using a novel airlift type photosynthetic microbial fuel cell | Split ARL cubic bioreactor with a baffle (8 cm in height) placed in the middle of the photobioreactor<br>$V_R$ = 0.95 L | 25 | - | Experimental | Li et al. (2019) |
| Oilfield produced water treatment using electrocoagulation/flotation technique | Internal-loop ARL reactor<br>Two acrylic concentric tubes<br>- Riser: $H_c$ = 20 cm, and $d_c$ = 4.7 cm<br>- Downcomer: $H_c$ = 27 cm, and $d_c$ = 8 cm<br>$A_r/A_d$ = 0.537, $H_0$ = 19 cm and $V_w$ = 1.75 L | 25 | 1.013 | Experimental | Ammar and Akbar (2018) |
| The production of polycyclic aromatic hydrocarbon-emulsifier protein produced by *"Aspergillus brasiliensis (niger)"* | Cylindrical glass ARL reactor<br>$V_w$ = 1 L | 40 – 92 | - | Experimental | Sánchez-Vázquez et al. (2018) |
| Carbon dioxide capture from air using biocatalyst | Internal-loop ARL reactor made of plexiglass<br>- Riser: $H_c$ = 100 cm, and $d_c$ = 10 cm<br>- Downcomer: $H_c$ = 200 cm, and $d_c$ = 15 cm<br>$H_0$ = 110 cm and $V_w$ = 20 L<br>Stainless-steal sparger ($d_0$ = 0.1 cm) | 30 | - | Numerical | Sadeghizadeh et al. (2018) |

## 1.2 Hydrodynamic and mass transfer aspects of BC and ARL reactors

The performance of bubble column and airlift reactors is a complex function of various mechanisms, which make their design and scaling-up fastidious because they are primarily linked, in addition to kinetics, to three major aspects, including hydrodynamics, and mass and heat transfer. Figure 1.3 depicts the relationship between these aspects and the BC and ARL performance, as well as the key parameters.

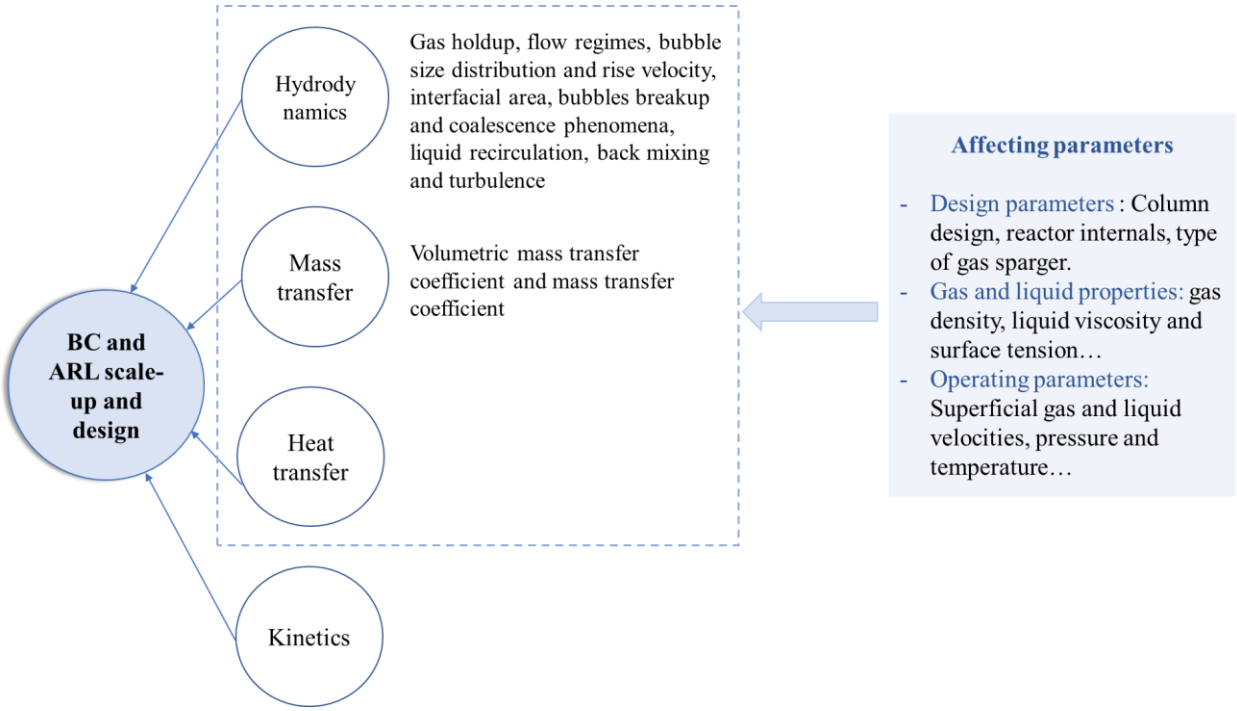


Figure 1.3 Key parameters governing hydrodynamics, and mass and heat transfer.

### 1.2.1 Hydrodynamics studies

#### *1.2.1.1 Bubble column reactors*

##### *1.2.1.1.1 Gas hold-up*

Gas hol-dup ($\varepsilon_g$) in the bubble column and airlift measures the fractional gas content in the reactor. It is extremely important to know the gas hold-up, as it is indicative of the residence time of the gas, flow regimes, effective interfacial area, and mass transfer coefficient. It is worth noting that gas hold-up is strongly related to column design, types of gas distributors, physical properties of the phases, and operating parameters, such as pressure and temperature.

The type and design of gas distributors have a profound effect on gas hold-up. Commonly, porous and membrane diffusers provide narrower size distributions, and thereby higher gas hold-up than perforated plates (Bouaifi et al., 2001; Kantarci et al., 2005; Leonard et al., 2015;

Zahradník et al., 1997). Camarasa et al. (1999) examined the effect of gas distributor by using three diverse static spargers: a single-orifice nozzle (5 mm in diameter), a multiple-orifice nozzle (62 holes of 1 mm uniformly spaced), and a porous glass plate (10–16 mm mean pore diameter, 5 mm in height). As a result, they found that the gas hold-up was higher with the porous plate than with the multiple-orifice nozzle because the first distributor produces smaller bubbles that do not coalesce in the homogeneous regime. When the porous plate or the multiple-orifice nozzle was used, the $\varepsilon_g$ versus $U_g$ curves exhibited a pronounced maximum reflecting the transition between the homogeneous and heterogeneous regime. On the contrary, the $\varepsilon_g$ versus $U_g$ curve with a single-orifice nozzle never augmented linearly and did not show a maximum, which indicated that heterogeneous conditions exist even at low superficial gas velocity. In this context, Besagni et al. (2018) classified gas distributors into two main categories "fine distributors" and "coarse distributors" (Figure 1.4). In case a "fine distributor" is used, the $\varepsilon_g$ curve increases linearly in the homogeneous flow regime, then reaches a peak and thereafter goes up again; conversely, in case a "coarse distributor" is used, the $\varepsilon_g$ curve rises continuously. Indeed, these distinct behaviors are attributed to bubble dynamics (i.e., bubble formation at the gas sparger and coalescence/breakup phenomena). In “coarse distributors” there is a continuous appearance of large bubbles, whereas, in “fine distributors” large bubbles start appearing after the flow transition. Thus, “fine distributors” exhibit higher $\varepsilon_g$ compared to “coarse distributors” because of their narrower bubble size distribution.

More interestingly, for the same distributor, the number and diameter of the openings also affect the gas hold-up (Hasanen et al., 2006; Polli et al., 2002; Zahradník et al., 1997). As a matter of fact, a decrease in the diameter of holes led to an increase in $\varepsilon_g$ (Jin et al., 2007; Şal et al., 2013). Gemello et al. (2018) studied the gas distribution in a 0.4 m diameter cylindrical BC reactor using two different perforated spargers: the first one had 92 holes of 2 mm in diameter, and the second one contained 7 holes of 9 mm, with one hole in the center of the sparger, while the other 6 holes create a hexagon for a dimensionless radial position equal to 0.65. Indeed, they reported that the initial radial profile of the gas fraction is almost flat using the gas distributor with small holes. However, the use of the gas distributor with big holes altered the radial profile which was caused by a strong accumulation of bubbles close to the holes. Furthermore, above an axial position of 50 cm, the gas fraction with the two spargers was approximately similar under the heterogeneous regime.

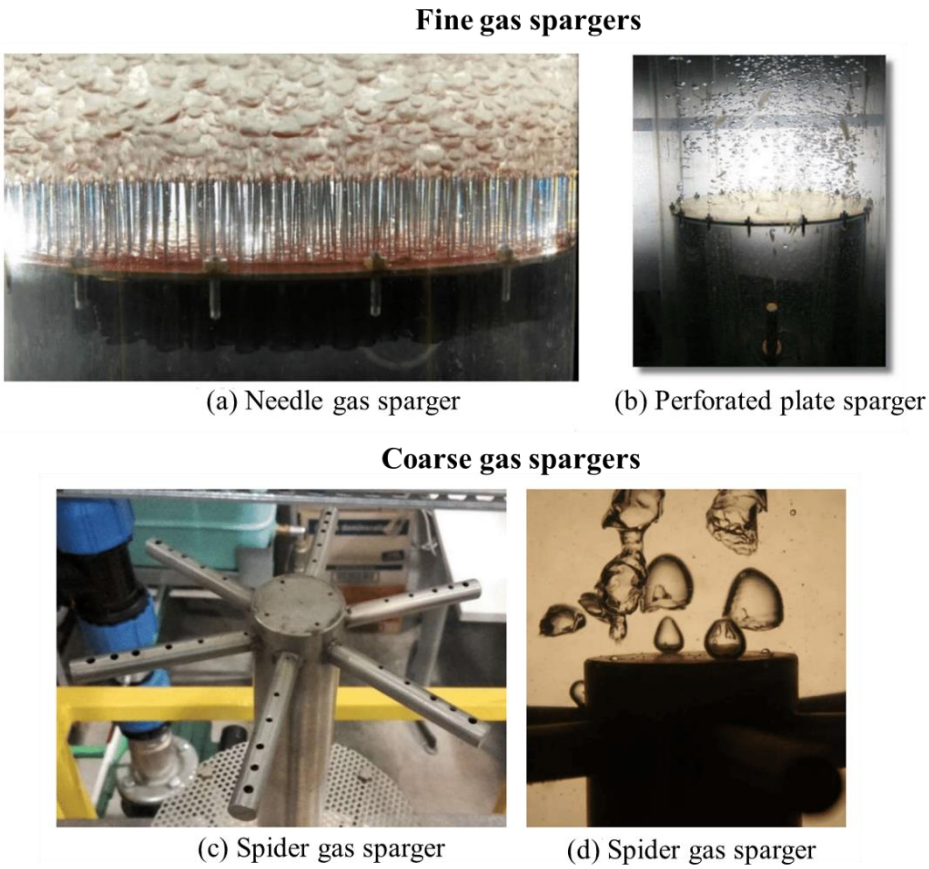


Figure 1.4 Fine and coarse gas spargers (Besagni et al., 2018).

Particular attention is also paid to the effects of additives and impurities contained in the liquid phase on the hydrodynamics of bubble column reactors as they lead to a change in the bubble's behavior. Indeed, when the liquid phase in the BC contains additives, bubble coalescence was suppressed. The coalescence inhibition mechanisms are different for various additives. These include hydration repulsive forces, the Gibbs–Marangoni effect, and reduction in hydrophobic and electrical repulsive forces (Kirkpatrick and Lockett, 1974; Martín et al., 2008; Weissenborn and Pugh, 1996). Sarhan et al. (2018) numerically investigated the effect of liquid and gas phases physico-chemical properties on bubble formation and the hydrodynamic characteristics in bubble column reactors. Indeed, they reported the increment in gas phase density resulted in a slight increase in the predicted gas hold-up, which can be ascribed to the fact that an augmentation in gas phase density stabilized the homogeneous flow regime and delayed the regime transition point. Meanwhile, a significant increase in the average gas hold-up values was observed when the lower-density paraffin oil was used as the liquid phase. This has been attributed to the reduced buoyancy force effect.

Gemello et al. (2018) carried out experiments with demineralized water, tap water, and demineralized water containing small quantities of ethanol. The findings indicated that the contaminants and the addition of alcohol inhibited bubble coalescence and caused a decrease in the average bubble size. Consequently, the addition of alcohol increased the gas hold-up in the heterogeneous regime and delayed the transition from the homogeneous to the heterogeneous regime. Mouza et al. (2005) studied the effect of liquids covering a various range of surface tension (48 – 72 $mN.m^{-1}$) on the hydrodynamics in a bubble column equipped with fine pore spargers. As a result, they observed an increase in gas hold-up when the lower surface tension butanol solutions were used as the liquid phase. In fact, positive surfactants (organic substances) are attracted to the bubble interface where they adsorb positively, leading to a diminution of the surface tension and inducing suppression of the coalescence phenomena. Notably, the alcohol molecules are formed of hydrophilic and hydrophobic parts which are adsorbed at the interface once they are dissolved in water. Similar outcomes were reported by (Camarasa et al., 1999; Gourich et al., 2005; Vial et al., 2001) who investigated the effect of non-coalescing media on gas hold-up. Likewise, Besagni et al. (2016) concluded that the addition of a low ethanol concentration resulted in an increment in the gas hold-up. Nevertheless, foam phenomena were observed when increasing the ethanol concentration (equal to 0.3 wt.%). Furthermore, the authors pointed out that the appearance of foam is not only related to the high concentration of ethanol but also the aspect ratio ($H_0/d_c$).

When compared to the case of the water-air system, $\varepsilon_g$ is always found higher for liquids with low surface tension (*i.e.*, mixtures of water and alcohols) (Figure 1.5a). However, Chaumat et al. (2007) examined the influence of surface tension in bubble column by using water ($\sigma$ = 72 $mN.m^{-1}$) and cyclohexane ($\sigma$ = 24.65 $mN.m^{-1}$) with similar viscosity. Hence, they found that the gas hold-up was smaller in cyclohexane than in water for both gas distributors with small and large holes. The authors stated that the use of pure solvent instead of aqueous solution with surfactant could be responsible for the identified discrepancy.

Regarding the rheological properties of the liquid phase, it has usually been shown that increasing the viscosity of the liquid phase diminishes the total gas hold-up and impedes the formation and stability of a homogeneous bubble bed. This adverse effect is primarily attributed to the existence of drag forces promoting bubble coalescence in the gas sparger region (Ruzicka et al., 2003; Urseanu et al., 2003; Zahradník et al., 1997). (Anastasiou et al., 2013) analyzed the behavior of shear-thinning non-Newtonian fluids in bubble columns equipped with a metal porous sparger. They reported that at very high viscosity values, larger bubbles were formed,

due to coalescence phenomena starting at the sparger surface. Thus, there is a clear relationship between gas hold-up and bubble size, *i.e.*, while larger bubbles rise at a higher velocity, this leads to a reduced gas residence time and, consequently, lower gas hold-up values. However, Esmaeili et al. (2015) studied the effects of elastic and viscous aspects of non-Newtonian fluids on the hydrodynamics of a pilot scale BC reactor, and revealed that the elasticity of the liquid phases shortened the average chord length of the bubbles and increased the total gas hold-up. Whilst viscosity tends to be more conducive to coalescence, the elasticity of the liquid phase can hinder the coalescence of bubbles by exhibiting solid-like behavior at the interface of two bubbles. Besagni et al. (2017b) noted that $\varepsilon_g$ rose continuously and nonlinearly as the mono-ethylene-glycol concentration increased to 5% ($\mu_L$ = 1.01 mPa.s), accompanied by the prevalence of small bubbles (Figure 1.5b). In contrast, as the concentration kept increasing from 5% to 80% ($\mu_L$ = 1.01 – 7.97 mPa.s) $\varepsilon_g$ decreased (Figure 1.5c). The authors commented that this behavior happened because at low viscosity, coalescence was restricted, and the large drag force reduced the rate of bubble rise, resulting in an increase in $\varepsilon_g$. However, with increasing viscosity, the coalescence trend prevailed, making large bubbles that moved up the column at a higher velocity, thereby minimizing $\varepsilon_g$.

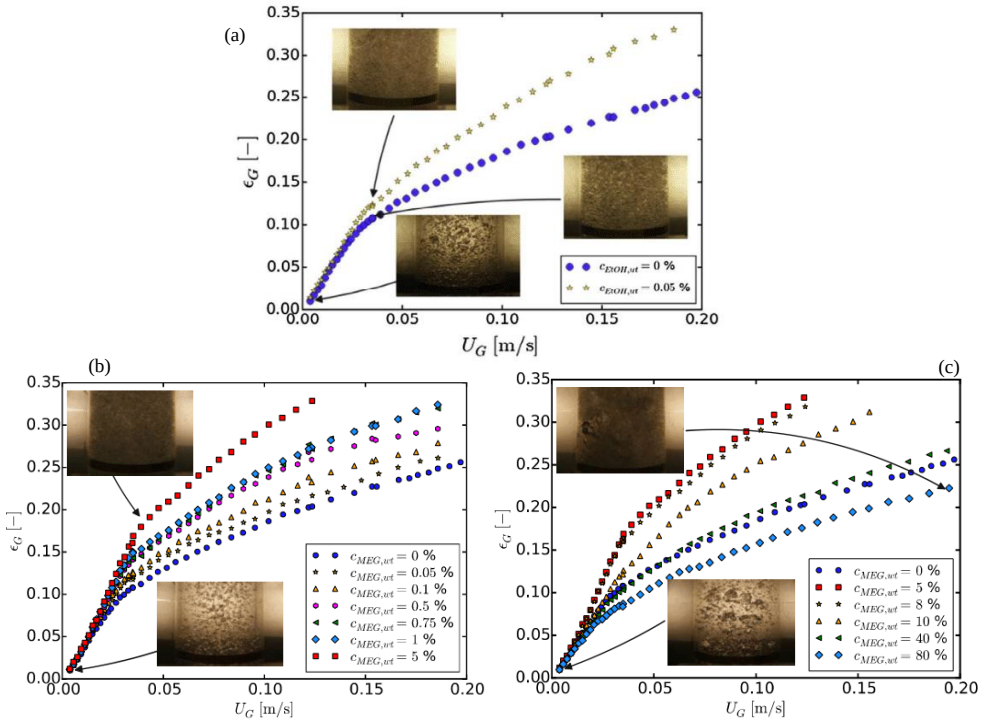


Figure 1.5 Global gas hold-up versus superficial gas velocity for (a) 0.05% ethanol–air, (b) water–MEG–air (low viscosities), and (b) water–MEG–air (moderate viscosities) systems (Besagni et al., 2017b, 2016).

Concerning the effect of temperature, there is no consensus in the literature. Leonard et al. (2019) and Pohorecki et al. (1999) found that temperature had no effect on gas hold-up which might be due to evaporation. Other authors observed a decrease in gas hold-up while increasing temperature (Deckwer et al., 1980b; Yang et al., 2001). Yang et al. (2001) described a decrease in interfacial area and gas hold-up in a homogeneous system in the presence of solid (5% by volume, system $H_2$/CO–viscous paraffin) and at different pressures (10 – 30 bar). Lin et al. (1998) reported an increase in the gas hold-up with the temperature at a pressure of 15.2 MPa, which can be linked to the bubble size distribution; it became narrower when the temperature was augmented. Actually, an increase in temperature leads to a decrease in surface tension and thus leads to a decrease in the film drainage speed, and subsequently a decrease in primary bubble size. A temperature increase also leads to a decrease in viscosity, which in turn can lead to a decrease in the primary bubble diameter. The viscosity has two effects on bubble coalescence. On the one hand, it increases film drainage speed and collision frequency, and thus, enhances coalescence phenomena. On the other hand, it decreases contact time. Therefore, it can be said that the increase in gas hold-up with the increase of temperature is related to the concomitant decrease in viscosity and surface tension. Viscosity and surface tension can have contradictory effects on bubble size through coalescence. The increase in gas hold-up is then linked to the effect on primary bubble size, maximum bubble size, and contact time for coalescence.

Increasing pressure also induced an increase in gas hold-up (Chilekar et al., 2010; Leonard et al., 2021, 2015). Indeed, for the air-water system, Schäfer et al. (2002) observed a notable decrease in bubble size while augmenting pressure with different types of gas distributor and at pressure up to 5 MPa and ambient temperature in the homogeneous regime. This positive impact can be related to the gas sparger. Maalej et al. (2003) found that the pressure effect is less important for porous plates than for perforated spargers. This can be explained by the fact that this influence was mainly due to the bubbles size that is generated through the various spargers (smaller for porous plates). Table 1.3 highlights the research works that investigated the effects of operating and design parameters on gas hold-up in BC reactors.

Many phenomenological correlations have been proposed in the last decades to predict gas hold-up in two-phase bubble columns. Among them, one of the most famous, which accounts for various parameters, was developed by Akita and Yoshida (1973). These authors studied the influence of liquid properties on the gas hold-up and proposed a correlation obtained on the

basis of dimensional analysis to predict gas hold-up in bubble columns for various fluid properties, superficial gas velocity, and column diameter. This correlation can be used for design calculations as it incorporates the effects of liquid properties. Its disadvantage is that it involves a trial-and-error calculation for the gas hold-up. Table 1.4 summarizes some of the frequently used correlations and their range of applicability.

*1.2.1.1.2 Flow regime*

Depending on the gas and liquid flow rates and the physical properties of the gas−liquid system, the flow regimes in bubble column reactors can be classified into the following types:

- Homogeneous flow regime: It occurs at low superficial gas velocities (*i.e.*, less than 5 $cm.s^{-1}$) and is characterized by a narrow bubble size distribution (BSD), lack of bubbles interaction, a uniform radial gas hold-up profile, and low liquid phase turbulence (Camarasa et al., 1999; Gourich et al., 2006b; Mudde, 2005; Sarrafi et al., 1999; Vial et al., 2001; Zahradník et al., 1997). From the observed bubble size distribution, the bubbly flow can be divided into mono-dispersed and poly-dispersed flow regimes depending on the design of the gas sparger used. In fact, fine spargers generate mono-dispersed BSD, whilst poly-dispersed BSD results from using coarse gas distributors (Besagni et al., 2019; Besagni and Inzoli, 2017; Mudde et al., 2009).
- Heterogeneous flow regime: At higher superficial gas velocities (*i.e.*, greater than 7 $cm.s^{-1}$), sufficient bubble coalescence occurs, and large bubbles appear in the gas−liquid system along with smaller bubbles. This regime is distinguished by the formation of broader BSD and non-uniform radial distribution of gas hold-up that causes high circulation of bulk liquid (Manjrekar and Dudukovic, 2019; Montoya et al., 2016; Zahradník et al., 1997). Furthermore, in the case of using very large spargers, a pure heterogeneous flow regime occurs right from the beginning (Ruzicka et al., 2001). As for the transitional regime, it is characterized either by clusters of bubbles (Takagi and Matsumoto, 2011) or coalescence-induced bubbles (Besagni and Inzoli, 2017, 2016) and this distinction is attributable to the physical properties of the liquid phase. Additionally, Besagni et al. (2017b) revealed that coalescence-induced bubbles, which destabilize the homogeneous flow regime, resulted from the lift force that drives the largest bubbles towards the center of the bubble column. Sarrafi et al. (1999) reported that the transition from homogeneous to heterogeneous flow generally occurred at a superficial gas velocity comprised between 0.02 and 0.06 $m.s^{-1}$.

- Slug flow regime: This regime occurs at large superficial gas velocities and in small diameter bubble columns (Deckwer et al., 1980b). Here, the diameter of bubbles formed by coalescence becomes comparable to the bubble column diameter. These bubbles are then stabilized by the bubble column wall and move as slugs in BC. This regime is, however, restricted to BC with small diameters and will not be considered in the next sections.

A schematic diagram of homogeneous and heterogeneous flow regimes is shown in Figure 1.6 with a transition region in which instability grows. If a small size of solid particles (such as catalyst) is used (i.e., less than 50 μm) and if the solid loading is less than 15%, the slurry may be treated as a pseudo-homogeneous phase and the hydrodynamics are similar to those of two-phase (gas−liquid) system.

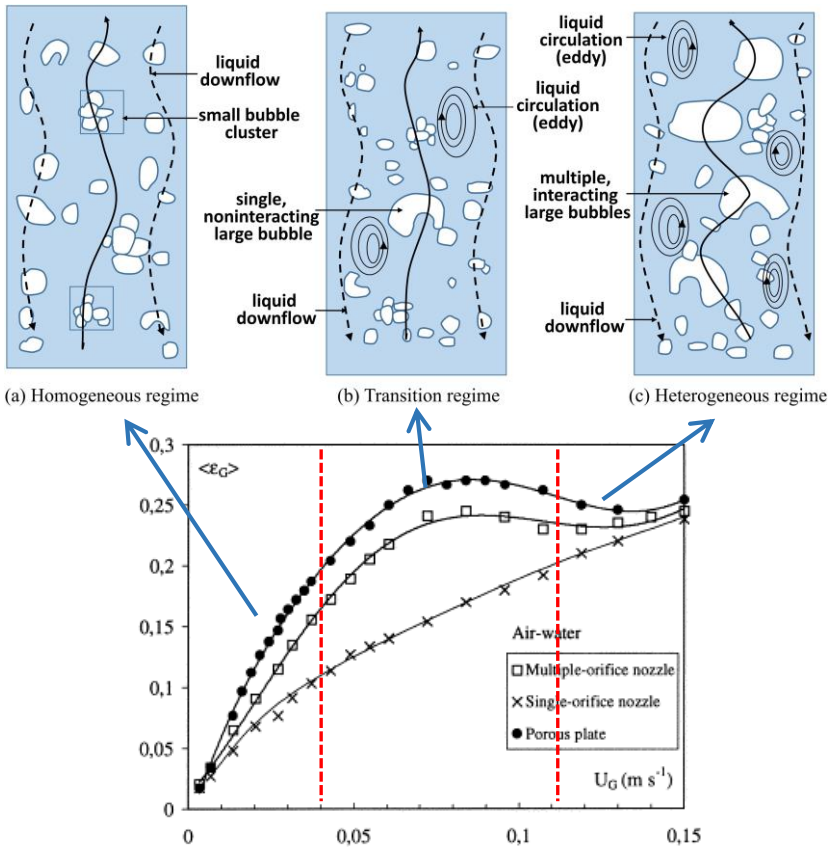


Figure 1.6 Observed flow regimes in a BC reactor (Fard, 2020).

As quoted above, the characteristic structure of each flow regime is quite different, thus requiring careful understanding to improve the industrial processes concerned (methanol synthesis, production of cell proteins, and Fischer-Tropsch synthesis…). For instance, the turbulence intensity is much greater in the heterogeneous regime, which leads to a significant

increase in the eddy diffusivities values for momentum, mass and heat transfer (Thorat and Joshi, 2004). Therefore, a large number of further research studies have been devoted to the accurate description of these flow regimes, notably the transition velocity, gas hold-up estimation, and bubbles characteristics. Bearing in mind that, column geometry, sparger design, operating pressure, gas and liquid phase properties (coalescing and non-coalescing liquids, foaming phenomena…) exhibit a complex interplay which is making the mission more delicate (Besagni and Inzoli, 2017; Camarasa et al., 1999; Chaumat et al., 2007; Gemello et al., 2018; Gourich et al., 2006b; Krishna et al., 2000, 1991; Schumpe and Deckwer, 1987; Vial et al., 2000).

*1.2.1.1.3 Regime transition determination*

As mentioned above, the flow regime transition from bubbly to churn-turbulent flow or from churn-turbulent to slug flow relies simultaneously on parameters such as superficial gas velocity, column diameter, liquid and gas phase properties, and distributor design. Figure 1.7 illustrates the flow regime maps of transition velocity as a function of column diameter that distinguishes between bubbly, transition, churn-turbulent, and slug flow (Shah et al., 1982; Shaikh and Al-Dahhan, 2007). Indeed, in some cases, it is hard to detect the slope (which represents the transition regime) of the gas hold-up versus $U_g$ curve. Therefore, there exists another method proposed by Wallis (1969) named the drift flux method. It is actually based on plotting the drift flux velocity $j_0 = U_g(1-\varepsilon_g)$ as a function of the gas hold-up $\varepsilon_g$. A change in the slope of this curve implies the appearance of the heterogeneous regime. Typically, the change in the drift flux is more pronounced compared to one in the gas hold-up versus the superficial gas velocity.

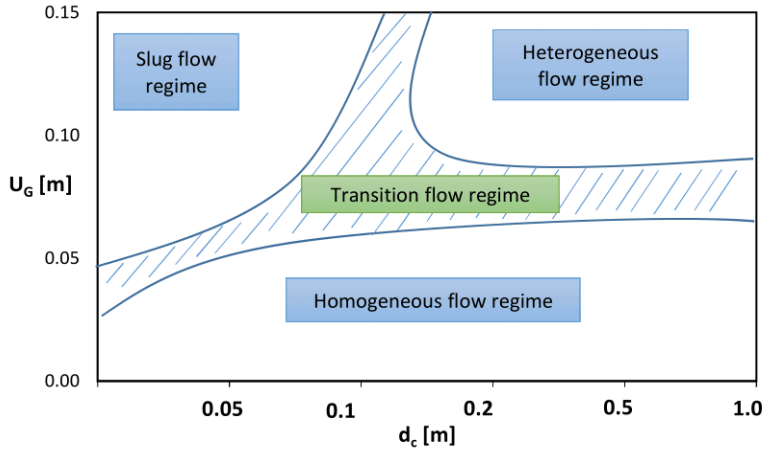


Figure 1.7 The flow regime map by (Shah et al., 1982).

### *1.2.1.2 Airlift reactors*

#### *1.2.1.2.1 Gas hold-up*

The overall gas hold-up is also the most important hydrodynamic parameter which affects the extent and degree of mixing as well as the overall mass transfer coefficient of the ARL reactor. Indeed, $\varepsilon_g$ is influenced by several parameters such as design parameters ($A_d/A_r$, $H_0/d_c$), gas sparger types, the physico-chemical properties of gas and liquid phases, and the operating conditions such as the superficial gas velocity. In this context, the gas hold-up g depends on the superficial gas velocity in the riser, as well as the increasing rhythm of $\varepsilon_g$ with $U_{gr}$ remains a function of the flow regime: the $\varepsilon_g$ increases with $U_{gr}$ faster in the homogeneous regime than in the transition and heterogeneous regime (Choi and Lee, 1993). Unlike bubble columns, the liquid circulation velocity in airlift reactors is found to have a large influence on gas hold-up (Choi and Lee, 1993; Siegel and Robinson, 1992). Actually, for a high liquid circulation velocity, the residence time of the bubble's decreases, thus leading to a decline in the gas hold-up.

The gas distributor type, design, and position have a significant effect on the bubble flow and distribution, which impacts gas hold-up and, consequently, the mass transfer characteristics in ARL reactors. Naidoo et al. (2021) examined the influence of three static gas spargers with different design (perforated plate ($d_0$ = 0.45 cm, $N_0$ = 21 holes), perforated disk ($d_0$ = 0.45 cm, $N_0$ = 20 holes), and perforated pipe ($d_0$ = 0.45 cm, $N_0$ = 21 holes)) on the gas hold-up for a water-air system in an external loop ARL reactor. Indeed, it was found that the perforated plate sparger was the best design and gave the largest overall gas hold-up values than the perforated disk and the perforated pipe. Similarly, Luo et al. (2011) used three different gas spargers with different diameters and hole numbers (2-orifice nozzle, O-ring distributor, and 4-orifice nozzle) to investigate the effect of gas distributor structure on the hydrodynamics of an internal loop ARL reactor. Therefore, they identified two flow regimes, *i.e.*, homogenous flow and heterogeneous flow as a function of the studied $U_g$ interval. In addition, the highest gas hold-up and downcomer liquid velocity were provided by the 4-orifice nozzle, followed by the O-ring distributor and the 2-orifice nozzle.

As for the effect of reactor geometry, Kilonzo et al. (2007) investigated the effect of the bottom and top clearances on $k_La_L$ measurements in a rectangular ARL reactor using water and carboxymethylcellulose (CMC) solutions with a range of viscosity varying from 0.02 to 0.5 Pa.s and surface tension from 65 to 85 $mN.m^{-1}$. Indeed, it was found that the downcomer gas

hold-up increased by two-fold when the bottom clearance was augmented from 0.014 to 0.094 m, whilst the bottom clearance showed no effect on gas hold-up. Drandev et al. (2016) studied the influence of the ratio between the downcomer and the riser areas on the hydrodynamics in a rectangular ARL bioreactor. Indeed, seven geometric configurations ($A_d/A_r$ = 0.2–5.0) were examined to determine an optimum value of $A_d/A_r$. In fact, they considered $A_d/A_r$ = 2 as an optimum ratio because it gave a higher $k_La_L$ coefficient. However, the majority of research studies (Choi et al., 1996; Couvert et al., 2004; El Azher et al., 2005; Gourich et al., 2006a; C. P. Huang, 1978) have used an $A_d/A_r$ ratio equal to 1.

On the other hand, authors such as (Chisti, 1989; Contreras et al., 1999; Kojić et al., 2015; Lin et al., 2004) are in consensus that the reactor geometry and the liquid phase properties are more influential in gas retention and mass transfer than the sparger design. In this respect, the impact of alcohol addition and three different gas diffusers (single orifice, perforated plate, and sintered plate) on gas hold-up in an external-loop airlift reactor were evaluated by Kojić et al. (2015). Based on their experimental results, it was concluded that the gas hold-up can be increased through a mutual influence of the alcohol addition and the sparger type (Figure 1.8). With the occurrence of small amounts of normal aliphatic alcohols, an increase in gas hold-up was observed compared to the air-water system, due to their coalescence-inhibiting nature. The air-water system exhibited the lowest $\varepsilon_g$ for all sparger types. Meanwhile, the effect of alcohol addition on $\varepsilon_g$ was more noticeable for both sintered and perforated plates than for a single orifice. Actually, the principal contributor to this phenomenon is the initial size of the bubbles at their onset. The sintered plate generated the smallest bubbles, so the inhibition of coalescence owing to the addition of alcohol was highlighted. Besides, the sintered plate was more effective than the perforated plate at $U_g \leq 10$ cm.s$^{-1}$. However, at higher $U_g$, the differences in $\varepsilon_g$ for these two gas spargers were under 3%. Likewise, Nandi and Jaju (2015) studied the effect of liquid surface tension ($\sigma_L$ = 72.6 – 22.8 mN.m$^{-1}$) by using organic alcohols (namely methanol, ethanol, n-propanol, and n-butanol) on the hydrodynamics of a pilot plant scale internal-loop ARL reactor. As a result, they reported that the addition of alcohols resulted in augmentation of the overall gas hold-up, which can be ascribed to the formation of a protective monolayer on the bubbles, thereby inhibiting the bubble coalescence phenomenon. Moreover, the probability of the formation of a protective layer became higher as the carbon chain length increased. These results are in agreement with those obtained by (Albijanić et al., 2007; El Azher et al., 2005; Moraveji et al., 2011). Furthermore, Moraveji et al. (2011) investigated the influence of various concentrations (0 – 5 ppm) of anionic (sodium dodecyl sulfate, SDS) and non-ionic (Tween-80

and Triton X-405) surfactants on gas hold-up and gas−liquid mass transfer in a split-cylinder ARL reactor. Therefore, it was found that surfactants strongly enhanced gas hold-up. Moreover, non-ionic surfactants were more effective in improving gas hold-up than anionic surfactants.

Regarding the effect of viscosity, Mendes and Badino (2016) investigated the influence of the superficial gas velocity in the riser, physical and rheological properties of twelve liquids, reactor geometry (draft tube and split cylinder airlift reactors), and scale (5 and 10 L) on gas hold-up. Consequently, they found that the gas hold-up values in the riser and downcomer were higher for the draft tube ARL reactors and the 10 L scale. However, it was observed that $\varepsilon_g$ values in the riser and downcomer were inversely proportional to the liquid viscosity. Deng et al. (2010) also indicated that the gas hold-up decreased with an increase in CMC concentration in a 5 m high internal-loop ARL reactor, which is due to the occurrence of larger bubbles in the viscous liquid. Large bubbles had a short residence time, thus leading to a decrease in the gas hold-up. Table 1.3 summarizes the research studies that examined the effects of operating and design parameters on gas hold-up in ARL reactors.

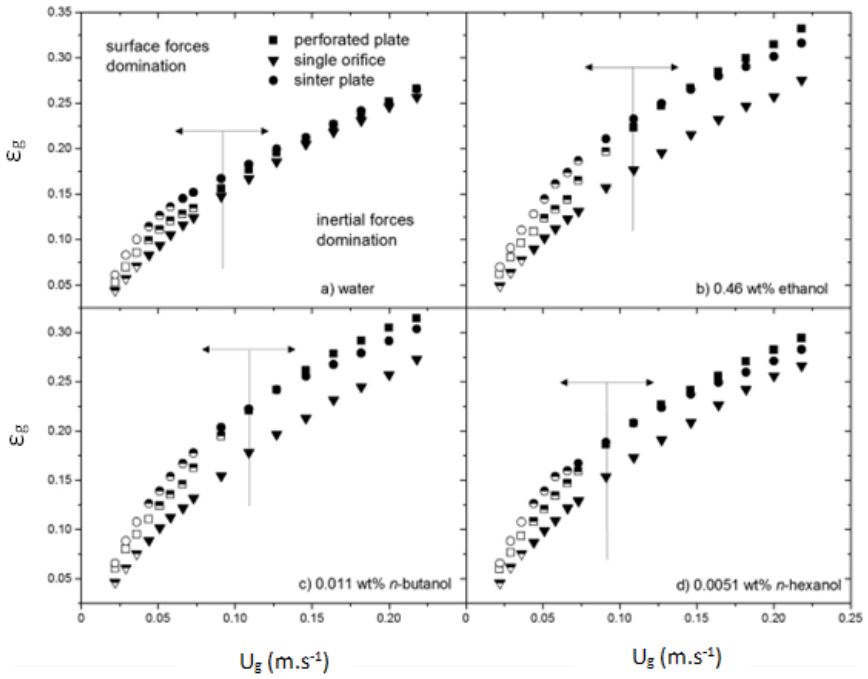


Figure 1.8 The mutual influence of the alcohol addition and the sparger type on gas hold-up in the ARL reactor (Kojić et al., 2015).

*1.2.1.2.2 Flow regime*

The flow regimes in ARL reactors vary considerably with gas flow rates; so, the transition of flow regimes obviously influences the hydrodynamics and mass transfer characteristics in

the reactor (Luo et al., 2012). Hence, this renders studies on flow regimes and their transition regularities of great importance for optimizing the design and operation of ARL reactors. The flow regimes in ARL reactors can be determined based on the distribution of bubbles in the risers or downcomers. With respect to gas distribution in the risers, the flow regimes in ARL reactors are shown to be similar to those in BC reactors, *i.e.*, homogeneous flow (bubbly), and heterogeneous flow (churn-turbulent) (Figure 1.9). Nevertheless, it is noteworthy that the operating range of the $U_g$ for each regime in ARLs can differ from that in BC reactors. Jin and Lant (2004) conducted a comparative study on both BC and inner-loop ARL reactors with similar geometry and concluded that the flow regimes in inner-loop ARLs are controlled by the induced liquid velocities and the solid loading. Homogeneous flow in the risers appears at a lower $U_g$ compared to BC reactors because of the smaller riser diameter. For the heterogeneous flow in the risers, it was observed in a larger $U_g$ range than in the BC reactors, thereby preventing the unfavorable slug flow regime in a wider range of gas superficial velocity (Zhang et al., 2019). Moreover, the transition between regimes is not quite as pronounced in ARL as in BC reactors.

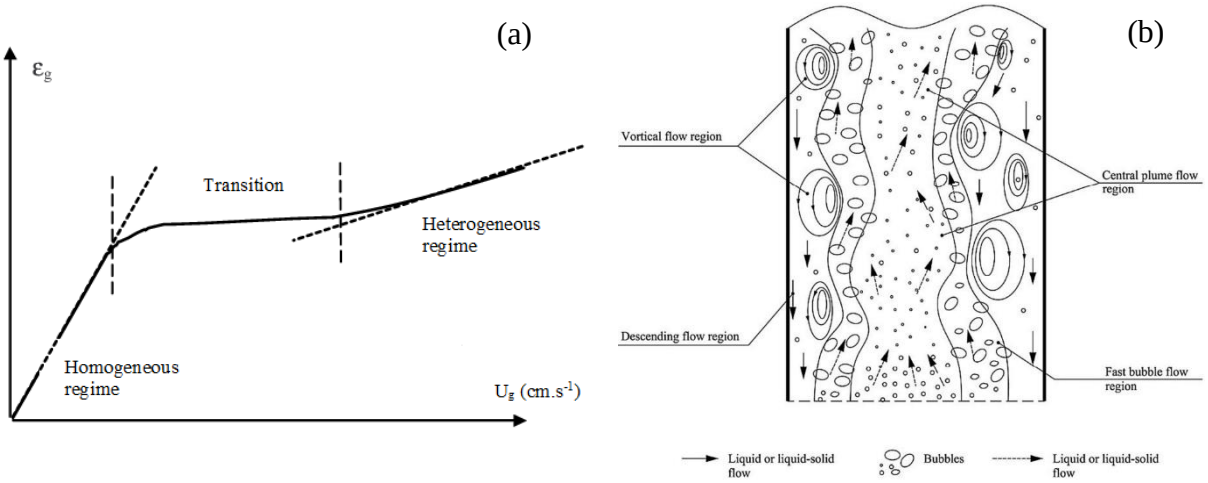


Figure 1.9 (a) Typical evolution of $\varepsilon_g$ as a function of $U_g$, and (b) Macroscopic flow structure in the gas−liquid ALR riser (Zhang et al., 2019).

Table 1.3 The effects of operating and design parameters on gas hold-up in BC and ARL reactors.

| Type of pneumatic reactor | Sparger and column design | Operating conditions | System | Influencing parameter | Impact | References |
|---|---|---|---|---|---|---|
| Cylindrical BC | $H_c$ = 600 cm, $d_c$ = 28 cm<br>Ring tube with 30 holes ($d_0$ = 0.3 cm)<br>Nozzle possessed a tangential fluid inlet and a circular orifice jet | $U_g$ = 1 – 13 cm.s$^{-1}$<br>$\rho_L$ = 998 kg.m$^{-3}$<br>$\sigma$ = 72 mN.m$^{-1}$<br>$\mu_L$ = 0.0009 Pa.s<br>T = 28 °C | Deionized water – air | Sparger: Jet mode > Bubbling mode | ↗ | Gong et al. (2022) |
| Cylindrical BC | $d_c$= 5 cm<br>$H_c$= 160 cm<br>Single nozzle ($d_0$= 0.68 cm) | $U_g$ = 0 – 40 cm.s$^{-1}$<br>$\rho_L$ = 915 – 970 kg.m$^{-3}$<br>$\sigma$ = 19.7 – 21.4 mN.m$^{-1}$<br>$\mu_L$ = 0.000018 – 5 Pa.s<br>P = 1 bar<br>T = 20 °C | Silicone oil – air | Viscosity ($\mu_L$ = 0.000018 – 5 Pa.s) | ↘ | Abdulkadir et al. (2021) |
| External loop ARL | Downcomer: $H_c$ = 310 cm, $d_c$ = 15 cm<br>Riser: $H_c$ = 295 cm, $d_c$ = 15 cm<br>$A_d/A_r$ = 1<br>Spargers: Perforated plate with 21 holes ($d_0$= 0.45 cm), perforated disk with 20 holes ($d_0$= 0.45 cm), perforated pipe with 21 holes ($d_0$= 0.45 cm) | $U_g$ = 1.5 – 7.5 cm.s$^{-1}$<br>$\rho_L$ = 997 kg.m$^{-3}$<br>$\sigma$ = 72 mN.m$^{-1}$<br>$\mu_L$ = 0.0011 Pa.s<br>Room temperature | Water – air | Sparger: Perforated plate > Perforated disk > Perforated pipe | ↗ | Naidoo et al. (2021) |
| Cylindrical slurry BC | $H_c$ = 270 cm, $d_c$ = 29.2 cm, $H_0$ = 110 cm<br>Perforated plate with 94 holes ($d_0$ = 0.1 cm) | $U_g$ = 0.5 – 20 cm.s$^{-1}$<br>$d_{particles}$ =35, 71, 156 µm | Water + (1-5vol %) glass beads – air | Solid concentration = 1, 3, 5 vol% | ↗ In homogeneuous<br>↘ In heterogeneous | Mokhtari and Chaouki (2021) |

Table 1.3 Continued.

| | | | | | | |
|---|---|---|---|---|---|---|
| Cylindrical BC | $H_c$ = 83 cm, $d_c$ = 4 cm, $H_0/d_c$ > 5<br>Sinter with an average pore diameter of 80 µm | $U_g$ = 0 – 0.8 cm.s$^{-1}$<br>T = 100 – 300 °C<br>P = 100 – 300 bar | Water – nitrogen | T = 100-300 °C | ↙ | Leonard et al. (2019) |
| Cylindrical BC | $H_c$ = 83 cm, $d_c$ = 4 cm, $H_0/d_c$ > 5<br>Sinter with an average pore diameter of 80 µm | $U_g$ = 0 – 0.8 cm.s$^{-1}$<br>T = 100 – 300 °C<br>P = 100 – 300 bar | Water – nitrogen | P = 100-300 bar | ↗ | Leonard et al. (2019) |
| Cylindrical BC | $d_c$= 40 cm<br>$H_0$= 160 cm<br>$H_c$= 325 cm<br>Perforated plate with 92 holes ($d_0$= 0.2 cm)<br>Perforated plate with 7 holes ($d_0$= 0.9 cm) | $U_g$ = 3 – 35 cm.s$^{-1}$<br>Atmospheric pressure | Demineralized water – air<br>Tap water – air<br>Water + 0.01 % ethanol – air<br>Water + 0.05 % ethanol – air | Liquid properties (decreasing surface tension) | ↗ | Gemello et al. (2018) |
| Cylindrical BC | $d_c$= 40 cm<br>$H_0$= 160 cm<br>$H_c$= 325 cm<br>Perforated plate with 92 holes ($d_0$= 0.2 cm)<br>Perforated plate with 7 holes ($d_0$= 0.9 cm) | $U_g$ = 3 – 35 cm.s$^{-1}$<br>Atmospheric pressure | Demineralized water – air<br>Tap water – air<br>Water + 0.01 % ethanol – air<br>Water + 0.05 % ethanol – air | Sparger: Perforated plate with 7 holes ($d_0$= 0.9 cm) > Perforated plate with 92 holes ($d_0$= 0.2 cm) | ↙ | Gemello et al. (2018) |
| Cylindrical BC | $d_c$= 24 cm<br>$H_c$= 530 cm<br>$H_0$= 24 – 360 cm<br>$H_0/d_c$= 1 – 15<br>Stainless steel spider ($d_0$= 0.2 – 0.4 cm) | $U_g$ = 0 – 20 cm.s$^{-1}$ | Water – air | $H_0/d_c$=1 – 15 | ↙ | Besagni et al. (2017a) |
| Cylindrical BC | $d_c$= 24 cm, $H_c$= 530 cm<br>$H_0$ = 30 cm<br>$H_0/d_c$ = 12.5<br>Stainless steel spider ($d_0$= 0.2 – 0.4 cm) | $U_g$ = 0 – 20 cm.s$^{-1}$<br>$\rho_L$ = 997 – 1094 kg.m$^{-3}$<br>$\sigma$ = 71.5 – 50.2 mN.m$^{-1}$<br>$\mu_L$ = 0.0009 – 0.00797 Pa.s<br>T= 21.8 °C | Water + (0 – 80 %) monoethylene glycol – air | Viscosity ($\mu_L$ = 0.0009 – 0.00797 Pa.s) | ↙ | Besagni et al. (2017b) |

Table 1.3 Continued.

| | | | | | | |
|---|---|---|---|---|---|---|
| Cylindrical BC | $d_c$= 24 cm<br>$H_0$= 30 cm<br>$H_c$= 530 cm<br>$H_0/d_c$= 12.5<br>Spider ($d_0$= 0.2 – 0.4 cm) | $U_g$ = 0 – 20 cm.s$^{-1}$<br>T= 21.8 °C | Water – air<br>Water + 0.05% ethanol – air | Liquid properties (decreasing surface tension) |  | Besagni et al. (2016) |
| Square BC | $d_c$= 20 cm<br>$H_c$= 200 cm<br>$H_0$= 30 – 100 m<br>$H_0/d_c$= 1.5 – 5<br>Perforated plate ($d_0$= 0.14 cm) | $U_g$ = 25 – 40 cm.s$^{-1}$ | Water – air | $H_0/d_c$= 1.5 – 5 |  | Sasaki et al. (2016) |
| Cylindrical BC | $d_c$= 24 cm, $H_c$= 530 cm<br>Stainless steel spider ($d_0$= 0.35 cm)<br>AG configuration: 2 PVC pipes, one centrally (d = 6 cm) and one asymmetrically (d = 7.5 cm).<br>OT configuration. | $U_g$ (AG) = 23 cm.s$^{-1}$<br>$U_g$ (OT) = 20 cm.s$^{-1}$<br>T=22°C | Water – air | Presence of internals |  | Besagni and Inzoli (2016) |
| Cylindrical BC | $d_c$= 29.2 cm, $H_c$= 270 cm, $H_0$= 110 cm<br>Perforated plate with 94 holes ($d_0$= 0.1cm) | $U_g$ = 0 – 22 cm.s$^{-1}$<br>$\rho_L$ = 997 – 995.31 kg.m$^{-3}$<br>$\sigma$ = 71.97 – 76.07 mN.m$^{-1}$ | Water – air<br>Water + 70% Glucose – air<br>Water + 60% Glucose + 0.04wt% PAA – air<br>Water + 0.5 wt% CMC – air<br>Water + 0.5 % Xanthan – air | Viscosity (increasing) |  | Esmaeili et al. (2015) |
| Internal loop ARL | Two concentric tubes<br>Downcomer: $H_c$ = 130 cm, $d_c$ = 28.4 cm<br>Riser: $H_c$ = 82 cm, $d_c$ = 7 cm<br>$H_0$ = 103.2 cm<br>Spargers: 2-orifice nozzle ($d_0$ = 0.26 cm), 4-orifice nozzle ($d_0$ = 0.184 cm), and O-ring distributor with 63 pores of ($d_0$ = 0.1 cm) | $U_g$ = 0.07 – 0.28 cm.s$^{-1}$<br>Room temperature and atmospheric pressure | Water – air | Sparger: 4-orifice nozzle > O-ring distributor > 2-orifice nozzle |  | Luo et al. (2011) |

Table 1.3 Continued.

| | | | | | | |
|---|---|---|---|---|---|---|
| Split rectangular ARL | $H_c$ = 200 cm, a = 20 cm, $H_0$ = 159 cm<br>Baffle: H = 130 cm<br>Single-orifice nozzle ($d_0$ = 0.35 cm) | $U_g$ = 1 – 8.5 cm.s$^{-1}$<br>$\sigma$ = 68.1 – 71.1 mN.m$^{-1}$ | Tap water – air<br>Tap water + 0.05 vol% 1-Propanol – air<br>Tap water + 0.1 vol% 1-Propanol – air<br>Tap water + 0.05 vol% 1-Butanol – air<br>Tap water + 0.05 vol% Methanol – air | Liquid properties (by decreasing surface tension) | ↗ | El Azher et al. (2005) |
| Internal loop ARL | Downcomer 1: $d_c$ = 10.8 cm<br>Downcomer 2: $d_c$ = 15.7 cm<br>Downcomer 3: $d_c$ = 29.4 cm<br>Riser 1: $H_c$ = 114.5 cm, $d_c$ = 7 cm<br>Riser 2: $H_c$ = 171 cm, $d_c$ = 10.6 cm<br>Riser 3: $H_c$ = 270 cm, $d_c$ = 20 cm<br>Perforated plate made of Teflon with 25 holes ($d_0$ = 0.05 cm)<br>Perforated plate made of stainless steel with 90 holes ($d_0$ = 0.1 cm) | $U_g$ = 0.07 – 0.28 cm.s$^{-1}$<br>T = 18 – 21 °C<br>Atmospheric pressure | Water – air | $H_0/d_c$ = 10 – 12 | ↙ | Blažej et al. (2004) |
| Internal loop ARL | Two concentric tubes<br>Downcomer: $H_c$ = 125 cm, $d_c$ = 11 cm<br>Riser: $d_c$ = 3.84 – 8.49 cm<br>Sintered steel tube ($d_0$ = 0.009 cm) | $U_g$ = 0 – 14 cm.s$^{-1}$ | Water – air | $A_d/A_r$ = 0.59 – 7.14 | ↗ | Korpijarvi et al. (1999) |

↗ Increased ↙ Decreased

Table 1.4 Summary of the major correlations for the gas hold-up in BC and ARL reactors.

| Type of reactor | Correlations | Medium | Operating conditions | Sparger and column design | References |
|---|---|---|---|---|---|
| External-loop ARL | $\varepsilon_{g,r} = 2.35U_g^{0.66}\sigma^{-0.47}\phi^{-0.045}(\frac{A_d}{A_r})^{-0.61}$<br>Where $\phi$ orifice size. | Tap water – air<br>Tap water + 0.1 wt.% ethanol – air<br>Tap water + 0.046 wt.% ethanol – air<br>Tap water + 1 wt.% ethanol– air<br>Tap water + 5 wt.% ethanol– air<br>Tap water + 0.011 wt.% n-butanol– air<br>Tap water + 0.0051 wt.% n-hexanol – air | $U_g$= 2 – 21.8 cm.s$^{-1}$<br>$\sigma$ = 56.41 – 72.4 mN.m$^{-1}$ | Reactor:<br>-Riser: $d_c$ = 5.4 cm $H_c$ = 200 cm<br>-Downcomer: $d_c$ = 2.5 cm $H_c$ = 195 cm<br>Gas distributors:<br>-Single orifice $d_0$ = 0.4 cm<br>-Perforated plate $d_0$ = 0.1 cm (7 holes, triangular pitch)<br>Sinter plate $d_0$ = 0.01 – 0.016 cm (porosity 8%). | Kojić et al. (2015) |
| External-loop ARL | $\varepsilon_{g,r} = 0.49U_g^{0.67}L_C^{-0.15}H_C^{-0.22}$<br>$\varepsilon_{g,d} = 0.29U_g L_C^{-0.45} H_C^{0.39}$ | Water – air | $U_g$= 0.5 – 10 cm s$^{-1}$ | Two vertical tubes:<br>-Riser: $d_c$ =10.4, $H_c$ = 100 – 140 cm<br>-Downcomer: $d_c$ =5.4 cm, $H_c$ = 100–140 cm<br>$L_C$ =20 – 40 cm | Rujiruttanakul and Pavasant (2011) |
| Internal loop ARL | Homogeneous flow:<br>$\varepsilon_g = 2.821U_g^{0.9548}$(2-orifice nozzle)<br>$\varepsilon_g = 0.7071U_g^{0.7264}$(4-orifice nozzle)<br>$\varepsilon_g = 3.574U_g^{0.9806}$(O-ring distributor)<br>Heterogeneous flow:<br>$\varepsilon_g = 0.3218U_g^{0.6118}$(2-orifice nozzle)<br>$\varepsilon_g = 0.9837U_g^{0.7761}$(4-orifice nozzle)<br>$\varepsilon_g = 0.3388U_g^{0.6078}$(O-ring distributor) | Tap water – air | $U_g$= 0.07 – 0.28 cm.s$^{-1}$<br>Room Temperature.<br>Atmospheric pressure. | $d_c$ = 28.4 cm<br>$H_c$ = 130 cm<br>$H_L$ = 103.2 cm<br>2-orifice nozzle, $d_0$ = 0.26 cm<br>4-orifice nozzle, $d_0$ = 0.184 cm<br>O-ring distributor, $d_0$ =0.1–0.6 cm | Luo et al. (2011) |

Table 1.4 Continued.

| | | | | | |
|---|---|---|---|---|---|
| Internal loop ARL | $\varepsilon_g = 0.499U_g$ | Water – air | $U_g$= 0 – 24 cm.s$^{-1}$ | $d_c$ = 6 cm<br>$H_c$ = 102 cm<br>O-ring distributor<br>$d_0$ = 0.08 cm<br>$A_d/A_r$ = 0.54<br>$H_L$ = 100 – 130 cm | Kilonzo et al. (2010) |
| External-loop ARL | $\varepsilon_{g,r} = 13.19U_g^{1.43}\ (1+\frac{A_d}{A_r})^{-0.62}(1+S)^{-0.58}(\frac{\mu_g}{\mu_{N_2}})^{-0.52}$ | Water – methane<br>Water – Oxygen<br>Water – 25 vol% methane +75 vol% oxygen<br>Water – 50 vol% methane+50 vol% oxygen<br>Water – 75 vol% methane+25 vol% oxygen | $U_g$= 1 – 6.5 cm s$^{-1}$<br>T= 30 °C | -Riser: $d_c$ = 3 – 9 cm, $H_c$ = 220 cm<br>-Downcomer: $d_c$ =3 cm, $H_c$ = 220 cm<br>$H_L$ = 10 cm<br>$A_d/A_r$ = 0.11 – 1<br>Sparger: $d_0$ = 0.01 cm (6 holes) | Yazdian et al. (2009) |
| Internal loop ARL | Bubble flow: $\varepsilon_g = 1.488U_g^{0.815}$<br>Churn flow: $\varepsilon_g = 0.371U_g^{0.449}$ | water – air | $U_g$= 0 – 3 cm.s$^{-1}$<br>T=18 – 21 °C<br>Atmospheric pressure. | Three reactors:<br>- Perforated plate (25 holes), $d_0$ = 0.05 cm<br>$V_w$= 10.5L, $d_c$ = 10.8 m, $H_L$ = 126 cm, $H_c$ =114.5 cm, $A_d/A_r$ = 0.81<br>- Perforated plate (25 holes), $d_0$ = 0.05 cm<br>$V_w$= 32L, $d_c$ = 15.7 cm, $H_L$ = 181.5 cm, $H_c$ = 171cm, $A_d/A_r$= 1.05<br>- Perforated plate (90 holes), $d_0$ = 0.1 cm<br>$V_w$= 200L, $d_c$ = 29.4 cm, $H_L$ =293.6 cm, $H_c$ = 270 cm, $A_d/A_r$ = 0.99 | Blažej et al. (2004) |

Table 1.4 Continued.

| | | | | | |
|---|---|---|---|---|---|
| Internal loop ARL | $\varepsilon_g \propto U_g^{0.647}$ | Tap water – air | $U_g$= 2 – 10 cm $s^{-1}$<br>T=25°C | Single nozzle<br>Round ARL loop: $d_c$ = 18.8 cm<br>$H_c$ = 200 cm, $A_d/A_r$ = 1.44<br>Modified square ARL: $d_c$ = 16.7 cm<br>$H_c$ = 200 cm<br>Square BC: $d_c$ = 16.7 cm<br>$H_c$ = 200 cm | Lu et al. (2000) |
| External loop ARL | $\varepsilon_g = 0.29\, U_g^{0.74}$ | Water – air | $0 \leq U_g \leq 2$ cm $s^{-1}$ | Perforated plate (193 holes)<br>$d_0$ = 0.01 cm<br>Riser: $d_c$ = 22.5 cm<br>$H_c$ = 675 cm<br>Downcomer: $d_c$ = 22.5 cm<br>$H_c$ = 675 cm<br>$V_w$ = 725 L | Abashar et al. (1998) |
| BC | $\frac{\varepsilon_g}{1+\varepsilon_g} = 0.0625\left(\frac{U_g}{\nu_L g}\right)^{1/4}$ | Water – air<br>Viscous Newtonian fluids – air<br>Non-Newtonian fluids – air | $2 \leq U_g \leq 20$ cm.$s^{-1}$<br>$0.0022 \leq \mu_L \leq$ 0.0192 Pa.s | $20 \leq d_c \leq 550$ cm | Kawase et al. (1992) |
| BC | $\varepsilon_g = 3.38\left(\frac{U_g^2}{g d_C}\right)^{1/3}$ | Water – air<br>Glycerine aq. sol. – air<br>Dextrose aq. sol – air<br>Fermentation medium (glucose + mineral salt)<br>Fermentation medium (molasses + mineral salt)<br>Fermentation medium (Alpha-floc + mineral salt)<br>Carboxy-methyl cellulose sol. – air<br>Carboxypolymethylene sol. – air<br>Polyacrylamide sol. – air | $\rho_L$ = 991–1009 kg.$m^{-3}$ | - 40 L bubble column<br>$d_c$ = 23 cm<br>$H_c$ = 122 cm<br>Perforated plate (20 holes with $d_0$ = 0.1 cm)<br>- 1000 L pilot plant fermenter<br>$d_c$ = 76 cm<br>$H_c$ = 321 cm<br>Ring sparger (100 holes with $d_0$ = 0.3 cm) | Kawase and Moo-Young (1987) |

Table 1.4 Continued.

| | | | | | |
|---|---|---|---|---|---|
| BC | $\frac{\varepsilon_g}{1-\varepsilon_g} = 0.115\left(\frac{U_g^3}{\nu_L g\left(\rho_L-\rho_g\right)/\rho_L}\right)^{0.23}$ | N-octanol – air<br>Tetrabromo-methane – air<br>1,3-butanediol – air<br>Glycol aq. sol. – air | $U_g$ = 1 – 20 cm.s$^{-1}$ | $d_c$ = 10 cm<br>$H_c$ = 120 cm | Schumpe and Deckwer (1987) |
| Internal loop ARL | Bubble flow:<br>$\varepsilon_g = 1.488U_g^{0.892\pm0.075}$<br>Coalesced bubble flow:<br>$\varepsilon_g = 0.371U_g^{0.430\pm0.015}$ | Water – air<br>Aqueous salt solution (0.15 kmol m$^{-3}$ NaCl) – air<br>Salt solution + 1, 2 or 3 dry wt./vol.% Solka-Floc (KS-1016) cellulose fibre– air | $U_g$= 1 – 40 cm s$^{-1}$<br>$\sigma$ = 80 – 83 mN.m$^{-1}$ | Riser : $d_c$ =17 cm<br>$H_c$ =105 cm<br>Riser :$d_c$ = 11.5 cm<br>$H_c$ = 105 cm<br>Perforated plate (20 holes), $d_0$ = 0.1 cm | Chisti and Moo-Young (1987) |
| BC | $\varepsilon_g = 296U_g^{0.44}\rho_L^{-0.98}\sigma^{-0.16}\rho_g^{0.19} + 0.009$ | Water – air<br>Varsol (hydrocarbon oil) – air<br>Trichloroethylene – air | $U_g$ = 1 – 40 cm.s$^{-1}$<br>$\rho_L$ = 788 – 1468 kg.m$^{-3}$<br>$\sigma$ = 28.3 – 72 mN.m$^{-1}$<br>$\mu_L$ = 0.609 × 10$^3$ – 1.236 × 10$^3$ Pa.s | $d_c$ = 30 cm<br>Perforated distributor plate (293 holes with $d_0$ = 0.15 cm) | Reilly et al. (1986) |
| BC | $\varepsilon_g = 0.239U_g^{0.634}d_C^{-0.50}$ | Carboxy-methyl cellulose sol. – air<br>Glycerine aq. sol. – air | $U_g$ = 4 – 28 cm.s$^{-1}$<br>$\rho_L$ = 996 – 1008 kg.m$^{-3}$<br>$\mu_L$ = 0.0013 – 0.246 Pa.s | $d_c$ = 30.5 cm<br>$H_c$ = 244 cm<br>Perforated plate (749 holes with $d_0$ = 0.166 cm) | Godbole et al. (1982) |
| BC | $\varepsilon_g = 0.728U^* - 0.485U^{*2} + 0.0975U^{*3}$<br>Where $U^* = U_g\left[\rho_L^2/\sigma\left(\rho_L-\rho_g\right)g\right]^{1/4}$ | Water–air<br>40 % aq. glycerol sol. – air<br>Kerosene – air<br>Reacting system: Air/$CO_2$ – aq. NaOH sol. (2 M) | $U_g$ = 0.22 – 6.89 cm.s$^{-1}$<br>$\rho_L$ = 787 – 1108 kg.m$^{-3}$<br>$\sigma$ = 31.19 – 74.5 mN.m$^{-1}$<br>$\mu_L$ = 0.00088 – 0.0115 Pa.s | $d_c$ = 5 – 10 cm<br>Perforated plate ($d_0$ = 0.087 – 0.309 cm) | Kumar et al. (1976) |

Table 1.4 Continued.

| | | | | | |
|---|---|---|---|---|---|
| BC | $\varepsilon_g = 0.505 U_g^{0.47} \left(\frac{72}{\sigma}\right)^{2/3} \left(\frac{1}{\mu_L}\right)^{0.05}$ | Water – air<br>8 wt.% aq. methanol sol. – air<br>15 wt.% aq. methanol sol. – air<br>53 wt.% aq. methanol sol. – air<br>35 wt.% aq. cane sugar sol. – air<br>50 wt.% aq. cane sugar sol. – air | $U_g$ = 4.30 – 33.80 cm.s$^{-1}$<br>$\rho_L$ = 911 – 1233 kg.m$^{-3}$<br>$\sigma$ = 38.2 – 75.5 mN.m$^{-1}$<br>$\mu_L$ = 0.001 – 0.0192 Pa.s | $d_c$ = 10 and 19 cm<br>$H_c$ = 150 and 240 cm<br>- Single nozzle gas sparger ($d_0$ = 1.3 cm)<br>- Three nozzles gas sparger ($d_0$ = 1.31, 2.06 and 3.62 cm) | Hikita and Kikukawa (1974) |
| BC | $\frac{\varepsilon_g}{(1-\varepsilon_g)^4} = C_1 \left(\frac{g d_c^2 \rho_L}{\sigma}\right)^{1/8} \left(\frac{g d_c^3}{\nu_L^2}\right)^{1/12} \left(\frac{U_g}{\sqrt{g d_c}}\right)$<br>where $C_1 = 0.20$ for non-electrolyte systems, $C_1 = 0.25$ for electrolyte systems. | Water – air<br>Water + 40% vol methanol – air<br>NaCl aq. sol. – air<br>Water + 70% vol glycol – air<br>Water – $O_2$<br>Water – $CO_2$<br>Water – He | $U_g$ = 1 – 24.75 cm.s$^{-1}$<br>$\rho_L$ = 790 – 1590 kg.m$^{-3}$<br>$\sigma$ = 22 – 74.2 mN.m$^{-1}$<br>$\mu_L$ = 0.00058 – 0.0211 Pa.s | $d_c$ = 15.2 cm<br>Single-hole gas sparger ($d_0$ = 0.5 cm) | Akita and Yoshida (1973) |
| BC | $\varepsilon_g = \frac{1}{2 + \left(\frac{0.35}{U_g}\right)\left[\left(\frac{\rho_L}{1}\right)\left(\frac{\sigma}{72}\right)\right]^{1/3}}$ | Water – air<br>Air-oil blend<br>Air-$ZnCl_2$ aq. sol.<br>Air – $Na_2SO_3$ aq. sol.<br>Air – glycerol<br>Air – kerosene | $U_g$ = 0.04 – 45 cm.s$^{-1}$<br>$\rho_L$ = 780 – 1700 kg.m$^{-3}$<br>$\sigma$ = 25 – 76 mN.m$^{-1}$<br>$\mu_L$ = 0.0009 – 0.0152 Pa.s | $d_c$ > 10 cm<br>Multi-orifice gas sparger | Hughmark (1967) |

### 1.2.2 Gas−liquid mass transfer

During chemical and biological processes, oxygen is transferred from an ascending gas bubble into a liquid phase and finally to the site of oxidative phosphorylation inside the cell, which can be viewed as a solid particle. The transport of oxygen from air bubbles to cells can be described by a number of steps and resistances (Chisti, 1989; Garcia-Ochoa et al., 2010):

- in a gas-film inside the bubble;
- at the gas−liquid interface;
- in a liquid film at the gas−liquid interface;
- in the bulk liquid;
- in a liquid film surrounding the cell;
- at the cell-liquid interface
- the internal cell resistance
- the resistance at the site of a biochemical reaction.

The most straightforward theory on gas−liquid mass transfer is the two-film model (Whitman, 1962), and the gas−liquid mass transfer rate is generally modeled according to this theory, which defines the flux through each film as the product of the driving force and the mass transfer coefficient, as follows:

$$J_0 = k_g(p_g - p_i) = k_L(C_i - C_L) \quad (1.1)$$

where $J_0$ is the molar flux of oxygen (mol.m$^{-2}$.s$^{-1}$) through the gas−liquid interface, $k_g$ and $k_L$ are the local mass transfer coefficients; $p_g$ is the oxygen partial pressure in the gas bubble, $C_L$ is the dissolved oxygen concentration in the bulk liquid, and index i refers to values at the gas−liquid interface.

As the interfacial concentrations are not directly measurable and considering the overall mass transfer coefficient, Eq (1.1) can be rewritten:

$$J_0 = K_g(p_g - p^*) = K_L(C^* - C_L) \quad (1.2)$$

where $p^*$ is the oxygen pressure in equilibrium with the liquid phase, $C^*$ is the oxygen saturation concentration in the bulk liquid in equilibrium with the bulk gas phase (according to Henry's law ($p^* = H \times C^*$)) and $K_g$ and $K_L$ are the overall mass transfer coefficients.

By combining Eqs. (1.1) and (1.2), the following equation is obtained:

$$\frac{1}{K_L} = \frac{1}{Hk_g} + \frac{1}{k_L} \tag{1.3}$$

Knowing that oxygen is only sparingly soluble in water (H is very large), it is usually assumed that the greatest resistance to mass transfer occurs on the liquid side of the interface and that the gas phase resistance can generally be ignored. Therefore, the overall mass transport coefficient is equal to the local coefficient: $K_L = k_L$.

The oxygen mass transfer rate per unit of reactor volume, $N_{O_2}$, is determined by multiplying the overall flux by the gas−liquid interfacial area per unit of liquid volume (a):

$$N_{O_2} = a \times J_0 = k_L a_L (C^* - C_L) \tag{1.4}$$

Since $k_L$ and a are hard to measure independently, the product $k_L a_L$; which is called the volumetric mass transfer coefficient; is usually measured and used to describe the transport of the gas to the liquid. The driving force is the gradient between the concentration of oxygen at the interface and that of the bulk liquid. Among the factors that control this gradient are solubility and metabolic activity. Actually, the gas solubility of the gas, $C^*$, in electrolyte solutions is generally lower than the gas in pure water ("salting-out effect"). Moreover, gas solubility is chiefly related to temperature, pressure, concentration and type of salts present, and chemical reactions.

The determination of $k_L a_L$ in chemical and biological reactors is vital for identifying the oxygenation capacity and quantifying the effects of operating variables on dissolved oxygen supply. The oxygenation capacity is an important criterion for comparing different aeration systems in terms of energy yield. It corresponds to the specific flow rate of oxygen transferred per kWh of energy dissipated and is expressed in kg $O_2$/kWh. Table 1.5 gives the oxygenation capacity of the bubble column and airlift reactors and their different designs for the water-air system. Indeed, it is difficult to compare the oxygenation capacity of the reactors since the operating conditions are not always similar. However, according to the data displayed in the table below, the ARL reactor can

provide an oxygenation capacity; at a low superficial gas velocity; almost equal to that of a cylindrical BC which is obtained at higher $U_g$.

Table 1.5 $k_La_L$ coefficient and oxygenation capacity of BC and ARL reactors.

| Type of reactor | $U_g$ range ($m.s^{-1}$) | $k_La_L$ ($h^{-1}$) | Oxygenation capacity (kg $O_2$ /kWh) | Reference |
|---|---|---|---|---|
| Square BC | 0.004 – 0.017 | 5.13 – 11.12 | 0.62 – 1.14 | Dong et al., (2019) |
| Cylindrical BC | 0.019 – 0.195 | 105.20 – 1151.17 | 4.68 – 4.98 | Zedníková et al. (2018) |
| Split-cylindrical ARL | 0.002 – 0.010 | 11.20 – 44.23 | 5.48 – 6.94 | Moraveji et al. (2011) |
| Split-square ARL | 0.009 – 0.083 | 11.70 – 222.60 | 2.53 – 4.95 | Gourich et al. (2006a) |
| External-loop cylindrical ARL | 0.002 – 0.009 | 3.35 – 22.84 | 1.45 – 2.70 | Nikakhtari and Hill (2005) |

(Garcia-Ochoa and Gomez, 2009) presented in their literature review, the different techniques available to measure the $k_La_L$ coefficient with or without biological consumption. Indeed, the techniques of measuring $k_La_L$ are divided into chemical (Cooper et al., 1944; Hegely et al., 2017) and physical methods (Mirón et al., 2000; Riet, 1979). Figure 1.10 provides a brief description of these techniques used to experimentally determine $k_La_L$ in the absence of biological consumption. However, Novák and Klekner (1988) outlined that several factors should be considered when choosing the technique for measuring $k_La_L$; namely: (1) the aeration and homogenization systems used, (2) the reactor type and its mechanical design, (3) the composition of the fermentation medium, and (4) the possible effect of the presence of the microorganisms.

The mass balance for the dissolved oxygen in the well-mixed liquid phase can be established as:

$$\frac{dC}{dt} = OTR - OUR \tag{1.5}$$

where dC/dt is the accumulation oxygen rate in the liquid phase, OTR corresponds to the oxygen transfer rate from the gas to the liquid described by equation (1.4), and OUR stands for the oxygen uptake rate by the microorganisms which can be defined as the product $q_{O_2} \times C_X$, (where $q_{O_2}$ is the specific oxygen uptake rate of the microorganism used and $C_X$ is the biomass concentration). Eq. (1.5) can be rewritten as:

$$\frac{dC}{dt} = k_L a_L (C^* - C_L) - q_{O_2} C_X \quad (1.6)$$

In the case when biochemical reactions do not take place, OUR = 0. Thus, Eq. (1.6) can be simplified as below:

$$\frac{dC}{dt} = k_L a_L (C^* - C_L) \quad (1.7)$$

#### *1.2.2.1 Volumetric mass transfer coefficient*

The liquid-side volumetric mass transfer coefficient $k_L a_L$ is an important parameter in the design of multiphase reactors. Indeed, considerable literature has been published on $k_L a_L$ in BC and ARL reactors. However, the investigations on the effects of physical properties for aqueous and inorganic systems (surface tension) on the $k_L a_L$ are limited. When considering the applications cited above, it is worth noting that bubble columns are mostly employed in slow reaction–absorption applications where the interphase mass transfer resistance on the gas side might be considered negligible compared with the gas−liquid side ($k_L$) (Deckwer and Schumpe, 1993).

##### *1.2.2.1.1 Volumetric mass transfer coefficient in BC reactors*

Similar to $\varepsilon_g$, $k_L a_L$ is strongly influenced by the operating and design parameters presented in Figure 1.2. Indeed, the gas distributor has a great influence on $k_L a_L$ (Shah et al., 1982). $k_L a_L$ increased with a decrease in opening diameter and increased (less than linearly) with an increase in the gas hold-up. The increase in the mass transfer with a decrease in the gas sparger openings is linked to the governing flow regime determined by the gas sparger (Besagni et al., 2018; Besagni and Inzoli, 2017). Deckwer et al. (1980a) discussed some aspects of the sparger design for bubble columns. It is indicated that sintered plates yield appreciably higher $k_L a_L$ values than perforated plates. However, the influence of sparger design may not be significant at higher velocities, where the coalescence of bubbles is very significant.

Additionally, $k_L a_L$ increased while augmenting pressure and temperature (Jin et al., 2014, 2004; Lau et al., 2004). As for the gas hold-up, it was reported that the increase in $k_L a_L$ with the gas density can be explained by either increasing pressure or changing the gas phase (Hashemi et al., 2009). Jin et al. (2014) studied the impact of temperature on $k_L a_L$ in a wide temperature range (from 25 to 200 °C) and for three pressures (10, 20, and 30 bar). As a result, they noted that $k_L a_L$ increased

with temperature for the three pressures. Furthermore, viscosity effects are linked to temperature as the liquid viscosity decreased when temperature increased. In this context, Shah et al. (2012) observed a decrease in $k_La_L$ by 67% while increasing liquid viscosity from 1 to 50 mPa.s.

Still, the properties of the liquid phase such as viscosity and surface tension exhibit a remarkable effect on $k_La_L$ (Deng et al., 2010; Hébrard et al., 2009; Kováts et al., 2020; Sardeing et al., 2006). (Dong et al. (2019) analyzed the mass transfer performance in tap water and CMC aqueous solutions with different weight percentages (0.3 wt.%, 0.4 wt.%, 0.5 wt.%, and 0.6 wt.%), and the apparent viscosity of the solutions ranged from 0.01 to 0.1 Pa.s. They reported that liquid phase rheology had a significant impact on the gas−liquid mass transfer performance. Actually, the $k_La_L$ coefficients in CMC aqueous solutions were much smaller than those in tap water, and the value diminished from $3.04 \times 10^{-3}$ $s^{-1}$ to $2.8 \times 10^{-4}$ $s^{-1}$ with the increase in the weight percentage of CMC aqueous solutions. By calculating the dimensionless diameter number of bubbles, it was found that the immobile gas−liquid interface was one of the reasons for the decrease in $k_La_L$ coefficients in CMC aqueous solutions. Additionally, Augier and Raimundo (2021) studied the effect of rheological properties on mass transfer and bubble sizes in a bubble column operated in the heterogeneous regime, and thus reported the coefficients of tap water were higher than those obtained when using viscous fluids (CMC solutions (0.25 wt.% and 0.50 wt.%), and xanthan gum solutions (0.1 wt.% and 0.25 wt.%)).

Sardeing et al. (2006) studied the effect of three types of surfactants (anionic, cationic, and non-ionic at concentrations up to 3.5 $mg.L^{-1}$) on the $k_La_L$ coefficient. Accordingly, in all liquid phases, it was reported that the $k_La_L$ coefficient increased with Ug, which in turn induced a systematic increase in the specific interfacial area. However, the $k_La_L$ coefficients of all the surfactant solutions were well below those of tap water ($k_La_L$ cationic < $k_La_L$ non-ionic < $k_La_L$ anionic < $k_La_L$ water). Furthermore, for a given Ug and surfactant solution, the smallest $k_La_L$ values were reached with the highest surfactant concentration (*i.e.*, surface coverage ratio at equilibrium equal to 1). Thus, it can be said that the type and the concentration of surfactants have a direct effect on gas−liquid mass transfer. Painmanakul et al. (2005) also related mass transfer coefficient, bubble diameter, and the surface coverage by surfactants to provide an understanding of the decrease in mass transfer performance in the presence of surfactants. Therefore, mass transfer in the presence of surfactants is thought to imply very complex mechanisms, as these agents affect the mass transfer in several

ways. Indeed, it has been pointed out that the head charge (Chen et al., 2003; Jia et al., 2015; Moraveji et al., 2012a; Painmanakul and Hébrard, 2008) or the length of the tail (García-Abuín et al., 2010; Vasconcelos et al., 2002) widely affected the mass transfer, as these parameters act on the affinity of the surfactants with the interface.

*1.2.2.1.2 Volumetric mass transfer coefficient in ARL reactors*

A thorough investigation of the volumetric mass transfer coefficient is of great importance for the design and scale-up of bioreactors and ARL reactors in particular. Common to BC reactors, the various factors that are known to affect gas−liquid mass transfer rate encompass superficial gas velocity, bubble size distribution, bubble coalescence, and breakage phenomena, liquid phase properties (Gharib et al., 2013; Moraveji et al., 2012b; Wei et al., 2014), gas distributor types (Luo et al., 2011; Wei et al., 2014), and downcomer to riser area ($A_d/A_r$) (Drandev et al., 2016). The volumetric mass transfer coefficient increased as $U_g$ increased. This is expected, as an increase in $U_{gr}$ resulted in a higher gas hold-up which induced an increment in interfacial area and also in mass transfer coefficient, and subsequently a higher oxygen supply. In contrast, an increase in bubble size led to a decrease in $k_La_L$ (Chisti, 1989; Chisti and Moo-Young, 1987; Merchuk, 2003).

Regarding liquid properties, Kumar et al. (2018) evaluated the effect of Newtonian (water and glycerol−water solutions) and non-Newtonian fluids (CMC and Xanthan aqueous solutions) on the $k_La_L$ coefficient in an internal loop ARL reactor. Therefore, it was found that the overall volumetric mass transfer coefficient decreased with an increase in viscosity/apparent viscosity of the Newtonian and non-Newtonian fluids. This finding was also reported by Cerri et al. (2008) and Mendes and Badino (2015) who proposed correlations for the $k_La_L$ coefficient by considering the effect of superficial gas velocity and viscosity for Newtonian fluids and consistency index for non-Newtonian fluids. Besides, Moraveji et al. (2012b) studied the effect of different types and concentrations of surfactant ((0 – 5 ppm) of anionic (sodium dodecyl sulfate, SDS) and non-ionic (Tween-80 and Triton X-405)) on the $k_La_L$ coefficient in split cylindrical ARL reactor, and found that overall gas−liquid volumetric mass transfer coefficient was diminished in the presence of surfactants, indicating that these agents significantly reduced the liquid mass transfer coefficient and that this reduction outweighed the interfacial surface enhancement effect. The same authors (Moraveji et al., 2012a) studied the mass transfer in a split-cylinder airlift bioreactor with a packed bed and in the presence of surface-active agents (containing SDS, HCTBr, and Tween 40) with

various concentrations (0 – 5 ppm). Therefore, they observed that surfactant occurrence significantly decreased the $k_La_L$ coefficients compared to those obtained in pure water. Besides, the packing installation improved the $k_La_L$ coefficient by augmenting flow turbulency and Reynolds number compared to an unpacked column. Furthermore, El Azher et al. (2005) evaluated the $k_La_L$ coefficient in a split rectangular ARL reactor using alcohol aqueous solutions. As a result, they pointed out that at low $U_g$, there was nearly no influence of propanol addition on the $k_La_L$ compared to water, whereas the presence of alcohol led to a significant decrease in the volumetric mass transfer coefficient at $U_{gr}$ values higher than 3.3 $m.s^{-1}$. However, Albijanić et al. (2007) examined the effect of 1 wt.% aqueous solution of five aliphatic alcohols on hydrodynamics and mass transfer in draft tube ARL reactor, and reported that alcohol addition improved gas hold-up and volumetric mass transfer coefficient, but induced a remarkable reduction of liquid velocity and hence elongation of circulation time, compared to the values obtained in the case for water–air system.

Luo et al. (2011) used three different gas spargers with different diameters and hole numbers (2-orifice nozzle, O-ring distributor, and 4-orifice nozzle) to analyze the effect of gas distributor structure on the mass transfer of an internal loop ARL reactor. As a result, they noted that the 4-orifice nozzle sparger enhanced the $k_La_L$ because it produced a smaller mean bubble diameter and thus a higher specific interfacial area compared to the other distributors. Moreover, it was found that the sparger structure had less effect on the oxygen mass transfer coefficient, whereas it significantly influenced the interfacial area. Recently, Naidoo et al. (2021) examined the influence of three static gas spargers with different design (perforated plate ($d_0$ = 0.45 cm, $N_0$ = 21 holes), perforated disk ($d_0$ = 0.45 cm, $N_0$ = 20 holes), and perforated pipe ($d_0$ = 0.45 cm, $N_0$ = 21 holes) on the hydrodynamics and mass transfer for a water-air system in an external loop ARL reactor. The gas distributor design was shown to impact the bubble size and distribution, and flow pattern in the riser. Indeed, it was found that the perforated plate sparger was the best design and led to the largest $k_La_L$ values than the perforated disk and the perforated pipe. Furthermore, the authors suggested that a low turbulence flow pattern resulted in an improvement in mass transfer performance.

Additionally, the geometry of airlift reactors is also a parameter to be considered for upgrading the performance of these reactors. Indeed, Merchuk and Gluz (2002) mentioned that ALRs with rectangular cross-sections are more versatile and provide better performance characteristics for a

given oxygen transfer rate. As well, large rectangular vessels are typically more easily constructed than cylindrical reactors (Couvert et al., 1999; Petersen and Margaritis, 2001). Drandev et al. (2016) studied the effect of the ratio between the downcomer and the riser areas on the mass transfer in a rectangular ARL bioreactor. Indeed, seven geometric configurations ($A_d/A_r$ = 0.2 – 5.0) were tested in order to determine an optimum value of $A_d/A_r$ in terms of the volumetric mass transfer coefficient. Through their results, it was shown that low $A_d/A_r$ ratios led to generally longer circulation times, and subsequently to smaller $k_La_L$ values than those achieved with higher $A_d/A_r$ ratios. Hence, it can be said that at very low $A_d/A_r$ ratios (when the width of the riser is less than or equal to the height of the base), the liquid circulation rate is insufficient for appropriate oxygen mass transfer. Kilonzo et al. (2007) investigated the effect of geometrical design on $k_La_L$ measurements in a rectangular ARL reactor using water and CMC solutions with a range of viscosity varying from 0.02 to 0.5 Pa.s and surface tension from 65 to 85 $mN.m^{-1}$. Thus, their findings revealed that an increment in the bottom clearance led to a decrease in the mass transfer by 50 % compared to 31 % when the top clearance was increased. Also, the gas−liquid separator was shown to exert a maximum influence of more than 65 % on the mass transfer compared to both bottom and top baffle clearances.

A summary of the studies performed to evaluate the effects of design and operating parameters on $k_La_L$ in BC and ARL reactors is given in Table 1.6. Ultimately, several empirical correlations describing the dependence of the $k_La_L$ coefficient on liquid and gas properties, operating and geometrical parameters in both BC and ARL reactors were developed to be used in the design and optimization of biochemical and other processes that require this type of reactors. Table 1.7 lists the commonly used correlations for estimating $k_La_L$ in the BC and ARL reactors.

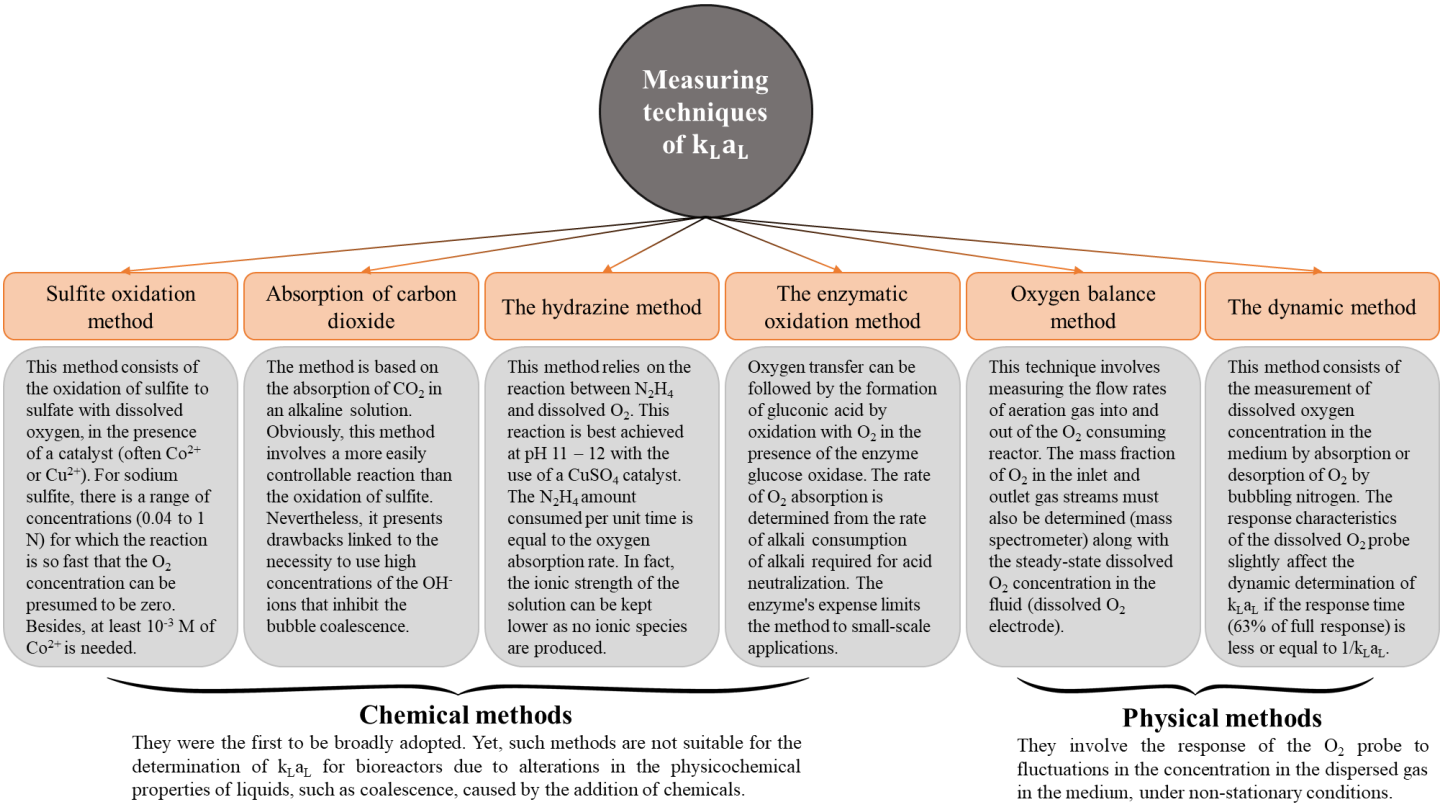


Figure 1.10 The principal measuring methods of $k_La_L$ coefficient.

Table 1.6 Summary of major investigations on the effects of operating and design parameters on $k_La_L$ in BC and ARL reactors.

| Type of pneumatic reactor | Sparger and column design | Operating conditions | System | Influencing parameter | Impact | References |
|---|---|---|---|---|---|---|
| External loop ARL | Downcomer: $H_c$ = 310 cm, $d_c$ = 15 cm<br>Riser: $H_c$ = 295 cm, $d_c$ = 15 cm<br>$A_d/A_r$ = 1<br>Spargers: Perforated plate with 21 holes ($d_0$= 0.45 cm), perforated disk with 20 holes ($d_0$= 0.45 cm), perforated pipe with 21 holes ($d_0$= 0.45 cm) | $U_g$ = 1.5 – 7.5 cm.s$^{-1}$<br>$\rho_L$ = 997 kg.m$^{-3}$<br>$\sigma$ = 72 mN.m$^{-1}$<br>$\mu_L$ = 0.0011 Pa.s<br>Room temperature | Water – air | Sparger: Perforated plate > Perforated disk > Perforated pipe | ↗ | Naidoo et al. (2021) |
| External loop ARL | Downcomer contained hydrocyclones with 8 cm in diameter: $H_c$ = 431 cm, $d_c$ = 20 cm<br>Riser : $d_c$ = 28 cm<br>$V_R$= 512 L, $V_w$= 400 L<br>Gas sparger with 160 needles ($d_0$= 0.086 cm) | $U_g$ = 1.4 – 8.1 cm.s$^{-1}$<br>$d_{particles}$= 66.11 – 109.7 µm | Water + (0 – 0.9 vol%) aluminum oxide-air | Solid concentration (0 – 0.9 vol%) | ↙ | Geng et al. (2020) |
| Cylindrical slurry BC | $H_c$ = 261cm, $d_c$ = 29.2cm<br>Distributor plate | $U_g$ = 0 – 25 cm.s$^{-1}$<br>$d_{particles}$= 35 – 156 µm | Tap water + (1 – 5 % (v/v)) glass beads-air | Solid concentration (1 – 5 % (v/v) | Neglected effect | Lakhdissi et al. (2020) |
| Square BC | $d_c$ = 12 cm, $H_c$ = 80 cm<br>Sintered glass gas dispenser ($d_0$= 0.0005–0.001 cm) | $U_g$ = 1.04 – 2.09 cm.s$^{-1}$<br>$\rho_L$ = 1026 – 1027 kg. m$^{-3}$<br>T = 25–27 °C | 0.003 M $K_2Cr_2O_7$+ 0.5 M $H_2SO_4$+ (15 to 100 ppm) SLS-air | Liquid properties (decreasing surface tension) | ↙ | Al-Shahrani et al. (2020) |

Table 1.6 Continued.

| | | | | | | |
|---|---|---|---|---|---|---|
| Slurry external loop ARL | Downcomer: $H_c$ = 420 cm, $d_c$ = 30 cm<br>3 Draft tubes: $H_c$ = 100 cm, $d_c$ = 20 cm<br>Needle distributor consisting of 109 needles ($d_0$ = 0.086 cm) | $U_g$ = 3 – 5.2 cm.s$^{-1}$<br>Solid concentration = 1 – 2 %<br>Room temperature<br>Atmospheric pressure | Water + (1 – 2%) alumina particles – air | Solid concentration | ↙ | Tao et al. (2020) |
| Square column | $d_c$ = 30 cm, $H_c$ = 60 cm, $H_0$ = 50 cm<br>Microporous distributeur | $U_g$ = 0.418 – 1.67 cm.s$^{-1}$<br>$\rho_L$ = 998 – 1008 kg.m$^{-3}$<br>$\sigma$ = 52.17 – 72.75 mN.m$^{-1}$<br>$\mu_L$ = 0.01 – 0.1 Pa.s | Tap water – air<br>tap water + CMC aqueous (0 – 0.6 wt.%) – air | Liquid properties (increasing viscosity) | ↙ | Dong et al. (2019) |
| Cylindrical BC | BC 1 without or with 22 % internals: $d_c$ = 19 cm, $H_0$ = 112 cm<br>Perforated plate with 225 holes ($d_0$ = 0.13 cm)<br>BC 2 without or with 22 % internals: $d_c$ = 45 cm, $H_0$ = 254 cm<br>Perforated plate with 241 holes ($d_0$ = 0.3 cm)<br>$H_0/d_c$ > 5 | $U_g$ = 20 – 45 cm.s$^{-1}$ | Water – air | With 22% internals > without internals | ↗ | Manjrekar et al. (2018) |
| Internal loop ARL | Downcomer: $H_c$ = 180 cm, $d_c$ = 20 cm<br>Riser: $H_c$ = 150 cm, $d_c$ = 12 cm<br>Perforated plate with 64 holes ($d_0$ = 0.05 cm) | $U_g$ = 0 – 2.5 cm.s$^{-1}$<br>$\rho_L$ = 1007 – 1192 kg.m$^{-3}$<br>$\mu_L$ = 0.001 – 0.0160 Pa.s<br>K = 0.007 – 0.162 Pa.s$^n$<br>Atmospheric pressure<br>room temperature | Tap water – air<br>Tap water + (25 – 65 % (v/v)) glycerin – air<br>Tap water + (0.15 – 0.45 % (w/v)) CMC – air<br>Tap water + (0.025 – 0.1 % xanthan (w/v)) CMC – air | Liquid properties (Increasing viscosity) | ↙ | Kumar et al. (2018) |

Table 1.6 Continued.

| | | | | | |
|---|---|---|---|---|---|
| Cylindrical slurry BC | $d_c$ = 10 cm, $H_0$ = 125 cm<br>Perforated plate with 4 nozzles ($d_0$= 0.8 cm) | $U_g$ = 3 – 10 cm.s$^{-1}$<br>T = 20 – 120 °C<br>P = 10 – 30 bar<br>$d_{particles}$ = 150–200 µm<br>$\rho_L$ = 835 – 890 kg.m$^{-3}$<br>$\mu_L$ = 0.0044 – 0.014 Pa.s | Paraffin – $H_2$<br>Paraffin – $CO_2$<br>Paraffin - CO | T = 20 – 120 °C ↗ | Jin et al. (2014) |
| Cylindrical slurry BC | $d_c$ = 10 cm, $H_0$ = 125 cm<br>Perforated plate with 4 nozzles ($d_0$= 0.8 cm) | $U_g$ = 3 – 10 cm.s$^{-1}$<br>T = 20 – 120 °C<br>P = 10 – 30 bar<br>$d_{particles}$ = 150 – 200 µm<br>$\rho_L$ = 835 – 890 kg.m$^{-3}$<br>$\mu_L$ = 0.0044 – 0.014 Pa.s | Paraffin – $H_2$<br>Paraffin – $CO_2$<br>Paraffin - CO | Slurry concentration = 0 – 20 wt. % ↙ | Jin et al. (2014) |
| Cylindrical slurry BC | $d_c$ = 10 cm, $H_0$ = 125 cm<br>Perforated plate with 4 nozzles ($d_0$= 0.8 cm) | $U_g$ = 3 – 10 cm.s$^{-1}$<br>T = 20 – 120 °C<br>P = 10 – 30 bar<br>$d_{particles}$ = 150 – 200 µm<br>$\rho_L$ = 835 – 890 kg.m$^{-3}$<br>$\mu_L$ = 0.0044 – 0.014 Pa.s | Paraffin - $H_2$<br>Paraffin - $CO_2$<br>Paraffin - CO | P = 10 – 30 bar ↗ | Jin et al. (2014) |
| Split rectangular ARL | $H_c$ = 200 cm, a = 20 cm, $H_0$ = 159 cm<br>Baffle: H = 130 cm<br>Single-orifice nozzle ($d_0$ 3.5mm) | $U_g$ = 1 – 8.5 cm.s$^{-1}$<br>σ = 68.1 – 71.1 mN.m$^{-1}$ | Tap water – air<br>Tap water + 0.05 vol% 1-Propanol – air<br>Tap water + 0.1 vol% 1-Propanol – air<br>Tap water + 0.05 vol% 1-Butanol – air<br>Tap water + 0.05 vol% Methanol – air | Liquid properties (by decreasing surface tension) ↙ | El Azher et al. (2005) |

↗ Increased ↙ Decreased

Table 1.7 Summary of major correlations for $k_La_L$ coefficients in BC and ARL reactors.

| Type of reactor | Correlation | Medium | Operating conditions | Sparger | $k_La$ method | Reference |
|---|---|---|---|---|---|---|
| BC | $k_La_L = 1.144U_g^{0.943}$<br>$k_La_L = 1.723U_g^{1.561}$ | Distillated water – air<br>Distillated water – pure oxygen | $d_c$ = 19 cm; $H_c$ = 400 cm; T = 25 ± 0.5; Atmospheric pressure<br>$U_g$ = 2 – 28 cm.s$^{-1}$ | Perforated plate and orifices of $d_0$ = 0.16 cm | Dynamic pressure method | Zedníková et al. (2018) |
| Annulus rising ARL | $k_La_L = 0.107U_g^{0.943}\mu_{ap}^{-0.234}$ | Tap water – air<br>(0.04 – 0.14 wt. %) CMC aqueous solutions–air | $U_g$ = 0.41 – 3.06 cm.s$^{-1}$<br>$\mu_{ap}$ = 0.0011 – 0.0351 Pa.s<br>$\rho_L$ = 1000.2 – 1001.9 kg.m$^3$<br>T = 20 ± 1 °C | O-ring distributor with 36 holes ($d_0$ = 0.05 cm) | Dynamic method (Nitrogen) | Han et al. (2017) |
| Internal loop ARL | $k_La_L = 0.02\left(\frac{P_M}{V_L}\right)^a U_g^b \upsilon^c$<br>With a = 0.10, b = 1.42, and c = -0.213 for 1.94 wt. % CMC<br>With a = 0.11, b = 0.99, and c = -0.08 for 1.8 wt. % Xanthan | 1.94 wt. % CMC aqueous solutions – air<br>1.8 wt. % xanthan aqueous solution – air | $U_g$ = 3.6 – 6 cm.s$^{-1}$<br>T = 25 °C | Circular perforated plate containing 90 equidistant holes | Dynamic method (Nitrogen) | de Jesus et al. (2015) |
| Split cylinder ARL | $k_La_L = 0.0024U_g^{0.605}\mu_L^{-0.655}$ | Water – air<br>Glycerol aqueous solution – air | $\mu_{ap}$ = 0.00084 – 0.03 Pa.s | Perforated sparger ($d_0$ = 0.05 cm) | Dynamic pressure-step method | Mendes and Badino (2015) |
| Internal loop ARL | $k_La_L = 0.107U_g^a\mu_{ap}^b$<br>For 0.3% CMC: a = 0.9144 and b = -0.1645<br>For 0.5% CMC: a = 0.8373 and b = 0.0406<br>For 0.3% CMC: a = 0.8803 and b = 0.4899 | (0.3 – 1.0 wt. %) CMC aqueous solutions-air | $U_g$ = 0.4 – 4 cm.s$^{-1}$ | Perforated plate sparger with 550 holes ($d_0$ = 0.2 cm)<br>Membrane-tube sparger (pore size = 5×10$^{-5}$ cm) | Dynamic method (Nitrogen) | Wei et al. (2014) |

Table 1.7 Continued.

| | | | | | | |
|---|---|---|---|---|---|---|
| Internal loop ARL | $k_L a_L = 0.1629 U_g^{0.6372}$ | Tap water – air | $U_g$ = 0.4 – 4 cm.s$^{-1}$ | Perforated plate sparger with 550 holes ($d_0$ = 0.2 cm) Membrane-tube sparger (pore size = 5×10$^{-5}$ cm) | Dynamic method (Nitrogen) | Wei et al. (2014) |
| Internal loop ARL | $k_L a_L = 0.0013 U_g^{0.803} \mu_L^{-0.492}$ | Tap water – air (0.1 – 0.35 % w/v) Glycerol aqueous solution – air | $U_g$ = 0.94 – 9.43 cm.s$^{-1}$ | Cross-piece type sparger ($d_0$ = 0.5 cm) | Dynamic pressure-step method | Cerri et al. (2008) |
| Internal loop ARL | $k_L a_L = 0.3039 U_g^{0.993} K^{-0.387}$ ($U_g$ < 5 cm.s$^{-1}$)<br>$k_L a_L = 0.0598 U_g^{0.438} K^{-0.35}$ ($U_g$ > 5 cm.s$^{-1}$) | (0.1– 0.35 % w/v) Xanthan gum aqueous solutions – air | $U_g$ = 0.94 – 9.43 cm.s$^{-1}$ | Cross-piece type sparger ($d_0$ = 0.5 cm) | Dynamic pressure-step method | Cerri et al. (2008) |
| BC | $k_L a_L = 0.48 \varepsilon_g$ | Demineralized water – air | $BC_1$: $d_{c1}$ = 10 cm; $BC_2$: $d_{c2}$ = 15 cm; $BC_3$: $d_{c3}$ = 38 cm; $H_0$ = 160 cm; $U_g$ = 0 – 35 cm.s$^{-1}$ | - Brace plate with 625 holes ($d_0$ = 0.05 cm) for $BC_2$ - Brace plate with 2750 holes ($d_0$ = 0.05 cm) for $BC_3$ | Dynamic oxygen absorption and desorption | Vandu and Krishna (2004) |
| BC | $k_L a_L = 1.77 \sigma_L^{-0.22} \exp(1.65 U_L - 65.3 \mu_L) \times \varepsilon_g^{1.2}$ | Gas: air Liquids: Paratherm NF heat transfer fluid, water | $BC_1$: $d_{c1}$ = 5.08 cm; $BC_2$: $d_{c2}$ = 10.16 cm; T = 92 °C; P = 4.24 MPa $U_g$ = 0 – 40 cm.s$^{-1}$ $U_L$ = 0.08 – 0.89 cm.s$^{-1}$ | Perforated plate with 120 square-pitched holes of $d_0$ = 0.15 cm | Oxygen desorption method with a discontinuous switch from air to nitrogen | Lau et al. (2004) |
| BC | $k_L a_L = 6.73 U_g^{1.22}$ | Deionized water – air | $d_c$ = 9.2 cm; $H_c$ = 130 cm; $H_0$ = 100 cm; Room temperature; $U_g$ = 0.28 – 2.2 cm.s$^{-1}$ | Perforated plate with 73 orifices of $d_0$ = 0.05 cm | Standard dynamic method (Nitrogen) | Vasconcelos et al. (2003) |

Table 1.7 Continued.

| | | | | | | |
|---|---|---|---|---|---|---|
| BC | $k_L a_L = \frac{\phi}{U_g^y - 1}$<br>$\phi = 0.874$; $y = -0.979$ for tap water;<br>$\phi = 2.222$; $y = -1.171$ for seawater | Tap water – air<br>Mediterranean Seawater – air | $d_c$ = 19.3 cm; $H_c$ = 230.6 cm; $H_0$ = 200 cm;<br>T = 22 ± 2 °C;<br>$U_g$ = 0 – 3.5 cm.s$^{-1}$ | A cross with 17 holes of $d_0$ = 0.1 cm | Dynamic gassing-in and gassing-out method (Nitrogen) | Mirón et al. (2000) |
| BC | $k_L a_L = 0.5\varepsilon_g$ | Demineralized water – air | $d_c$ = 15 cm; $H_c$ = 122 cm;<br>P = 0.1 – 1.0 MPa;<br>$U_g$ = 0 – 30 cm.s$^{-1}$ | Perforated plate with 200 orifices of $d_0$ = 0.05 cm | Dynamic pressure method | Letzel et al. (1999) |
| BC | $k_L a_L = 10^{-3.08} d_c \left(\frac{d_c U_g \rho_g}{\mu_L}\right)^{0.254}$ | CMC aqueous solution – air | $d_c$ = 15.2 cm; $H_c$ = 200 cm; P = 0.1 – 0.6 MPa;<br>$U_g$ = 2 – 20 cm.s$^{-1}$ | Grid having 12 holes with $d_0$ = 0.1 cm, and 0.3 cm internal diameter perforated pipes drilled horizontally in the grid | Dynamic oxygen absorption and desorption (Nitrogen) | Kang et al. (1999) |
| BC | $k_L a_L = 2.39 \times 10^{-4} \left(\frac{P_g}{V_L}\right)^{0.86}$ | Water – air | $d_c \geq 10$ cm<br>$200 \leq \frac{P_g}{V_L}(W.m^{-3}) \leq 1000$<br>$\frac{H_0}{d_c}$ up to 25 | | | Chisti (1989) |
| BC | $k_L a_L = K U_g^{0.82} \mu_{eff}^{-0.39}$<br>K = 0.063 in case of salt solutions<br>K = 0.042 in case of salt-free systems | Gas: air<br>Liquids: Water, $Na_2SO_4$ (0.8 M) aqueous solution | $d_c$ = 9.5 cm; $H_0$ = 85 cm;<br>T = 25 °C;<br>$U_g$ = 0.83 – 8 cm.s$^{-1}$ | Sigle orifice ($d_0$ = 0.09 cm) | Dynamic oxygen absorption and desorption (Nitrogen) | Schumpe and Deckwer (1987) |
| BC | $\frac{k_L a_L d_c^2}{D_L} = 6.8n^{-6.72} \left(\frac{d_c U_g \rho_L}{\mu_L}\right)^{0.38n+0.52} \times \left(\frac{\mu_L}{\rho_L D_L}\right)^{0.38n+0.14}$ | Gases: air, carbon dioxide<br>Liquids: Water, CMC aqueous solutions, glycerin solutions + silicone antifoam emulsion | $d_c$ = 23 cm; $H_c$ = 122 cm; $H_0$ = 92 cm; T = 24 - 29 °C;<br>$U_g$ = 0.8 – 8.4 cm.s$^{-1}$ | Perforated plate with 20 orifices of $d_0$ = 0.1 cm | Dynamic carbon dioxide gas method | Kawase and Moo-Young (1987) |

Table 1.7 Continued.

| | | | | | | |
|---|---|---|---|---|---|---|
| BC | $\frac{k_L a_L d_b^2}{D_L} = 0.62\left(\frac{\mu_L}{\rho_L D_L}\right)^{0.5}\left(\frac{d_b^2 \rho_L g}{\sigma_L}\right)^{0.33} \times \left(\frac{d_b^3 \rho_L^2 g}{\mu_L^2}\right)^{0.29}\left(\frac{U_g}{\sqrt{g d_b}}\right)^{0.68} \times \left(\frac{\rho_g}{\rho_L}\right)^{0.04}$ | Gases: air, nitrogen, helium, hydrogen, carbon dioxide<br>Liquids: tap water, methanol, ethanol, 2-propanol, 1-butanol, glycol (22, 60, 80, 100 wt. %), xylene, acetone, carbon tetrachloride, 1,2-dichloroethane, ethylbenzene, nitrobenzene, 1,4-dioxane, ethyl acetate, aniline, ligroin A, ligroin B, decalin | $d_c$ = 9.5 cm; $H_0$ = 85 cm; T = 20 °C; $U_g$ = 0.8 – 10 cm.s$^{-1}$ | Sigle orifice ($d_0$ = 0.3 cm) | Dynamic oxygen absorption and desorption (Nitrogen) | Öztürk et al. (1987) |
| BC | $k_L a_L = 8.35 \times 10^{-4} U_g^{0.44}\left[K\left(5000 U_g\right)^{n-1}\right]^{-1.01}$ | Gas: air<br>Liquids: CMC pure solutions, CMC + Triton X-114, CMC + sodium sulfate (0.8 M), CMC + sodium sulfide (0.8 M) solutions | $d_c$ = 30.5 cm; $H_c$ = 340 cm; $H_0$ = 250 cm; T = 25 °C; $U_g$ = 3 – 25 cm.s$^{-1}$ | Perforated plate with 479 holes of $d_0$ = 0.166 cm | Oxygen absorption and desorption Nitrogen and sulfite oxidation | Godbole et al. (1984) |
| BC | $k_L a_L = \frac{14.9 g f}{U_g}\left(\frac{U_g \mu_L}{\sigma_L}\right)^{1.76}\left(\frac{\mu_L^4 g}{\rho_L \sigma_L^3}\right)^{-0.248} \times \left(\frac{\mu_g}{\mu_L}\right)^{0.243}\left(\frac{\mu_L}{\rho_L D_L}\right)^{-0.604}$<br>f = 1 for non-electrolytes, $f = 10^{0.0681 \times I}$ for ionic strength I ≤ 1.0 kg ion.m$^{-3}$, and $f = 1.114 \times 10^{0.021 \times I}$ for I >1.0 kg ion.m$^{-3}$ | Gases: air, oxygen, hydrogen, methane, carbon dioxide<br>Liquids: deionized water, sucrose (30 and 50 wt. %), n-butanol, methanol (15 and 53 wt. %), $Na_2SO_4$ (0.2 – 2 M), KCl (0.8 – 3 M), $K_2SO_4$ (0.1 – 0.5 M), NaCl (0.3 – 5 M), $KNO_3$ (0.2 – 1.5 M), $AlCl_3$ (0.1 – 1 M), $CaCl_2$ (0.1 – 2 M) | $BC_1$: $d_{c1}$ = 10 cm; $H_{c1}$ = 150 cm; $H_{01}$ = 130 cm; $BC_2$: $d_{c2}$ = 19 cm; $H_{c2}$ = 240 cm; $H_{02}$ = 220 cm; $U_g$ = 4.2 – 38 cm.s$^{-1}$ | $BC_1$: single nozzle type ($d_0$ = 0.9 cm and 1.3 cm)<br>$BC_2$: single nozzle type ($d_0$ = 1.31; 2.06 and 3.62 cm) | Dynamic oxygen absorption and desorption (Nitrogen) | Hikita et al. (1981) |
| BC | $k_L a_L = 2.08 \times 10^{-4} U_g^{0.59} \mu_{eff}^{-0.84}$ | CMC aqueous solutions (0.7, 1.0, 1.3, 1.6 wt. %) – air | $d_c$ = 14 cm; $H_c$ = 270 cm; T = 20 °C; $U_g$ = 0 – 5 cm.s$^{-1}$ | -Perforated plate with 73 holes ($d_0$ = 0.1 cm) - Perforated plate with 19 holes ($d_0$ = 0.2 cm) - Sintered plate (0.02 cm) | Dynamic oxygen absorption and desorption (Nitrogen) | Deckwer et al. (1981) |

Table 1.7 Continued.

| | | | | | | |
|---|---|---|---|---|---|---|
| BC | $\frac{k_L a_L d_c^2}{D_L} = 0.09\left(\frac{\mu_L}{\rho_L D_L}\right)^{0.5}\left(\frac{d_c^2 \rho_L g}{\sigma_L}\right)^{0.75} \times \times \left(\frac{d_c^3 \rho_L^2 g}{\mu_L^2}\right)^{0.39}\left(\frac{U_g}{\sqrt{g d_c}}\right)^{1.0}\left(1 + C\left(\frac{U_B \lambda}{d_{vs}}\right)^m\right)^{-1}$<br>C=0 (inelastic fluids) or C=0.133 (elastic fluids) | Gas: air<br>Liquids: water, sucrose (10 %, 30 %, 50 %), carboxy methyl cellulose (CMC) (0.3 %, 0.5 %, 1.0 %) and sodium polyacrylate (0.01 %, 0.05 %, 0.1 %) aqueous solutions | $d_c$ = 14.55 cm; $H_c$ = 190 cm; $H_c$ = 110 cm; T = 30 °C | Sigle orifice ($d_0$ = 0.4 cm) | Dynamic oxygen absorption and desorption (Nitrogen) | Nakanoh and Yoshida (1980) |
| BC | $\frac{k_L a_L d_c^2}{D_L} = 0.6\left(\frac{d_c^2 \rho_L g}{\sigma_L}\right)^{0.62}\left(\frac{d_c^3 \rho_L^2 g}{\mu_L^2}\right)^{0.31} \times \left(\frac{\mu_L}{\rho_L D_L}\right)^{0.5} \varepsilon_g^{1.1}$ | Water – air<br>Water – oxygen<br>Methanol – oxygen<br>Glycerol aqueous solution – air<br>$Na_2SO_3$ (0.15 M) – air | $d_c$ = 15.2 cm; $H_c$ = 400 cm; $H_0$ = 200 – 300 cm; T = 20 °C ; $U_g$ = 0.40 – 8.86 $cm.s^{-1}$ ; $U_g$ = 2.00 – 8.03 $cm.s^{-1}$ ; $U_g$ = 0.66 – 10.08 $cm.s^{-1}$ ; | Single hole ($d_0$ = 0.5 cm) | Dynamic oxygen absorption and desorption (Nitrogen) | Akita and Yoshida (1973) |

## 1.3 Conclusions

In this chapter, an overview of the main research works in the literature concerning the hydrodynamic and gas−liquid mass transfer characteristics of bubble columns and airlift reactors has been provided. Indeed, this part highlights the complexity of studying the hydrodynamics and mass transfer of these reactors, as several parameters are involved and affect these two aspects. Besides, the advantages offered by these pneumatic reactors have rendered them indispensable in many fields, especially for processes involving slow reactions.

Notwithstanding the enormous number of studies that have been published on these multiphase reactors, there are still many questions that remain to be answered. For instance, the interaction between the different phases, which are intimately linked, and the effect of their physical properties (*i.e.,* liquid surface tension) on the bubble dynamics and mass transfer are not yet well comprehended. Therefore, principles of bubble columns and airlift reactors design and operating parameters have primarily been guided by empirical or semi-empirical correlations, that are essentially based on experimental data and plant experience. Actually, the reason behind this is that the multiphase flow behavior in these devices is typical of complex structures.

Ultimately, the next chapters will be dedicated to the study of the effect of surface-active agents on hydrodynamics and oxygen mass transfer in a square bubble column. Additionally, the application of a gas−liquid reaction in these two types of multiphase reactors will be investigated in order to evaluate and compare their performance in the field of water treatment.

# Chapter 2: Experimental analysis of the effects of liquid phase surface tension on the hydrodynamics and mass transfer in a square bubble column


## Abstract

The effects of liquid surface tension were investigated on gas−liquid interfaces in bubbly flows through the analysis of hydrodynamic and mass transfer features. Tap water and aqueous solutions with two types of surfactants (cationic and anionic) are used as aqueous liquid phases. In fact, these surfactants are organic collectors consisting of an amine and ester. The influences of surfactant concentration and superficial gas velocity on the volumetric mass transfer coefficient and the gas hold-up were highlighted. The experimental findings revealed that although the two surfactants tested generated a decrease in surface tension, their effects on gas hold-up and flow regimes are very different. First, it was observed that the gas hold-up in amine aqueous solutions was very close to that in tap water, but it increased once the superficial gas velocity was above 7 $cm.s^{-1}$. Conversely, the presence of ester decreased the overall gas hold-up since bubble net coalescence was enhanced, and the heterogeneous flow regime prevailed above 2.9 $cm.s^{-1}$. Thus, the homogeneous regime prevailed with a superficial gas velocity of less than 4.4 $cm.s^{-1}$ for tap water and amine aqueous solution, which corresponds to the transition point. Experimental findings exhibited also that the power spectral density of pressure fluctuations is a convenient tool to identify the prevailing flow regimes even in surfactant aqueous solutions. Besides that, both organic surfactants strongly reduced the volumetric mass transfer coefficient in comparison to tap water, mainly by inducing an additional resistance to gas−liquid mass transfer through interfacial adsorption for the cationic amine, but by promoting bubble coalescence for the anionic ester aqueous solution.



**Keywords:** Bubble column; Gas−liquid interfaces; Surface tension; Gas hold-up; Flow regime transition; Bubble size; Mass transfer

## 2.1 Introduction

Gas−liquid and gas−liquid−solid contactors constitute vital components for many industrial processes. Bubble columns are one of the most widely used multiphase reactors, that are found in many industries such as chemical, biochemical, biotechnology, environmental separation, and wastewater treatment industries (Chalupa et al., 2020; Gallucci et al., 2019). In fact, the extensive use of bubble columns is attributed to the advantages they offer, which are mainly good mixing, better mass and heat transfer rates with low energy intake (Besagni and Inzoli, 2017; Shah et al., 1982). Meanwhile, optimization and design of bubble columns involve thorough comprehension of the different flow regimes, as the hydrodynamic characteristics of these regimes are often quite distinct (Shiea et al., 2013). Essentially, two flow regimes are observed: the homogeneous bubbly flow, and the heterogeneous or churn-turbulent flow regimes. The former is associated with low superficial gas velocities and characterized by a uniform bubble size distribution. The latter is commonly observed at relatively high superficial gas velocities and marked by a wide variety of bubble sizes as a consequence of high coalescence and breakage phenomena.

The knowledge of the hydrodynamic parameters is crucial since it affects the mass and heat transfer phenomena as well as the mixing time in the reactor, which then leads to the reaction rate determination. However, the gas hold-up, which is a key hydrodynamic parameter, is strongly influenced by the geometrical parameters of the column (which usually cover the column diameter $d_C$ and the ratio between the liquid free level $H_0$ and $d_C$), sparger design, and the physico-chemical properties of gas and liquid phases. Among the liquid properties, surface tension and viscosity were the focus of several investigations (Besagni et al., 2017b; Besagni and Inzoli, 2017; Esmaeili et al., 2015; Kelkar et al., 1983; Lu et al., 2019). Since modifying the surface tension through surfactants is of prime importance in most industrial applications, researchers used a variety of organic (alcohols such as ethanol) and inorganic surfactants (electrolytes like $NaCl, CaCl_2, Na_2SO_4$) to provide insight into the effect of surface tension changing on gas hold-up as well as flow regimes. In addition, in the literature, there is an agreement that diminishing the surface tension has been associated with a decrease in bubble coalescence frequency, and then bubbles became smaller, which subsequently leads to an increase in gas hold-up compared to that of the water-air system (Camarasa et al., 1999; Gourich et al., 2006b). Bearing in mind that Lu et al. (2019) reported that surfactants delay coalescence by slowing the drainage of the liquid film separating the approaching bubbles before they make contact. Furthermore, many correlations have been proposed to properly predict the gas hold-up in two-phase bubble columns, taking into account the type of liquid phase and other parameters (Table 1.4).

The flow regime in the bubble column is a multifaceted function of fluid properties, column diameter, gas sparger design, and operating conditions. Thus, several experimental techniques have been developed and used for this end, including particle image velocimetry (Delnoij and Kuipers, 2000), electrical resistance tomography (Toye et al., 2008), laser Doppler anemometry (Olmos et al., 2003), bed vibration signature (Sheikhi et al., 2013), optical fiber signals (Chen et al., 2003) and pressure fluctuations (Vial et al., 2000). Particularly, the measurement of pressure fluctuations is experimentally simple and inexpensive. It can be used on a laboratory and industrial scale without altering the flow in the reactor (Vial et al., 2000). For this reason, the pressure fluctuations are sampled by a series of pressure transducers located along the column and several approaches, and data analysis techniques are applied to determine the hydrodynamic features and characterize the flow dynamics within the column. Table 2.1 reports some studies based on pressure fluctuations analysis.

As previously quoted, surfactants play a prominent role in several industrial applications, one illustrative example of which is the flotation process in the mining industry. Indeed, collectors are part of the most important components involved in the flotation process of minerals, such as phosphate, to separate the ore from impurities (*i.e.*, silicates and carbonates in the case of phosphate ore) (Blazy and Jdid, 2000). The main objective of the collector is to selectively form a hydrophobic layer on a mineral surface in the flotation pulp, and hence ensure the conditions for the attachment of hydrophobic particles to the air bubbles and recovery of these particles in the froth (Bulatovic, 2007). Basically, a flotation collector is composed of polar and non-polar groups. The non-polar part, as a linear, branched, or cyclic hydrocarbon group is referred to as a hydrophobic group. The polar part, which has a high affinity for mineral surfaces, is known as the minerophilic group (Liu et al., 2017). Depending on the tendency of collectors to dissociate in water, they can be divided into three separate groups: cationic, anionic, and non-ionic surfactants (Ruan et al., 2019; Sis and Chander, 2003). Moreover, the surface-active character is imparted by the affinity of the hydrocarbon chain to the gaseous phase, and by that of the polar head to the liquid phase. The surfactant molecule is therefore oriented at the air-water interface (Blazy and Jdid, 2000). However, as surface-active agents, these collectors significantly affect gas−liquid interfaces. The aim of this study is, therefore, to investigate these specific effects.

Table 2.1 A few studies that used the pressure fluctuation methods for regime flow identification in bubble columns.

| Authors | Medium | Column dimension (cm) | Methods | Highlights |
|---|---|---|---|---|
| Vial et al. (2000) | Water – air | $d_c = 10$<br>$H_c = 200$ | - Statistical analysis<br>- Spectral analysis<br>- Fractal analysis<br>- Chaos analysis | - Statistical analysis can detect the transition, but it does not provide more information than conventional methods based on gas hold-up measurements.<br>- Spectral analysis can identify the governing flow regime in the bubble reactor (with the perforated or the porous plates, the homogeneous flow was characterized by a peak at 0.1 Hz, whereas the heterogeneous regime by 3–5 Hz)<br>- Fractal and particularly chaos approaches accurately indicate the transition regime. |
| Lin et al. (2001) | Water – air | $d_c = 17$<br>$H_c = 250$ | - Chaos analysis | - Four chaotic invariants (Lyapunov exponent, metric entropy, correlation dimension, and mutual information) were used to identify the transition velocity. -- Two transitions velocities were found; 4 and 10 $cm.s^{-1}$. |
| Gourich et al. (2006b) | Water – air<br>Aqueous alcohol solutions – air | $d_c = 10$<br>$H_c = 300$ | - Standard deviation<br>- Spectral analysis<br>- Fractal analysis<br>- Chaos analysis | - Pressure fluctuation methods successfully identify the boundary of flow regimes but there is no clear transition. |
| Chilekar et al. (2005) | Demineralized water – air | $d_c = 30$<br>$H_c = 200$ | - Power spectral density | - Large bubbles of 4 to 5 cm generate pressure fluctuations in the range of 2 to 5 Hz, and that small bubbles of around 4 mm can induce fluctuations up to 50 Hz. |
| Sheikhi et al. (2013) | Tap water – air | $d_c = 9$<br>$H_c = 200$ | - Statistical analysis<br>- Spectral analysis | - The analysis of the signals in the frequency domain suggested the way of the alteration of the behavior of the bubbles according to their size under different operating conditions of gas and liquid velocities.<br>- The kurtosis of pressure fluctuations could only detect the main transition point of the column at moderate liquid velocities. |
| Tchowa Medjiade et al. (2017) | Water – nitrogen | $d_c = 10.2$<br>$H_c = 240$ | - Standard deviation<br>- Fractal analysis<br>- Kolmogorov entropy<br>- Power spectral density | - The homogeneous regime was characterized by a zone without any peaks.<br>- The heterogeneous flow was characterized by the presence of pronounced spikes at up to 20 $s^{-1}$ and less pronounced peaks from 35 to 45 $s^{-1}$.<br>- The transition between the two-above mentioned regimes was observed at 4.5 $cm.s^{-1}$. |

Another determining factor in the performance of multiphase contactors is the gas−liquid mass transfer, which is characterized by the volumetric mass transfer coefficient $k_La_L$. In the mineral processing of phosphate ore, a large amount of freshwater (around 500 $m^3.h^{-1}$) is consumed and subsequently about 10,000 $m^3$ of wastewater effluents are generated (case of a Jordanian phosphate industry) (Al-Zoubi and Al-Thyabat, 2012). However, flotation wastewaters which contain excess and unreacted concentrations of organic surfactants, lead to a serious environmental pollution by degrading water quality and aquatic life (Chockalingam et al., 2003; Deo and Natarajan, 1998). Hence, chemical treatments such aeration, oxygenation, ozonation and peroxide or permanganate treatment have been carried out to remove these organic chemicals, though these methods are costly and can bring about a secondary pollution (Chen et al., 2011; Chockalingam et al., 2003). Furthermore, biodegradation techniques have attracted interest as a versatile, low-cost, stable and environmentally friendly technique for flotation wastewater treatment (Chen et al., 2011; Dong et al., 2014). On the one hand, in such treatments, mass transfer is a major limiting factor as the oxygen transfer process requires a large amount of energy and of course a high investment cost (Jia et al., 2015). On the other hand, the presence of surfactant in wastewater has a very pronounced effect on gas−liquid mass transfer through a modification of the solubility, mobility and specifically the surface tension of the fluids (Jia et al., 2015).

However, the mass transfer rate strongly relies on the hydrodynamic conditions in bubble columns; and so many parameters affect $k_La_L$, such as design parameters (column geometry and gas distributor design, etc.) and liquid properties (viscosity, presence of ions inhibiting coalescence, or surfactants adsorption, etc.) (Vasconcelos et al., 2003; Zedníková et al., 2018). Regarding the specific effect of surfactants, it is reflected in the increase in the bubble drag force coefficient and the decrease in the bubble rise velocity since these substances tend to accumulate at the bubble gas−liquid interfaces (Alves et al., 2005). Bubbles generated in the presence of surfactants have a tendency to be smaller and slower due to the decline in the coalescence phenomenon (Loubière and Hébrard, 2004). This could have a positive impact on the interfacial area, unlike the liquid side mass transfer coefficients ($k_L$) which considerably decreases (Vasconcelos et al., 2003). A study was accomplished by Sardeing et al. (2006) on the impact of non-ionic, anionic, and cationic surfactants on the liquid-side mass transfer coefficient in gas−liquid systems. They reported that regardless of the liquid phase, three zones could be distinguished with respect to the liquid-side mass transfer coefficient variation with the bubble diameter. For mean bubble diameters less than 1.5 mm, $k_L$ values were

approximately constant about $10^{-4}$ m.s$^{-1}$ and no effect of the surfactants was observed. For mean bubble diameters higher than 3.5 mm, $k_L$ values were almost constant with the diameter but depended on surfactant concentration. For bubbles with diameters varying from 1.5 to 3.5 mm, $k_L$ increased from $10^{-4}$ m.s$^{-1}$ to reach between 1 and $3.10^{-4}$ m.s$^{-1}$ at 3.5 mm diameter based on the charge and the concentration of surfactant. Besides, Jamnongwong et al. (2010) concluded that the hydrodynamic characteristics were almost constant for each surfactant concentration examined; hence, only a change in oxygen diffusion coefficient could be responsible for the $k_L$ decline.

It can be said that no investigations on the effect of collectors as surface-active agents in a two-phase bubble column reactor are reported in the literature. Therefore, this work is aimed at studying the gas hold-up and gas−liquid mass transfer rate in a square bubble column reactor with tap water and aqueous solution of cationic and anionic collectors (an amine and an ester, respectively) which are widely used in phosphate flotation. The influences of the collector concentration and superficial gas velocity ($U_g$) on the overall gas hold-up, the flow regime, and the volumetric mass transfer coefficient $k_La_L$ are examined.

## 2.2 Materials and methods

### 2.2.1 Experimental setup

The experimental setup consists of a square bubble column made of Plexiglas with dimensions 0.2 m × 0.2 m × 3 m (L×W×H). Gas sparging is performed through a perforated plate with 246 holes of 0.9 mm in diameter at the bottom of the column providing uniform aeration. The gas phase consists of compressed air. The air flow rate is controlled using a calibrated rotameter (Brooks Instrument®, GT1000, with a precision of 2 %), and the superficial gas velocity under atmospheric pressure ranges from 0.75 to 9.44 cm.s$^{-1}$. The liquid phase is fed into the column through a valve placed at the bottom of the column. The liquid phase is operated in a batch mode and the clear liquid height $H_0$ is adjusted to 1.65 m. All experiments are carried out at ambient temperature and atmospheric pressure. Figure 2.1 displays a schematic drawing of the experimental setup.

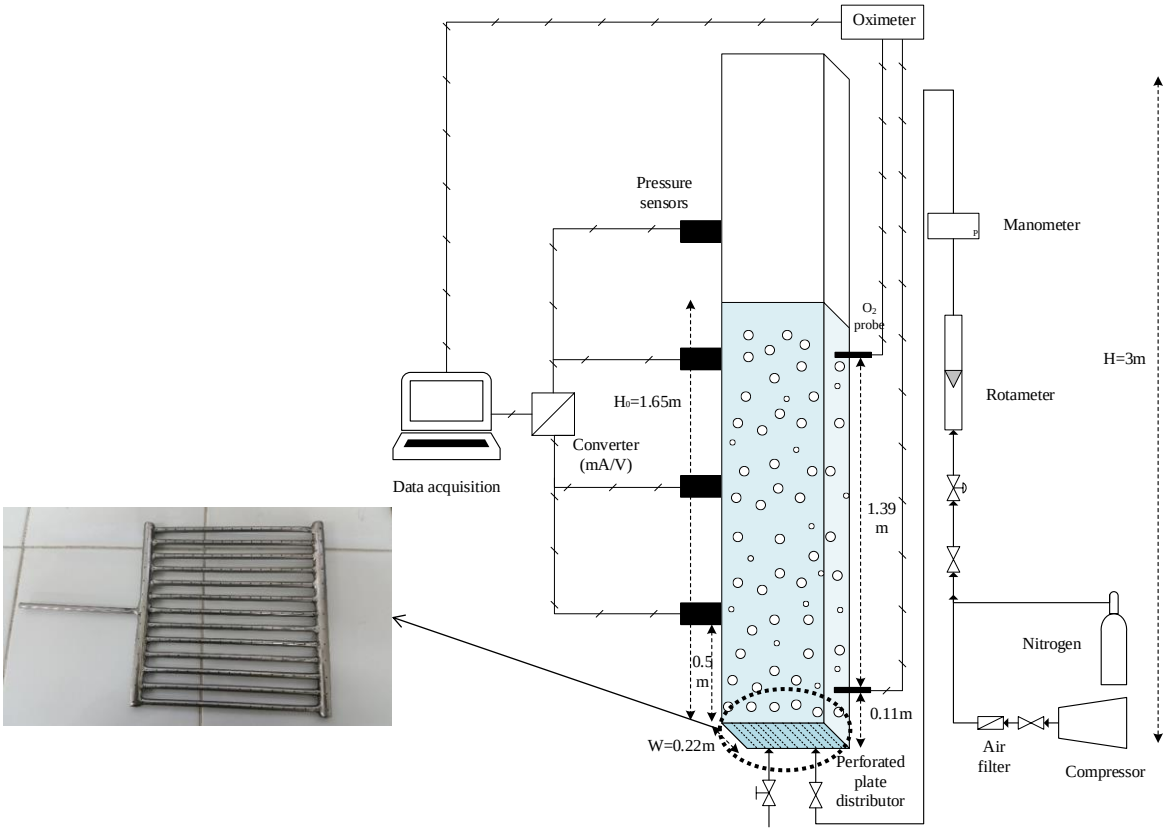


Figure 2.1 Schematic of the experimental setup.

### 2.2.2 Surfactant preparation and characterization

The experiments are conducted by using various liquid phases, which are tap water and surfactants aqueous solution. It is worth noting that surfactants have been carefully selected according to their nature and applications. Thus, two types of commercial collectors are tested, namely, an amine and an ester, which are cationic and anionic surfactants, respectively, supplied by OCP Group (Office Chérifien des Phosphates, Morocco, https://www.ocpgroup.ma/). These collectors were chosen mainly because of their wide use for the flotation of oxidized ores, such as phosphate and industrial minerals. The concentrations studied vary between 5 and 50 ppm. All solutions were prepared by adding each of the two collectors to tap water while stirring for 10 to 15 minutes at a temperature of 25°C. Experiments are also repeated with tap water as the reference fluid. The surface tension of each solution is measured using a Krüss tensiometer (K12-Krüss©, Germany) and the Wilhelmy plate method with an accuracy of ±1 $mN.m^{-1}$. Surface tension always reached the equilibrium value immediately, so that only the static surface tension value was retained. The surface tension of tap water and aqueous solutions in different concentrations are summarized in Table 2.2. From

this table, it can be deduced that the Critical Micellar Concentration, which corresponds to a saturated interface, is achieved when collector content is about 20 ppm and 24 ppm for the amine and the ester, respectively.

The rheological studies of the solutions are accomplished by means of an AR-G2 rheometer (TA Instruments, USA) with a 40 mm − 2° steel cone geometry. A simple shear study with a shear rate ranging from 1 to 1000 $s^{-1}$ is performed to determine the apparent viscosity value at 25°C. The measured apparent viscosity of the solutions is represented in Table 2.2. In the case of tap water, the obtained surface tension and apparent viscosity are in accordance with literature data (Jamnongwong et al., 2010).

Table 2.2 Surface tension and apparent viscosity of the liquid phases at 25 °C.

| Aqueous solution | Concentration (ppm) | Surface tension ($mN.m^{-1}$) | Apparent viscosity (mPa.s) |
|---|---|---|---|
| Tap water | - | 72.9 ± 0.9 | 1.10 ± 0.05 |
| Amine | 5 | 63.1 ± 1.4 | 1.20 ± 0.15 |
| | 10 | 48.4 ± 1.8 | 1.11 ± 0.01 |
| | 15 | 43.5 ± 1.8 | 1.11 ± 0.01 |
| | 20 | 29.9 ± 1.6 | 1.10 ± 0.01 |
| | 30 | 30.3 ± 1.7 | 1.11 ± 0.13 |
| | 40 | 28.9 ± 0.9 | 1.09 ± 0.02 |
| | 50 | 28.5 ± 0.5 | 1.10 ± 0.09 |
| Ester | 5 | 55.0 ± 1.5 | 1.20 ± 0.14 |
| | 10 | 55.1 ± 1.5 | 1.13 ± 0.05 |
| | 15 | 48.5 ± 1.2 | 1.10 ± 0.04 |
| | 20 | 40.8 ± 0.8 | 1.10 ± 0.03 |
| | 30 | 34.0 ± 1.4 | 1.11 ± 0.08 |
| | 40 | 34.3 ± 1.3 | 1.10 ± 0.04 |
| | 50 | 32.7 ± 0.7 | 1.09 ± 0.02 |

### 2.2.3 Measuring methods in bubble column

#### *2.2.3.1 Gas hold-up measurement*

The overall gas hold-up in the column is measured using the manometric method. Omitting the acceleration and wall friction participation in the momentum balance, and assuming that $\rho_G \ll \rho_L$, the gas hold-up can be deducted by the following expression:

$$\varepsilon_g = 1 - \frac{\Delta P}{\rho_L \times g \times \Delta H} \tag{2.1}$$

where ΔP is the difference of static pressure between two sensors placed at a distance ΔH. Pressure measurements are performed using four piezo-resistive sensors embedded in the wall (Keller PR-25/8797.1), with respective pressure ranges 0 – 500 mbar (for the two lowest sensors), 0 – 150 mbar (for the two top sensors), with an accuracy of 0.02 % of the full scale. The distance between the pressure sensors is 0.5 m (from 0.5 m to 2 m above the gas sparger). Pressure signals are sampled with a 16-bit acquisition card (Adlink-1901, *Adlink Technology Inc.*, Taiwan) and stored in a PC. The *Adlink® Utest* software is employed to control data acquisition. Pressure signals are sampled with a frequency of 100 Hz and duration of 200 s. Thus, the acquisition length is 20,000 points for each experiment. Three samples for each condition are conducted to diminish statistical error.

#### *2.2.3.2 Flow regime*

Spectral analysis of pressure signals based on Fast Fourier transform (FFT), which is in the frequency domain analysis, has been illustrated as a simple and robust tool to determine the hydrodynamic regime in bubble columns when water corresponds to liquid phase (Vial et al., 2001). However, few studies (Esmaeili et al., 2015; Gourich et al., 2006b; Tchowa Medjiade et al., 2017) have applied this tool for systems that contain water contaminated with surfactants or viscous liquids.

In this work, spectral analysis of pressure fluctuations is applied using the equipment used for gas hold-up measurements. Fourier transform allows transposing pressure signals expressed in the time domain into the frequency domain. This leads to the identification of the main frequencies contained in the initial signal. The Fourier transform is given as:

$$\mathcal{F}_x(f) = \frac{1}{T}\int_0^T P_x(t)e^{-2\pi i f t}dt \tag{2.2}$$

The power spectral density (PSD) expresses the contributions of the elementary sine functions to the whole signal:

$$PSD = \frac{1}{T}E(\mathcal{F}_x.\mathcal{F}_x^*) \tag{2.3}$$

where E is the expectation of $\mathcal{F}_x(f)$ and $\mathcal{F}_x^*$ is the complex conjugate of the Fourier transform.

It is worth mentioning that the pressure signal in the bubble column changes depending on different fluctuation sources with specific characteristic frequencies, comprising bubble formation, rise, coalescence and breakage, and liquid level fluctuations. Therefore, the

amplitude, dominant frequency, and frequency distribution of a PSD curve can be employed to characterize the properties and behavior of the bubbles and to identify the flow patterns in a bubble column.

#### *2.2.3.3 Volumetric mass transfer coefficient and bubble size measurements*

The volumetric mass transfer coefficient $k_L a_L$ is measured using the dynamic deoxygenation method, which is based on oxygen elimination by bubbling nitrogen followed by reoxygenation using compressed air. In the batch liquid phase, the variation of dissolved oxygen concentration in the batch liquid phase with time is measured using two dissolved oxygen electrodes (WTW Cellox 325) located at 0.11 m and 1.50 m above the perforated plate, and horizontally immersed to a depth of 9 cm. These sensors are connected to a DO-meter (WTW OXI 197i) and to a data acquisition system (Adlink-1901) allowing the recording of concentration values. The time constant ($k_p$) of the oxygen sensors is measured by the method described by Vandu and Krishna (2004), which give $k_p = 0.14\ s^{-1}$. A mass balance on dissolved oxygen (and assuming a perfectly stirred bubble column) gives:

$$\frac{dC_t}{dt} = k_L a_L (C_s - C_t) \tag{2.4}$$

where $C_s$ is the dissolved oxygen concentration at saturation and $C_t$ is the instantaneous dissolved oxygen concentration measured by experiments. The integrated formula of Eq. (2.4) is as follows:

$$\ln \frac{C_s - C_0}{C_s - C_t} = k_L a_L\, t \tag{2.5}$$

where $C_0$ is the initial dissolved oxygen concentration. The value of $k_L a_L$ is obtained from the slope of the curve of $\ln \frac{C_s - C_0}{C_s - C_t}$ versus t.

The volumetric oxygen transfer coefficients measured at the temperature T ($k_L a_{L_T}$), are reported at 20 °C ($k_L a_{L_{20}}$) using the following temperature correction:

$$k_L a_{L_{20}} = k_L a_{L_T} \times \theta^{(20-T)} \qquad \text{with } \theta = 1.024 \tag{2.6}$$

Bubble sizes were measured using image analysis. Pictures of the bubbly flow were taken and analysed using the free *ImageJ* software package (https://imagej.nih.gov/). However, this technique was limited to low gas hold-up, *i.e.*, to low superficial gas velocity, due to the influence of light obscuration by the bubbles on flow imaging.

## 2.3 Results and discussion

The following section outlines and discusses the experimental results obtained. A contribution to the assessment of the influence of surfactant addition on the hydrodynamics and oxygen mass transfer of bubble column is provided through the analysis and comparison with the literature of parameters such as gas hold-up, transition velocity, and volumetric mass transfer coefficient.

### 2.3.1 Gas hold-up and flow regime transition

The overall gas hold-up is one of the foremost hydrodynamic and design parameters of bubble columns. It is also strongly affected by surfactants. Figures 2.2a and 2.2b depict the global gas hold-up in tap water and surfactant aqueous solutions as a function of superficial gas velocity. $\varepsilon_g$ augments with the increase in $U_g$ for any liquid phase. This can be explained by an increase in the number of bubbles in the liquid phase with superficial gas velocity. Besides, at the same superficial gas velocity, the overall gas hold-up of ester aqueous solutions is smaller than that of tap water and this is due to net bubble coalescence that quickly takes place (Figure 2.2b). Conversely, the overall gas hold-up in amine aqueous solutions is almost equal to that in tap water at a relatively low gas flow rate, but this is no longer the case for $U_g$ greater than 7.3 $cm.s^{-1}$ (Figure 2.2a). This increase in $\varepsilon_g$ is due to froth formation with a height approximately of 15 to 18 cm at high superficial gas velocities (exceeding 7.3 $cm.s^{-1}$). As mentioned by Besagni et al. (2019), the formation of a thick cap was noticed in the upper part of the column; thus, this cap hinders air disengagement and subsequently causes bubble accumulation and a significant increase in $\varepsilon_g$.

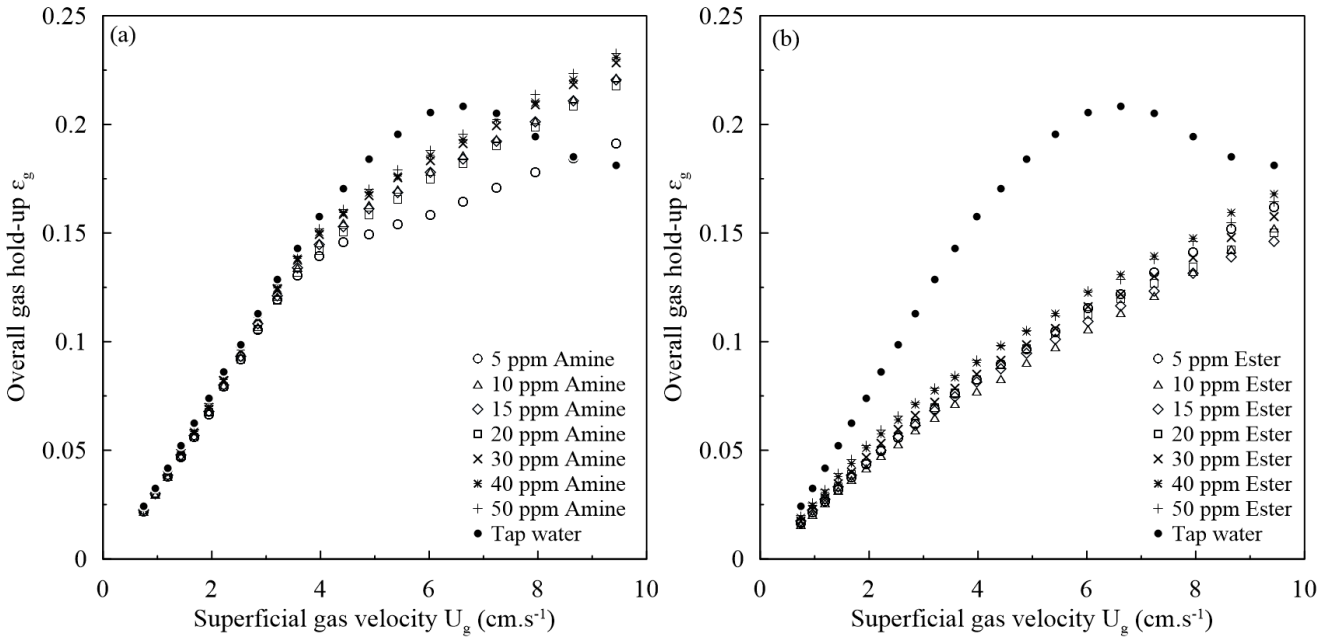


Figure 2.2 Overall gas hold-up versus superficial gas velocity for (a) air−tap water-amine, and (b) air−tap water-ester.

Figure 2.3a displays the overall gas hold-up differences between the amine and the ester compared to tap water at a concentration of 50 ppm. The difference between both surfactants seems to result from their charge at constant pH, as surface tension does not strongly differ (Table 2.2) and gas−liquid interfaces seem to be saturated by adsorbed species above 10 ppm for both surfactants whatever the superficial gas velocity (Figures 2.3b and 2.3c). Similarly, the effect of the axial position in the column does not strongly affect these conclusions (Figure 2.4). The obtained findings are in line with those of Koide et al. (1985), and Yagi and Yoshida (1974) by using surfactants and antifoam agents. Conversely, the majority of studies found that $\varepsilon_g$ improved in the presence of surface-active agents (Camarasa et al., 1999; Gourich et al., 2006b; Kelkar et al., 1983). Hence, it emerges from the literature that the effect of surfactants can be complex and does not always induce an increase in the gas hold-up.

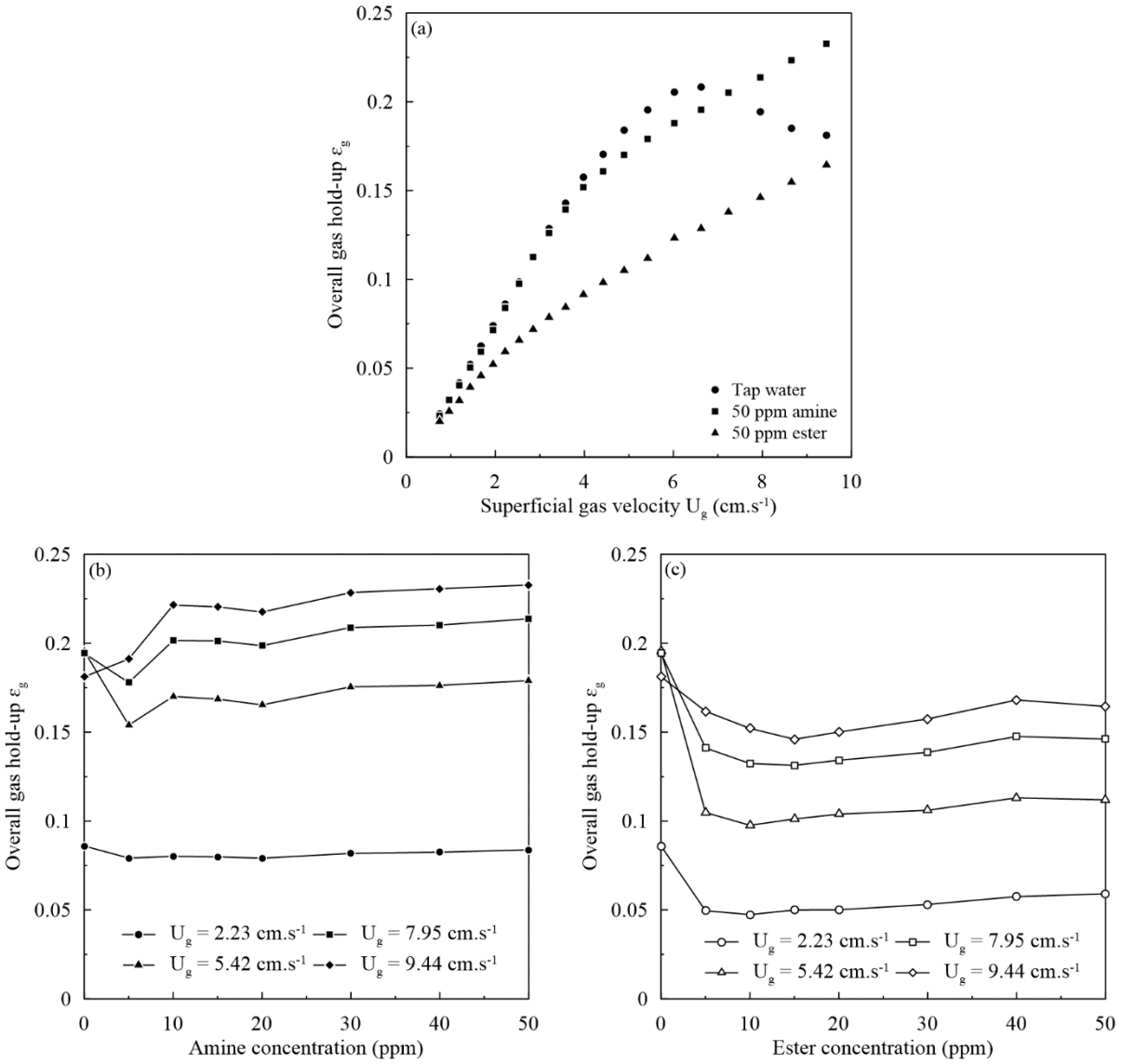


Figure 2.3Influence of the liquid phase properties on overall gas hold-up measurements (air−tap water, amine and ester aqueous solutions); (a) overall gas hold-up versus surfactant concentrations for different superficial gas velocities: (b) tap water and amine aqueous solution, and (c) tap water and ester aqueous solution.

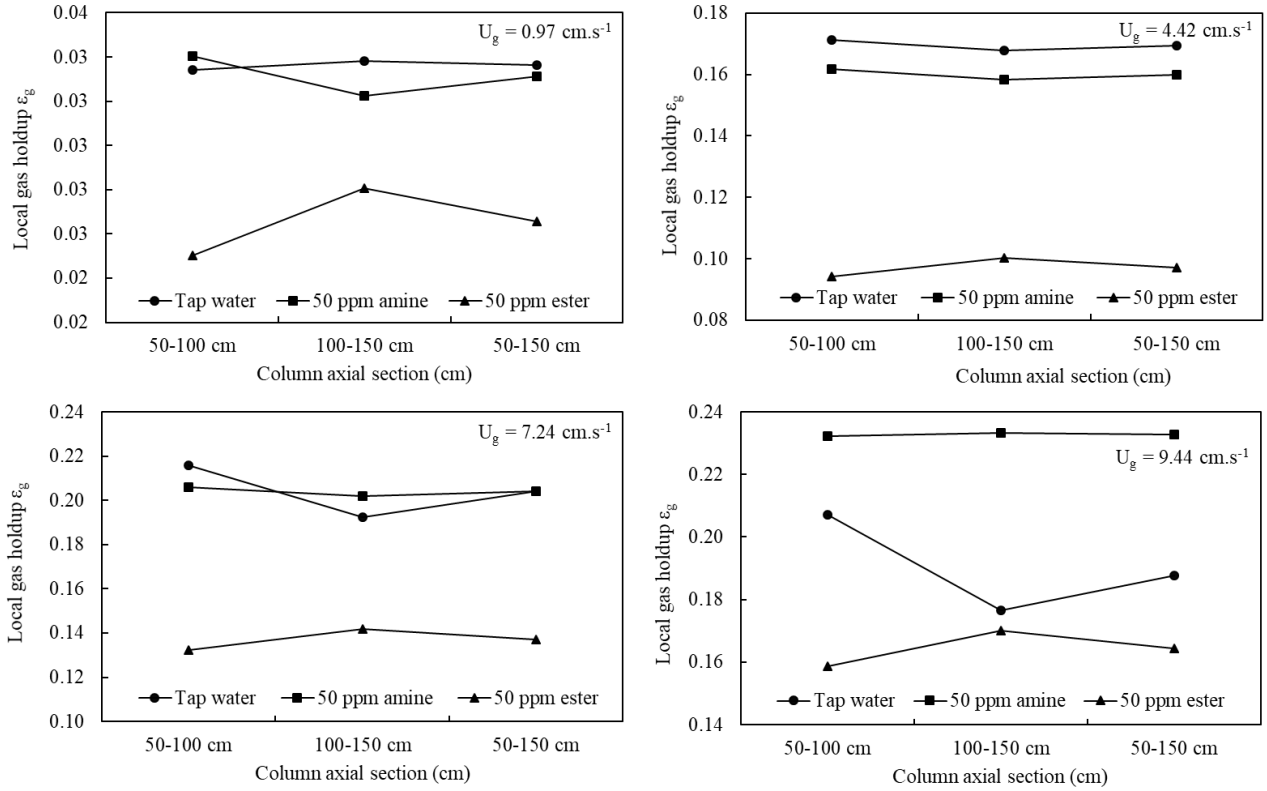


Figure 2.4 Local gas hold-up axial profiles at different superficial gas velocity.

The experimental data were compared to five correlations found in the literature (Table 1.4) to examine their validity in this case. Figure 2.5 depicts the comparison between experimental and predicted $\varepsilon_g$ for tap water and surfactant aqueous solutions. For the case of tap water (Figure 2.5(a)), most correlations were approximately able to predict $\varepsilon_g$ in the homogeneous regime, but then the $\varepsilon_g$ was overpredicted for $U_g > 2$ cm.s$^{-1}$. Whereas, the correlations by Kumar et al. (1976) and Hikita and Kikukawa (1974) better predict $\varepsilon_g$, Meanwhile, these correlations overpredict $\varepsilon_g$ for both amine and ester aqueous solutions (50 ppm), which means that it is unable to predict the effect of liquid phase properties on gas hold-up through these correlations (Figures 2.5b and 2.5c). However, for amine aqueous solution (50 ppm) and at all $U_g$, the correlation suggested by Hughmark (1967) better predicts $\varepsilon_g$ than other correlations, while the $\varepsilon_g$ values predicted by the Reilly et al. (1986) correlation are very close to the experimental values but at high velocities (Figure 2.5b).

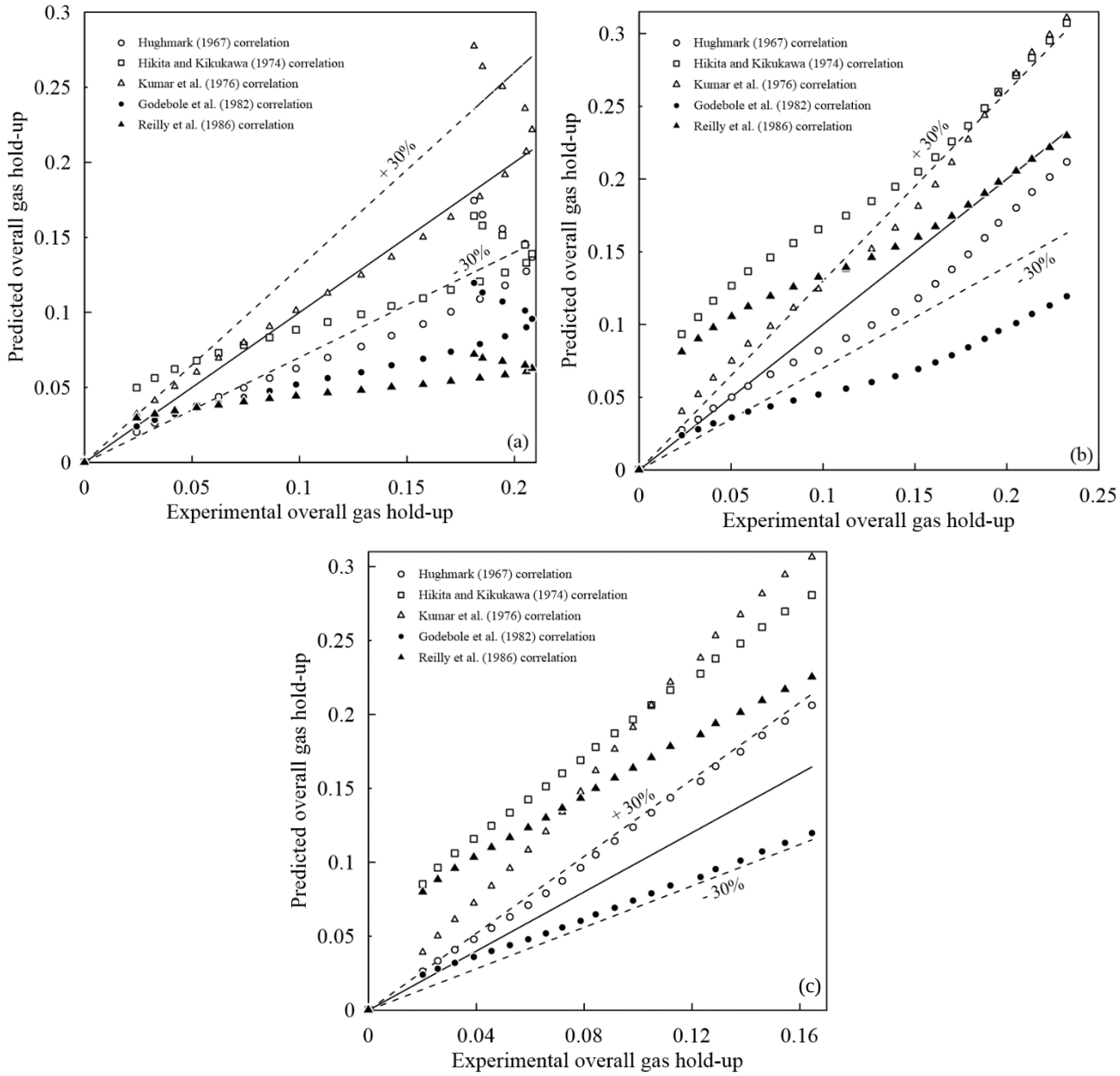


Figure 2.5 Comparison between predicted and experimental gas hold-up values for (a) tap water–air, (b) 50 ppm amine aqueous solution–air, and (c) 50 ppm ester aqueous solution–air (dash lines correspond to ± 30% error).

Concerning the flow regime, it is clear from Figure 2.3a that up to 4.42 $cm.s^{-1}$, the relationship between $\varepsilon_g$ and $U_g$ is linear for air−tap water or air−tap water−amine, which means that amine concentration has no effect on $\varepsilon_g$ in this range of superficial gas velocity. However, the gas hold-up is influenced by the type of gas distributor used which mostly generates gas bubbles with a diameter of around 1 mm. The linearity of the curve thus shows that the homogeneous regime prevails at $U_g$ less than 4.4 $cm.s^{-1}$. Beyond this critical gas superficial velocity, the gas hold-up keeps augmenting, but the slope is gradually reduced. This means that the transitional regime takes place. The slope and shape of the gas hold-up curve for the water-

air system are those generally found for a similar type of gas distributor used in this study (Camarasa et al., 1999). During the transition flow regime, clusters of bubbles appear and rise through the column center with lower mean residence time of the gas phase, thing that was also noticed in the literature. As for the air−water−ester system, bubble coalescence occurs even at low superficial gas velocity, leading to the onset of the heterogeneous flow regime from the beginning. Thus, large bubbles appear and rise more rapidly than the smaller ones, which reduces the overall gas hold-up. These findings are in agreement with literature data (Besagni and Inzoli, 2017; Camarasa et al., 1999; Gemello et al., 2018).

Furthermore, two different methods were utilized by several authors (Besagni and Inzoli, 2017; Gourich et al., 2006b) to detect the regime transition point: swarm velocity method and the drift flux model. The first one was developed by Zuber and Findlay (Zuber and Findlay, 1965) and based on the swarm velocity:

$$U_{swarm} = \frac{U_g}{\varepsilon_g} \tag{2.7}$$

The swarm velocity $U_{swarm}$ is plotted against the superficial gas velocity. $U_{swarm}$ remains constant in the homogeneous regime but starts to augment when the system reaches the heterogeneous regime. Indeed, the sudden increase of the swarm velocity; which is due to the occurrence of the first large bubble; is a sign of the flow regime transition.

The second method to determine the transition velocity was the drift flux model proposed by Wallis (1969). In a bubble column operated in the batch mode for the liquid phase, the drift flux is expressed as:

$$j_{gl} = U_g\left(1 - \varepsilon_g C_0\right) \tag{2.8}$$

$C_0$ is the distribution parameter which equals to 1 when the flow is radially uniform.

Assuming $C_0$ = 1 in the homogeneous flow regime, a change in the slope in the $j_{gl}=U_g\left(1-\varepsilon_g\right)$ drift flux versus $\varepsilon_g$ plot can be regarded as a transition point. Figures 2.6a and 2.6b represent the drift flux and the swarm velocity plot for all solutions. According to Figure 2.6a, a rapid change in slope was observed in the drift flux curve for the 50 ppm ester aqueous solution which corresponds to a superficial gas velocity of 2.9 $cm.s^{-1}$. Similar results have been reported in the literature in the case of viscous liquids, such as glucose, and carboxymethyl cellulose (CMC) aqueous solution (Esmaeili et al., 2015). Meanwhile, the drift flux curve of

the water–air system shows notable change at a gas hold-up of about 18 %, which confirms that the transition occurs at a superficial gas velocity of 4.42 $cm.s^{-1}$. Moreover, Figure 2.6b clearly exhibits the influence of ester addition on the flow regime by advancing the occurrence of large coalesced bubbles (Figure 2.7), which leads to a destabilization of the homogeneous flow, and therefore, the transition appears earlier and then, the heterogeneous flow regime is rapidly developed, even at relatively low ester concentration. This finally highlights that despite the adsorption of the ester collector, this does not prevent bubble coalescence.

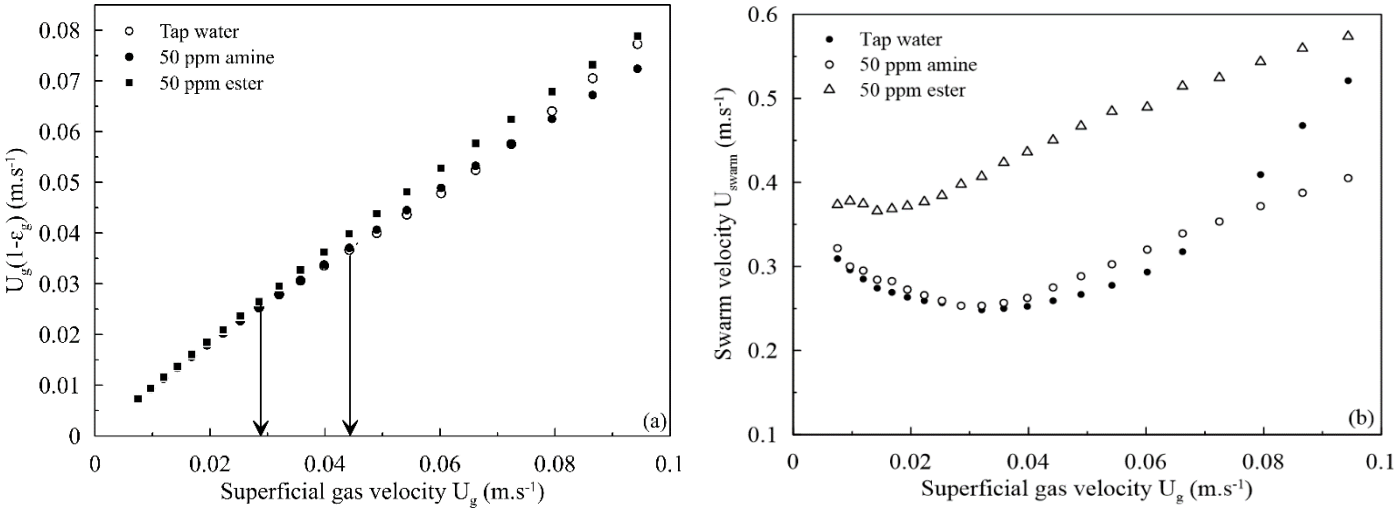


Figure 2.6 Regime transition analysis: the drift flux plot and the swarm velocity (Eq. (2.7)).

Figure 2.7 Example of bubbles using 30 ppm of ester, and $U_g$ = 2.53 $cm.s^{-1}$.

### 2.3.2 Spectral analysis of the pressure time series

In this section, the pressure time series recorded by the sensors in position 1 and 3 for tap water and surfactant aqueous solutions and different superficial gas velocities are processed. The PSD of the pressure signal is estimated on time series of 20,000 points, divided into segments of 512 points each; with an overlap of 10 % of this block length, and a Hamming window as the window function. Given that in bubble columns only phenomena with a frequency range between 0 and 20 Hz happen (Drahoš et al., 1991), the PSD curves are, therefore, plotted only in this range. Figures 2.8a, 2.8b and 2.8c exhibit the PSD for different operating solutions at three superficial gas velocities: 2.2 $cm.s^{-1}$, 5.4 $cm.s^{-1}$, and 9.4 $cm.s^{-1}$, respectively. At low superficial gas velocity ($U_g = 2.2$ $cm.s^{-1}$), and for both tap water and amine aqueous solution (50 ppm) (Figures 2.8a and 2.8b), the PSD plots show a peak at 0.1 Hz, which corresponds to the homogeneous regime. Hence, for the tap water−air system, the obtained results are in accordance with Drahoš et al. (1991) and Vial et al. (2001) who reported that the homogeneous regime was dominated by very low frequencies of the order of 0.1 Hz, corresponding to liquid level oscillations. In contrast, the PSD plot of an ester aqueous solution (Figure 2.8c) exhibits a dominant peak at a frequency of about 5.8 Hz, indicating the formation of large bubbles even at low superficial gas velocity, corresponding to frequency of the alternative upward-downward move of the bubble close to the wall. As this could have been noticed early, the addition of ester decreases the liquid turbulence and promotes bubble coalescence.

As illustrated in Figures 2.8a-c, the increase in the superficial gas velocity (5.4 $cm.s^{-1}$) is accompanied by the appearance of secondary peaks at low frequency, as well as the increase in the amplitudes of the dominant peaks. This is due to the increase in the gas throughputs by augmenting the superficial gas velocity, which leads to an increase in the coalescence rate and, subsequently, of the bubble size. Moreover, for ester aqueous solution, the dominant peak appears this time at lower frequency of about 4.2 Hz (less than that for lower $U_g$), which confirms that the bubble coalescence becomes dominant, leading to the formation of larger bubbles. On the other hand, the transition region is characterized by the presence of two peaks, as seen in the PSD plot of tap water (Figure 2.8a and at $U_g = 5.4$ $cm.s^{-1}$). At high superficial gas velocity such as 9.4 $cm.s^{-1}$ (Figures 2.8a-c), for both tap water and amine aqueous solution (50 ppm), the PSD plots show a broader peak in the range 2 – 5 Hz, which corresponds to the heterogeneous regime. In addition, the secondary peaks mentioned above are fully developed

in almost all cases, which can be caused by the existence of two different bubble populations at this high superficial gas velocity (due to the phenomena of bubble coalescence and break-up).

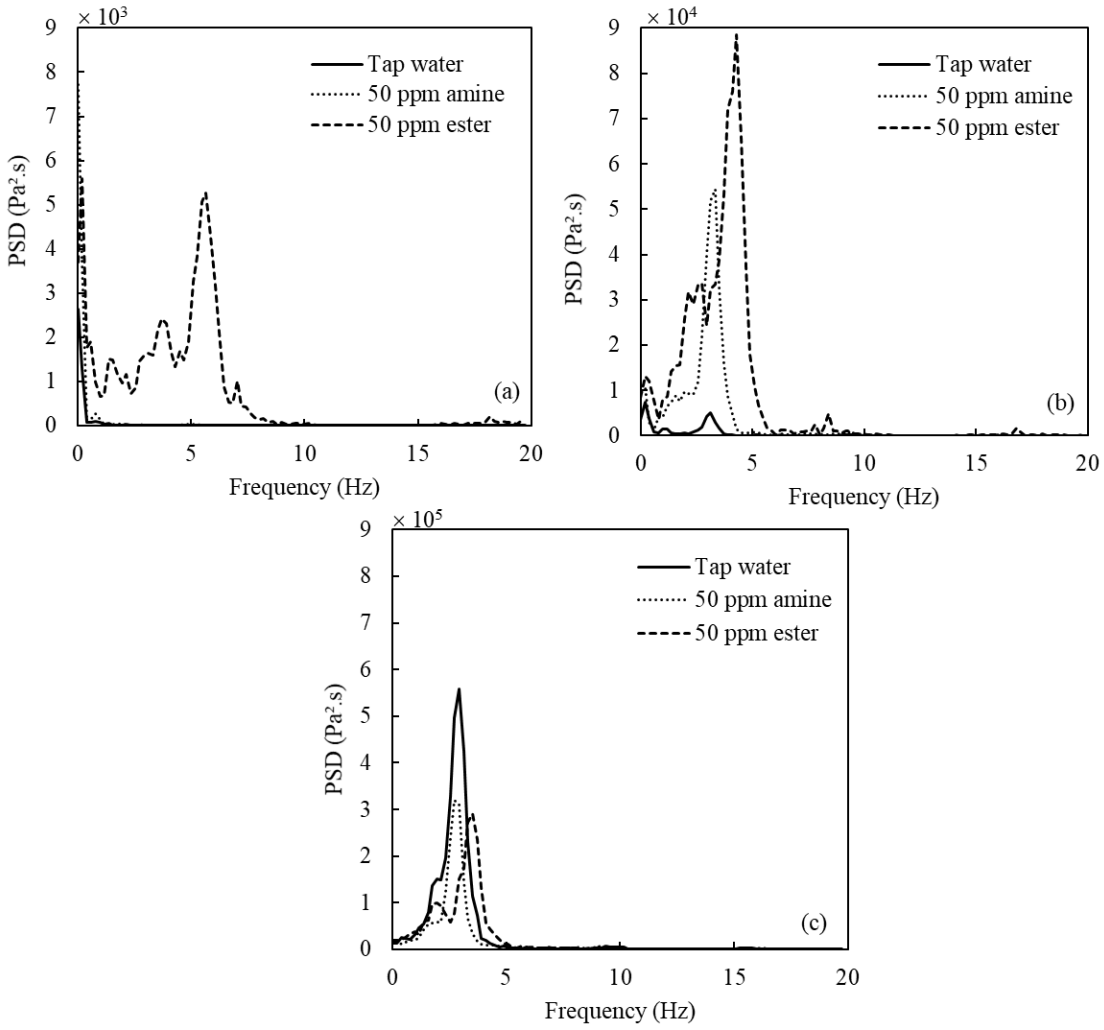


Figure 2.8 Power spectral density of the pressure time series for different operating aqueous solutions at superficial gas velocity (a) 2.23 cm.s$^{-1}$, (b) 5.42 cm.s$^{-1}$, and (c) 9.44 cm.s$^{-1}$.

The average frequency of the spectrum, $f_m$, is another valuable parameter that may provide useful information about the phenomena that occur in the bubble column. The average frequency of a spectrum is given as:

$$f_m = \frac{\int [P_{xx}(f)] f df}{\int [P_{xx}(f)] df} \tag{2.9}$$

where $P_{xx}(f)$ is the average power spectral density (Pa$^2$.s). The average frequency versus superficial gas velocity for tap water and surfactant aqueous solutions is plotted in Figure 2.9. This shows that the average frequency $f_m$ increases by rising the gas velocity. In fact, the

average frequency is close to 0 in the homogeneous regime, whereas it is between 3 and 5 Hz in the heterogeneous regime.

In conclusion, the findings derived from the power spectral density of the pressure time series are in good agreement with those obtained by other measuring techniques in this study.

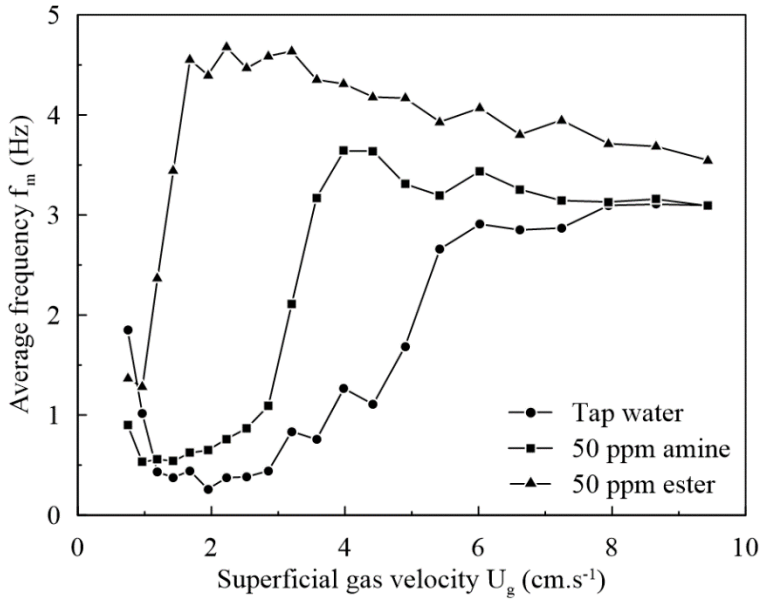


Figure 2.9 Average frequency of the spectrum versus superficial gas velocity for tap water and surfactant aqueous solutions.

### 2.3.3 Gas−liquid mass transfer performance in bubble column

After identifying the different flow regimes from the evolution of the gas fraction and the analysis of pressure time series, the volumetric mass transfer coefficient has still to be measured, as it both results from bubble size and it assesses the role of surface-active agents at the gas−liquid interface. Figure 2.10 represents the temporal variation of dissolved oxygen concentration in tap water and surfactant aqueous solutions at a concentration of 50 ppm and a superficial gas velocity of 2.2 cm.s$^{-1}$. From this figure, it can be deduced that the mass transfer rate in tap water was greater than surfactant aqueous solutions, especially at the initial stage. This proves that the liquid phase properties have a significant effect on the gas−liquid mass transfer performance.

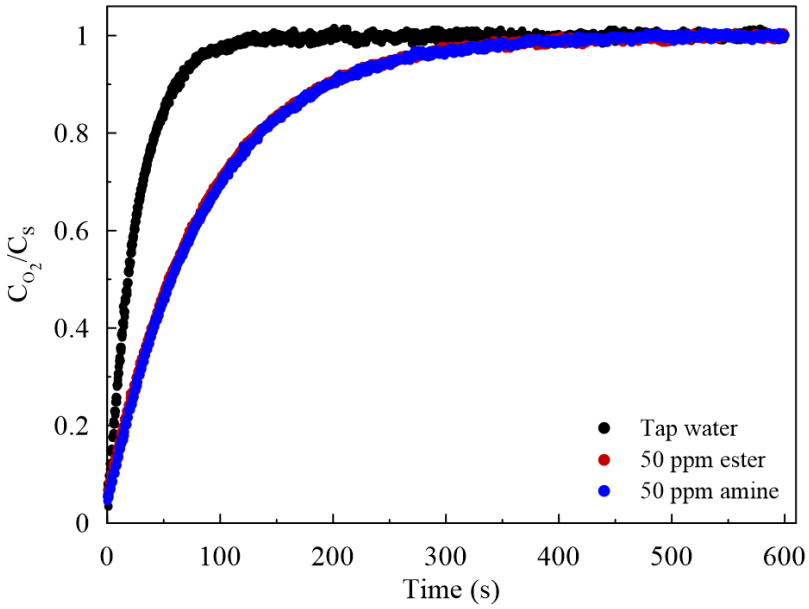


Figure 2.10 Temporal variation of dissolved oxygen curves in tap water and collector aqueous solutions.

As is well known, the volumetric mass transfer coefficient is strongly dependent on the superficial gas velocity (Figure 2.11). Therefore, for all operating conditions, $k_La_L$ increased with superficial gas velocity. In fact, as mentioned by Dong et al. (2019), with the increase in $U_g$, the number of bubbles in the liquid phase raised and the turbulence induced by the rising bubbles was enhanced, which allowed to drastically increase the gas−liquid contact area and subsequently improve the performance of the gas−liquid mass transfer. This is due to the fact that any surface-active agent, as the amine or the ester, reduced surface tension (Table 2.2). However, adsorbed species are also known to induce an additional interfacial resistance to mass transfer, especially when a saturated interface which creates an additional interfacial resistance to mass transfer; small bubbles behave with rigid interfaces, resulting in a lower mass transfer coefficient. Thus, by reducing the surface tension, adsorbed surfactants influence the gas−liquid interface as well as the gas−liquid mass transfer.

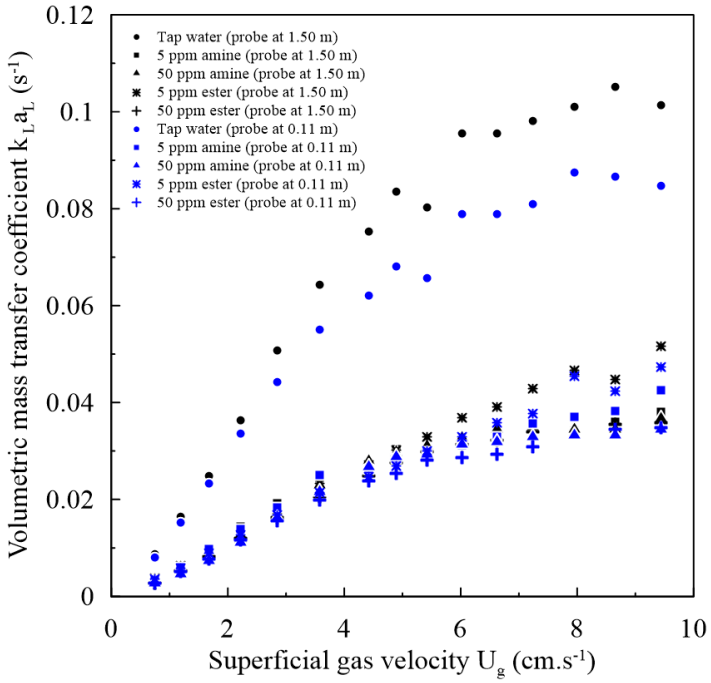


Figure 2.11 Volumetric mass transfer coefficient $k_La_L$ versus the superficial gas velocity for tap water and surfactant aqueous solutions.

Figure 2.11 shows the evolution of volumetric mass transfer coefficient $k_La_L$ depending on the superficial gas velocity for tap water and surfactant aqueous solutions under different concentrations. In this figure, $k_La_L$ in tap water was higher than in amine and ester aqueous solutions, which means that these two surfactants have a large effect on gas−liquid mass transfer. Furthermore, for both types of surface-active agent, the volumetric mass transfer coefficient decreased slightly with increasing surfactant concentration from 5 ppm to 50 ppm, except for the case of high superficial gas velocities ($\geq 6.02$ $cm.s^{-1}$) where $k_La_L$ at 50 ppm was distinctly lower from that at 5 ppm. This slight effect of surfactant concentration was also shown in the case of gas hold-up (Figure 2.3). According to Nock et al. (2016), when attaching to a bubble, the surface flow around the bubble redistributes the surfactants to the base of the bubble, producing a surface tension gradient and a Marangoni effect. Indeed, the decrease in the surface tension can reduce the internal circulation within a bubble, which increases the drag force and decreases the rise velocity, and then causes a decrease in $k_L$. In contrast, as the diameter of the bubble was larger in aqueous ester solutions, the increase in the gas−liquid contact area with the superficial gas velocity was limited. Hence, the reinforcing effect of the increase in the superficial gas velocity on the volumetric mass transfer coefficient of oxygen in surfactant aqueous solutions was attenuated.

Besides the liquid phase properties, other parameters influence the volumetric mass transfer coefficient estimation: namely, the operating conditions, and the geometrical parameters of the bubble column, but also the position of the oxygen sensor. Actually, there are two main cases reported in the literature; the oxygen sensor placed either at 5 cm to 10 cm from the gas distributor (Vandu and Krishna, 2004), or far from the gas sparger (Dong et al., 2019). Figures 2.12a and 2.12b illustrate the change of volumetric mass transfer coefficient with the variation of oxygen sensor position for tap water and the ester aqueous solution. In these figures, the volumetric mass transfer coefficient obtained at 0.11 m from the gas sparger was lower than those obtained at 1.50 m. This can be explained by the fact that in the area close to the gas distributor (11 cm), $k_La_L$ is measured in the region where the primary gas distribution predominates, which can widely differ from the bubble size distribution in the bulk particularly for ester aqueous solution where coalescence occurred easily; this means that the bubble size distribution changed above the first 0.11 m close to the sparger. However, when the probe is far from the sparger, there may be a time lag between the change in gas composition and the start of the effective measurement at the probe level (Gourich et al., 2008). For these reasons, Shioya and Dunn (1978) suggested that the oxygen sensor should be placed at liquid mid-height in bubble columns.

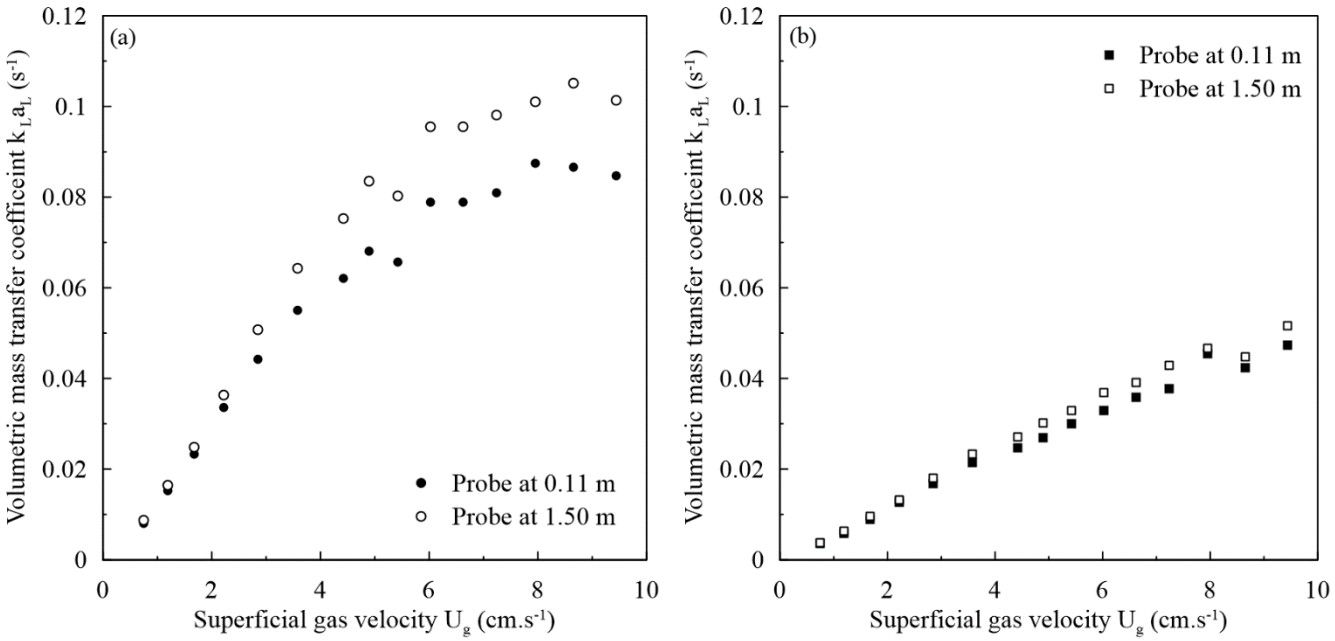


Figure 2.12 Effect of the oxygen sensor position on the volumetric mass transfer coefficient $k_La_L$ ((a) tap water−air, and (b) 5 ppm ester−tap water−air).

According to Chisti (1989), the volumetric mass transfer coefficient ($k_L a_L$), the gas hold-up ($\varepsilon_g$), the mean bubble diameter ($d_B$) and the mass transfer coefficient ($k_L$) are known to be linked by Eq. (2.10):

$$\frac{k_L}{d_B} = k_L a_L \frac{(1-\varepsilon_g)}{6\varepsilon_g} \tag{2.10}$$

For the air-water and air-water-surfactant systems, the calculation of the $\frac{k_L}{d_B}$ ratio from the measured $k_L a_L$ and $\varepsilon_g$ is illustrated in Figure 2.13. As shown in this figure, the plot of $k_L a_L$ against $\frac{6\varepsilon_g}{(1-\varepsilon_g)}$ is nearly linear until a superficial gas velocity of 4.90 cm.s$^{-1}$ and for a value of $\frac{6\varepsilon_g}{(1-\varepsilon_g)}$ equals to 1.4, which matches with the transition flow regime. Then the $\frac{k_L}{d_B}$ ratio (corresponding to the slope of the curve) is constant and has a value of around 0.063 s$^{-1}$. The values of $\frac{k_L}{d_B}$ for each liquid phase have been summarized in Table 2.3.

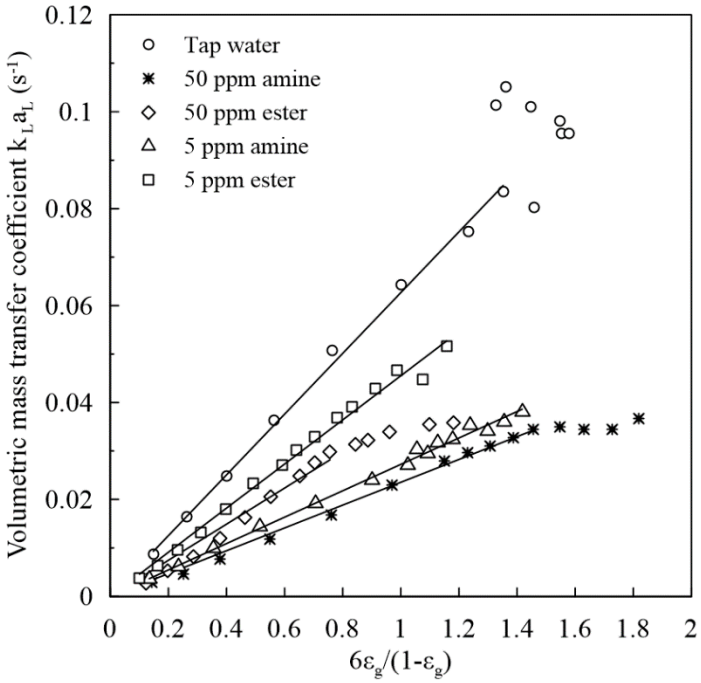


Figure 2.13 Correlation of the measured $k_L a_L$ and gas hold-up $\varepsilon_g$ according to Eq. (2.10).

In the presence of surfactants, the $\frac{k_L}{d_B}$ ratio becomes lower compared to that in tap water and it is even lower for the ester solutions than for the amine solutions. Concerning the ester aqueous solutions, data from image analysis highlight that the mean bubble size is smaller than in tap water at low ester content (5 ppm), but also that the mean bubble diameter becomes higher and the bubble size distribution wider than in tap water when ester concentration increases. For the

ester, the comparison to tap water in Table 2.3 confirms, first, that the decrease in $\frac{k_L}{d_B}$ ratio against that of tap water is due to sharp decrease in $k_L$ at low ester concentration, and then, that this decrease is enhanced by an increase in bubble size at higher ester content. Conversely, for the cationic amine aqueous solutions, bubble diameter is nearly independent from the amine content and always smaller than in tap water, which should lead to an enhancement in the $\frac{k_L}{d_B}$ ratio; but it is not the case, and this trend proves a sharp decrease in $k_L$. The strong decrease in $k_L$ observed with both collectors can be attributed to the resulting adsorbed layer which induces a strong additional interfacial resistance to gas−liquid mass transfer by rigidifying the air-water interface.

Table 2.3 Comparison of $k_L/d_B$ ratio for tap water and surfactant aqueous solutions.

| System | $k_L/d_B$ ($s^{-1}$) |
|---|---|
| Air-tap water | 0.063; $R^2$ = 99.67 |
| Air-tap water-5 ppm amine | 0.027; $R^2$ = 99.42 |
| Air-tap water-50 ppm amine | 0.024; $R^2$ = 99.48 |
| Air-tap water-5 ppm ester | 0.046; $R^2$ = 99.01 |
| Air-tap water-50 ppm ester | 0.037; $R^2$ = 97.04 |

## 2.4 Conclusions

The present chapter experimentally investigates the effects of the liquid surface tension, by using organic collectors as surface-active agents, on hydrodynamics (gas hold-up and flow regimes) and mass transfer ($k_La_L$) within a two-phase bubble column. The prominent results are outlined as follows:

- The addition of ester liquid leads to a decrease in gas hold-up due to primary bubble coalescence phenomena. Meanwhile, the gas hold-up has been shown to increase for amine aqueous solutions at superficial gas velocity higher than 7.24 $cm.s^{-1}$ because of foam formation.
- Spectral analysis reveals that homogeneous flow prevailed until $U_g \leq 4.4$ $cm.s^{-1}$ and was depicted by a peak at 0.1 Hz in the PSD. For ester aqueous solutions, a dominant peak at a frequency of about 5.8 Hz emerged, which indicated the formation of large bubbles even at low superficial gas velocity.
- The gas−liquid mass transfer was shown to decrease dramatically with collector addition due to surface tension decrease. Taking into account that, the apparent decrease in $k_La_L$ can

be explained by a strong decrease in $k_L$ values due to the presence of surfactant, which has been proved by the study of the $\frac{k_L}{d_B}$ ratio and the bubble size diameter, but this effect is reinforced in the case of the ester solutions by an increase in bubble size when ester concentration is increased.

It can be said that the present work is only a preliminary study focusing on the gas−liquid flow in flotation wastewaters treatment, but it however provides significant information on the possible specific effect of remnant additive residues at the bubble interface in subsequent treatments involving bubbly two-phase flows. So, the perspectives include, first, the experimental analysis of gas−liquid-solid flow by adding solid particles on the one hand, and the modeling of gas−liquid and gas−liquid-solid flows by tools such as Computational Fluid Dynamics (CFD) on the other hand.

# Chapter 3: Experimental investigation on Manganese(II) removal from drinking water by aeration process in in pneumatically agitated reactors


## Abstract

The aim of this study is the mitigation of soluble manganese Mn(II) from drinking water by aeration process using pneumatically agitated reactors including square bubble column and split-rectangular airlift reactor operating in semi-batch conditions. The effects of operating conditions such as aeration flow rate, initial pH, Mn(II) concentrations, and amount of $MnO_2$ particles on the Mn(II) removal efficiency were investigated. The major findings revealed that the variation of air flow rate had no effect on Mn(II) removal yield which means that the mass transfer is not a limiting step for Mn(II) oxidation by the aeration process. Additionally, the oxidation of Mn(II) was improved when augmenting pH and initial Mn(II) concentrations and it corresponded to a kinetically-slow reaction that is strongly pH-dependent. The kinetic data showed also an autocatalytic behavior due to the oxidation of Mn(II) on the $MnO_2$ surface, which allows the conversion to go to completion. Indeed, this behavior was confirmed by the addition of $MnO_2$ fine particles that led to a significant increase in the reaction rate. At high initial Mn(IV) concentrations, the kinetic law was shown to be pseudo-first order in Mn(II), with an apparent kinetic constant depending on the initial amount of Mn(IV) compounds. This constant was fitted by a linear model as a function of Mn(IV) concentration. Besides, it was concluded that the Mn(II) removal efficiency achieved using the airlift reactor is significantly higher than that attained using the bubble column for pH ranging from 9.2 to 9.8 with an energy consumption 2.44 times lower than that required in the bubble column reactor. Besides, the chemical characterization revealed that the increase in pH from 9.2 to 10 led to an alteration in crystallographic structure, morphology, shape, and size of obtained manganese oxides. Eventually, compared to other techniques, aeration is an efficient process because it gives us a removal efficiency of 90 % in less than 40 min at pH 9.5 and initial soluble Mn(II)and insoluble Mn(IV) concentrations between 5 and 20 and 0 – 500 $mg.L^{-1}$, respectively, while avoiding the drawbacks of strong oxidizers and biological oxidation processes.



**Keywords:** Airlift reactor; Bubble column; Aeration process; Manganese(II) removal; Drinking water; Autocatalytic mechanism; Precipitate characterization.

## 3.1 Introduction

As the world's population is continuing to swell, most of the world's available freshwater is being heavily utilized to meet the agricultural, industrial, and domestic needs of human beings (Mukhopadhyay et al., 2022). However, the sustainability and quality of surface and groundwater resources are increasingly impaired due to urban development, industrialization, anthropogenic pollution, and the natural geochemical environment (Patel et al., 2016). Therefore, the occurrence of metals in water can bring serious concerns for human health, animals, and plant growth as well as the ecosystem. Specifically, manganese (Mn) is a rich transition metal and ranked fifth in the metal abundance in the earth's crust, and can be found in both surface water as well as groundwater (Singh Thakur et al., 2022). Manganese exists generally in three oxidation states which are the divalent cation (Mn(II)) and the oxides/hydroxides consisting of Mn(III) and Mn(IV), including $MnO_2$ and MnOOH. Actually, Mn(II) is thermodynamically stable primarily in the absence of oxygen ($O_2$) (at low pH) while Mn(III) and Mn(IV) are essentially stable in the presence of oxygen ($O_2$) (at high pH) (Lanson et al., 2000). In other words, Mn(III) and Mn(IV) are prevalent under alkaline and aerobic conditions whilst Mn(II) dominates under conditions where the pH is < 6 or anaerobic.

At a specific level, manganese is considered an essential micronutrient for the health and efficient growth of various living organisms. As well, manganese depletion can cause toxicity to organisms in aquatic and terrestrial ecosystems (Nkele et al., 2022). Aesthetically, manganese contamination of water can result in discoloration of water (brownish red color), which can taint plumbing equipment and clothing, and impart an unpleasant taste or odor and metallic taste to drinking water (Aydin et al., 2000; Gerke et al., 2016; WHO, 2017). From a health aspect, consuming drinking water with abnormally high levels of manganese can cause health trouble to individuals such as "manganism". This disorder is manifested by clumsiness and slow body movements, as well as emotional and mental difficulties (Nkele et al., 2022). Moreover, (Mthombeni et al., 2016) studied the health behavior of children who are exposed to higher concentrations of manganese from the drinking water and those receiving permissible limits of manganese, and found that these children experienced health troubles in the form of degenerative brain disorders, short-term memory, altered attention, speed, manual dexterity as well as visual deficits.

To mitigate the impact of manganese exposure on humans, the World health organization (WHO, 2017) has specified that the health threshold limit for manganese in drinking water is 100 $\mu g.L^{-1}$. The Moroccan guidelines of drinking water set a recommended limit for manganese to 50 $\mu g.L^{-1}$. For this purpose, numerous techniques have been developed to remove this element from different kinds of water including physicochemical treatments by precipitation (Zhang et al., 2010), ion exchange (Kononova et al., 2019), coagulation/flocculation (Zhao et al., 2009), oxidation/ filtration using strong oxidation agents (Deborde and von Gunten, 2008; El Araby et al., 2009; Gregory and Carlson, 2001; Sallanko et al., 2005), electrochemical treatments such as electrocoagulation with aluminum electrodes (Ganesan et al., 2013; Shafaei et al., 2010), adsorption (Al-Wakeel et al., 2015; Anbia and Amirmahmoodi, 2016; Ates and Akgül, 2016; Islam et al., 2015; Khobragade and Pal, 2014), membrane processes i.e., nanofiltration (Al-Rashdi et al., 2011) and microfiltration (Ellis et al., 2000; Teng et al., 2001), and biological processes (Katsoyiannis and Zouboulis, 2004; Piazza et al., 2019). As indicated in Table 3.1, despite the inherent benefits of these techniques, they still suffer from a number of shortcomings, such as high energy consumption, high operating cost, membrane fouling, and the formation of by-products (Deborde and von Gunten, 2008; Gregory and Carlson, 2001; Sorlini et al., 2014; von Gunten, 2003)

Among the methods mentioned above, oxidation constitutes the most common method for removing manganese by using several types of stronger oxidizing agents such as chlorine dioxide ($ClO_2$), chlorine ($Cl_2$), potassium permanganate ($KMnO_4$) or ozone ($O_3$) (El Araby et al., 2009; Tobiason et al., 2016). It enables to oxidize the dissolved Mn into insoluble products (mainly $MnO_2$) that will be subsequently separated from the water by filtration. Indeed, the removal of manganese by this type of oxidant is viewed as an effective, simple, and fast method and it also helps to disinfect the water. In contrast, it is constrained due to the excessive demand for chemical products which influences the overall cost of the treatment, and the production of secondary pollution (Crini and Lichtfouse, 2019). For these reasons, the aeration process can be considered an alternative to chemical oxidation since it avoids the use of chemicals and their additional cost. As a matter of fact, aeration has proven its ability to remove ferrous iron from waters containing iron concentrations exceeding 5 $mg.L^{-1}$ (El Azher et al., 2008; Wong, 1984). El Azher et al. (2008) studied the effect of operating parameters on the elimination of ferrous iron from drinking water using iron oxidation by aeration in a split-rectangular airlift reactor. Thus, it was found that the iron

oxidation kinetics was strongly sensitive to the pH and it exhibited an autocatalytic behavior that played an important role in waters with high levels of ferrous iron, such as groundwaters (> 5 $mg.L^{-1}$). Furthermore, they concluded that the split airlift reactor was shown to be appropriate for Fe(II) removal because it offers good mixing, mass transfer, and pH control properties.

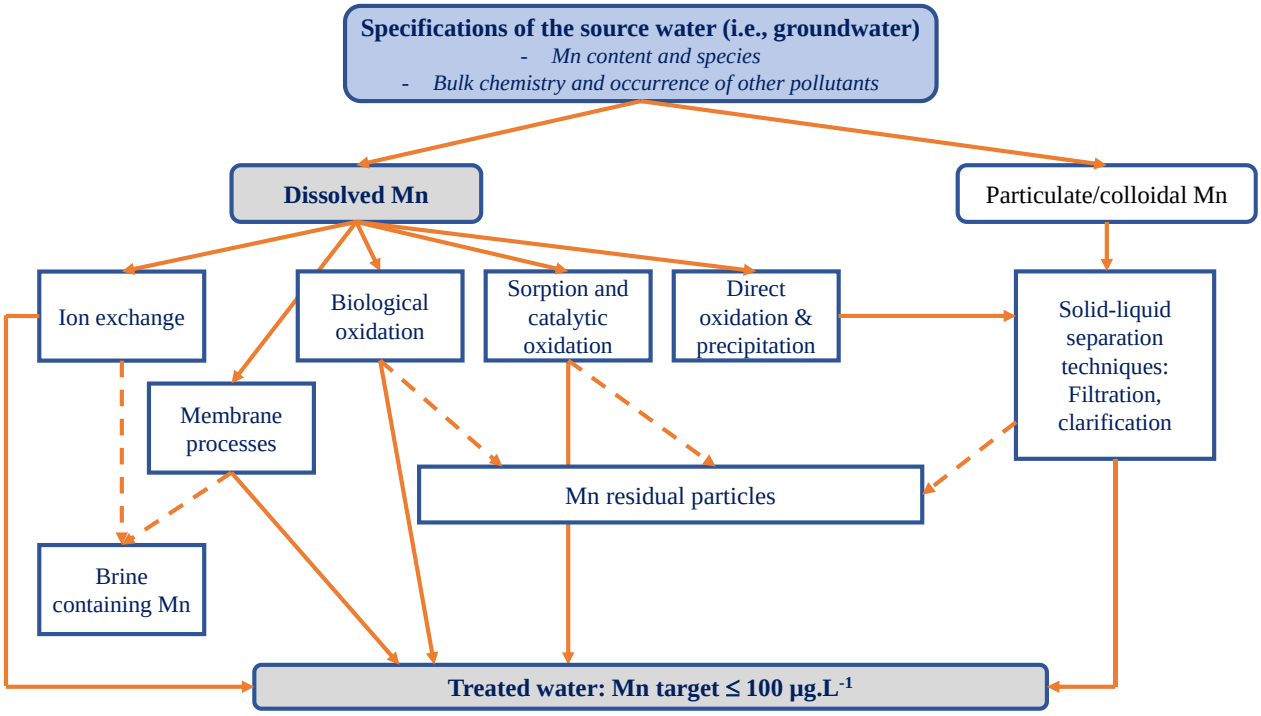


Figure 3.1 Manganese removal processes from water sources (adapted from (Tobiason et al., 2016)).

Accordingly, the present study is devoted to investigating the removal kinetics of soluble Mn(II) from potable water by oxidation with atmospheric oxygen in order to oxidize it into highly insoluble manganese compounds in a square bubble column and split-square airlift reactors. These pneumatic reactors are known for their benefits such as low operating and maintenance costs, good mixing and higher mass transfer rate as it was outlined in chapter 1. In addition, the hydrodynamic, liquid mixing, and gas−liquid mass transfer characteristics of the bubble column were described in chapter 2 while those of the airlift reactor were reported in previous work and compared with literature data and correlations (Gourich et al., 2006a, 2005). The effects of operating conditions such as the pH, superficial gas velocity, initial concentrations of soluble Mn(II), and insoluble Mn(IV) manganese forms were examined. Furthermore, the characterization of the resulting solid was thoroughly studied through the measurement of particle size distribution and semi-quantitative

chemical and morphological analyses to shed light on the mechanisms responsible for manganese removal by atmospheric oxygen from drinking waters. Besides, the applicability of the aeration process in the bubble column and the airlift reactors in terms of manganese removal was evaluated by comparing their oxidation efficiency and energy requirements. Ultimately, to evaluate the demanganization of drinking water by the aeration process in pneumatic reactors, a comparison of the removal efficiency to that of other physicochemical techniques was performed.

Table 3.1 Advantages and disadvantages of physicochemical techniques for Mn removal.

| Techniques | Advantages | Disadvantages | Refs. |
|---|---|---|---|
| Hydroxide precipitation | Simple operation, integrated physicochemical process, advantageous and economically efficient. | High pH requirement, high chemicals demand, production of voluminous sludge, and issues of sludge handling and disposal. | Crini and Lichtfouse (2019) |
| Coagulation/ flocculation | Sludge settling, dewatering characteristics, bacterial inactivation capability, and sludge stability, economically feasible and not complex, availability of a wide range of chemicals, and simplistic operation. | Require pH adjustment, high chemical dosage, and sludge generation. | Crini and Lichtfouse (2019) |
| Ion exchange | Can be regenerated without regeneration loss, simple technology, and the procedures are well tested, documented and established, easy to control. | Not all ion exchange resins are suitable for metal removal, expensive technique, only used for a trace amount of metals in water due to clogging, regeneration of resins causes secondary pollution. | Kononova et al. (2019) |
| Oxidation/ filtration | Most of the iron and manganese treatment systems employ this method. The process is proficient and fast. | Difficulty in storage and transport of the oxidant, corrosion, requires high energy, produces by-products, and requires chemicals and has limited effect on salinity. | Tobiason et al. (2016) |
| Electrocoagulation | Required low chemicals, production of less sludge. | High capital cost, high energy consumption, anodic/cathodic surface passivation. | Barrera-Díaz et al. (2018) |
| Adsorption | Adsorbents have high capacity, and they are effective. Moreover, the adsorbents are locally available and cheap. | Loss of adsorbent, limited capacity on concentrated solutions, and regeneration is very costly. Regenerants require proper disposal and recovery is not viable unless pre-concentration is pursued. | Ates (2014) |
| Membrane filtration | High efficiency, no need for chemicals, no production of solid waste, compact, simple automation. | Membrane fouling, high operational cost, low permeate flux, the production of brine that poses secondary pollution. | Tang et al. (2021) |

## 3.2 Kinetics of manganese oxidation by dissolved oxygen

Manganese dioxide is slightly soluble; in addition, its solubility varies with pH (Table 3.2). At the higher pH levels, the Mn(II) in solution is similar to the Mn(IV) solubility. In parallel, air oxidation of Mn(II) to insoluble $MnO_2$ is an extremely slow process at pH values typical of natural waters (6 – 8). Thus, to achieve a higher oxidation rate, an increase in pH is required (Hao et al., 1991).

The kinetic studies have generally shown that the oxidation of Mn(II) to Mn(IV) includes an autocatalytic mechanism in addition to a term proportional to the reduced metal ion concentration. However, some researchers have concluded that this mechanism of auto-oxidation does not take place between Mn(II) and insoluble $MnO_2$ particles at pH values below 9 (Pankow and Morgan, 1981; Stumm and Morgan, 2012). The oxidation of dissolved manganese with dissolved oxygen can be described by the following mechanism (Kessick and Morgan, 1975):

$$\mathrm{Mn(II)} + \mathrm{O_2} \overset{k_1}{\rightarrow} \mathrm{MnO_2} \tag{3.1}$$

$$\mathrm{Mn(II)} + \mathrm{MnO_2} + \mathrm{O_2} \overset{k_2}{\rightarrow} 2\mathrm{MnO_2} \tag{3.2}$$

At constant pH and under constant oxygen partial pressure, the reaction rate is therefore commonly expressed as a function of Mn(II) and Mn(IV) concentrations (Aydin et al., 2000; Kessick and Morgan, 1975):

$$r_{Mn^{2+}} = (k_1 + k_2[\mathrm{Mn(IV)}])[\mathrm{Mn(II)}] \tag{3.3}$$

However, as the reaction produces a solid phase and because autocatalysis is a heterogeneous mechanism that competes with homogeneous oxidation, a precise estimation of kinetic constants is difficult. According to (Davies and Morgan, 1989), the rate of oxidation of Mn(II) in homogeneous and heterogeneous solutions under transient conditions in a perfectly mixed tank is described by the equation below:

$$-\frac{d[\mathrm{Mn(II)}]}{dt} = k_1[\mathrm{Mn(II)}] + k_2[\mathrm{Mn(II)}][\mathrm{MnO_x}] \tag{3.4}$$

where $k_1$ and $k_2$ are the homogeneous and heterogeneous rate constants for Mn(II) oxidation, respectively.

Table 3.2 Solubility of $MnO_2$ as a function of pH.

| pH | Solubility of $MnO_2$ ($mg.L^{-1}$) |
|---|---|
| 2.1 | 1.3 |
| 3.0 | 0.9 |
| 5.4 | 0.5 |
| 6.9 | 0.1 |
| 7.0 | 0.1 |
| 8.4 | 0.3 |
| 8.7 | 0.02 |
| 10.2 | 0.1 |
| 10.6 | 0.2 |

## 3.3 Materials and methods

### 3.3.1 Reagents

Manganese sulfate monohydrate ($MnSO_4.H_2O \geq 99$ %), sodium hydroxide ($NaOH \geq 98$ %), and sulfuric acid ($H_2SO_4$, 95 % – 97 %) used in this investigation were supplied from Merck (Germany) and used without any further purification. Actually, manganese sulfate was selected since sulfate anions are a common constituent of most groundwater. Mn(II) stock solution was prepared by dissolving manganese sulfate monohydrate in tap water (the properties of which are reported in Table 3.3). Distilled water was used to dissolve NaOH for preparing an alkaline medium (1 N), and to dilute sulfuric acid to obtain an acidic solution (1 N) for pH adjustment during oxidation assays.

Table 3.3 Tap water properties.

| pH | 7.85 |
|---|---|
| Alkalinity (°f) | 15 |
| Total hardness (°f) | 35 |
| Turbidity (NTU) | 0.15 |
| Conductivity ($\mu S.cm^{-1}$) | 1600 (20 °C) |
| Chloride [$Cl^-$] ($mg.L^{-1}$) | 392 |

### 3.3.2 Experimental setup and procedure

As previously outlined, the oxidation of dissolved manganese was investigated in both square BC column and split ARL reactors made of Plexiglas.

The split-square ARL consisted of a square column (20 cm × 20 cm) with 2 m in total height, divided into a riser and a downcomer by a Plexiglas baffle with 0.204 m in width, 0.006 m in thickness, and 1.30 m in total height. The riser-to-downcomer cross-sectional area ratio was equal to 1. The baffle was located at a distance of 0.115 m from the bottom of the reactor. The gas-free liquid height was about 1.59 m. The gas distributor was situated at the bottom of the riser and was a single orifice of 3.5 mm in diameter. Compressed air was injected into the reactor and controlled using calibrated rotameters (model 1355, Emerson Brooks, UK). The reactor volume was approximately 63 L. A schematic diagram of the experimental setup for this work is shown in Figure 3.2. As for the experimental apparatus of the square BC, it is the one illustrated in Figure 2.1 and has been already described in sub-section 2.2.1 of chapter 2.

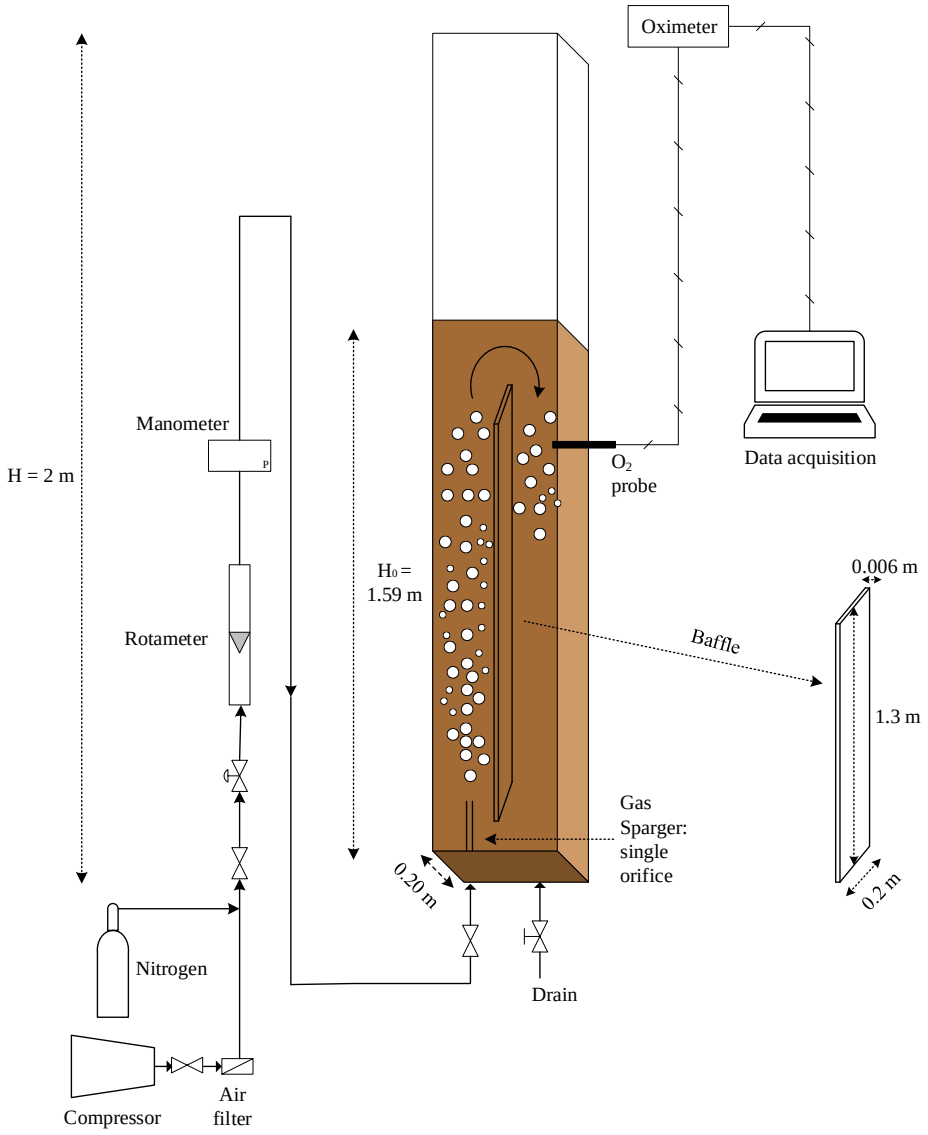


Figure 3.2 Schematic diagram of the experimental setup.

All experiments were carried out in semi-batch flow conditions and at a temperature of 25 ºC. During experimental runs, pH and dissolved oxygen were monitored over time. The pH of the medium was measured using a pH-meter (pH197i, WTW, Germany) and maintained constant by controlled additions of 1 N NaOH and 1 N $H_2SO_4$ aqueous solutions. The dissolved-oxygen levels were recorded using a DO-meter (OXI197i, WTW, Germany). All sensors were connected to a data acquisition system. The influence of operating parameters such as pH ranging from 9.2 to 10, gas flow rate ($Q_{air}$) from 1.07 $m^3.h^{-1}$ to 3.21 $m^3.h^{-1}$, and initial Mn(II) concentration varied from 5 $mg.L^{-1}$ to 20 $mg.L^{-1}$ was examined. Indeed, it was opted to vary the initial Mn(II) concentration within this interval as the highest Mn(II) concentration found in Moroccan groundwater is 20 $mg.L^{-1}$. In addition, for investigating the autocatalytic effect of insoluble manganese dioxide, commercial $MnO_2$ particles (~ 85 %, < 10 µm, Honeywell Fluka) were added to the liquid phase with a concentration ($[MnO_2]_0$) between 0 $mg.L^{-1}$ and 500 $mg.L^{-1}$.

### 3.3.3 Analytical methods

For the measurements of residual Mn(II) concentration, 20 mL of solution samples were collected as a function of time. Each sample was filtered through a 0.45 µm syringe filter and acidified with 1 mL of a 15 % $H_2SO_4$ aqueous solution to limit further oxidation and stored for subsequent analysis. The initial and residual concentrations of Mn(II) were analyzed using calibrated atomic absorption spectrophotometer (PinAAcle 900T, Perkin Elmer, USA).

The removal efficiency of manganese ions from tap water was calculated using the following equation (Eq. (3.5)):

$$\text{Mn(II) removal} = \frac{[\text{Mn(II)}]_0 - [\text{Mn(II)}]_{\text{resid}}}{[\text{Mn(II)}]_0} \quad (3.5)$$

where $[Mn(II)]_0$ ($mg.L^{-1}$) and $[Mn(II)]_{resid}$ ($mg.L^{-1}$) are the initial manganese concentration and that remaining after the oxidation reaction at a given time, respectively.

Once each experiment was accomplished, the solution in the reactor was filtered and the resulting precipitate was collected, rinsed with deionized water, and dried. The precipitates were then analyzed using X-ray diffraction (XRD) conducted with a Bruker D8 Discover diffractometer ($Cu - K\alpha$ radiation, $\lambda$ = 1.5406 Å, 30 kV and 10 mA). The instrument was configured for scanning in the range of 5° to 80° at $2\theta$. The software "X'PertHigh score" was employed for data processing. The Fourier-transform infrared spectroscopy (FTIR) spectra

were measured using a Shimadzu IRAffinity-S1 spectrometer with 4 $cm^{-1}$ resolution in a wavelength range of 500 $cm^{-1}$ to 4000 $cm^{-1}$. Samples were mixed with KBr and pressed into a 1 mm thick pellet. Scanning Electron Microscope (SEM) imaging was performed with JEOL JSM-IT500HR and elemental composition of the precipitate was carried out with Energy Dispersive X-ray Spectrometer (EDS) (JEOL Ex-74600U4L2Q detector enclosed with JSM-IT500HR).

## 3.4 Results and discussion

### 3.4.1 Influence of operating parameters on Mn(II) oxidation by aeration

#### *3.4.1.1 Effect of gas flow rate*

Figure 3.3 depicts the evolution of the normalized Mn(II) concentration with time for different gas flow rates ranging from 1.07 $m^3.h^{-1}$ to 3.21 $m^3.h^{-1}$ in bubble column. From this figure, regardless of the gas flow rate, it is clear that the Mn(II) concentration decreased with increasing time. However, augmenting the flow rate had no remarkable effect on the manganese removal efficiency. In fact, the flow rate increase from 1.07 $m^3.h^{-1}$ to 3.21 $m^3.h^{-1}$ led to a slight improvement in Mn(II) removal efficiency from 85.47 % to 92.55 %. Furthermore, during the experiments, it was observed that the dissolved oxygen concentration remained constant throughout the experiments and its average value was quite approximate to that of the oxygen solubility. Therefore, it can be said that oxygen mass transfer is not a limiting step for manganese oxidation by aeration. Besides, the calculation of the dimensionless Hatta number using the following equation (Eq. (3.6)):

$$\mathrm{Ha} = \frac{\sqrt{r_{Mn^{2+}} D_{O_2}}}{k_L \sqrt{C^*}} \tag{3.6}$$

where $[Mn(II)]_0 = 10\ mg.L^{-1}$, $D_{O_2} = 2 \times 10^{-9}\ m^2.s^{-1}$ is the oxygen diffusivity at 20 °C, and using Eq. (3.3) for calculating the maximum kinetic rate $r_{Mn^{2+}}$ ($mg.L^{-1}.s^{-1}$), $C^*$ is the oxygen solubility ($mg.L^{-1}$), and $k_L \approx 4 \times 10^{-4}\ m.s^{-1}$ is the mass transfer coefficient. It was found that the Ha number was always lower than 0.01 for Mn(II) oxidation in bubble column and airlift reactors, which corresponds to kinetically-slow gas−liquid reactions in the film (Ha < 0.3), which implies that the reaction occurs mainly in the liquid bulk.

For the sake of simplicity, the experimental results of the evolution of the residual Mn(II) concentration as a function of the gas flow rate in the case of carrying out the reaction in the

airlift were not shown. Moreover, the previous work of El Azher et al. (2008) proved that the variation of the gas flow rate had no effect on iron removal by aeration in the same ARL reactor.

Therefore, since they gave similar specific energy input (~ 164 $W.m^{-3}$), superficial gas velocities of 0.033 $m.s^{-1}$ ($Q_{air}$ = 2.38 $m^3.h^{-1}$) and 0.017 $m.s^{-1}$ ($Q_{air}$ = 2.42 $m^3.h^{-1}$) were selected to perform all experiments in ARL and BC reactors, respectively.

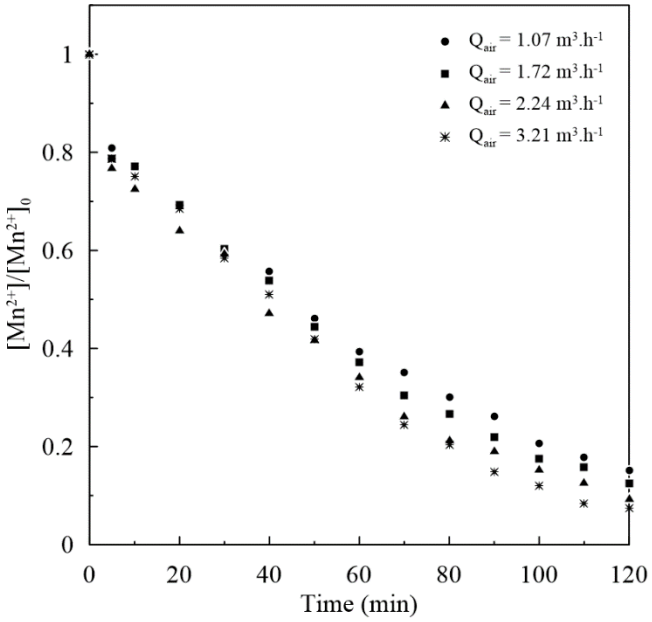


Figure 3.3 Effect of gas flow rate on Mn(II) oxidation in bubble column at pH 9.5 and [Mn(II)] = 10 $mg.L^{-1}$.

### *3.4.1.2 Effect of pH*

pH is one of the pivotal parameters for the oxidation of Mn(II) by the aeration process. Figure 3.4 displays the evolution of the normalized Mn(II) concentration as a function of time for different pH values ranging from 9.2 to 10. According to this figure, the oxidation of Mn(II) using atmospheric oxygen in pneumatic reactors is strongly favored at pH > 9.2. Indeed, it is obvious that the increase in pH from 9.2 to 10 induced an improvement of the Mn(II) removal efficiency from 52.31 % to 99.82 % and from 36.05 % to 98.03 % for a reaction time set to 40 min, for the airlift and the bubble column cases, respectively (figures 3.4a and 3.4c). Moreover, the slight increment in the pH resulted in a shortening of the reaction time. For instance, the time required to reach an Mn(II) removal efficiency of 90 % in the BC reactor decreased significantly from 119 min to 25 min by augmenting the pH from 9.5 to 10.

Besides, it can also be noticed that the Mn(II) removal effectiveness achieved by the airlift aeration process was higher than that by the bubble column. Indeed, for a reaction time of 40 min, the yield obtained in the ARL reactor was 98.66 % while that in the BC was 71.64 % for

a pH of 9.8. Therefore, to reach Mn(II) removal yield levels equal to or higher than those obtained with the airlift reactor, it was necessary to increase the reaction time to 120 min.

Figures 3.4b and 3.4d show that the evolution of the normalized Mn(II) concentration with time followed an exponential decrease and can be considered a first-order mechanism if one neglected the initial part of the curves corresponding to the mixing time (Gourich et al., 2006a). By fitting experimental data to Eq. (3.4), the rate constant $k_1$ values were determined from the slopes of lines in Figure 3.4b. Consequently, Figure 3.5 depicts the plot of k versus the hydroxide anion concentration and indicates that the rate constant k is proportional to $[OH^-]^2$.

Table 3.4 Average k values in the homogeneous systems.

| pH | $[OH^-]$ (mol.L$^{-1}$) | $[Mn(II)]_0$ (mg.L$^{-1}$) | ARL reactor | |
|---|---|---|---|---|
| | | | $k_1$ (min$^{-1}$) | $R^2$ |
| 9.2 | $1.584 \times 10^{-5}$ | 10 | 0.017 ± 0.002 | 0.9824 |
| 9.5 | $3.162 \times 10^{-5}$ | 10 | 0.038 ± 0.001 | 0.9946 |
| 9.8 | $6.309 \times 10^{-5}$ | 10 | 0.070 ± 0.006 | 0.9957 |
| 10 | $1.000 \times 10^{-4}$ | 10 | 0.102 ± 0.015 | 0.9815 |
| 9.5 | $3.162 \times 10^{-5}$ | 5 | 0.028 ± 0.008 | 0.9902 |
| 9.5 | $3.162 \times 10^{-5}$ | 10 | 0.038 ± 0.001 | 0.9946 |
| 9.5 | $3.162 \times 10^{-5}$ | 15 | 0.055 ± 0.003 | 0.9817 |
| 9.5 | $3.162 \times 10^{-5}$ | 20 | 0.079 ± 0.002 | 0.9871 |

For pH ≥ 9.8, an increase in the reaction rate after 10 min was noticed. This trend appeared when [Mn(II)] is about 3 mg.L$^{-1}$, which corresponds to an insoluble $MnO_2$ concentration of about 5 mg.L$^{-1}$, and means that the amount of insoluble $MnO_2$ increased with the pH. Indeed, it can be concluded that the autocatalytic effect became significant and therefore the removal efficiency of soluble Mn(II) increased with increasing pH (Aydin et al., 2000; Kessick and Morgan, 1975). In other words, at a higher concentration of $OH^-$, it was found that the oxidation of Mn(II) occurred rapidly (Table 3.4). Figure 3.5 which highlights a homogeneous reaction mechanism close to the first-order kinetics with respect to the $OH^-$ anions.

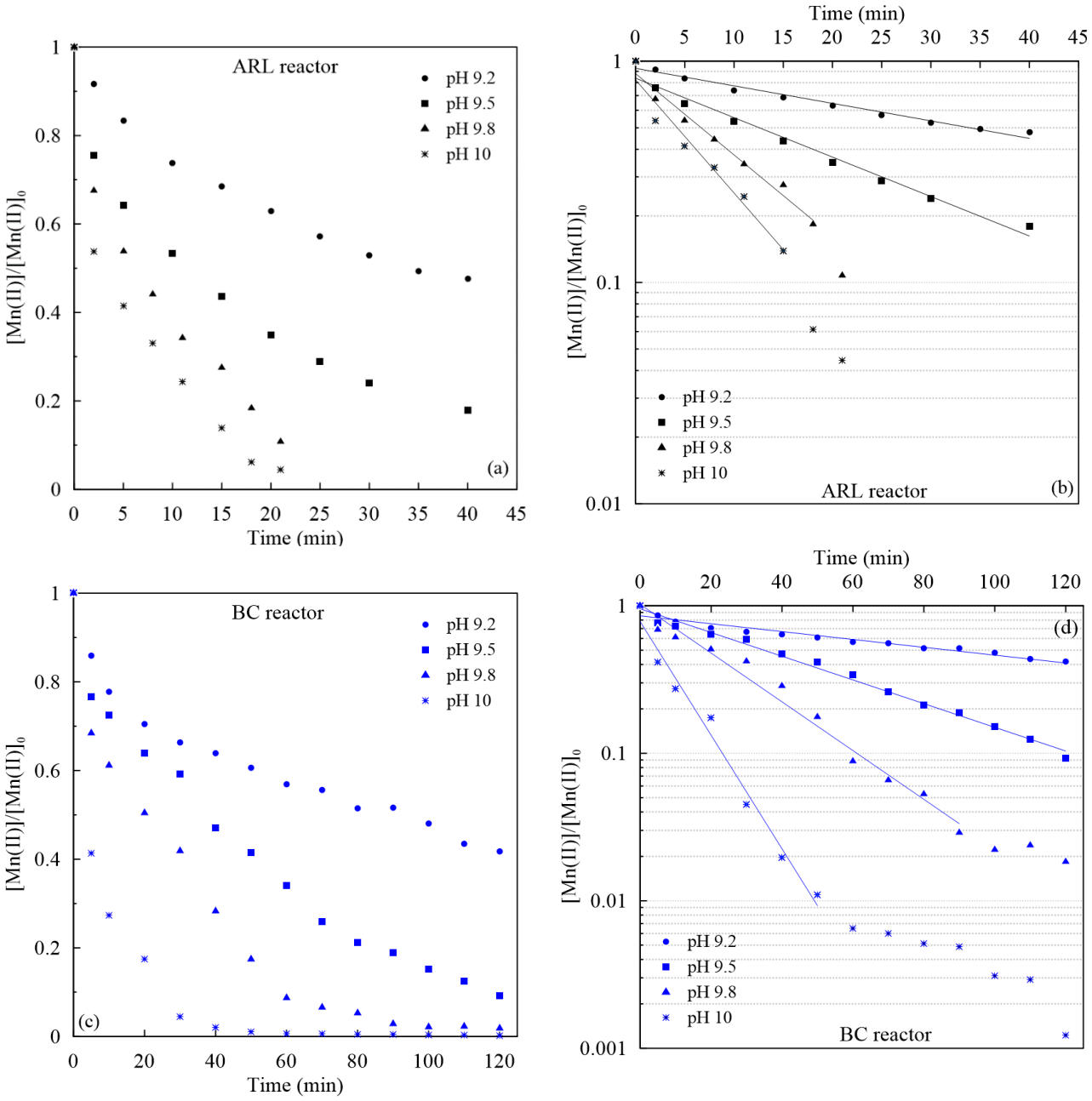


Figure 3.4 Evolution of normalized Mn(II) concentration with time for different pH in ARL and BC reactors ($[Mn^{2+}]_0$ = 10 mg.L$^{-1}$): (a) and (c) linear plot; (b) and (d) semilog plot.

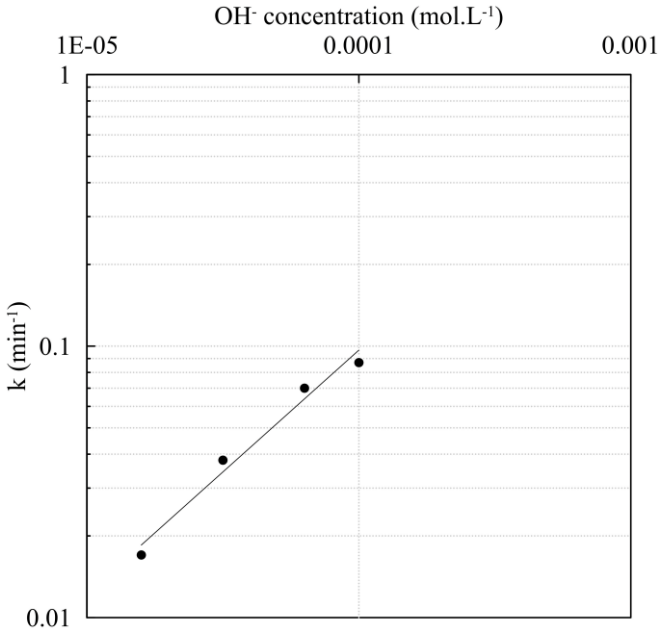


Figure 3.5 Evolution of the kinetic constant of the homogeneous oxidation mechanism as a function of $OH^-$ concentration in ARL reactor ($[Mn(II)]_0$ = 10 $mg.L^{-1}$).

### *3.4.1.3 Effect of the initial Mn(II) concentration*

The experimental results obtained in semi-batch experiments for an initial concentration of Mn(II) equal to 5, 10, 15, and 20 $mg.L^{-1}$ in ARL and BC reactors, keeping all other experimental conditions identical, are depicted in Figures 3.6a and 3.6b. According to the Figure 3.6, it is shown that Mn(II) oxidation was much faster when $[Mn^{2+}]_0$ increased from 5 $mg.L^{-1}$ to 20 $mg.L^{-1}$, and subsequently the Mn(II) removal efficiency is gone up from 68.52 % to 96.12 %, and from 43.45 % to 80.48 % for a reaction time equal to 40 min, using ARL and BC reactors, respectively. The acceleration of the oxidation rate at high initial Mn(II) concentrations can be attributed to the speciation of manganese when pH is modified and the air is introduced, which favored oxidation and mixing at the same time.

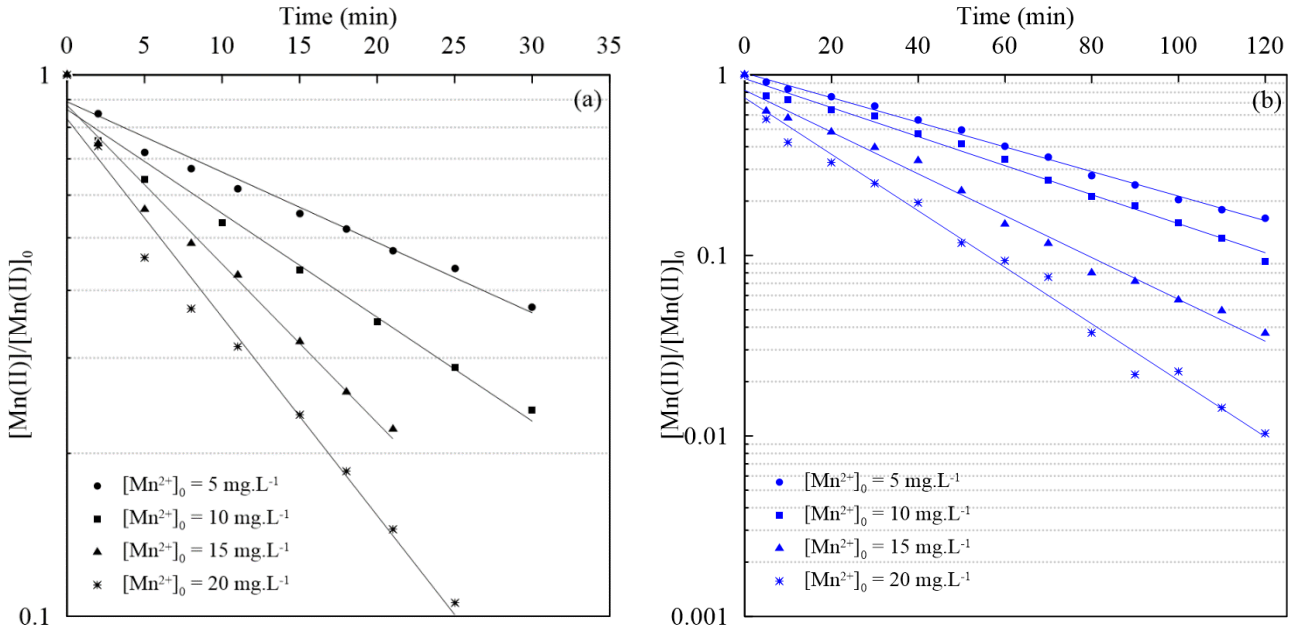


Figure 3.6 Evolution of Log [Mn(II)] with time for different initial Mn(II) concentrations and pH 9.5 in (a) ARL and (b) BC reactors.

Figure 3.6 indicates also that the first-order mechanism determined in the previous section is pseudo-first-order kinetics. The apparent homogeneous reaction rate constant values, $k_1$ were derived from the slopes of the lines plotted in Figure 3.6 and are summarized in Table 3.4 for the different operating conditions investigated. Additionally, it was found that the change in the homogeneous rate constant with initial Mn(II) concentration was identified as a linear function and the quantitative data are reported in Figure 3.7.

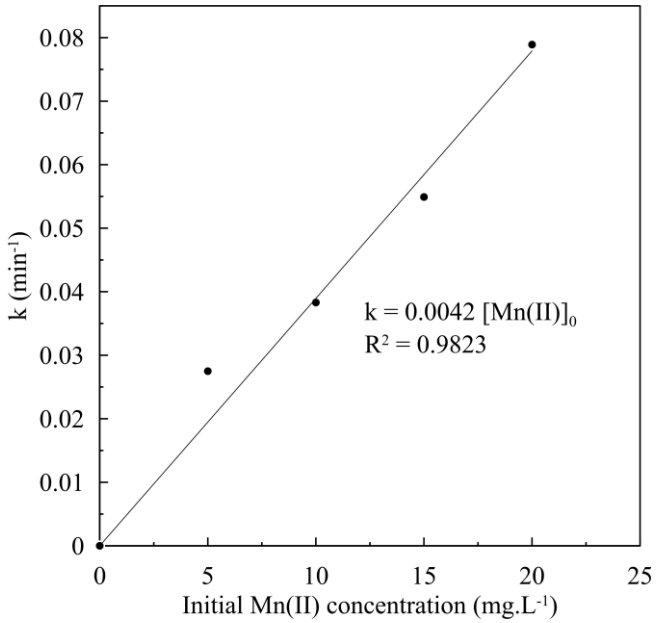


Figure 3.7 Evolution of the kinetic constant of the homogeneous mechanism as a function of $[Mn(II)]_0$ in ARL reactor.

### *3.4.1.4 Effect of $MnO_2$ addition*

In order to study the effect of $MnO_2$ addition on manganese removal by aeration, known concentrations of manganese oxide comprised between 5 and 500 $mg.L^{-1}$ were dispersed into a 5 $mg.L^{-1}$ Mn(II) aqueous solution (pH 9.5). It is noteworthy that this initial Mn(II) concentration was chosen to minimize autocatalytic effects attributed to the Mn(IV) formed by Mn(II) conversion. Figure 3.8 depicts the evolution of $[Mn(II)]/[Mn(II)]_0$ as a function of time while varying the concentration of added $MnO_2$. According to Figure 3.8, the rate of manganese oxidation was significantly influenced by the presence of manganese oxide and increased with $[MnO_2]_0$. Additionally, the time needed to reach 90 % conversion was about 76 min when no Mn(IV) was present in the reactor. Conversely, the reaction time (the time required to achieve maximal removal yield) was reduced to about 18 minutes when 500 $mg.L^{-1}$ of Mn(IV) was added initially into the ARL reactor. Thus, the reaction time is drastically reduced with increasing initial Mn(IV) concentrations.

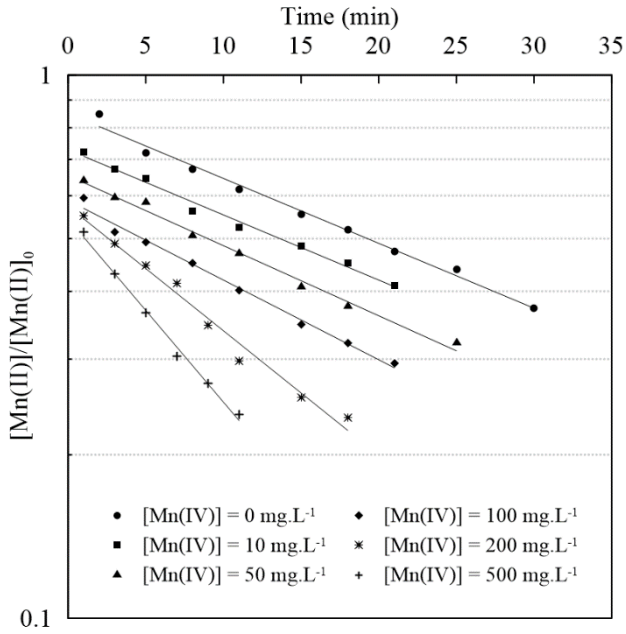


Figure 3.8 Evolution of Log $[Mn(II)]/[Mn(II)]_0$ against time for different initial Mn(IV) concentrations and pH 9.5 in ARL reactor.

The catalytic rate constant ($k_{cat}$) was calculated from the slopes of the lines on semi-logarithmic plots of $[Mn(II)]/[Mn(II)]_0$ and time. Quantitative data are reported in Figure 3.9. By fitting $k_{cat}$ as a function of $[Mn(IV)]_0$ expressed in $mg.L^{-1}$, the following equation was obtained:

$$k_{cat}(min^{-1}) = 10.6 \times 10^{-5}[Mn(IV)]_0 + 0.0259 \quad (3.7)$$

From Eq. (3.7), the two contributions are equal when $[Mn(IV)]_0$ is 245 $mg.L^{-1}$ and the heterogeneous term is ten times higher than the homogeneous term when $[Mn(IV)]_0$ is 2450 $mg.L^{-1}$, which proves that the homogeneous mechanism cannot be disregarded in practice compared to the heterogeneous mechanism of Mn removal. This result is strengthened by the fact that the intercept is very close to the value of k in Table 3.4.

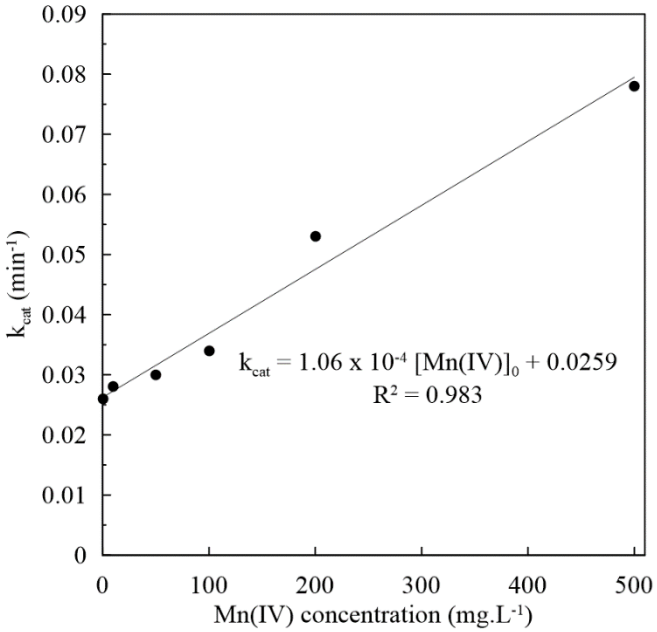


Figure 3.9 The evolution of $k_{cat}$ as a function of Mn(IV) concentration.

### 3.4.2 Solid characterization

After completing the reaction of Mn(II) mitigation from drinking water by atmospheric oxygen in the BC reactor, the resulting solid was in the form of a brown-black to-black powder (Figure 3.10).

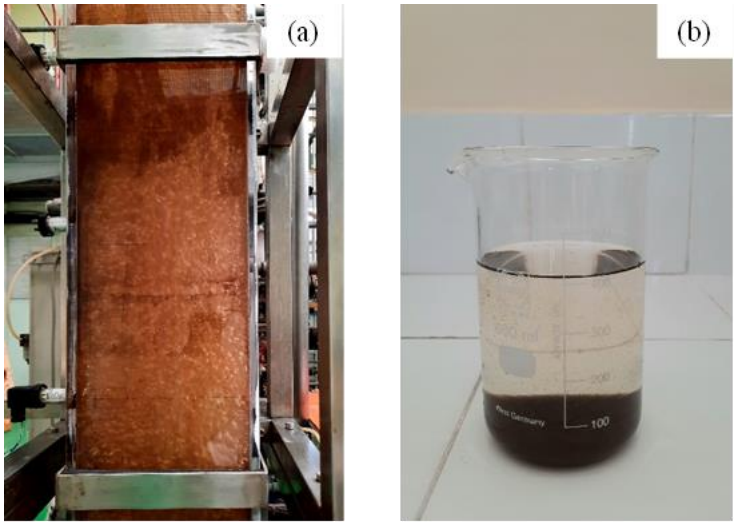


Figure 3.10 (a) The solid formation owing to the reaction between Mn(II) and atmospheric $O_2$ in the BC reactor. (b) The resulting solid after settling.

To explore the characteristics of the formed solid, XRD was used to analyze and identify the crystallographic structure of solid samples collected for pH ranging from 9.2 to 10. Figure 3.11a displays the XRD patterns of the manganese oxides derived from different pH conditions. For

the three samples obtained for pH values 9.5, 9.8 and 10, the diffraction patterns were seen to be nearly identical. Thus, the diffraction peaks occurred at 27.24°, 29.67°, 45.92°, 48.41°, 50.26°, 52.48°, 53.01°, and 59.36, respectively should be ascribed to monoclinic hydrated $MnO_2$ (todorokite; PDF no. 01-084-1713). Additionally, the diffraction peaks occurred at 26.27°, 41.23°, 48.82°, and 76.92° should be attributed to γ-MnOOH (manganite; PDF 96-101-1013), while the 33.16°, 38.55°, 45.90°, 50.25°, 56.86°, 63.46° should be indexed to orthorhombic α-MnOOH (groutite; PDF 01-075-1199). For pH 9.2, monoclinic manganite was the prevailing phase represented by the diffraction peaks 26.59°, 39.70°, 49.02°, 57.86°, and 65.14. As for pH 9.8, the orthorhombic γ-$MnO_2$ (ramsdellite; PDF 96-900-3476) and hexagonal ε-$MnO_2$ (Akhtenskite, PDF 96-901-4107) were attributed to the diffraction peaks observed at 38.53°, 50.26°, 53.03°, and 37.31°, 42.99°, respectively. Regarding pH 10, the diffraction peaks occurred at 42.99°, 56.87°, and 65.02° should be allotted to the tetragonal β-$MnO_2$ (pyrolusite; PDF 96-151-4102). Moreover, orthorhombic γ-$MnO_2$ was also identified at diffraction peaks 38.56°, 43.43°, 50.26°, and 63.41°, whereas the diffraction peaks at 23.23° and 33.16° should be ascribed to orthorhombic α-$MnO_2$ (cryptomelane; PDF 96-151-4104).

The FT-IR spectra of $MnO_2$ resulting from different pH conditions within the wavenumber vary from 400 – 4000 $cm^{-1}$ and are represented in Figure 3.11b. Several absorption bands at 3396.64, 1631.77, 1438.89, 1082.6, 856.39, 713.66, 501.49, and 418.55 $cm^{-1}$ can be distinguished. The band around 3396.64 $cm^{-1}$ should be ascribed to the presence of the O–H stretching vibration and the presence of traces of absorbed water (Mylarappa et al., 2016; Wan et al., 2014). Besides, the 1631.77, 1438.89, 1082.6, 856.39 $cm^{-1}$ absorption bands generally corresponded to the O–H bending vibrations associated with Mn atoms (Jaganyi et al., 2013; Yuan et al., 2009). Whereas the bands at around 713.66, 501.49, and 418.55 $cm^{-1}$ can be attributed to the Mn–O vibrations in $MnO_6$ octahedra (Wang et al., 2007; Yuan et al., 2009). It can be noticed from Figure 3.11b that the absorption peak intensity at 713.66 and 501.49 $cm^{-1}$ which are allotted to the Mn–O band are shown to get more and more intense with increasing pH from 9.2 to 10. Thus, the IR scans confirmed the findings provided by the XRD analysis.

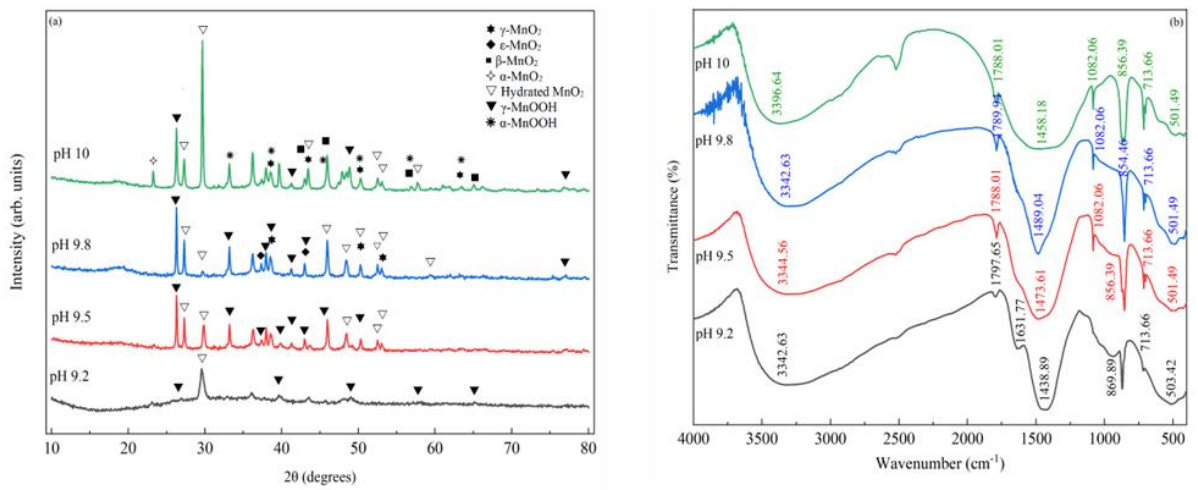


Figure 3.11 (a) XRD patterns and (b) FT-IR spectra of manganese oxides derived from pH ranging from 9.2 to 10.

The chemical composition of the formed $MnO_2$ was determined by performing an EDS analysis. As shown in Figure 3.12c, oxygen and manganese are observed in the composite structure of the samples for the different pH considered, along with other elements such as magnesium and calcium which were also detected as they constitute the major components of the tap water.

SEM images of $MnO_2$ derived from the reaction between the dissolved form of manganese and atmospheric oxygen for different pH conditions are provided by Figure 3.12b. At pH 9.2, the SEM image revealed that the morphology of the $MnO_2$ powder was in the form of agglomerates with no distinctive orientation or shape and it can be noticed that coarse and fine particles coexist. Besides, the enlarged micrograph shows that the particles are scattered in the form of spheres or polyhedral and some of them have irregular shapes. At pH 9.5, aggregated spherical or rod-like structures were observed. However, a dense cluster of rods $MnO_2$ particles was formed at pH 9.8. Lastly, the high magnification micrograph associated with pH 10 indicated that the particle had mainly a flower-like morphology.

Figure 3.12a displays the trend in the particle size distribution (PSD) in volume percentage of the $MnO_2$ formed for different pH. Indeed, increasing the pH from 9.2 to 10 induced a reduction in the particle size and it was found that the median diameter decreased from 39.90 µm to 23.72 µm, respectively. Additionally, for a pH of 9.2 to 9.5, the PSD was broad and reached the larger sizes, however, as the pH further increased the PSD became narrower and skewed towards the smaller sizes. Actually, it is a known fact that manganese dioxide particles are negatively charged in natural waters since their isoelectric point (IEP) is inferior to pH 3

(Morgan and Stumm, 1964). When pH is augmented, the more negatively charged surfaces induced greater electrostatic double layer (EDL) repulsions between the particles, which in turn lessened the particle aggregation. The obtained results are in line with those found by (Kenari and Barbeau, 2016) who investigated the effect of pH on the size and Zeta Potential of oxidized iron and manganese in water treatment. Starting from all these findings, it can be said that the pH of the solution plays a major role in controlling the size, shape, and morphology of the resulting $MnO_2$ during manganese oxidation by atmospheric oxygen.

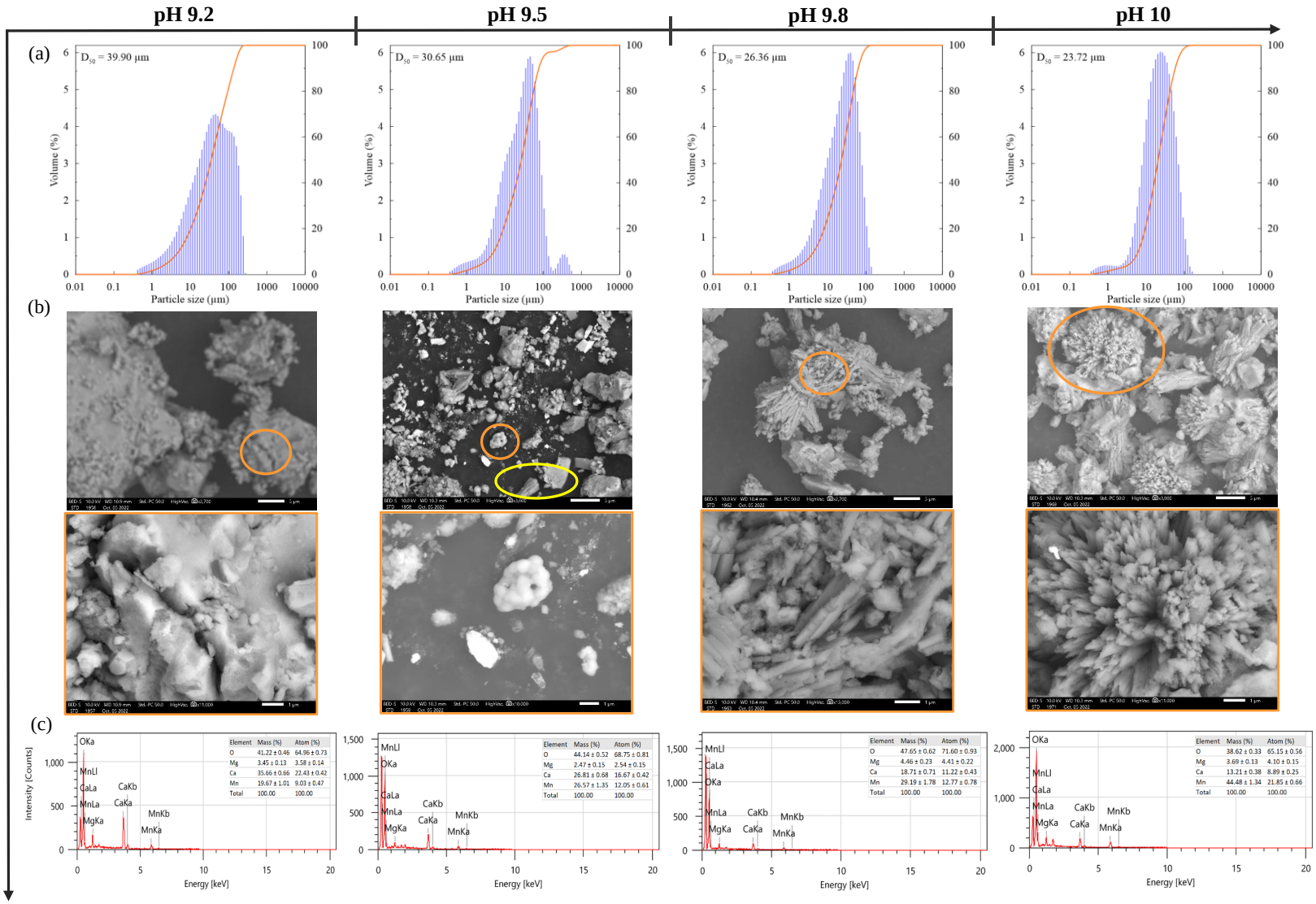


Figure 3.12 (a) Particle size distribution, (b) SEM images, and (c) EDS analysis of manganese oxide resulted from Mn(II) oxidation by aeration for pH varying from 9.2 to 10.

### 3.4.3 Comparison of ARL and BC reactors performance in Mn(II) removal by aeration process

In order to assess the performance of the two reactors involved in this investigation, the removal efficiency of Mn(II) by the aeration process was plotted as a function of pH as well as the initial soluble manganese concentration for a treatment time of 40 min (Figure 3.13). Indeed, it is noteworthy that the manganese removal efficiency achieved using the airlift reactor is significantly higher than that attained using the bubble column for a pH ranging from 9.2 to 9.8 and an initial Mn(II) concentration between 5 $mg.L^{-1}$ and 20 $mg.L^{-1}$. Besides, it can also be noticed that the Mn(II) removal effectiveness achieved by the airlift aeration process was higher than that by the bubble column.

Although the bubble column offered a higher oxygenation capacity than the airlift reactor at approximately the same specific power input, the use of the aeration process in the airlift is still privileged over the bubble column. Therefore, the reasons behind the better performance of the ARL reactor over the bubble column with respect to the manganese oxidation can be attributed to the fact that the mixing time in the ARL reactor is shorter than in the bubble column (Mirón et al., 2004). In addition, a defined cyclic mixing pattern was identified in the airlift reactor (Gourich et al., 2006a) in contrast to a chaotic mixing in the bubble column which may be an indication of the occurrence of dead zones in the column. While, at a pH 10, the deviation between the removal yield reached by the aeration bubble column process (98.03 %) and that by the airlift (99.82 %) became minor as the increase in pH to this value shortened the required reaction time and ameliorated the reaction rate. The improved performance of the airlift rather than the bubble column has also been pointed out in the literature, for instance in the biological field (*i.e.*, microalgae cultivation) (Kumar and Das, 2012).

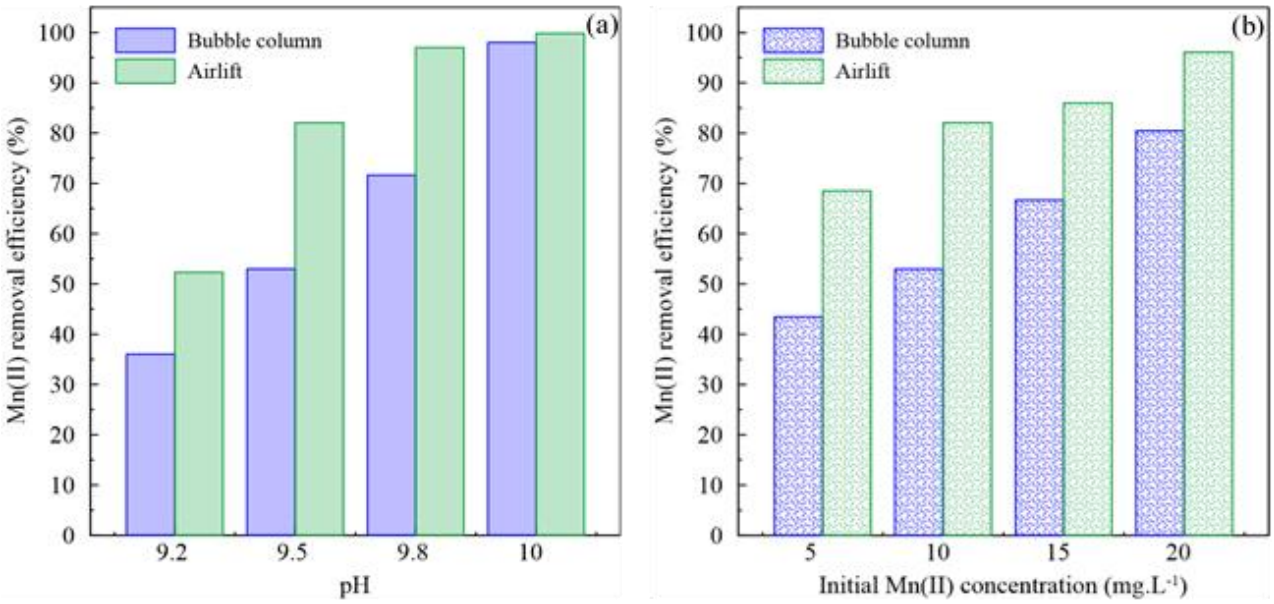


Figure 3.13 Evaluation of Mn(II) removal efficiency using bubble column and airlift aeration process (a) versus pH and (b) versus the initial Mn(II) concentration.

From the standpoint of industrial applications, the most relevant factors for evaluating the performance of certain water treatment processes are energy consumption and the corresponding operating cost. In this respect, Bolton et al. (1996) proposed applicable standard figures-of-merit for comparing the treatment technologies, which involved the electrical energy consumption within two phenomenological kinetic order regimes (zero or first order). Thus, the electrical energy per order (EE/O) figure-of-merit is the electrical energy in kilowatt-hours (kWh) needed to abate a contaminant by one order of magnitude (90 %) in 1 $m^3$ of polluted water or air. This figure-of-merit is most adequate for cases where the contaminant concentration is low and the required energy is independent of the contaminant concentration, in other words, the removal of the pollutants follows pseudo-first order kinetics. For a batch reactor system, the EE/O value ($kWh.m^{-3}$) can be determined by the following formula (Bolton et al., 2001; Vanraes et al., 2017):

$$EE/O = \frac{P \times t \times 1000}{V \times 60 \times \log\left(\frac{C_0}{C_f}\right)} \quad (3.8)$$

where P stands for the power introduced into the reactor (kW), t is the treatment time (min), V is the liquid volume (L), $C_0$ and $C_f$ are the initial Mn(II) concentration ($mg.L^{-1}$) and the final Mn(II) concentration at time t ($mg.L^{-1}$), respectively.

Energy consumption for the Mn(II) oxidation in the bubble column and airlift reactors are listed in Table 3.5.

According to the results reported in Table 3.5, the energy consumption to achieve 90 % Mn(II) removal by aeration in the bubble column is greater than in the airlift reactor. In fact, Mn(II) removal from effluent containing 10 $mg.L^{-1}$ of soluble manganese in the bubble column required 2.44 times more energy than an airlift reactor. Nevertheless, these findings emphasized that the Mn(II) mitigation in water by the aeration process in pneumatic reactors remains effective compared to the ozonation process as far as energy consumption is concerned. Moreover, to get an economic indication of the aeration process, the operating cost of manganese removal in bubble column and airlift reactors was calculated taking into account that the industrial electricity cost is 0.1 USD/kWh (Zhuk et al., 2022). Thus, it can be said that the Mn(II) removal through oxidation in ARL was cost-effective as compared to the BC reactor.

Table 3.5 Comparison of energy efficiency and operating cost for the Mn(II) removal by aeration process in the bubble column and the airlift reactor.

| | BC reactor | ARL reactor |
|---|---|---|
| Specific power input ($Watt.m^{-3}$) | 164.70 | 161.97 |
| Power input (kW) | 0.011 | 0.010 |
| Oxygenation capacity (kg dissolved $O_2.kWh^{-1}$) | 4.68 | 3.68 |
| Treatment time (min) | 60 | 25 |
| Liquid volume (L) | 68.22 | 63 |
| Initial Mn(II) concentration ($mg.L^{-1}$) | 10 | 10 |
| Final Mn(II) concentration ($mg.L^{-1}$) | 1 | 1 |
| EE/O ($kWh.m^{-3}$) | **0.072** | **0.029** |
| Operating cost ($USD.m^{-3}$) | **0.007** | **0.003** |

### 3.4.4 Comparison of physicochemical processes for Mn(II) removal

Obviously, using an airlift reactor in order to remove manganese is an appreciable method because this type of reactor is used for slow gas−liquid reaction, which is the case of manganese. On the other hand, this technique leads to a removal rate of 90 % and the time needed to reach it is 76 min at low $[Mn]_0$ values. Table 3.6 summarizes and compares the manganese removal efficiency achieved by the aeration process using an airlift reactor and the processes mentioned above. This emphasizes that the aeration process is effective over a wide range of initial Mn concentrations, providing a flexible, safe, and yet inexpensive process.

Table 3.6 Comparison of manganese removal efficiency of various techniques.

| Techniques | Initial Mn (II) concentration ($mg.L^{-1}$) | Time (min) | Removal efficiency (%) | pH | Comments | Ref. |
|---|---|---|---|---|---|---|
| Hydroxyde precipitation | 1791 | | 71.4 | 8.2 | Synthetic laterite waste solution | Zhang et al. (2010) |
| Coagulation/ flocculation | 1085 | | 99.83 | 11 | Synthetic wastewater | Charerntanyarak (1999) |
| Flottation | 5.5 | | 96 | 8 – 12 | Precipitate flotation | Gregory et al. (1980) |
| Ion exchange | 5000 | 1440 | > 90 | NA | $MnCl_2$ Feed solution (20 ± 1) °C Resin mass of 0.1 – 0.2 g | Kononova et al. (2015) |
| Oxidation/filtration | 1.81 | | 95 | 8.5 | $KMnO_4$ oxidation followed by flocculation, settling, and filtration | Roccaro et al. (2007) |
| Ozonation process | 1.0 | | 89 | 9 – 12 | Ozone dose of $3mg.L^{-1}$ at 20 °C | El Araby et al. (2009) |
| Electrocoagulation | 100 | | 87.9 | 7.0 | Current density 1.5 – 9.4 $mA.cm^{-2}$ Aluminum electrodes | Shafaei et al. (2010) |
| Adsorption | 50 | 420 | 82.2 | 7 | Carbon impregnated with cetyltrimethylammonium ammonium bromide | Anbia and Amirmahmoodi (2016) |
| Membrane filtration | 1000 | | 89 | 1.5 ± 0.2 | Type of membrane : NF270 | Al-Rashdi et al., (2011) |
| Aeration process using an airlift reactor | 5 | 76 | 90 | 9.5 | | This study |

## 3.5 Conclusions

Manganese removal from drinking was studied using an oxidation process based on aeration in bubble columns and split-rectangular airlift reactors. In this work, experiments were carried out under semi-batch conditions on tap water enriched in Mn(II). The effect of operating conditions on the Mn(II) removal efficiency using atmospheric oxygen was examined, including the air flow rate, pH, as well as the initial concentrations of dissolved manganese and the manganese oxide. As a result, it was found that the oxygen mass is not a limiting step for Mn(II) removal by oxidation. Increasing the pH from 9.2 to 10 and the initial Mn(II) concentration resulted in an increase in Mn(II) removal efficiency with a remarkable shortening of the treatment time. Indeed, the time required to reach an Mn(II) removal yield of 90 % in the BC reactor diminished significantly from 119 min to 25 min by augmenting the pH from 9.5 to 10. Moreover, experimental data proved that the Mn(II) oxidation kinetics was strongly sensitive to the pH and that it exhibited an autocatalytic behavior. Hence, the kinetic of manganese oxidation by aeration was shown to be pseudo-first order in Mn(II), with an apparent kinetic constant depending on the initial amount of Mn(IV) compounds. Meanwhile, by analyzing XRD, FT-IR, SEM, and PSD, the formation of manganese oxides with different size and morphology caused by pH variation (9.2 – 10) was confirmed.

While comparing the performances of the two reactors, it is worth noting that the aeration in the airlift made it possible to reach an Mn(II) removal efficiency of 90 % for a treatment time of 25 min and an energy requirement of 0.029 $kWh.m^{-3}$ with an operating cost of 0.003 $USD.m^{-3}$ as opposed to the BC reactor which required a time of 60 min and energy consumption of 0.072 $kWh.m^{-3}$. Thus, airlift reactors appear to be adequate for Mn(II) oxidation by atmospheric air thanks to their internal liquid recirculation between the riser and downcomer compartments, and good mixing time that maintain a better homogeneity of $MnO_2$ particles in the reactor, which subsequently accelerate the Mn(II) oxidation.

# Chapter 4: Comparative analysis of industrial processes for cadmium removal from phosphoric acid: a review


## Abstract

The manufacture of phosphoric acid by wet process, where the phosphates are solubilized by mineral acids, frequently gives a product that inevitably contains several impurities. Some of these elements are detrimental to the quality of the acid for its end use in fertilizers or food industries. Among these impurities, one can find cadmium whose final content in fertilizers depends both on the type of raw materials and the chemical synthesis pathway. Hence, the wet phosphoric acid (WPA) must be purified. The present review compares and analyzes the different industrial processes for cadmium removal from WPA, starting with solvent extraction which has always been the most widely used technique in this field, but also considering precipitation, ion exchange, adsorption, flotation, and even the more recent membrane processes that can become a relevant alternative. The efficiency of cadmium removal techniques is assessed, and their advantages and limitations are discussed. This review also provides insights into the thermodynamic modeling of the $H_3PO_4/H_2O$ system and compares the ability of current models to predict thermodynamic properties, including osmotic coefficient and speciation, in a wide range of phosphoric acid concentrations. Besides, the cost and the environmental impact of WPA production have also been evaluated using Life Cycle Assessment and available cost data which reveals that thermal phosphoric acid is still economically and environmentally more onerous than purified WPA.



**Keywords:** Wet phosphoric acid; Cadmium removal; $H_3PO_4$ purification; $H_3PO_4$ thermodynamics; Decadmiation cost; Decadmiation environmental impact

## 4.1 Introduction

World's natural phosphorus resources are used primarily for the production of phosphate fertilizers and are essential to global agriculture, so that it can keep pace with global population growth. Morocco, China, the USA, and Russia are among the most important producers of phosphates, and 70% of global phosphate rock reserves are located in Morocco (De Ridder et al., 2012; Mar and Okazaki, 2012; U.S. Gelogical Survey, 2012) (Figures 4.1 and 4.2). Moreover, about 95% of the world's phosphate rock production, which approaches 150 million tons annually, is consumed for manufacturing phosphate fertilizers (Abouzeid, 2008).

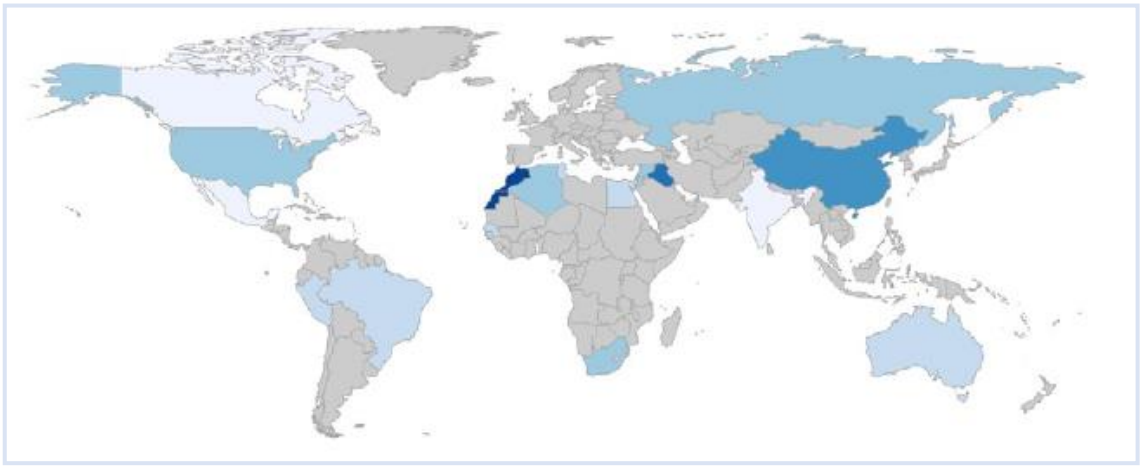

Figure 4.1 Map of countries by phosphate rock reserves (in blue gradient depending on their phosphate rock reserves) (De Ridder et al., 2012).

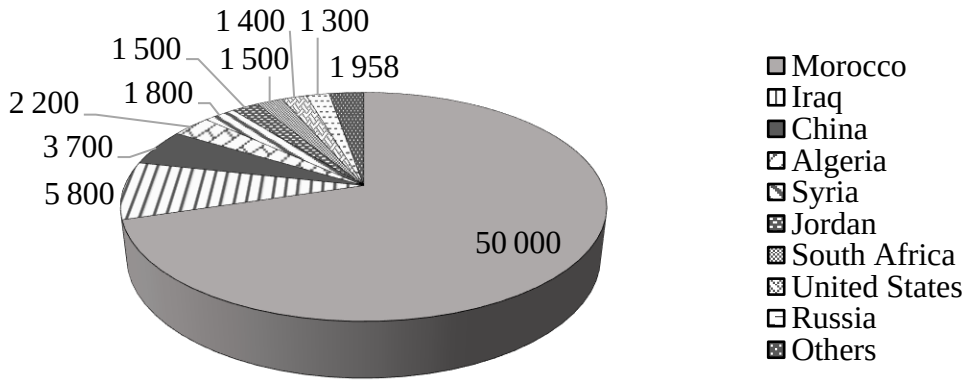


Figure 4.2 Phosphate rock reserves per country in MMt (U.S. Geological Survey, 2012).

The production of phosphate fertilizers requires an intermediate step: the production of phosphoric acid. Indeed, there are two main production processes of phosphoric acid from phosphate ores: the thermal process and the wet process. About 90% of the world's production

of this acid is manufactured using the wet process (Becker, 1989). Thus, the formation of large volumes of phosphogypsum releases and the presence of impurities initially contained in phosphate rocks, such as organic matter and heavy metals constitute the main disadvantages of wet phosphoric acid production. One of these contaminants is the cadmium element, one of the minor components in phosphate rock (Ukeles et al., 1994). Indeed, phosphate ores contain from 10 to 80 $g.ton^{-1}$ cadmium depending on the deposit, and then it can be found in wet phosphoric acid as well as in phosphate fertilizers.

According to the World Health Organization (WHO), cadmium is a toxic chemical and is known to accumulate in soils, leach into ground and surface waters, leading to increased uptake by crops, which results in increased levels in animals and food, and could cause damage to human health. Based on this risk analysis, several countries have established cadmium limits in their fertilizers, among which Belgium 90 mg of Cd/kg of $P_2O_5$, Austria 75 mg Cd/kg of $P_2O_5$, Denmark 48 mg Cd/kg of $P_2O_5$, Sweden 44 mg Cd/kg of $P_2O_5$, Poland 50 mg Cd/kg of $P_2O_5$, or Hungary 20 mg Cd/kg of $P_2O_5$ (Roberts, 2014; Ulrich, 2019). Additionally, in 2016, the revision of Fertilizers Regulation (European Commission) No 2003/2003 was proposed to set harmonized environmental standards to minimize adverse effects on human health and the environment by reducing cadmium in fertilizers, which is currently unrestricted, to an initial limit of 60 mg Cd/kg $P_2O_5$. The limit would be constricted to 40 mg Cd/kg of $P_2O_5$ after three years and then to 20 mg Cd/kg of $P_2O_5$ after 12 years. Consequently, the introduction of stringent limit on Cd content in phosphate fertilizers may lead to serious disturbances on the market. For this reason, the removal of cadmium from WPA is of major importance for the scientific community as well as for the phosphate industries.

In fact, there is an effective method to eliminate Cd from raw phosphate which is calcination, but it is seen as not cost-effective given the required energy to heat at a temperature of 850−1150°C (Cichy et al., 2014; Syers, 2001). On the other hand, various processes have been developed for the removal of Cd from phosphoric acid solutions, such as solvent extraction, adsorption, ion exchange, precipitation, flotation, and membrane processes. However, the use of these techniques was limited because of several economical, technical, and environmental constraints including high energy requirements, limited efficiency, complicated treatment process, and a risk of secondary pollution.

The present chapter focuses on a comparative analysis of different available processes that have been used for cadmium removal from WPA, with an evaluation of their respective

advantages and limitations. A comprehensive approach has been followed to cover all the significant works done in this field to date, including the thermodynamic modeling of $H_3PO_4/H_2O$ system, which can provide essential information for designing and simulating different processes. Furthermore, the cost of phosphoric acid production has been discussed, while comparing the price of thermal and wet phosphoric acid, and the purified wet phosphoric acid. Finally, the most common problems regarding the environmental impact of phosphate fertilizer use are the harmful phenomenon of eutrophication (Schröder et al., 2010; United Nations Environment Program and International Fertilizer Industry Association, 2001) and the accumulation of cadmium in the soil (Cichy et al., 2014). In order to obtain more insight into the environmental impacts of phosphoric acid, the last section is devoted to detailing the harmful effect of the production and use of phosphoric acid on the environment by evaluating available life cycle assessment studies.

## 4.2 Phosphoric acid: an overview

Phosphoric acid is a major intermediate chemical product. In 2014, the global phosphoric acid production capacity was about 55 million tons (Food and Agriculture Organization of the United Nations, 2015). It is mainly employed in fertilizers production. In fact, from about 84% to 90% of the worldwide phosphoric acid (Becker, 1989; Toama, 2017) is dedicated to the manufacture of phosphate fertilizers (Figure 4.3). Besides, phosphoric acid is indispensable for the production of several products in the process industries (Boussen, 2007; González et al., 2002; Mecibah, 2013), including the pharmaceutical industry, the production of detergents, and the treatment of metal surfaces such as pickling, polishing, antirust, treatment of wastewater; also, it is used in the food products, cosmetics, and paints.

To meet the phosphoric acid needs, it is necessary to mine phosphate which is the main raw material in the phosphoric acid industry. Indeed, phosphate ores have two major geological origins: Sedimentary and igneous (Becker, 1989; European Fertilizer Manufacturer's Association, 2000).

- Igneous is found in Kola (Russia), South Africa, Brazil, etc.
- Sedimentary is found in Morocco, Algeria, Jordan, USA, etc.

Phosphoric acid is manufactured using different processes, the most commonly used are: the thermal and wet processes (European Fertilizer Manufacturer's Association, 2000). An overview of the global phosphate industry is given in Figure 4.4.

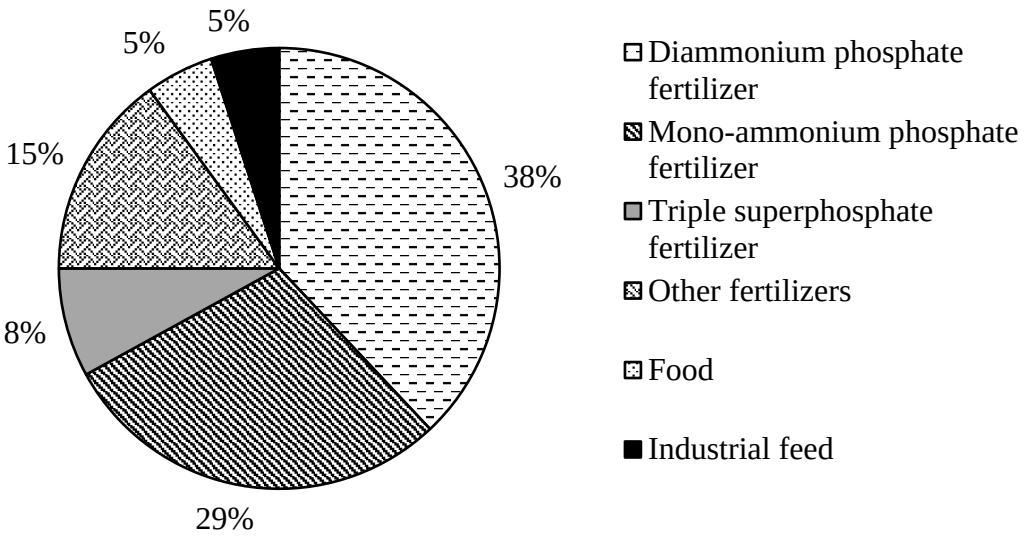


Figure 4.3 Phosphoric acid uses by sectors (Toama, 2017).

### 4.2.1 Thermal process

The production of phosphoric acid by thermal route is conducted in two steps. First, elemental phosphorus is produced from phosphate rock. Next, the elemental phosphorus is oxidized with air to $P_2O_5$, which is then hydrated to produce phosphoric acid. This process consists in mixing the ground phosphate rock with a slurry of water, clay, and various waste streams containing phosphorus. The mixture is then heated at a temperature ranging between 1450 °C and 1500 °C (Boussen, 2007; Mecibah, 2013) in an electric resistance furnace together with cokes and gravel (slag formation) to obtain phosphorus. As indicated in the reaction below (Eq. (4.1)), this method produces gaseous phosphorus, carbon monoxide, and a liquid slag (European Commission, 2007).

$$2Ca_3(PO_4)_2 + 6SiO_2 + 10C \rightarrow P_4 + 10CO + 6CaSiO_3 \quad (4.1)$$

The second stage to produce phosphoric acid is the oxidation of elemental phosphorus with the air to $P_2O_5$. Thereafter, the resulting $P_2O_5$ is contacted with dilute phosphoric acid and reacts with water present in the acid to form phosphoric acid according to reactions (Eqs. (4.2) and (4.3)).

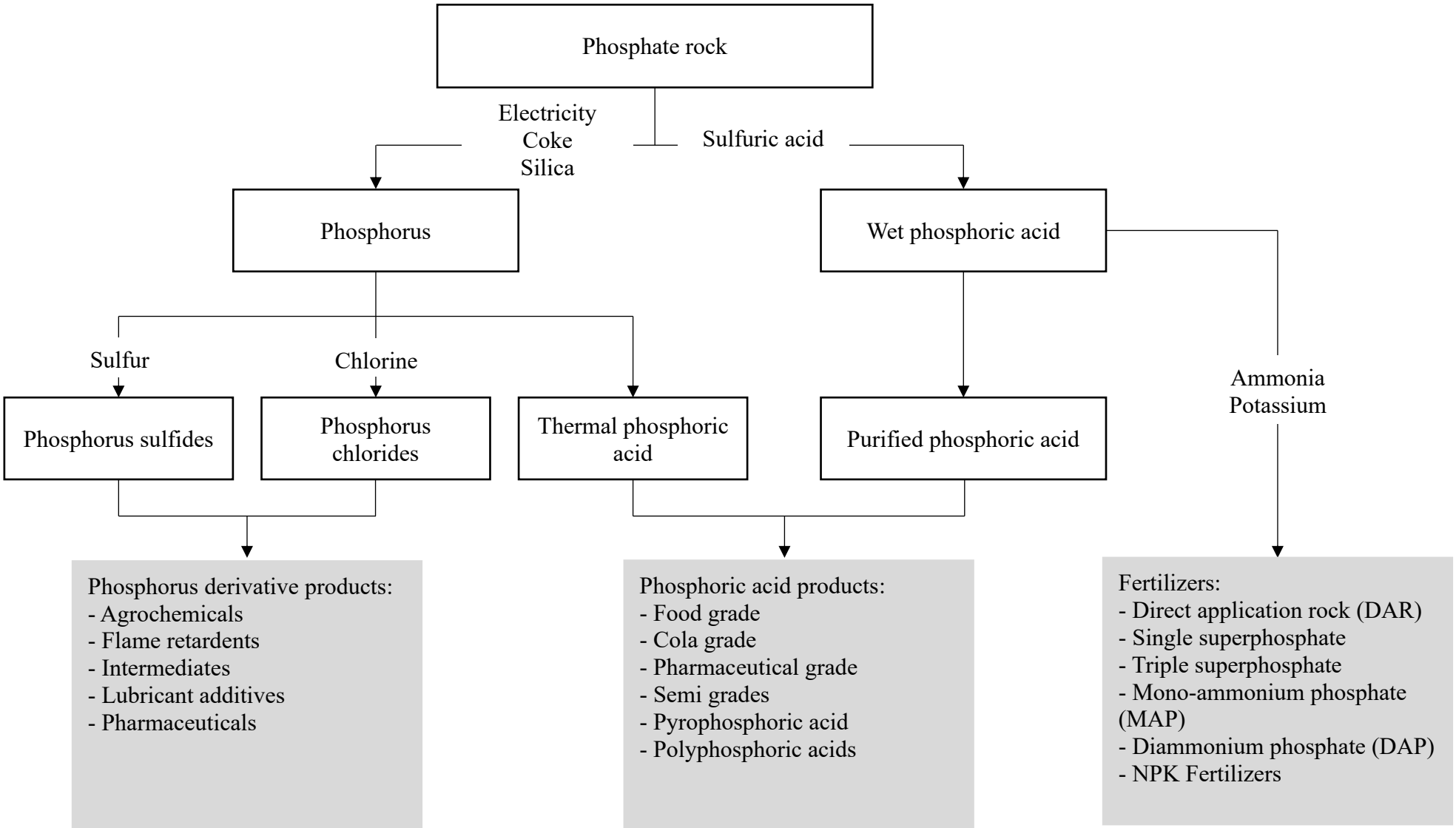


Figure 4.4 Overview of phosphate industry.

It should be noted that these reactions are exothermic, and heat released is used for steam generation at high temperatures.

$$P_4 + 5O_2 \rightarrow 2P_2O_5 \quad (4.2)$$

$$P_2O_5 + 3H_2O \rightarrow 2H_3PO_4 \quad (4.3)$$

Thermal phosphoric acid is pure but is expensive because it requires a huge amount of energy (Boussen, 2007; Ennaassia et al., 2002). That is why it is almost manufactured for specific applications which require a very pure acid quality, such as metal surface treatment in the micro-electronics industry and the acidulation of beverages (European Commission, 2007).

### 4.2.2 Wet process

The wet process is by far the most widely used process for the manufacture of phosphoric acid. This consists in digesting phosphate rock in a mineral acid (Toama, 2017). Phosphate acidulation is performed using either sulfuric acid, nitric acid, or hydrochloric acid, whereas wet digestion of phosphate rock with $H_2SO_4$ is the preferred method in terms of volume (European Commission, 2007).

Typically, the term "wet process" is employed when sulphuric acid is applied. The tri-calcium phosphate from the phosphate rock reacts with concentrated $H_2SO_4$ to produce phosphoric acid and an insoluble calcium sulfate salt, which facilitates the separation of phosphoric acid directly by filtration. Eq. (4.4) displays the overall reaction for producing the phosphoric acid using the $H_2SO_4$ attack (European Commission, 2007; Toama, 2017).

$$CaF_2.3Ca_3(PO_4)_2 + 10H_2SO_4 + 20H_2 \rightarrow 10(CaSO_4.2H_2O) + 2HF + 6H_3PO_4 \quad (4.4)$$

The resulting phosphoric acid is called "weak acid" and has a different percentage of $P_2O_5$ content according to the used process route. Indeed, there are five well-known process routes using $H_2SO_4$ to manufacture phosphoric acid (European Commission, 2007; European Fertilizer Manufacturer's Association, 2000; Toama, 2017):

- Dihydrate process (DH)
- Hemihydrate process (HH)
- Hemi-dihydrate process recrystallization process, single-stage filtration
- Hemi-dihydrate process recrystallization process, double-stage filtration
- Di-hemihydrate process recrystallization process, double-stage filtration

The dihydrate process is adaptable to a wide range of phosphate rocks, and the weak acid contains 26 – 30 % $P_2O_5$. Then, this weak acid is concentrated to 50 – 54 % by evaporation to meet fertilizer production requirements.

The di-hemihydrate method with two-stage filtration (also called Central Prayon process) is used to produce around 50 % of phosphoric acid and it reaches an efficiency of 98 % in $P_2O_5$. The reaction between tri-calcium phosphate and $H_2SO_4$ is limited by an insoluble layer of $CaSO_4$ but it can be minimized by recirculation of phosphoric acid which allows the solubilization as monocalcium phosphate which becomes calcium sulfate after precipitation with sulfuric acid (Figure 4.5). The following equations (Eqs. (4.5)-(4.7)) summarize the chemical reactions between rocks and sulfuric acid (European Commission, 2007; European Fertilizer Manufacturer's Association, 2000).

$$Ca_3(PO_4)_2 + 3H_2SO_4 \rightarrow 2H_3PO_4 + 3CaSO_4 \quad (4.5)$$

$$Ca_3(PO_4)_2 + 4H_3PO_4 \rightarrow 3Ca(H_2PO_4)_2 \quad (4.6)$$

$$3Ca(H_2PO_4)_2 + 3H_2SO_4 \rightarrow 3CaSO_4 + 6H_3PO_4 \quad (4.7)$$

Due to its low cost, the production of phosphoric acid by means of the wet process is the most widespread in the world. However, the major drawback of this process is that the WPA contains a high content of cationic impurities, which is why it must be purified before use.

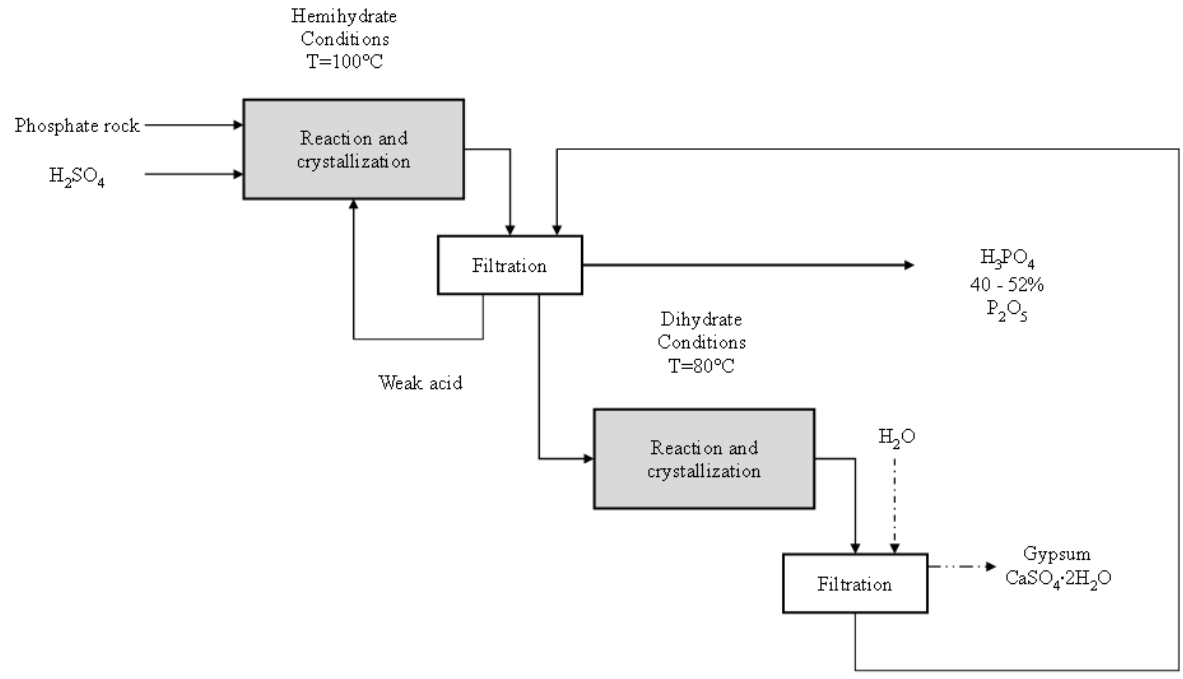


Figure 4.5 Overview of the Hemi-dihydrate recrystallization process with double stage filtration (European Commission, 2007).

### 4.2.3 Impurities contained in the wet phosphoric acid

As pointed out above, the majority of phosphate rock is converted into phosphoric acid by the wet route. The phosphate acid attack solubilizes partially, or totally organic and inorganic impurities contained therein. Subsequently, the impurities such as iron, vanadium, cadmium, copper, manganese, aluminum, lead, and chromium (Boussen, 2007; Mecibah, 2013; Monser et al., 1999) end up in WPA, and the byproduct $CaSO_4.2H_2O$. These impurities affect the color, density, and viscosity of WPA (Boussen, 2007). An overview of the different impurities and their concentrations in the phosphate rock of the Khouribga site in Morocco, in WPA, and phosphogypsum is given in Table 4.1.

Table 4.1 Composition of the phosphate ore (Khouribga), the phosphoric acid solution (29 % $P_2O_5$), and the phosphogypsum (Tjioe, 1987).

| Component (%) | Ore | Acid | Gypsum | Element ($mg.L^{-1}$) | Ore | Acid | Gypsum |
|---|---|---|---|---|---|---|---|
| $P_2O_5$ | 31 | 29 | 0.40 | Cr | 170 | 160 | 5 |
| CaO | 52 | 0.5 | 32.5 | Mn | 14 | 10 | 3 |
| $SO_3$ | 2 | 2.0 | 45.3 | Ni | 34 | 30 | 2 |
| F | 4.2 | 1.7 | 1.1 | Cu | 32 | 25 | 4 |
| $SiO_3$ | 2.2 | - | 0.6 | Zn | 310 | 300 | <10 |
| $Al_2O_3$ | 0.54 | 0.33 | 0.14 | As | 10 | 10 | 1 |
| $Fe_2O_3$ | 0.19 | 0.18 | 0.005 | **Cd** | **23** | **19** | **2 – 3** |
| $Na_2O$ | 0.73 | 0.09 | 0.47 | Pb | 4 | <1 | 2 |
| | | | | V | 240 | 15 | - |
| | | | | U | 118 | 100 | <15 |
| | | | | Ra | 40 ppb | - | - |

#### *4.2.3.1 Cadmium in phosphoric acid*

Cadmium can be found in the WPA at varying concentrations depending on the origin of phosphates: the phosphate rocks of volcanic origin among like Russia and South Africa contain very small amounts of Cd (igneous deposits represent only 5 % of global reserves and 13 % of world production (Kauwenbergh, 1997)), while sedimentary rocks exhibit a wide range of Cd content (Ukeles et al., 1994), as reported in Table 4.2.

In addition to the raw material type, the final content of cadmium in WPA and, of course, in the fertilizers depends also on the manufacturing method (Tjioe, 1987). In fact, the sulfuric acid

attack (70 % of the phosphoric acid produced) solubilizes about 66 % of the cadmium present in the raw phosphates (Boussen, 2007).

Table 4.2 The content of cadmium in phosphate ore depending on its country-of-origin (Boussen, 2007; Ukeles et al., 1994).

| Country | Cd content ($g.t^{-1}$) |
|---|---|
| Algeria | 18 |
| Brazil | - |
| Israel | 10 |
| Egypt | - |
| Jordan | 10 |
| Morocco (Khouribga) | 18 |
| Morocco (Youssoufia) | 40 |
| Senegal | 76 |
| Togo | 48 |
| Tunisia | 18 |
| USA (North Carolina) | 45 |
| Russia (Kola) | 0.3 |
| South Africa | 0.15 |

#### *4.2.3.2 Toxicity of cadmium*

Along with manure, biosolids, and atmospheric deposition from the incineration of town wastes, non-ferrous metal production, iron and steel production, and fossil fuel combustion, the phosphorus fertilizers contribute to the anthropogenic input of cadmium to agricultural soils (McLaughlin and Singh, 1999). Furthermore, the extensive use of these fertilizers can increase the cadmium content of agricultural soils from 9 ppb to 162 ppb after adding superphosphates for 40 years (Tjioe, 1987). Previous estimates of annual cadmium intake in arable land in some European countries are shown in Table 4.3.

Cadmium is a toxic contaminant that can accumulate in crops and possibly ingested by human beings (Jiao et al., 2012; Wei et al., 2016). Estimates of the daily intake of cadmium by man via food and water vary from 40 μg to 70 μg, whereas the World Health Organization has recommended a maximum absorption of 7 μg Cd per day (Tjioe, 1987). Accordingly, it represents a potential risk to human health by damaging the kidneys and causing anemia and bone disease (Cichy et al., 2014; Tjioe, 1987).

Table 4.3 Estimated annual cadmium input to arable land in 1980 (Tjioe, 1987).

| Country | Cadmium input ($g.ha^{-1}$) |
|---|---|
| Italy | 1.6 |
| France | 5.4 |
| United Kingdom | 6.5 |
| Irish Republic | 6.6 |
| The Netherlands | 4.6 |
| Belgium | 9.4 |
| Denmark | 2.4 |
| West Germany | 4.6 |

Since it has been proven that one of the major sources of soil pollution by Cd is fertilizers, it is important to develop techniques for the removal of Cd from phosphoric acid as an action to prevent environmental pollution. However, it is first necessary to know the thermodynamic and kinetic properties of the $H_3PO_4/H_2O$ system, which is essential to understand the reactions involved in the manufacturing of phosphoric acid and phosphate fertilizers. This is possible through experimental study and thermodynamic modeling of the $H_3PO_4/H_2O$ system by using a model that can predict with good accuracy the speciation in the bulk solution. Therefore, the following section will be dedicated to discussing experimental studies and modeling, while citing the different thermodynamic models that have been used to study the behavior of the $H_3PO_4/H_2O$ system by determining the chemical composition of phosphoric acid solutions and the species effectively present in these aqueous solutions.

## 4.3 Thermodynamic modeling

### 4.3.1 Chemical equilibria involved in the $H_3PO_4/H_2O$ system

Wet-process acid provides a mixture which is a good example of weak and complex electrolytes. The latter dissociates in three incomplete steps and presents three equilibrium reactions. Numerous authors (Barta and Bradley, 1983; Elmore et al., 1965; Robinson and Stokes, 2002) have determined the equilibrium constants in question and they were assembled by Zemaitis et al. (2010).

$$H_3PO_4 \rightleftharpoons H_2PO_4^- + H^+ \qquad K_1 = \frac{a_{H_2PO_4^-} \times a_{H^+}}{a_{H_3PO_4}} = 0.0007107 \tag{4.8}$$

$$H_2PO_4^- \rightleftharpoons HPO_4^{2-} + H^+ \qquad K_2 = \frac{a_{HPO_4^{2-}} \times a_{H^+}}{a_{H_2PO_4^-}} = 6.3387 \times 10^{-8} \tag{4.9}$$

$$HPO_4^{2-} \rightleftharpoons PO_4^{3-} + H^+ \qquad K_3 = \frac{a_{PO_4^{3-}} \times a_{H^+}}{a_{HPO_4^{2-}}} = 4.5301 \times 10^{-13} \qquad (4.10)$$

Compared to the second and the third reactions, the first one (Eq. (4.8)) is more important because it represents the acid weakness and it is the most used for thermodynamic modeling by several authors, such as Pitzer and Silvester (1976) who used this mechanism to predict the osmotic coefficient ($\phi$) for a molality range from 0 to 6 mol.kg$^{-1}$. However, it could not describe all the reactions happening in the system (Haghtalab and Nosrati, 1998).

Indeed, Elmore et al. (1965) studied the degree of dissociation of phosphoric acid based on vapor pressure, conductance, and pH data at 25 °C and they concluded that for a concentration range of 0.1 to 10 molal, the equilibrium reactions that describe properly this system are:

$$H_3PO_4 \rightleftharpoons H_2PO_4^- + H^+ \qquad K_1 = \frac{a_{H_2PO_4^-} \times a_{H^+}}{a_{H_3PO_4}} = 0.0007107 \qquad (4.11)$$

$$H_3PO_4 + H_2PO_4^- \rightleftharpoons H_5P_2O_8^- \qquad K_4 = \frac{a_{H_5P_2O_8^-}}{a_{H_3PO_4} \times a_{H_2PO_4^-}} = 1.263 \qquad (4.12)$$

$$H_6P_2O_8 \rightleftharpoons H^+ + H_5P_2O_8^- \qquad K_5 = \frac{a_{H^+} \times a_{H_5P_2O_8^-}}{a_{H_6P_2O_8}} = 0.3 \qquad (4.13)$$

In the same way as Elmore et al. (1965), other authors (Ruiz-Beviá et al., 1995; Selvaratnam and Spiro, 1965) noticed that the anion generated from the first dissociation stage (Eq. (4.8)), $H_2PO_4^-$, has a good trend to pair with the undissociated $H_3PO_4$ and eventually to form $H_5P_2O_8^-$ anion. The presence of $H_5P_2O_8^-$ species in aqueous phosphoric acid solutions was proved by Raman spectra study (Cherif et al., 2000b). In addition, it is considered that at $m_{H_3PO_4}$> 2 mol.kg$^{-1}$, $H_5P_2O_8^-$ concentration is not negligible. For the entire concentration range, the main species are considered as $H_5P_2O_8^-$, $H^+$, $H_2PO_4^-$, $H_3PO_4$. Thus, by combining Eqs. (4.8) and (4.11), the overall equilibrium reaction may be written as:

$$H_6P_2O_8 \leftrightarrows H^+ + H_5P_2O_8^- \qquad K_6 = \frac{a_{H^+} \times a_{H_5P_2O_8^-}}{(a_{H_3PO_4})^2} = K_1 \times K_4 = 0.0089 \qquad (4.13)$$

### 4.3.2 Thermodynamic modeling of the $H_3PO_4/H_2O$ system

As described above, the industrial phosphoric acid solutions are composed of a multitude of molecular and ionic entities interacting between them according to different reactions (Eq. (4.8) and Eqs. (4.11)-(4.13)).

The thermodynamic modeling of such electrolyte system is based on (i) the choice of the thermodynamic model, (ii) the chemical reactions, and (iii) the available experimental data (Messnaoui and Bounahmidi, 2005). Indeed, for such complex and concentrated aqueous solutions, the model of Pitzer (1973), and Bromley (1973a) based on the concept of the total composition, and the electrolyte-NRTL model (Kontogeorgis and Folas, 2010), the Cruz model (Cruz and Renon, 1978), and Extended-Uniquac model (Thomsen, 2009) based on the concept of the local composition are the most frequently used. The Pitzer and electrolyte-NRTL models are employed to represent the nonideality of complex and concentrated solutions and offer a database which covers a diverse range of single electrolytes systems with the richest interactions parameters (Messnaoui and Bounahmidi, 2005).

The study of the thermodynamic properties of phosphoric acid has been the aim of several articles (Christensen and Thomsen, 2003; Haghtalab and Nosrati, 1998; Jiang, 1996; Pitzer and Silvester, 1976; Rumpf and Maurer, 1994). For this type of complex electrolytes, various models have been developed to estimate the excess Gibbs energy, and the corresponding adjustable parameters were defined from vapor-liquid equilibrium experimental data and derived properties values (Gibbs free energy, enthalpy…). In this context, Haghtalab and Nosrati (1998) used the NRTL-NRF model to calculate the mean ionic activity coefficient and pH for various concentrations of $H_3PO_4$. According to their results, they noticed that a disagreement between the activity coefficient obtained by this model and the one calculated by the Pitzer and Silvester (1976) and Cruz and Renon (1978) models. This discrepancy can be explained by the fact that in the Cruz-Renon model, the values are based on the complete dissociation of $H_3PO_4$ into $H^+$ and $H_2PO_4^-$; while the values of the Pitzer-Silvester model are related to the partial dissociation based on the Eq. (4.8) up to a molality of 6 mol.kg$^{-1}$.

Messnaoui and Bounahmidi (2005) used the electrolyte-NRTL model to estimate the excess properties and the vapor-liquid equilibrium of the aqueous phosphoric acid. Hence, to describe the $H_3PO_4/H_2O$ system, they investigated two mechanisms; in the first one, they considered only the first dissociation of the phosphoric acid (Eq. (4.8)), and in the second mechanism, they took into account the first dissociation of $H_3PO_4$ and the chemical reaction of dimer formation $H_5P_2O_8^-$ (Eqs. (4.8) and (4.11)). As a result, they reported that the electrolyte-NRTL model considering only the first dissociation successfully predicts the osmotic coefficient ($\phi$), the undissociated $H_3PO_4$ activity ($a_{H_3PO_4}$), and the total vapor pressure ($P^0$) for molalities up to 36 mol.kg$^{-1}$ and at different temperatures varied between 298.15 and 428.15 K. Besides, the integration of the $H_5P_2O_8^-$ formation permits a good estimation of the parameters mentioned

above ($\phi$, $a_{H_3PO_4}$, p). In the electrolyte-NRTL model (1st mechanism), the adjusted parameters $\beta_{(H^+,H_2PO_4^-)-H_3PO_4}$ and $\beta_{H_3PO_4-(H^+,H_2PO_4^-)}$ have to be reexamined to obtain satisfactory results. However, Cherif et al. (2000a) reported that the adjusted parameter $\beta_{(H^+,H_2PO_4^-)}$ in Pitzer model had no significant improvement in the data representation.

In order to compare the different findings of thermodynamic models, we chose three parameters (pH, osmotic coefficient, and speciation) that are considered as important; a disagreement can be noticed between the models and the experimental data. Figure 4.6 summarizes the results obtained for pH calculation based on different models compared to experimental data of Elmore et al. (1965) at 25 °C (Table 4.4). The pH data obtained by the approach of Rumpf and Maurer (1994) agreed with those calculated by Cherif et al. (2000a) and at higher concentrations, there is a concordance between the experimental and calculated pH values (-0.28 – 1.57) by the NRTL-NRF model (Haghtalab and Nosrati, 1998). However, using Pitzer model (Pitzer and Silvester, 1976), Jiang's approach (Jiang, 1996) failed to represent these data, especially at high concentrations. The pH calculated with electrolyte-NRTL model (using the first mechanism) deviated from Elmore et al. (1965) data with an increase in $H_3PO_4$ concentration with an increase in the average error until it reached 16.2%, whereas the inclusion of the chemical equilibrium that involves $H_5P_2O_8^-$ formation reduced the pH deviation to 5.2 %. In addition, with Pitzer and Silvester model (Pitzer and Silvester, 1976), the pH values were underestimated for acid molality greater than 2 mol.kg$^{-1}$ (Rumpf and Maurer, 1994).

Table 4.4 Summary of different experimental studies of $H_3PO_4/H_2O$ system.

| Authors | Molality range (mol.kg$^{-1}$) | Temperature (K) | Measured parameters |
|---|---|---|---|
| Elmore et al. (1965) | 0.1 – 10 | 298.15 | pH |
| Elmore et al. (1965) | 0.1 – 10 | 298.15 | Speciation |
| Cherif et al. (2000b) | 0.3 – 9.7 | 298.15 | Speciation |
| Preston and Adams (1977) | 0 – 4.9 | 298.15 | Speciation |
| Platford (1975) | 0.1236 – 18.541 | 298.15 | Osmotic coefficient |
| | 1.648 – 10.845 | 273.15 | Osmotic coefficient |
| Elmore et al. (1946) | 0.1389 – 35.773 | 298.15 | Osmotic coefficient |

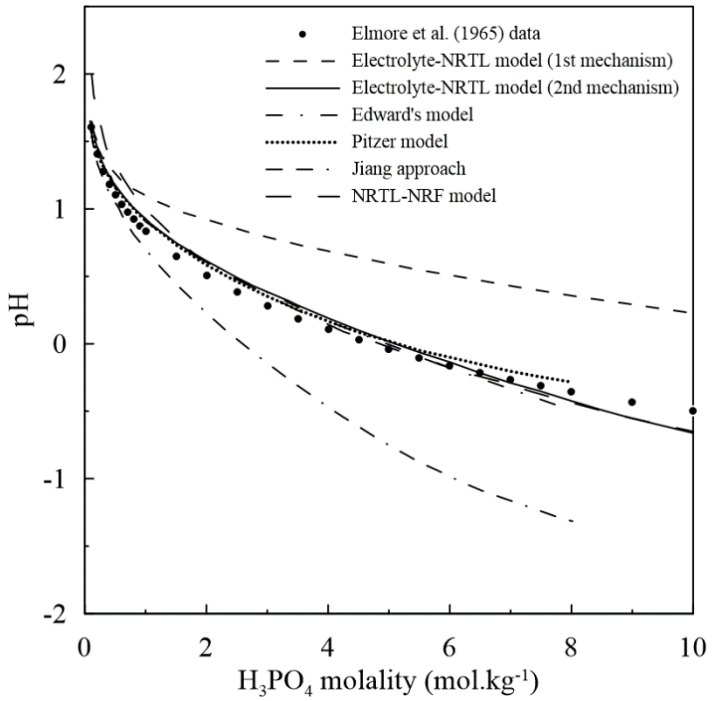


Figure 4.6 Comparison between experimental and calculated pH values in phosphoric acid solutions at 298.15 K.

Osmotic coefficient is used for representing the activity of solvents in electrolyte solutions, its definition depends on the ways of expressing the chemical composition of mixtures (Kontogeorgis and Folas, 2010). Because of the low volatility of phosphoric acid, the vapor phase in equilibrium with the $H_3PO_4/H_2O$ solutions contains only water; so, it is feasible to determine the osmotic coefficient with high accuracy using the isopiestic method (Platford, 1975). This is very relevant because osmotic coefficients are real excess properties, and subsequently, much more sensitive to the influence of the γ model parameters (γ: activity coefficient is a fractional number which when multiplied by the molar concentration of a substance in solution yields the chemical activity). This term provides an approximation of how much interaction exists between molecules at higher concentrations. Besides, activity coefficients of ions are determined using electromotive force, freezing point, and solubility measurements or are calculated using the theoretical equation of Debye and Hückel (Considine, 2005). Platford (1975) measured the osmotic coefficients at 25 °C in the 0.1236 – 18.541 molality range using the isopiestic method. It should be emphasized that the osmotic coefficients are evaluated based on the total dissociation of $H_3PO_4$ into $PO_4^{3-}$ and $H^+$. This must be indicated because the experimental values of the osmotic coefficients may have different definitions in the case of partial dissociation. From Figure 4.7, it can be noticed that the calculated values of the osmotic coefficient by Cherif et al. (2000a) and Jiang (1996) (for

the entire studied molality range from 0 to 9 mol.kg$^{-1}$) are in agreement with the experimental data (Elmore et al., 1946; Platford, 1975). Hence, for both mechanisms, the electrolyte-NRTL model (Messnaoui and Bounahmidi, 2005) showed high performance in estimating the osmotic coefficient for aqueous solutions of $H_3PO_4$ from low molalities up to 36 mol.kg$^{-1}$. The root mean standard deviation from experimental values was equal to 0.0102 for the first mechanism and to 0.006 for the second one.

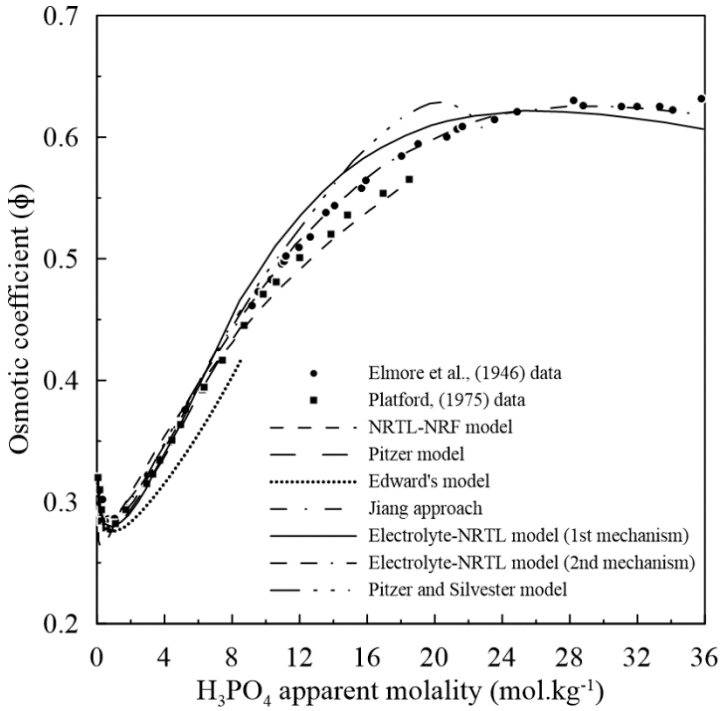


Figure 4.7 Representation of osmotic coefficients in aqueous solutions of phosphoric acid at 298.15 K.

Finally, for speciation, the approach of Jiang (1996) and Rumpf and Maurer (1994) model failed to calculate the $H_3PO_4$ molality, especially at higher acid apparent molality, as observed in Figure 4.8. Therefore, the results obtained by the model proposed by Cherif et al. (2000a) were consistent with the experimental data presented in their earlier work (Cherif et al., 2000b) where they determined the species present in aqueous phosphoric acid at concentrations of 2.1 % to 47.09 % $P_2O_5$ at 25 °C using Raman spectroscopy, whereas the calculation of speciation for the $H_3PO_4/H_2O$ system by Electrolyte-NRTL model (Messnaoui and Bounahmidi, 2005) using the two mechanisms gave contradictory results. Thus, the estimated value agreed with the experimental data of Preston and Adams (1977) and Cherif et al. (2000b), respectively. It is, therefore, important to identify the species present in the $H_3PO_4/H_2O$ system through new experimental studies, which will determine the appropriate mechanism for species estimation.

The approach on which Pitzer and Silvester (1976) relied did not consider the $H_5P_2O_8^-$ formation; also, the Haghtalab and Nosrati model Haghtalab and Nosrati (1998) model ignored the $H_2PO_4^-$ species, so that both of them could fail in the distribution of species calculation because it is clear that $H_2PO_4^-$ is present in a large amount.

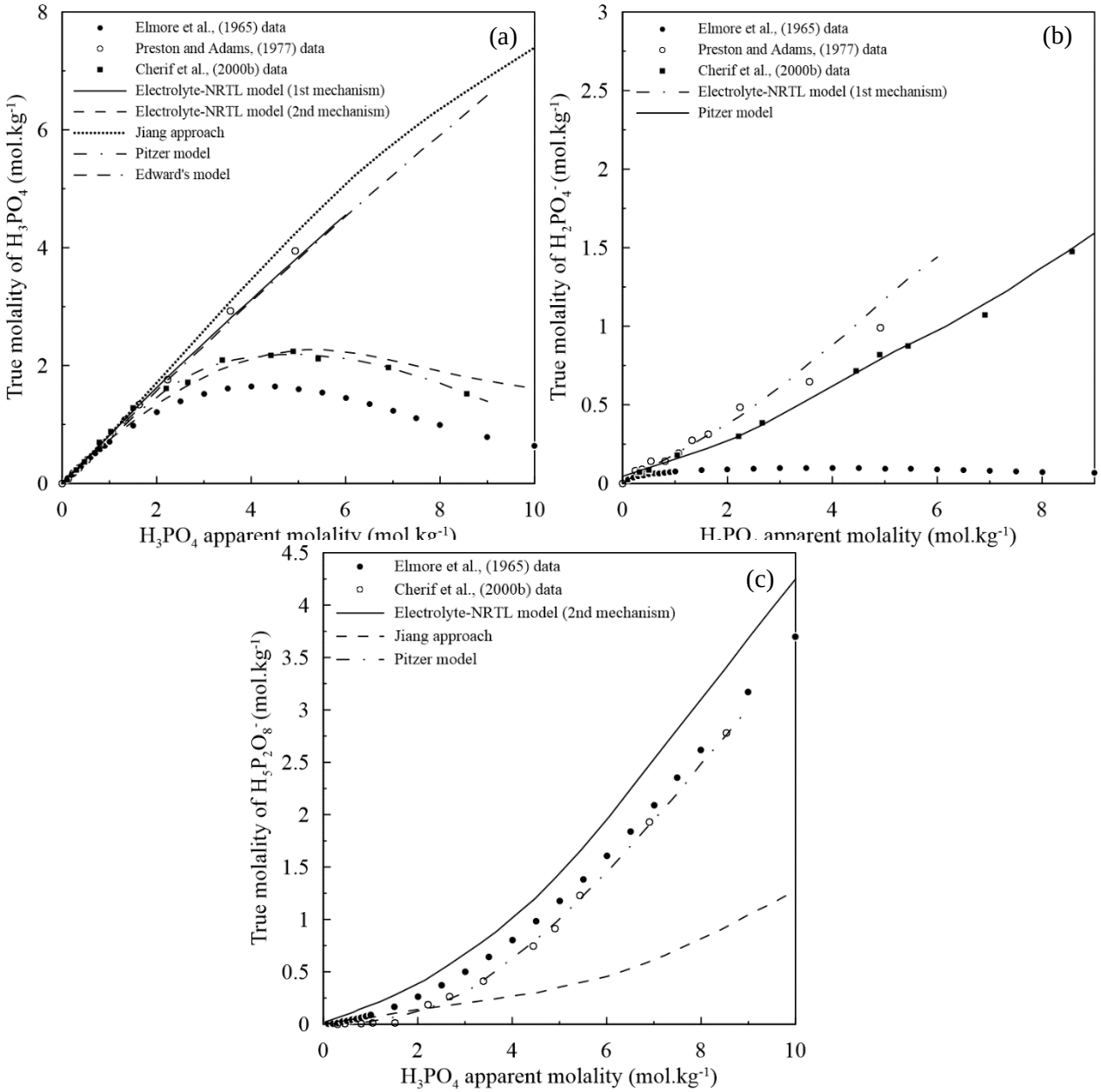


Figure 4.8 Calculated and experimental distribution of species in aqueous phosphoric acid solutions at 298.15 K ((a) $H_3PO_4$, (b) $H_2PO_4^-$, (c) $H_5P_2O_8^-$).

Comparing the works carried out on the thermodynamic modeling of the $H_3PO_4/H_2O$ system (Table 4.5), it is worth noting that most of the models are limited because they describe only diluted media at a temperature of 25 °C. Hence, it is not the case of industrial phosphoric

acid which generally has a concentration of 29 % and 54 % $P_2O_5$, and a temperature of about 70 °C. With the exception of Electrolyte-NRTL model (Table 4.6) used by Messnaoui and Bounahmidi (2005) which covers the operating conditions of industrial phosphoric acid manufacture (temperature, concentration), but taking into account the contradiction between mechanisms 1 and 2, it would be difficult to decide about the choice of the suitable mechanism. Therefore, it is necessary to carry out experimental studies in order to identify the species present in the $H_3PO_4/H_2O$ system. Moreover, further experimental studies are needed to test the reliability of the proposed models, because a realistic modeling approach must include not only phase equilibria data, but also liquid phase composition data.

Table 4.5 Summary of different studies for modeling of $H_3PO_4/H_2O$ system.

| Thermodynamic models | Reactions chemical equilibrium | Molality range (mol.kg$^{-1}$) | Temperature (K) | Thermodynamic properties | Relative deviation (%) | Ref. |
|---|---|---|---|---|---|---|
| Pitzer model | $H_3PO_4 \rightleftharpoons H^+ + H_2PO_4^-$ | 0 – 6.0<br>0 – 6.0<br>0 – 5.0 | 298.15<br>298.15<br>298.15 | Osmotic coefficient<br>Orthophosphoric activity<br>Speciation | 0.93<br>1.21<br>5.12 | Pitzer and Silvester (1976) |
| Bromely model | $H_3PO_4 \rightleftharpoons H^+ + H_2PO_4^-$<br>$H_3PO_4 + H_2PO_4^- \rightleftharpoons H_5P_2O_8^-$<br>$H_6P_2O_8 \rightleftharpoons H^+ + H_5P_2O_8^-$ | 0.1 – 10.0 | 298.15 | Degree of dissociation coefficient | 0.93 | Bromley (1973) |
| Edward model | $H_3PO_4 \rightleftharpoons H^+ + H_2PO_4^-$<br>$H_2PO_4^- \rightleftharpoons H^+ + HPO_4^{2-}$<br>$HPO_4^{2-} \rightleftharpoons H^+ + PO_4^{3-}$<br>$H_3PO_4 + H_2PO_4^- \rightleftharpoons H_5P_2O_8^-$ | 0 – 4.0<br>4.0 – 9.0 | 298.15<br>298.15 | Water activity<br>Water activity | 1.00<br>2.00 | Rumpf and Maurer (1994) |
| Pitzer model | $H_3PO_4 \rightleftharpoons H^+ + H_2PO_4^-$<br>$H_3PO_4 + H_2PO_4^- \rightleftharpoons H_5P_2O_8^-$ | 0 – 24.0 | 298.15 | Water activity<br>Orthophosphoric Activity | 0.80<br>12.10 | Jiang (1996) |
| NRTL-NRF model | $2H_3PO_4 \rightleftharpoons H^+ + H_5P_2O_8^-$ | 18.5 | 298.15 | Osmotic coefficient<br>pH | 1.30<br>5.47 | Haghtalab and Nosrati (1998) |
| Pitzer model | $H_3PO_4 \rightleftharpoons H^+ + H_2PO_4^-$<br>$H_3PO_4 + H_2PO_4^- \rightleftharpoons H_5P_2O_8^-$ | 9.0<br>8.75 | 298.15<br>298.15 | Osmotic coefficient<br>Speciation | 1.32<br>4.76 | Cherif et al. (2000a) |
| Extended-Uniquac model | $H_3PO_4 \rightleftharpoons H^+ + H_2PO_4^-$<br>$H_2PO_4^- \rightleftharpoons H^+ + HPO_4^{2-}$ | 9.9<br>5.0 | 273.5-298.15<br>298.15 | Osmotic coefficient<br>Speciation | 5.20<br>3.96 | Christensen and Thomsen (2003) |
| Electrolyte-NRTL model | $H_3PO_4 \rightleftharpoons H^+ + H_2PO_4^-$ | 0 – 5.0<br>0 – 10.0<br>> 36.0<br>0 – 36.0<br>0 – 36.0<br>> 36 | 298.15<br>298,15<br>293.15 – 373.15<br>298.15<br>298.15<br>373.35 – 431.15 | Speciation<br>pH<br>Total vapor pressure<br>Osmotic coefficient<br>Orthophosphoric activity<br>Normal temperature boiling point | 5.40<br>16.2<br>2.50<br>1.02<br>2.10<br>0.43 | Messnaoui and Bounahmidi (2005) |
| Electrolyte-NRTL model | $H_3PO_4 \rightleftharpoons H^+ + H_2PO_4^-$<br>$H_3PO_4 + H_2PO_4^- \rightleftharpoons H_5P_2O_8^-$ | 0 – 10.0<br>0 – 10.0<br>> 36.0<br>0 – 36.0<br>0 – 36.0 | 298.15<br>298.15<br>293 – 303<br>298.15<br>298.15 | Speciation<br>pH<br>Total vapor pressure<br>Osmotic coefficient<br>Orthophosphoric activity | 8.92<br>5.20<br>0.46<br>0.6<br>1.93 | Messnaoui and Bounahmidi (2005) |

Table 4.6 Interactions parameters estimated for Electrolyte-NRTL model for two mechanisms at 298.15 K (Messnaoui and Bounahmidi, 2005).

| Model | Mechanism | System of equations | Interaction parameters | Values estimated |
|---|---|---|---|---|
| Electrolyte-NRTL model | $H_3PO_4 \rightleftharpoons H^+ + H_2PO_4^-$ | $m_{ap} = m_{H_3PO_4} + m_{H_2PO_4^-}$ | $\tau_{H_2O-H_3PO_4}$ | 6.8686 |
| | | | $\tau_{H_3PO_4-H_2O}$ | -4.9068 |
| | | $k_1 = \frac{m_{H^+} m_{H_2PO_4^-}}{m_{H_3PO_4}} \frac{\gamma_{H^+}\gamma_{H_2PO_4^-}}{\gamma_{H_3PO_4}}$ | $\tau_{H_2O-(H^+,H_2PO_4^-)}$ | 9.5129 |
| | | | $\tau_{(H^+,H_2PO_4^-)-H_2O}$ | -4.2157 |
| | | $m_{H^+} = m_{H_2PO_4^-}$ | $\tau_{H_3PO_4-(H^+,H_2PO_4^-)}$ | 1.2279 |
| | | | $\tau_{(H^+,H_2PO_4^-)-H_3PO_4}$ | -1.2618 |
| Electrolyte-NRTL model | $H_3PO_4 \rightleftharpoons H^+ + H_2PO_4^-$<br>$H_3PO_4 + H_2PO_4^- \rightleftharpoons H_5P_2O_8^-$ | $m_{ap} = m_{H_3PO_4} + m_{H_2PO_4^-} + 2m_{H_5P_2O_8^-}$ | $\tau_{H_2O-H_3PO_4}$ | 2.3235 |
| | | $k_1 = \frac{m_{H^+} m_{H_2PO_4^-}}{m_{H_3PO_4}} \frac{\gamma_{H^+}\gamma_{H_2PO_4^-}}{\gamma_{H_3PO_4}}$ | $\tau_{H_3PO_4-H_2O}$ | -3.1996 |
| | | | $\tau_{H_2O-(H^+,[H_2PO_4^-,H_5P_2O_8^-])}$ | 12.193 |
| | | $k_2 = \frac{m_{H_5P_2O_8^-}}{m_{H_3PO_4} m_{H_2PO_4^-}} \frac{\gamma_{H_5P_2O_8^-}}{\gamma_{H_3PO_4}\gamma_{H_2PO_4^-}}$ | $\tau_{(H^+,[H_2PO_4^-,H_5P_2O_8^-])-H_2O}$ | -5.5949 |
| | | | $\tau_{H_3PO_4-(H^+,[H_2PO_4^-,H_5P_2O_8^-])}$ | 3.7428 |
| | | $m_{H^+} = m_{H_2PO_4^-} + m_{H_5P_2O_8^-}$ | $\tau_{(H^+,[H_2PO_4^-,H_5P_2O_8^-])-H_3PO_4}$ | 8.1038 |

## 4.4 Processes for Cd(II) removal from WPA

### 4.4.1 Solvent extraction

In general, solvent extraction is one of the most commonly used methods for purifying phosphoric acid; it has been the subject of several studies (Awwad et al., 2013; Hannachi et al., 2007; Mellah and Bauer, 1995; Mellah and Benachour, 2006a; Stenström and Aly, 1985). Similarly, solvent extraction coupled with emulsion liquid membrane has been used to extract Cu and Cd from WPA (Lizon and Ortiz, 1997; Urtiaga et al., 2000).

At the industrial scale, purification of phosphoric acid by solvent extraction is difficult, because WPA is rich in organic matter. Indeed, during the intimate mixture of the crude aqueous phase and the extractive organic phase, an emulsion is formed by the presence of organic matter, so it is almost impossible to obtain a settling of the phases. In addition, the phosphoric acid color turns to very dark brown, which is not acceptable in the food industry; so, it is necessary to reduce the organic content by calcination of phosphate rock before digestion. Furthermore, this treatment does not generate an extracted colorless acid (Boussen, 2007).

Mellah and Benachour, (2007a, 2006b) used Kelex100 and TBP (Tri-nbutyl phosphate) in kerosene for the extraction of cadmium in the presence of zinc and chromium contained in phosphoric acid solutions (29 % $P_2O_5$). They found that the increase in Kelex 100 concentration led to an increase in the metal ions extraction. In the optimal conditions, the loading capacities were found to be 83 %, 80 %, and 71 % for Zn, Cr, and Cd, respectively, which indicates that the extractant is highly selective for the metal ions considered in phosphoric acid solutions. Unlike Zn(II) and Cr(III), the cadmium extraction rate decreased with increasing aqueous phase pH; thus, Cd extraction requires lower pH due to the high complexing ability of phosphoric acid.

Cyanex 301 and 302 are among the extractants introduced commercially by Cytex Industries, these are the monothio- and dithio- substituted analogs of Cyanex 272 (bis(2,4,4-tri-methylpentyl)phosphinic acid) (Sole and Hiskey, 1995), respectively. These extractants have been used to extract Cd(II) and Pb(II) from phosphoric acid and chloride solutions (Almela et al., 1998; Almela and Elizalde, 1995; Alonso et al., 1997; Menoyo et al., 2001), and other metals, such as Cu(II), Zn(II), Fe(III), Fe(II), Co(II), Ni(II) and Mn(II) from sulfate solutions (Reddy et al., 2006; Tait, 1992). According to Almela et al. (1998) and Tait (1992), Cyanex 302 and Cyanex 301 are suitable and effective in metals extraction from acidic solutions. In this context, (Boussen, 2007) employed Cyanex 302 for the extraction of Cd from synthetic and

industrial phosphoric acid solutions; as a result, they found that Cyanex 302 has good stability in all phosphoric acid media [5 % − 60 % $P_2O_5$], which confirms that its performance is not affected by the variation of phosphoric acid concentration. Another studied parameter was temperature; indeed, they reported that temperature (20 °C, 50 °C, and 70 °C) has no effect on the cadmium removal rate, so phosphoric acid can be treated without having to be cooled.

Touati et al. (2009) proposed a mixer-settler extraction stripping process using di(2-ethylhexyl) dithiophosphoric acid ($D_2$EHDTPA denoted HR) in dodecane for extraction of cadmium from phosphoric acid solution (30 % $P_2O_5$). In preliminary batch tests, they reported that a small concentration of extractant (0.02 M) was sufficient to achieve a complete extraction of cadmium from phosphoric acid; however, ten times higher concentrations were required to achieve the same performance as Cyanex 302. Under steady-state conditions, the yields of extraction and stripping were more than 99 % and 96 %, respectively, by using a continuous micro-pilot scale mixer-settler. They found that experimental results were in good agreement with those predicted based on the McCabe-Thiele method. Then, the authors proposed a flow sheet for a counter-current multistage process including two extraction ideal stages and six stripping ones (Figure 4.9) to purify the WPA and to recover a relatively concentrated cadmium solution.

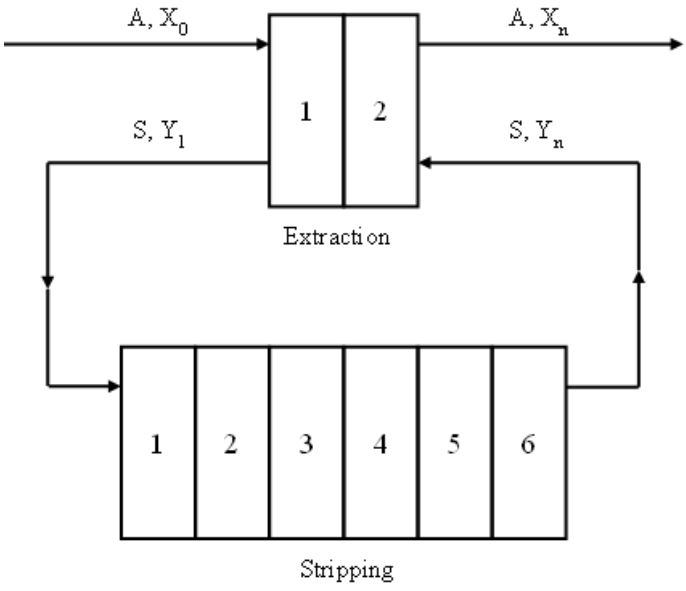


- A and S are respectively the flow rate of the aqueous and the organic phases for the extraction step.

- $X_0$ is the initial cadmium amount, and $X_n$ is the cadmium amount in the aqueous phase leaving stage n.

- $Y_1$ and $Y_n$ are the cadmium amount in the organic phase leaving the first and $n^{th}$ extraction stage.

Figure 4.9 Flowsheet for a counter-current multistage process proposed by (Touati et al., 2009).

The thermodynamic aspect of the extraction of $Zn(II)$, $Cd(II)$, and $Cr(III)$ from phosphoric acid solutions by TBP (tri-*n* butyl phosphate) relying on the effect of the extractant concentration and temperature on the efficiency process were studied by Mellah and Benachour (2007a). Under the operating conditions of equilibrium pH 1.5 ± 0.1, phase ratio O/A = 1, contact time = 30 min at 25 °C, sodium nitrate (5 M $NaNO_3$) was added to the mixture as a source of nitrate ions by the salting-out action in order to increase the distribution coefficient of the metals. These authors found that the distribution coefficients D increased with increasing phosphoric acid concentration to a maximum value ($[H_3PO_4]$ = 30 % $P_2O_5$) at 20 % vol TBP in kerosene, and then decreased rather rapidly with further increase in phosphoric acid concentration (Figure 4.10). This phenomenon was due to the formation of other species, $Zn(H_2PO_4)^+$, $Cd(H_2PO_4)^+$, and $Zn(H_2PO_4)^{2+}$, which are less extractable by TBP. On the other hand, they reported that the cadmium distribution coefficient ($D_{Cd}$) increased with increasing temperature (from 20 °C to 75 °C) showing that the process is endothermic. As a result, they expressed the dependence between the distribution coefficients, temperature, and TBP concentration by the following equation (Mellah and Benachour, 2007a):

$$\log D_{Cd} = \frac{-2.37}{T} + 7.19 + 2\log[NO_3^-]_{aq} + 1.96\log[TBP]_{org} \quad (4.14)$$

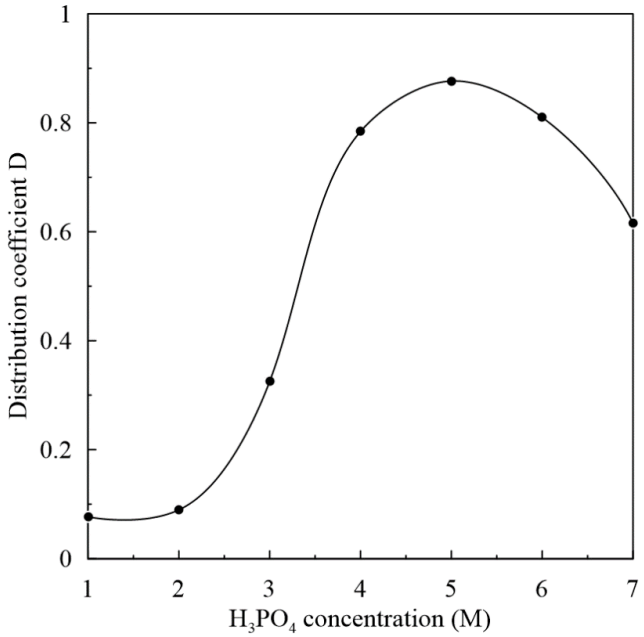


Figure 4.10 Extraction of cadmium from $H_3PO_4$ by 20 % (v/v) TBP in kerosene (Mellah and Benachour, 2007a). Operating conditions: $[Cd^{2+}] = 0.05 \times 10^{-2}$ mol.L$^{-1}$, equilibrium pH 1.5 ± 0.1, phase ratio O/A = 1, and contact time 30 min at 25 °C.

However, it turned out that the extraction of Cd by TBP requires significant solvent flow compared to the flow rate of the phosphoric acid aqueous solution to be purified, which leads to the use of very large installations and thereby, high investment.

In order to intensify the extraction and separation of metals from aqueous solutions, such as sulfate solutions, several researchers used mixed extractants (Gotfryd and Cox, 2006; Preston and Preez, 1994). Elyahyaoui and Bouhlassa (2001) investigated the extraction of Cd with a mixture of HDEHP (di(2-ethylhexyl) phosphoric acid), TBP, TOPO (trioctyl phosphine oxide), and TPPO (triphenyl phosphine oxide). Nevertheless, they found that the recovery of cadmium from phosphoric acid solutions was less than with HDEHP alone. Besides, they reported that the addition of sulfate anions to $H_3PO_4$ solutions does not affect the recovery of cadmium. However, the addition of iodide anions improved the extraction of Cd(II) from$H_3PO_4$ and also $HClO_4$ media by HDEHP because they lead to the formation of $CdI^+$ and $CdI_2$, in the aqueous medium, which are extractable by HDEHP.

Another approach for the extraction of cadmium from phosphoric acid solutions is to use amine-based extractants (viz. trioctyl amine and Alamine 336) (Skorovarov et al., 1998; Stenström and Aly, 1985). In this context, Nazari et al. (2005) used Alamine 336 to extract Cd from WPA. B-65 kerosene was chosen as a diluent because of its low cost, safety, and higher process efficiency compared to A-55 kerosene and 1-2-4 trimethylbenzene. They concluded that the Cd extraction increased with increasing extractant concentration, but then it decreased; this can be explained by the polymerization of Alamine 336. Conversely, the temperature has no significant effect on Cd extraction, which is an advantage in the extraction process. However, Nazari et al. (2005) reported that the pretreatment of WPA by the addition of 250 µm activated charcoal improved Cd extraction because it reduced fine suspended particles and organics, and also Cd was adsorbed onto activated charcoal.

Purification of phosphoric acid by liquid-liquid extraction is a complex process that simultaneously involves chemical and physical equilibria. Thus, most of the reported research works have an experimental nature and just a few are based on modeling. In this context, Boulkroune and Meniai (2012) studied the case of purification of WPA contaminated with cadmium by $D_2$EHDTPA diluted in dodecane based on the experimental study of Touati et al. (2009) using modified UNIQUAC model to calculate the interaction parameters and, thereby, to predict the activity coefficients.

According to this model, the activity coefficient is expressed as follows:

$$\ln \gamma_n = \ln \gamma_n^{DH} + \ln \gamma_n^{C} + \ln \gamma_n^{R} \quad (4.15)$$

$$\ln \gamma_b^{*} = \ln \gamma_b^{*,DH} + \ln \gamma_b^{*,C} + \ln \gamma_b^{*,R} \quad (4.16)$$

n and b referred to the solvent and the ion, respectively. $\ln \gamma_n^{DH}$ , $\ln \gamma_n^{C}$, and $\ln \gamma_n^{R}$ are the Debye-Hückel, combinatorial, and residual terms.

Indeed, the different chemical equilibria taking place in the aqueous phase are Eqs. (4.8)-(4.13), and the following complexation reaction (Bendada et al., 2001):

$$Cd^{2+} + 2HR \rightleftharpoons CdR_2 + 2H^{+} \qquad K_7 = 11 \times 10^{6} \quad (4.17)$$

Through their study, the authors found that for a small quantity of extracting agent, a rapid increase in the ratio of the complex is noted and even for low concentrations of the metal. It was also reported that an increase in $H_3PO_4$ concentration led to a decrease in the ratio of complexation, which agrees with the experimental results.

Besides phosphoric acid, some authors extracted cadmium from phosphates, Benredjem and Delimi (2009) carried out tests on Gebel El Onk phosphates to remove cadmium by using three extracting agents (ammonium acetate salt, diamine tetra-acetic, and hydrochloric acids), and through this study, the authors showed that HCl presents the highest content of cadmium extract that corresponds to an extraction rate of 71 %. To strengthen their research, they investigated the influence of some parameters on the HCl extraction of cadmium. They found that the concentration of the cadmium extracted increased when the concentration of HCl varied from 0.1 to 0.5 M, but it became constant once [HCl] > 0.5 M. A second parameter was studied, the temperature (25 – 55 °C), and they found that an increase in the temperature generated a slight increase in the amount of cadmium eliminated. Moreover, these authors investigated the ratio effect (mass ore/volume of HCl); they found that the extraction rate was over 71 % when the ratio was less than 1/25.

In another work, Benredjem et al. (2016) performed tests on cadmium extraction from phosphates by using $Na_2EDTA$ and have studied the effect of the consecutive extractions number, microwave power, and microwave irradiation time on cadmium extraction. They deduced that the cumulative removal of cadmium from phosphate after the first and third extraction cycles were 38.9 % and 55.9 %, respectively. The increase in the extraction number leads to an increase in the amount of cadmium extracted, and an increase in microwave power

(100 – 400 W) results in a higher extraction rate of cadmium; it reached 40.1 % when the microwave power was set at 400 W. The extraction efficiency increased also with the time of radiation exposure; therefore, to preserve the properties of ore, the time exposure should not exceed 5 min. Furthermore, microwave technology has been rarely employed on a large-scale due to the limitations that it presents against scale-up, such as high energy consumption, safety, and design issues.

A few studies carried out on solvent extraction are detailed in Table 4.7.

Table 4.7 Overview of Cd removal from WPA by solvent extraction.

| Extractant | Diluent | Extractant concentration (M) | $H_3PO_4$ concentration (% $P_2O_5$) | Initial Cd concentration ($mg.L^{-1}$) | Equilibrium pH | Temperature (°C) | Set-up | Extraction efficiency (%) | Remarks | Ref. |
|---|---|---|---|---|---|---|---|---|---|---|
| $D_2$EHDTPA | Dodecane | 0.02 | 28 | 40 | 0.16 | 20±2 | Continuous experiments in mixer-settler system of 0.25 L | 99.1 | The cadmium in the organic phase was recovered and stripped by HCl 4 M. | Touati et al. (2009) |
| Cyanex 302 | - | 0.005 | 30 | 3.26 | - | 20 and 50 | - | 80 | Mixing time was from about 2 to 15 min. The phosphoric acid used is an industrial phosphoric acid. Temperature does not affect the efficiency of the extractant. | Boussen (2007) |
| Cyanex 302 | - | 0.005 | 52.7 | 3.26 | - | 70 | - | 80 | | |
| Kelex 100 | Kerosene | 0.4 | 29 | 56.21 | 1.5 ± 0.1 | 25 | Batch tests in thermostatic mechanically agitated beakers, the volume of solution 50 mL | 71 | As a modifier, n-decanol was added to improve phase separation and to enhance the rate of extraction. | Mellah and Benachour (2006a) |
| D2EHPA | Kerosene | 0.5 | 29 | 56.21 | 2.0 ± 0.1 | 25 | Batch tests in thermostatic mechanically agitated beakers, volume of solution 50 mL | 65.46 | Beyond 0.3 M, the D2EHPA concentration had no effect on the metal extraction. | Mellah and Benachour (2006b) |

Table 4.7 Continued.

| | | | | | | | | | | |
|---|---|---|---|---|---|---|---|---|---|---|
| Alamine336 | B-65 Kerosene | _ | 51 | 50 | - | 29 | Batch tests in stirred beakers, the volume of the solution not given | 74 ± 2.54 | Mixing time was 5 min Organic phase containing 1% Alamine336 +1.5% iso-decanol in B-65 kerosene. | Nazari et al. (2005) |
| Cyanex 302 | Kerosene | 0.01 | 23.72 | 50 | 0.17 | - | Batch tests in stoppered shaken tubes, the volume of solution 20 mL | 90 | During extraction, $Cd(II)$ forms $CdR_2(HR)$ complex in the organic phase. | Almela et al. (1998) |
| Trioctyl amine | Kerosene | 0.05 | 33 | 52 | - | - | - | 95 | 2.2 vol.% decanol was added and the optimal mixing time was 5 min. | Skorovarov et al. (1998) |
| p-(1,1,3,3-tetra methylbutyl) phenyl phosphoric acid | Kerosene | 0.2 | 28.61 | 1124 | - | 20 | Batch tests, volume of solution 20 mL | 58.6 | During extraction of metals under different concentrations, order was Ti>Cr>Cd for $H_3PO_4$>7 M, and Cr>Cd>Ti for $H_3PO_4$<5 M. | Mellah and Bauer (1995) |
| Alamine336 | - | 0.1 | 30 | 8.54 | - | 22 | Batch tests in 100 mL separatory funnels, the volume of solution 50 mL | 95 | Tertiary amine extracts Cd from phosphoric acid solution forming a complex of $CdCl_4^{2-}$. | Stenström and Aly (1985a) |

### 4.4.2 Adsorption

The adsorption of inorganic impurities from different aqueous solutions using activated carbon has been the subject of several studies (C.P. Huang, 1978; Jusoh et al., 2007; Kang et al., 2008) for its stability, as well as its large micropore and mesopore volumes and the resulting high surface area, and is still being used with several sorts of modifications. The adsorption capacity of activated carbon depends on: (a) the nature and concentration of the adsorbate, (b) the nature of the adsorbent, (c) the pH of the solution (Purkayastha et al., 2014). According to Babić et al. (2002), $Cd^{2+}$ adsorption on activated carbon cloth was negligible at pH < 3.5 and increased sharply between pH 4 and 9 with a maximum value at pH > 9.5.

Indeed, the elimination of cadmium from phosphoric acid aqueous solutions has rarely been studied using activated carbon or charcoal. Monser et al. (1999) used activated carbon (with a particle size of 100 – 150 μm and a specific area of 1100 $m^2.g^{-1}$) modified with sodium dodecyl sulfate (SDS) to remove Zn, Cr, Cd, Ni, and V from Tunisian WPA (5 % $P_2O_5$). SDS was adsorbed on the surface of activated carbon from a solution of $5 \times 10^{-3}$ M SDS, and the amount adsorbed was $5.03 \times 10^{-4}$ $mol.g^{-1}$ of activated carbon. Through their investigation, they reported that the concentration of Cd decreased from 3.2 $mg.L^{-1}$ to 0.01 $mg.L^{-1}$ (a removal yield of 99 %). Besides, the adsorption efficiency was affected by the increase in the concentration of WPA, for a concentration of 10 % $P_2O_5$, the removal yield of Cd was reduced to reach 44 %.

Another adsorbent that is known for its high adsorption capacity in solution (Kurniawan et al., 2006) and its cheap market price (Virta, 2002) (US$ 0.04-0.12/kg) is clay; this natural material locally available in some regions (like Tunisia) was used as low-cost adsorbents to bind heavy metals such as Cd(II), Ni(II), Cr(III), Zn(II) and organic matter (OM) from wastewater and phosphoric acid solutions (Kaya and Ören, 2005; Lin, 2002; Mellah and Benachour, 2007b; Sultanbayeva et al., 2013). In addition to heavy metals, it must be pointed out that WPA is rich in organic matter such as humic substances like fulvic and humic acids which are chemically reactive. In this context, Omri and Batis (2013) employed different modified clays by insertion or impregnation to eliminate cadmium from WPA (51.65 % $P_2O_5$), because they have a large adsorption capacity. They used six types of adsorbents, namely kaolinite, kaolinite impregnated by *Posidonia oceanica*, K10 montmorillonite, EDTA inserted in K10 montmorillonite, iron oxide inserted in K10 montmorillonite, and activated carbon. These authors studied the effect of contact time between the clay and the adsorbate, and the temperature ($T_1$= 300 K, $T_2$= 313 K, and $T_3$= 333 K) on the kinetics of adsorption and on the cadmium removal efficiency. The obtained results

showed that the increase in adsorbent concentration lead to an increase in the cadmium removal rate (the maximum sorption capacity of kaolinite impregnated by *Posidonia oceanica*, K10 montmorillonite modified by EDTA, and K10 montmorillonite modified by iron oxide were 4.798, 7.535, and 12.97 $mg.g^{-1}$, respectively). They also noticed that cadmium elimination was proportional to temperature, but this was not applicable at high temperature (superior or equal to 60°C). Comparing the adsorption on different clays, they reported that the inserted montmorillonite with EDTA was the best Cd adsorbent (the concentration of cadmium decreased from 15.8 $mg.L^{-1}$ to reach 3.16 $mg.L^{-1}$ at 40 °C). Conversely, Cd concentration decreased from 15.8 $mg.L^{-1}$ to reach 12.04 $mg.L^{-1}$ by using activated carbon, even if this had the highest specific surface (1200 $m^2.g^{-1}$). These findings revealed that the modified clays were effective and economical adsorbents for the removal of cadmium from phosphoric acid solutions. The kinetics study of adsorption also showed that the model of pseudo-second order was better suited to describe the kinetics of adsorption of cadmium on various kind of adsorbents at different temperatures and the equilibrium adsorption of Cd(II) onto different modified clays followed the Freundlich isotherm (Omri and Batis, 2013).

Clay was also used to eliminate copper from phosphoric acid, which confirms the power of clay against heavy metals contained in phosphoric acid. Abdennebi et al. (2013) studied the possibility of copper removal from phosphoric acid (6.77 % $P_2O_5$) using Tunisian bentonite (clay dose ranging from 0.5 g/100 mL acid to 3 g/100 mL acid). They found that bentonite was not effective at a low initial concentration of 3 ppm copper, and the removal yield was 23 %.

Hamza et al. (2016) conducted a study on adsorption of OM (491 $mg.L^{-1}$), Cr(III) (380.2 $mg.L^{-1}$), and Zn(II) (337.4 $mg.L^{-1}$) by Fe-pillared bentonite (Fe-PILB) from industrial WPA (54 % $P_2O_5$). They concluded that the OM removal efficiency by Fe-PILB increased from 48 to 80% with the increase in adsorbent dose from $5 \times 10^3$ to $2 \times 10^4$ $mg.L^{-1}$; this was due to the increase of the available surface area and adsorption capacity. Moreover, a similar trend was observed for Cr(III) and Zn(II) adsorption onto Fe-PILB. However, the authors also found that Fe-PILB is more able to remove OM and cationic impurities from industrial phosphoric acid than raw bentonite, which confirmed the results obtained by Abdennebi et al. (2013). To explain that iron oxide modified the adsorptive properties of clays by their introduction into interlayer spaces. This developed the contact surface and possibly promoted nature's fixation sites of heavy metals and OM.

In order to be close to the actual composition of effluent and quantify the adsorption competition between derived compounds, Zermane and Meniai (2012) studied the elimination of a mixture of four constituents: Cu, Cd, Zn and DBP (dibutylphthalate) from phosphoric acid, using the bentonite,

activated carbon, and coal from olive pits; as a result, they found that the higher removal yield was given by coal from olives pits (19 % and 30.45 % for activated carbon and coal from olive pits, respectively). Besides, they studied the effect of some parameters (stirring rate, time of contact, solid/liquid ratio, and adsorption isotherms). By comparing different stirring rates, the authors noted that 500 rpm gave the best result and low stirring speed did not promote better contact between the adsorbate and the adsorbent. Nevertheless, intensive stirring can have an adverse effect on performance due to the large amount of adsorbent that transferred the solution to the walls of the beaker. Concerning the contact time, the adsorption equilibrium was reached after 30 min in all ratios (R = 1, 2, 3 $g.L^{-1}$), and the kinetics of competitive adsorption of these impurities on activated carbon trading was very fast. They noted that the efficiency of competitive adsorption of inorganic impurities ($Cu^{2+}$, $Cd^{2+}$, and $Zn^{2+}$) and organic matter (DBP) was affected by pH: this increased with augmenting the pH of the solution.

In practice, OM in phosphoric acid decreases the separation efficiency of other impurities, such as cations. That is why it may be important to remove OM before applying any technique to purify phosphoric acid. Hanna and Ali (2007) used animal charcoal powder as an adsorbent to remove OM from wet-process phosphoric acid. They found that the removal of OM decreased as the acid concentration increased, where the removal rate decreased from 75.74 % at a concentration of 20 % $P_2O_5$ to 69.86 % at a concentration of 50 % $P_2O_5$. These authors explained that this decrease could be due to the viscosity of the acid, by dilution, which enabled the charcoal particles to spread and penetrate more easily through the more dilute medium.

A summary of different adsorption studies for the removal of Cd from WPA is presented in Table 4.8.

Table 4.8 Summary of different adsorption studies for the removal of Cd from WPA.

| Adsorbent | Adsorbent dose (g) | $H_3PO_4$ concentration (% $P_2O_5$) | Initial Cd concentration ($mg.L^{-1}$) | Temperature (°C) | pH | Cd removal yield (%) | Remarks | Ref. |
|---|---|---|---|---|---|---|---|---|
| K10 Montmorillonite modified by EDTA | 2 | 51.65 | 15 | 39.85 | - | ≈ 45 | The kinetic of cadmium adsorption was studied during 96 h | Omri and Batis (2013) |
| *Posidonia Oceanica* impregnated kaolinite | 2 | 51.65 | 15 | 39.85 | - | 30 | | |
| K10 Montmorillonite modified by iron oxide | 2 | 51.65 | 15 | 39.85 | - | 27 | | |
| Coal from olives pits | 1 | 3.62 | 11 | 23 | 1.50 | ≈ 25 | Equilibrium time = 60 min | Zermane and Meniai (2012) |
| | 1 | 6.77 | 11 | 23 | 1.44 | 30.45 | Stirring rate = 500 rpm | |
| | 1 | 28 | 11 | 23 | 1.15 | 11.72 | | |
| Activated carbon | 1 | 6.77 | 11 | 23 | 1.44 | 16.25 | | |
| | 2 | 6.77 | 11 | 23 | 1.44 | 18.94 | | |
| | 3 | 6.77 | 11 | 23 | 1.44 | 19.06 | | |
| Activated bentonite | 0.5 – 2.5 | 30 | - | 20 – 70 | 1.25 – 2.50 | 89 | The activation of bentonite was carried out by a chemical process, by using $H_2SO_4$. | Mellah and Benachour (2007b) |
| Activated carbon-Sodium diethyldithiocarbamate | 12 | 10 | 5.2 | 50 | - | 63.46 | SDDC was adsorbed on the surface of activated carbon from a solution of $5.3 \times 10^{-3}$ $mol.L^{-1}$ SDDS. The amount adsorbed was 295 μmol SDDC $g^{-1}$ of activated carbon. | Monser et al. (1999) |
| | 12 | 28 | 9.6 | 50 | - | 23.96 | | |
| Activated carbon-Sodium dodecyl sulfonate | 12 | 10 | 5.2 | 50 | - | 44.23 | SDS is a moderately hydrophobic ion-pairing agent and its adsorption oh the surface of activated carbon changed its characteristics. | |

### 4.4.3 Ion exchange

Ion exchange is the process of purification, separation, and decontamination of aqueous or other ion-containing solutions with solid polymeric or mineral ion exchangers. This technique is widely used in different industries, especially in heavy metal removal from wastewaters due to its high exchange capacity, high removal efficiency, and fast kinetics (Kang et al., 2004). For instance, this technology was set up to extract inorganic impurities, such as cadmium and uranium from industrial WPA using the Purolite S940 resin (Ortiz et al., 1999).

Among the various materials used in ion exchange processes, synthetic resins are mainly preferred, as they are particularly effective in heavy metals removal from aqueous solutions (Alyüz and Veli, 2009). Bearing this in mind, the macroporous sulfonic acid resin, Duolite C264, was found to be the most suitable for Cd(II) removal from phosphoric acid (28 % $P_2O_5$) (Booker, 1989).

Kabay et al. (1998a) carried out tests on the elimination of Cd(II) and Cr(III) from phosphoric acid using different chelating ion-exchange resins, such as Diphonix, Actinide-CU, Diaion CRP200, and RSPO resins. They studied the effect of exchange time, temperature, and acid concentration on Cd removal using 2 h and 24 h exchange time, 30 °C and 50 °C temperature, and 1 %, 3.62 %, 6.77 % and 20 % $P_2O_5$ concentrations. They reported that the batch exchange of Cd(II) decreased when the acid concentration increased, which was due to an increase in proton concentration; they also found that the exchange capacities of the resins were ranked in the following order: Diphonix > Actinide-CU >> Diaion CRP200 >> RSPO. Even if they have a higher capacity than Diphonix, Diaion CRP200 and RSPO resins are ineffective in highly acidic solutions, because they are weak acids and the exchange process in a chelating resin is usually slower than that in strong acid resins of the sulfonic type and it is controlled by the kinetics of exchange reaction. However, the strong acid cation-exchange resin Dowex 50W(X8) exhibited higher performance than chelating resins. For instance, when the temperature was 30 °C, the initial cadmium concentration was 50 $mg.L^{-1}$, and $H_3PO_4$ concentration was 6.77 % $P_2O_5$; the cadmium removal was 5 $mg.g^{-1}$ of resin and 25 $mg.g^{-1}$ of resin for Actinide-CU and Dowex 50X(X8), respectively.

In order to improve the adsorption capacity and kinetic performance of resins, several impregnation techniques have been developed, including resin impregnation using organophosphorus extractants such as Cyanex 272, Cyanex 301, and 302. Kabay et al. (1998b) investigated the use of Amberlite XAD-7 impregnated with Cyanex 302, packed into a column

with an internal diameter of 0.7 cm to remove 1124.1 mg.$L^{-1}$ Cd(II) and 635.46 mg.$L^{-1}$ Cu(II) from WPA solution (28.97 % $P_2O_5$). The column breakthrough curve was reasonably steep, and the column reached saturation after about 3 h at a flow rate of 0.5 $cm^3.min^{-1}$. The elution of loaded solvent impregnated resin was performed in 4.0 M and 6.0 M HCl, respectively. The elution of Cd(II) was reasonable but not totally complete after 4 h; thereby, the Cd(II) elution efficiency was 68.2 % and 65.3 %, respectively.

Because of its high macroporosity, hydrophobicity, and efficiency for solvent impregnation, Reyes et al. (2001) intensified the elimination of Cd from phosphoric acid aqueous solutions using resin-impregnated (Amberlite XAD-2 and XAD-7) with organophosphorus extractant (Cyanex 301) in both batch and column systems. Comparing the two commercial resins, they found that Amberlite XAD-7 was very efficient in removing Cd from dilute phosphoric acid solutions and at high concentrations as 54.33 % $P_2O_5$, whereas a significant decrease in Cd removal for Amberlite XAD-2/Cyanex 301, so it was necessary to dilute the solution when Amberlite XAD-2/Cyanex 301 was used. In the batch system, these authors reported that a few hours were sufficient to reach 90% of the total extraction even under unfavorable conditions (which means high acid and Cd concentrations), but less than 1 h to completely eliminate 10 mg.$L^{-1}$ Cd from phosphoric acid solutions (20 % $P_2O_5$). Besides, Cd can also be efficiently removed in the column. However, for the industrial phosphoric acid, Hinojosa Reyes et al. (2001) noted that the efficiency of Cd removal strongly decreased due to the presence of large concentrations of competitive ions (Fe(III) and Cu(II)). Consequently, the authors concluded that pretreatment with reducing agents, such as $Na_2S_2O_4$, is required in order to improve the Cd removal efficiency.

According to Booker (1989) and Kabay et al. (1998b), Cd(II) does not form complexes with phosphoric acid. Therefore, Cd(II) extraction can be carried out by complex formation with the impregnated extractants onto the resin (for example, di(2,4,4-trimethylpentyl = HL) phosphinic acid) following the reaction below (Cortina et al., 1996):

$$Cd^{2+} + 2HL_r \rightleftharpoons CdL_{2,r} + 2H^+ \quad (4.18)$$

The studies carried out cadmium removal by ion exchange in WPA are detailed in Table 4.9.

Table 4.9 Summary of different ion exchange studies for the removal of Cd from WPA.

| Resin | Resin dose (g) | $H_3PO_4$ concentration (% $P_2O_5$) | Initial Cd concentration ($mg.L^{-1}$) | Temperature (°C) | Sorption time (h) | Removal efficiency or capacity | Setup | Comments | Ref. |
|---|---|---|---|---|---|---|---|---|---|
| Duolite C264 | 20 | 30 | 29 | 60 | | 98.28 | Fixed bed with an internal diameter of 38 mm<br>Flow rate = 3.8 $BV.h^{-1}$ | The size of resin particle was 1 mm. | Booker (1989) |
| Diphonix | 0.1 | 6.77 | 50 | 50 | 2 | 9.38 $mg.g^{-1}$ | Batch tests in magnetic stirred container. Volume of solution 100 mL | The total exchange capacity of Diphonix is 7.31 mequiv/g. | Kabay et al. (1998a) |
| Dowex 50W(X8) | 0.1<br>0.1 | 6.77<br>20 | 50<br>50 | 50<br>50 | 2<br>2 | 28.02 $mg.g^{-1}$<br>7.89 $mg.g^{-1}$ | Batch tests in magnetic stirred container. Volume of solution 100 mL. | The measurements performed at 30°C and with 24 h of sorption gave similar results. | Kabay et al. (1998a) |
| Amberlite XAD-8 impregnated with Cyanex 302 | 0.05 | 32.6 | 50 | 30 | 24 | 39.76 % | Batch tests. | The surface area of XAD-8 is 160 $m^2/g$. | Kabay et al. (1998b) |
| Amberlite XAD-7 impregnated with Cyanex 301 | 1.4 | 20 | 10 | 25 | _ | 11.1 $mg.g^{-1}$ | Column system (column depth = 9.8 cm)<br>flow rate = 54 $mL.h^{-1}$ | The total stripping impregnation method was used for the impregnation of the resin. | Reyes et al. (2001) |
| Amberlite XAD-7 impregnated with Cyanex 301 | 1.4 | 54 | 45 | 25 | _ | 9.7 $mg.g^{-1}$ | Column system (column depth = 9.8 cm).<br>Flow rate = 54 $mL.h^{-1}$ | Pretreated industrial phosphoric acid with $Na_2S_2O_4$. | Reyes et al. (2001) |
| Amberlite XAD-2 impregnated with Cyanex 301 | 0.5 | 20 | 10 | 25 | 24 | 4 – 4.5 $mg.g^{-1}$<br>35 – 40 % | Batch tests in thermostatic stirred container. Volume of solution 50 mL | The equilibrium impregnation method was used for the impregnation of the resin. | Reyes et al. (2001) |

### 4.4.4 Chemical precipitation

By far the most widely used process for the removal of heavy metals from aqueous solutions is chemical precipitation. Sulfide precipitation can be performed employing either solid (FeS, CaS), aqueous ($Na_2S$, NaHS, $NH_4S$) or gaseous sulfide sources ($H_2S$). The thermodynamic equilibria involved in metal sulfide precipitation can be expressed as (Lewis, 2010):

$$H_2S \rightleftharpoons HS^- + H^+ \qquad K_1 = \frac{(HS^-)(H^+)}{(H_2S)} \qquad pK_1 = 6.99 \text{ at } 25\ ^\circ C \qquad (4.19)$$

$$HS^- \rightleftharpoons S^{2+} + H^+ \qquad K_2 = \frac{(S^{2-})(H^+)}{(HS^-)} \qquad pK_2 = 17.4 \text{ at } 25\ ^\circ C \qquad (4.20)$$

$$M^{2+} + S^{2-} \rightleftharpoons MS(s) \qquad (4.21)$$

$$M^{2+} + HS^- \rightleftharpoons MS(s) + H^+ \qquad (4.22)$$

Sulfides have been studied as potential inorganic reagents for the removal of heavy metals from various wastewaters (Bhattacharyya et al., 1979) and wet phosphoric acid (Tjioe, 1987). In this context, Norwood and Tate (1992) worked with sulfide precipitation using sodium sulfide and polysulfide solutions to remove heavy metals (Cd, Hg, Pb) from WPA (30 % $P_2O_5$) and observed that only a minor amount of cadmium was precipitated, which indicates that cadmium sulfide concentration is significantly affected by low pH value ($H_2S$ is the major element at low pH). To deal with this issue, some patent applications tried a partial neutralization of the acid before the addition of the sulfide source (Berglund, 1981; Plessen et al., 1983; Wolstein et al., 1983). Boliden AB Company (Berglund, 1981) found that the concentration of cadmium contained in phosphoric acid solution (44.88 % $P_2O_5$) decreased from 20 mg.L$^{-1}$ to 2.5 mg.L$^{-1}$ after neutralization with NaOH to Na/P = 1/10 mol/mol at a temperature of 60 °C. Hoechst AG (Plessen et al., 1983) also carried out the neutralization of 15.20 % – 20.27 % $P_2O_5$ with ammonia until pH 1 and reported that the cadmium content was reduced from 3-6 ppm to 0.2 ppm.

Other patent applications used an overpressure to obtain low residual cadmium concentrations. Chemische Fabrik Kalk GmbH (Taubert and Boehm, 1975) investigated the use of an overpressure of 5 bar at 20 °C and subsequently, they found that the cadmium content in 54.3 % $P_2O_5$ decreased from 65 ppm to 13 ppm. Then, the precipitate was separated by filtration. Tjioe (1987) reported that no CdS precipitation can occur in $H_3PO_4$ solutions with concentrations greater than 43.46 % $P_2O_5$ at 1.01325 bar of $H_2S$.

Ennaassia et al. (2002) studied the elimination of Cd(II) from phosphoric acid solutions by precipitation into CdS using $Na_2S$. The influences of temperature, $H_3PO_4$ concentration, $Na_2S/Cd(II)$ molar ratio, and the addition of $(NH_4)_2SO_4$ on the precipitation of CdS were investigated. They found that the cadmium removal rate decreased both with the increase in the acidity level (from 10 % $P_2O_5$ to 30 % $P_2O_5$) and the increase in the temperature (from 20 to 70 °C), hence an increase in the molar ratio of sulfide to cadmium enhanced the precipitation efficiency. A discrepancy was observed between experimental data and theoretical curves (calculated using equilibrium solubilities). Therefore, this was attributed to the slowness of the precipitation process by the phenomenon of supersaturation and the formation of CdS colloidal particles.

As mentioned above, the formation of the CdS precipitate takes place according to Eq. (4.23):

$$Cd^{2+} + S^{2-} \rightleftharpoons CdS(s) \qquad K_s = (Cd^{2+})(S^{2-}) \qquad (4.23)$$

Nevertheless, in this case, cadmium was removed from acidic solutions where $S^{2-}$ ions exist as $H_2S$ (Figure 4.11), Eq. (4.23) can be considered alternatively:

$$Cd^{2+} + H_2S \rightleftharpoons CdS(s) + 2H^+ \qquad K_s' = \frac{(H^+)^2}{(Cd^{2+})\,(H_2S)} \text{ and } K_s' = \frac{K_1 K_2}{K_s} \qquad (4.24)$$

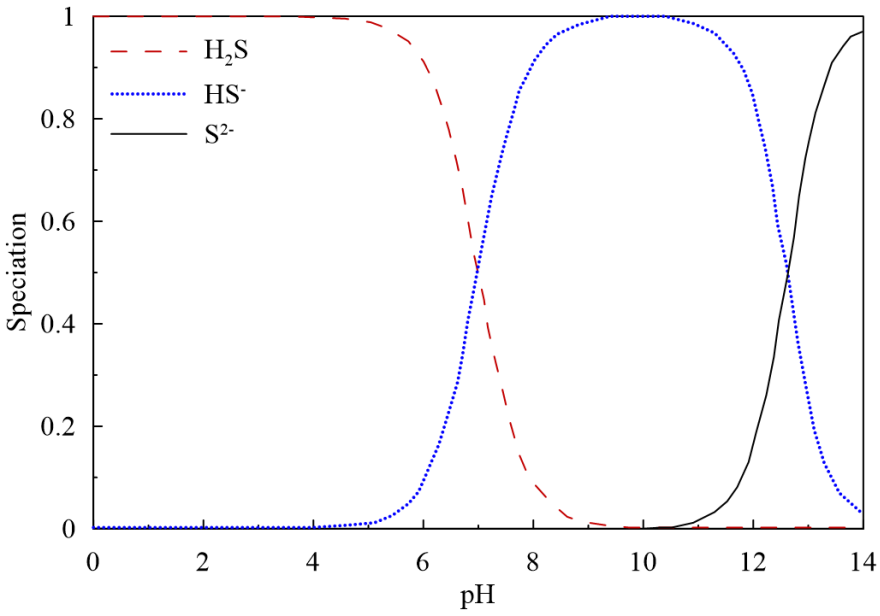


Figure 4.11 pH dependence of sulfide speciation (Lewis, 2010).

According to Ennaassia et al. (2002) experimental data (Figure 4.12), and using the following equations:

$$v = -\frac{dC(t)}{dt} \qquad \text{with } C = C_0(1 - X) \tag{4.25}$$

where v is the reaction rate, $C_0$ is the initial $Cd^{2+}$ concentration and $C(t)$ is the instantaneous $Cd^{2+}$ concentration. The integrated formula of Eq. (4.25) is as follows:

$$\frac{1}{(1 - X)^{n-1}} - 1 = (n - 1)\frac{k.C_0^{n-1}}{v}t \tag{4.26}$$

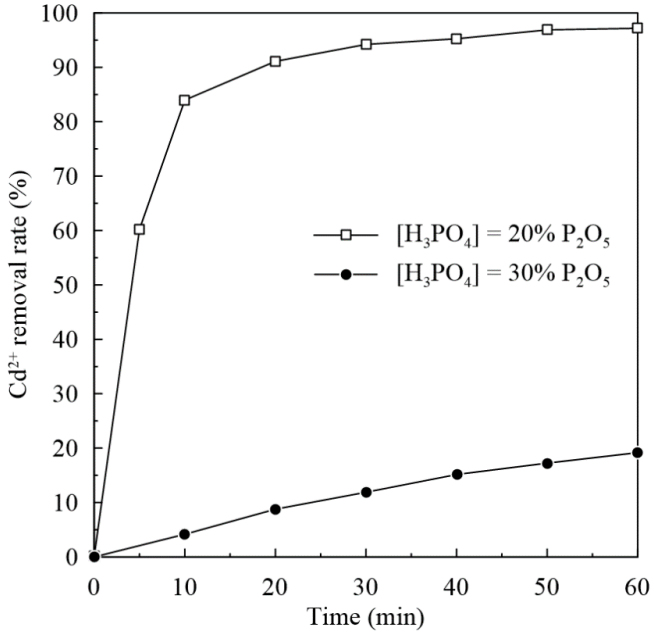


Figure 4.12 Kinetics of CdS precipitation from 20 % $P_2O_5$ and 30 % $P_2O_5$ at 20 °C using $[Na_2S]/[Cd^{2+}]$ = 10/1 (Ennaassia et al., 2002).

By plotting $\frac{1}{(1-X)^{n-1}} - 1$ versus time, and considering n = 2, it is obvious that for both phosphoric acid concentrations (20 % and 30 % $P_2O_5$), the kinetics of $CdS$ precipitation using $Na_2S$ is a second-order kinetics (Figure 4.13**)**.

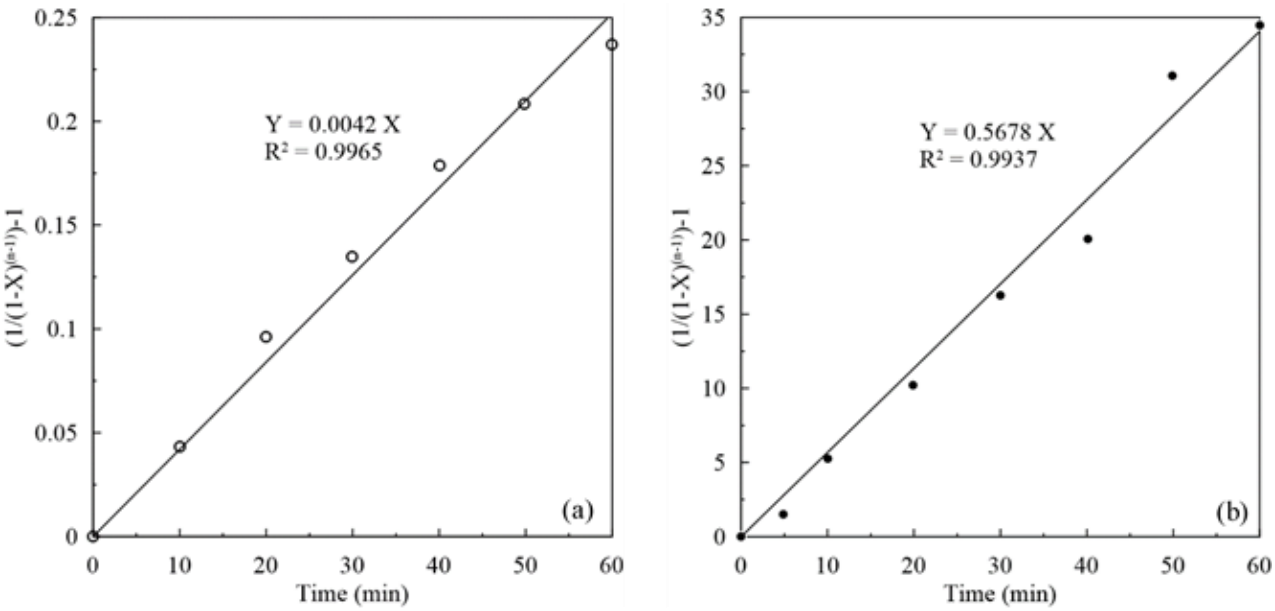


Figure 4.13 $(1/(1-X)^{(n-1)})-1$ versus time for (a) 20 % $P_2O_5$ and (b) and 30 % $P_2O_5$.

Ukeles et al. (1994) developed a process based on the precipitation of cadmium and copper from WPA through the simultaneous addition of iron powder and a dithiophosphinate reagent. The separation characteristics were evaluated using both dilute (25 % $P_2O_5$) and concentrated (54 % $P_2O_5$) phosphoric acid solutions. When the residence time was 60 minutes, it was observed that the cadmium concentration was lowered by about 82 % of its initial level (from 28 ppm to 5 ppm). At a dosage of 4 kg iron powder per ton of $P_2O_5$, slightly more than 80 % of cadmium was removed, while almost 70 % of cadmium removal was reached when the dosage was 3 kg iron powder per ton of $P_2O_5$. To explain this result, it is known that $Cd^{2+}$and $Cu^{2+}$ had a strong affinity to dithiophosphinate (DTPN), Cd begins to precipitate only after total Cu consumption. That is why iron powder was added to promote the cementation of the $Cu^{2+}$ species to copper metal and thus, prevent $Cu^{2+}$ from reacting with DTPN.

Similarly, the decrease in the dithiophosphate dosage led to a diminution in cadmium removal rate. For 1 kg of dithiophosphinate per ton of $P_2O_5$, a maximum cadmium removal rate of 15 % was achieved. The authors found that the removal rate of cadmium at 55 °C was higher than at 35°C. Eventually, the process was tested in continuous pilot operations, and the authors reported that the concentration of cadmium and copper was reduced from 27 ppm to 2 – 4 ppm and from 37 ppm to 2 ppm, respectively. The crystals of the Cd-DTPN precipitate were very small; thus, it was possible to separate them by pressure filtration with other solids present in the WPA.

Trisodium trithiocyanuric acid (TMT-15), sodium trithiocarbonate (5 wt. %), and sodium polythiocarbonate (Thio-Red II) were evaluated as precipitating agents for heavy metals (Cd, Cu, Hg, Mn, Pb, Cr, Zn) in a 10-34-0 (N-$P_2O_5$-$K_2O$) grade fertilizer solution and WPA by Norwood and Kohler (1990). These authors showed that cadmium and chromium can be precipitated by adding 5 wt. % $Na_2CS_3$. A 1.5 equivalent of 5 wt. % $Na_2CS_3$ was added for each equivalent of heavy metal, the cadmium concentration was reduced from 130 ppm to 80 ppm. Therefore, Thio-Red II and TMT-15 did not precipitate Cd, Mn, Cr, and Zn. The 5 wt. % $Na_2CS_3$ was shown to be the most effective organic reagent for removing heavy metals from 10-34-0 (N-$P_2O_5$-$K_2O$) grade fertilizer, as well. Ennaassia et al. (2002) concluded that a large excess of $S^{2-}$ ions (up to 20/1 molar ratio of $Na_2S$ to Cd) was required to purify phosphoric acid solutions to international regulatory levels (< 20 mg Cd/kg $P_2O_5$). The studies carried out on Cd elimination by precipitation from WPA are summarized in Table 4.10.

Table 4.10 Summary of different precipitation studies for the removal of Cd from WPA.

| Precipitating agent | Precipitating agent concentration (a) or molar ratio (b) | $H_3PO_4$ concentration (% $P_2O_5$) | Initial Cd concentration ($mg.L^{-1}$) | Temperature (°C) | Residence time (a) or equilibrium time (b) (min) | Residual Cd concentration (ppm) | Removal efficiency (%) | Setup | Comments | Ref. |
|---|---|---|---|---|---|---|---|---|---|---|
| Quaternary amine (TBAI) | 10[(b)] | 30 | 36 | 60 | 30[(b)] | 1.20 | 96.66 | Batch tests | Optimum stirring rate = 350 rpm | Boussen (2007) |
| | 8[(b)] | 54 | 36 | 70 | 30[(b)] | 2.88 | 92.00 | | | |
| $Na_2S$ | 2[(b)] | 10 | 56.2 | 20 | 60[(b)] | 10.40 | 81.50 | Batch tests in thermostatic cell, hermetically closed and equipped with capillary tube for $Na_2S$ addition, volume of solution 50 mL | The addition of $(NH_4)_2SO_4$ had almost no effect on the yield of Cd(II) removed. | Ennaassia et al. (2002) |
| | 2[(b)] | 10 | 56.2 | 70 | 60[(b)] | 51.62 | 8.15 | | | |
| | 10[(b)] | 10 | 56.2 | 40 | 60[(b)] | 1.59 | 97.17 | | | |
| | 10[(b)] | 10 | 56.2 | 70 | 60[(b)] | 6.87 | 87.77 | | | |
| | 4[(b)] | 20 | 56.2 | 20 | 60[(b)] | 10.48 | 81.36 | | | |
| | 4[(b)] | 20 | 56.2 | 60 | 60[(b)] | 56.20 | 0.00 | | | |
| | 7[(b)] | 20 | 56.2 | 20 | 60[(b)] | 5.06 | 90.99 | | | |
| | 7[(b)] | 20 | 56.2 | 70 | 60[(b)] | 26.53 | 52.79 | | | |
| | 10[(b)] | 30 | 56.2 | 20 | 60[(b)] | 49.37 | 12.15 | | | |
| | 10[(b)] | 30 | 56.2 | 20 | 60[(b)] | 45.33 | 19.35 | | | |
| DTPN | 2 kg DTPN/ton $P_2O_5$ [(a)] | 25 | 28 | 55 | 60[(a)] | 5 | 82 | Reactor constructed from PVC having an active volume of 50 L. Flow rate = 60 L/h | The amount of iron powder was 4 kg of iron powder/ton $P_2O_5$ | Ukeles et al. (1994) |
| | | 25 | 28 | 35 | 60[(a)] | 16.8 | 40 | | | |
| | | 25 | 28 | 55 | 30[(a)] | 12.69 | 54.67 | | | |
| $Na_2S$ | - | 30 | - | 22.77 ± 2 | - | - | 5 | | $Na_2S/P_2O_5$= 0.0030 | Norwood and Tate (1992) |
| $Na_2S_{2.32}$ | - | 30 | - | 22.77 ± 2 | - | - | 5 | | $Na_2S_{2.32}/P_2O_5$= 0.0057 | |

### 4.4.5 Flotation

Dissolved air flotation (DAF), foam flotation, ion flotation, precipitate flotation, and adsorbing colloid flotation are the main flotation processes for the removal of metal ions from aqueous solutions. This technique has a good trend for the removal of heavy metal ions from wastewaters even at high ionic strength and it is insensitive to large pH ranges (Huang and Wilson, 1976).

Ion flotation, first described by Sebba (1959), is a separation technology for recovering and removing metal ions from dilute aqueous solutions (Matis and Mavros, 1991). Jdid et al. (1982) proposed to float uranium (IV) in concentrated phosphoric acid (30 % $P_2O_5$) using anionic collectors belonging to the organophosphorus family. Bessiere et al. (1986) carried out ion flotation for the removal of Cd(II) and As(III) from phosphoric acid solutions (6.77% $P_2O_5$ to 37 % $P_2O_5$) by using sodium diethyldithiophosphate ($(CH_3CH_2O)_2PS_2Na$), which is marketed by Hoechst under the name of LET. This collector is able to provide poorly soluble complexes with cadmium, arsenic, mercury, silver, lead, and copper. LET is, however, oxidized by Fe(III); hence, this reaction is susceptible to disrupt ion flotation operations in industrial phosphoric acid, which are sometimes rich in Fe(III). Results revealed that the removal efficiency of $Cd^{2+}$ was 75 % when the molar ratio of the collector to metal was 2, initial cadmium concentration 60 mg.$L^{-1}$, and acid concentration (30 % $P_2O_5$) (Table 4.11).

Despite the high acidity and ionic strength of phosphoric acid solutions, ion flotation of cadmium and arsenic can be achieved using anionic collectors (Bessiere et al., 1986). The latter precipitate Cd(II) and As(III) species to give stable complexes ($Cd(LET)_2$ (s) in the case of cadmium). However, the optimization of ionic flotation recovery processes in phosphoric acid solutions requires a better knowledge of ions reactivity and also the acid-base and complexing properties of the surfactants.

In the same context, Jdid et al. (1987) investigated the removal of (73.5 mg.$L^{-1}$) cadmium from (29.1 % $P_2O_5$) WPA by flotation using an anionic surface-active agent (sodium diethyldithiophosphate) as a cadmium collector and an injected gas in the presence of other impurities, including iron and possibly uranium. As a result, they found that the degree of cadmium removal by flotation increased proportionately with the reduction in trivalent iron content in the treated industrial phosphoric acid solution. In fact, the trivalent iron reduction operation in the industrial phosphoric acid solution can be carried out using known means, such

as electrolytic reduction, the addition of iron in powder form, or by circulating industrial phosphoric acid over metal waste preferably containing iron. The reduction operation of the trivalent iron present in the industrial phosphoric acid was continued until the ratio $[Fe^{2+}]/[Fe^{3+}]$ obtained was at least 4 and was reasonably between 6 and 40 for economic reasons in order to promote the elimination of cadmium and at the same time to reduce the collector agent consumption. Table 4.11 shows the obtained findings.

Table 4.11 Cadmium removal from WPA by flotation.

| Collector | Molar ratio [Collector]/ $[Cd^{2+}]$ | $H_3PO_4$ concentration (% $P_2O_5$) | Initial Cd concentration ($mg.L^{-1}$) | Removal efficiency (%) | Residual Cd concentration ($mg.L^{-1}$) | Comments | Ref. |
|---|---|---|---|---|---|---|---|
| $(CH_3CH_2O)_2$ $PS_2Na$ | 4 | 6.77 | 56.21 | 22 | 43.84 | pKs $Cd(LET)_2$ = 11.5 in a 5.5M $H_2O$-$H_3PO_4$ mixture | Bessiere et al. (1986) |
| | 4 | 13.04 | 56.21 | 66 | 19.11 | | |
| | 4 | 22 | 56.21 | 94 | 3.37 | | |
| | 1 | 30 | 56.21 | 33 | 37.66 | | |
| | 2 | 30 | 56.21 | 74 | 14.61 | | |
| | 4 | 30 | 56.21 | 95 | 2.81 | | |
| | 4 | 30 | 112.41 | 96 | 4.50 | | |
| | 4 | 30 | 21.36 | 81 | 4.06 | | |
| Sodium diethyldithio-phosphate | 2 | 29.1 | 73.5 | 0.95 | 72.8 | Without trivalent iron reduction | Jdid et al. (1987) |
| | 3 | 29.1 | 73.5 | 1.20 | 72.6 | | |
| | 4 | 29.1 | 73.5 | 9.65 | 66.4 | | |
| | 2 | 29.1 | 73.5 | 52.2 | 35.1 | With trivalent iron reduction | |
| | 3 | 29.1 | 73.5 | 93.1 | 5.04 | | |
| | 4 | 29.1 | 73.5 | 93.0 | 1.45 | | |

### 4.4.6 Membrane processes

Membrane technologies with different types of membranes show great promise for heavy metal removal due to their high efficiency, easy operation, and space-saving (Fu and Wang, 2011); thus they may provide an interesting alternative for the purification of phosphoric acid (Skidmore and Hutter, 1999). González et al. (2002) studied the removal of cadmium and other impurities from phosphoric acid solutions by reverse osmosis (RO) and nanofiltration (NF) using different membranes (Table 4.12). Experimental results exhibited that RO was suitable to purify $H_3PO_4$ solutions up to 13.04 % $P_2O_5$. High pressures (68.95 − 124.11 bar) have to be applied to obtain acceptable flux due to the high osmotic pressure of the solutions. However, NF was the best for purifying acid solutions with high concentrations up to 40.93% $P_2O_5$. For higher acid concentrations, the flux and selectivity of the membrane decreased in a considerable manner (González et al., 2002). The $H_3PO_4$ permeability and the reflection coefficient were calculated using the irreversible thermodynamics model of Kedem-Katchalsky (Mulder, 1998);

the phosphoric acid permeability was 4.86 $10^{-4}$ and 7.13 $10^{-2}$ $m^3.m^{-2}.h^{-1}$ for the SX01 membrane (RO) and DS5DL membrane (NF), respectively.

Nanofiltration membranes were also used by Khaless (2006) to obtain purified acid and to retain multivalent contaminants (Al, Fe, V, Cd, Cu). This work was carried out by operating a frontal filtration with membranes of different molecular weight cut-off (MPF-34, MPF-36, Desal5-DL, Desal KH, and PES 10) in a pressure range not exceeding 40 bar and at an ambient temperature of 20 ± 5 °C. The experiments were carried out in a filtration stainless-steel cell equipped with a mechanical stirrer, which allowed filtering a volume of 300 mL through a plane membrane with an area of 43 $cm^2$. The filtration performance study revealed that NF at ambient temperature was only suitable for the treatment of a phosphoric acid solution ≤ 29 % $P_2O_5$. Indeed, the permeation flux was almost zero at the maximum pressure of the cell (40 bar), with an MPF-36 membrane, due to the viscosity of pure phosphoric acid (58 % $P_2O_5$) which is equal to 20 cP.

Comparing the different membranes, it appears that the Desal5-DL membrane displays the highest reduction of multivalent metallic contaminants (the Cd(II) removal rate was 80 % at a pH < 0, a pressure of 30 bar, a stirring rate of 200 rpm, and a temperature of 21 ± 1 °C). However, the Desal5-DL membrane presents an insufficient chemical resistance: in fact, phosphoric acid gradually degrades the active layer of this polyamide membrane, and subsequently modifies its performance, *i.e.*, with a lifetime of less than two months in a phosphoric acid solution 29 % $P_2O_5$) at ambient temperature.

To improve the performance (flux and selectivity) of the commercial NF membranes (MPF, Desal KH, and PES 10), Khaless (2006) investigated the modification of NF membranes by polymer deposition (polymers A, B, C, D, and E which are different in chain length or function) on the active surface to reduce pore size, increase the steric effect, and modify the electrostatic repulsion. After the deposition of polymers (C and D) on the PES membrane, a strong improvement in cationic impurities reduction (from 6 % to 76 % for Cd(II)) was reported. On the other hand, in the case of the Desal KH membrane modified with polymer C, a slight decrease in the reduction of divalent contaminants (from 75 % to 69 %) was noted. Moreover, the use of modified membranes generated an increase in the removal rate of contaminants and a decrease in permeate flux.

Table 4.12 RO and NF membrane characteristics which were evaluated by González et al. (2002) and Khaless (2006).

| Membrane processes | Supplier | Reference | Composition | MWCO (Da) | NaCl retention (%) | Water permeability at 25 °C ($L.h^{-1}.m^{-2}.bar^{-1}$) | Recommended pressure (bar) | Maximum operating Temperature (°C) | pH range |
|---|---|---|---|---|---|---|---|---|---|
| Nanofiltration | Nadir | PES 10 | Polyethersulfone | 1000 | 5 – 15 | - | - | 95 | 0 – 14 |
| | Koch membrane | MPF-36 | Polyacrylonitrile + composite | 1000 | 10 | 8 – 10 | 35 | 40 – 70 | 0 – 14 |
| | Koch membrane | MPF-34 | Polyacrylonitrile + composite | 300 | 35 | 4 | 35 | 40 – 70 | 0 – 14 |
| | Ge-Osmonics | Desal5-DL | Polyamine / Polysulfone | 150 – 300 | 50 | 3 | 40 | 90 | 2 – 12 |
| | Ge-Osmonics | Desal KH | Polysulfonamide | 300 | - | 3 | - | 90 | 0 – 14 |
| | Ge-Osmonics | BQ01 | Anion rejection | 500 – 1000 | 20 – 30 | - | 7 | 100 | 0.5 – 11 |
| Reverse osmosis | Ge-Osmonics | SX01 | Cellulose acetate | 300 – 500 | 50 – 70 | - | 14 | 50 | 2 – 8 |
| | Ge-Osmonics | MX07 | Polyamide | 300 – 600 | 50 – 70 | - | 7 | 80 | 2 – 12 |
| | Ge-Osmonics | ST10 | Cellulose acetate | 150 – 220 | ≥ 95 | - | 28 | 50 | 2 – 8 |
| | Ge-Osmonics | SR10 | Cellulose acetate | 200 – 300 | ≥ 92 | - | 28 | 50 | 2 – 8 |
| | Ge-Osmonics | MS19 | Polyamide | 125-200 | ≥ 99 | - | 14 | 80 | 2 – 12 |

Electrodialysis (ED) has also been proposed as a feasible method to separate a wide variety of metal ions from phosphoric acid solutions (Duan et al., 2018)**.** This other membrane process uses an electric field as the driving force for the separation of ions across charged membranes (ion-exchange membranes) from one solution to another one (Fu and Wang, 2011). The membranes are actually of two basic types: cation-exchange and anion-exchange membranes. Mecibah et al. (2012) studied cadmium removal by electrodialysis by using CMX (Asahi Glass Japan) as a cation-exchange membrane and ADS (Morgane-Solvay France) as an anion-exchange membrane. The phosphoric acid (28 % $P_2O_5$) to be treated contained 20 $mg.L^{-1}$ of $Cd^{2+}$. The results revealed that the increase in current density (from 5 to 20 $mA.cm^{-2}$) and the circulation flow (from 2 to 16 $mL.min^{-1}$) promoted the removal of cadmium. The thickness of the receiver compartment also had an effect on the electrodialysis. Hence, the optimal thickness was found to be 0.8 cm.

Among all the studies conducted in membrane processes, the highest Cd removal efficiency reported was 98.26 % using NF, which confirms that NF is a more suitable choice. Nevertheless, electrodialysis can ensure a good purification of phosphoric acid, but it requires an optimization of the parameters, such as membrane choice and current density. Finally, Table 4.13 summarizes the studies conducted on membrane processes.

Table 4.13 Summary of different membrane processes studies for the removal of Cd from WPA.

| Membrane | $H_3PO_4$ concentration (% $P_2O_5$) | Initial Cd concentration ($mg.L^{-1}$) | Residual Cd concentration ($mg.L^{-1}$) | Removal efficiency (%) | Comments | Ref. |
|---|---|---|---|---|---|---|
| **Reverse Osmosis (RO)** | | | | | | |
| SX01 | 8.58 | 46.6 | 2.66 | 94.29 | Experiments were conducted in a stainless-steel cell with magnetic stirring under the pressure of an inert gas ($N_2$)<br>SX01 is an asymmetric cellulose acetate membrane<br>P = 124.11 bar | González et al. (2002) |
| **Nanofiltration** | | | | | | |
| DS5DL | 33.4 | 46.6 | 0.81 | 98.26 | DS5DL is a thin-film membrane<br>P = 68.95 bar | González et al. (2002) |
| MPF-36 | 29 | 18 | 13.86 | 23 | Batch tests<br>P = 30 bar<br>pH < 0<br>Stirring rate = 200 rpm<br>T= 21 ± 1°C<br>[Polymer] = 0.01 M to 0.05 M | Khaless (2006) |
| PES-10 | 29 | 18 | 16.92 | 6 | | |
| Desal5-DL | 29 | 18 | 3.6 | 80 | | |
| Desal KH | 29 | 18 | 4.5 | 75 | | |
| MPF-36 + Polymer A | 29 | 18 | 9.54 | 47 | | |
| PES 10 + Polymer A | 29 | 18 | 12.78 | 29 | | |
| PES 10 + Polymer C | 29 | 18 | 4.32 | 76 | | |
| PES 10 + Polymer D | 29 | 18 | 5.22 | 71 | | |
| Desal KH + Polymer C | 29 | 18 | 5.58 | 69 | | |
| **Electrodialysis** | | | | | | |
| CMX-ADS | 28 | 20 | 13.718 | 31.41 | Circulation flow = 16 mL/min<br>Current density = 10 $mA/cm^2$ | Mecibah et al. (2012) |

### 4.4.7 Comparison between different WPA purification techniques

In the light of these works, solvent extraction technique was frequently used to purify WPA (Feki et al., 1994), and a wide variety of extractants was tested. it is worth noting that $D_2$EHDTPA and Kellex 100 are adequate extracting agents for the extraction of cadmium from phosphoric acid solutions, in contrast to Cyanex 302 which is limited by a relatively high concentration. It has also been found that amines do not have performance for the cadmium removal as it requires a high concentration; so, they must be pre-equilibrated, as they have the ability to extract the acid, which subsequently generates an increase in the stage number. Moreover, it has been established that the extraction of cadmium from phosphoric acid using amines starts at a certain concentration of $H_3PO_4$ within the range of $28.61\% - 30\%$ $P_2O_5$. However, this technique is limited by several drawbacks, such as the formation of a third phase in which the extracted element is present in a highly concentrated form, and also the fouling of the extraction system caused by the precipitated sulfate during the addition of sulfuric acid to the crude acid to activate the transfer of additional phosphoric acid in the organic solvent phase of the extraction system. In fact, periodic cleaning is necessary.

Moreover, sulfide precipitation has been the subject of several patents and they reported that sulfide precipitation of cadmium from concentrated phosphoric acid can be accomplished but it is not widely used due to the concerns about sulfide excess, also the poor filterability of the precipitate because of the small size of the precipitate particles. Therefore, the size of the crystals can be influenced by controlling the precipitation conditions (seed crystals, slow release of ligand) (Tjioe, 1987). Other ways to obtain larger particles are co-precipitation and the use of adsorbents. Instead of filtration or adsorption, the precipitate can also be concentrated by flotation.

Adsorption process can also be used for low concentration heavy metals removal, especially cadmium. But it is important to note that the metal adsorption capacities of low-cost adsorbents strongly vary, depending on the characteristics of the individual adsorbent, the extent of surface modification, the initial concentration of adsorbate, and the temperature.

Ion exchange can be used to remove cadmium from dilute phosphoric acid by means of cation and anion exchangers. Hence, a pretreatment of WPA is required in order to remove insoluble substances which will avoid clogging the ion exchanger and reduce its lifetime, and also improve the Cd removal efficiency by reducing the impurities. In addition, membrane filtration and flotation were also used and showed their feasibility in terms of cadmium removal

from phosphoric acid solutions up to a concentration of 30 % $P_2O_5$, however, further studies are needed.

The benefits and disadvantages of each technique are given in Table 4.14. In particular, the increase in the cost of WPA production due to the integration of the different purification techniques mentioned above as well as the environmental pollution generated during this manufacturing process will be detailed in the following sections.

Table 4.14 Advantages and disadvantages of diverse techniques for Cd removal from WPA.

| Techniques | Advantages | Limitations | Ref. |
|---|---|---|---|
| Solvent extraction | Simple technique, widely used method | High cost of the extractant, extractant dispersion, loss of solvent, pollution impact, inadequate control: phase continuity, equilibrium pH, interface, agitation, cross-circuit | (Ennaassia et al., 2002; Hinojosa Reyes et al., 2001; Omri and Batis, 2013) |
| Ion-exchange | High treatment capacity, good heavy metals removal, fast kinetics, high metal selectivity, no sludge generation | Resins more often not regenerable, high cost, second pollution | Omri and Batis, (2013); Purkayastha et al. (2014); Sobhanardakani et al. (2013) |
| Adsorption | Flexibility in design and operation, effective and economic method, inexpensive locally and naturally available material, high-quality of treated effluent | A large amount of reagent, the expensive adsorbent had to be regenerated by desorption, high cost and low availability of some adsorbents, low-cost adsorbents show poor adsorption capacity | Bishnoi et al. (2004); Hamza et al. (2016); Purkayastha et al. (2014) |
| Precipitation | Potential for selective metal removal, fast reaction rates, better settling properties | Technically difficult, expensive, difficult to control sulfide dosing | Lewis (2010); Ukeles et al. (1994) |
| Flotation | High metal selectivity, high removal efficiency, high overflow rates, production of concentrated sludge | High initial cost, high operational and maintenance costs, it depends upon several factors | Purkayastha et al. (2014); Sobhanardakani et al. (2013) |
| Membrane technologies | Easy operation, save spacing, good pollutant removal efficiency | Membrane fouling, high energy consumption, high operational cost | Mulder (1998); Purkayastha et al. (2014) |

## 4.5 The production cost of phosphoric acid

The economy of the phosphate industry is largely dependent on the prices of phosphate rock and sulfur (65 % of the annual world production of sulfuric acid is devoted to the production of phosphoric acid), as well as electricity. Phosphate rock is mined and provided by industry for use in other product manufacturing (Table 4.15). so, its price is fixed by the industry of the phosphate ore sector (Gilmour, 2013). Figure 4.14 shows the evolution of Moroccan phosphate rock prices during the years 2015 to 2018.

Table 4.15 The energy required for phosphate rock mining (Belboom et al., 2015).

| Origin | Moroccan phosphate rock | American phosphate rock | Phosphate rock[a] |
|---|---|---|---|
| Energy required to rock mining ($GJ.ton^{-1}$) | 1.15 | 1.29 | 0.5-2.8 |

[a] In general, the mining of phosphate rock requires an energy between 0.5 – 2.8 $GJ.ton^{-1}$.

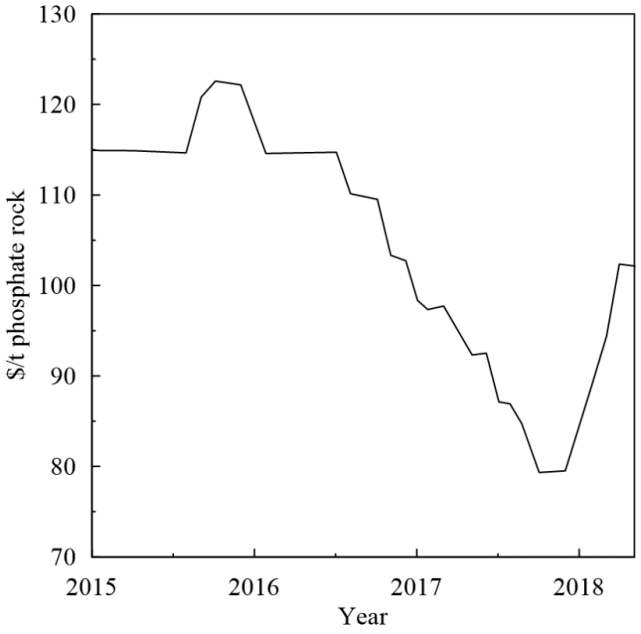


Figure 4.14 Moroccan phosphate rock data prices from 2015 to 2018 (Direction des études et des prévisions financières, 2018).

The cost estimation of producing phosphoric acid, either wet or thermal, is based on the cost of several components. Tables 4.16 − 4.18 list all cost elements, usages, and costs per unit, and they include: raw materials in order of diminishing importance; chemical services, which are not part of the product but are essential for its manufacturing (for example, antifoam or solvent in a solvent extraction facility); utilities, such as steam, water and nitrogen; direct labor that is

the personnel required to operate, maintain, develop and supervise the plant; maintenance, mostly budgeted at 1 % − 5 % of the capital or the cost of replacement of the plant-based on the technology; and indirect costs, which include administrative expenses, depreciation, taxes and insurance (Gilmour, 2013). Comparing the total production cost of WPA and thermal phosphoric acids (Tables 4.17 − 4.18), it is clear that the latter is much more expensive and about twice as much, for the same $P_2O_5$, utility, labor, and overhead rates. Therefore, any phosphate derivatives made from thermal acid are much more expensive than those from purified acid. That is why most of the phosphoric acid produced worldwide is obtained by the wet process and it seems cheaper to purify it than to invest large sums of money to produce thermal phosphoric acid. Furthermore, this process has been abandoned in the majority of European countries due to the high energy requirement (European Fertilizer Manufacturer's Association, 2000). Thus, by far, this process is still employed in China and Kazakhstan.

Table 4.16 WPA cost plant sheet (Gilmour, 2013).

| Phosphoric acid plant | | Capacity 1000 t/Day $P_2O_5$ | | 330 Days/Year | |
|---|---|---|---|---|---|
| | Usage/t $P_2O_5$ | Price | Unit | \$/t $P_2O_5$ | % |
| **Raw materials** | | | | | |
| Phosphate rock[a] | 3.29 | 158 | \$/t | 519.8 | 76 |
| Sulfuric acid[b] | 2.76 | 35 | \$/t | 95.7 | 14 |
| Additives | | | | 5.0 | 1 |
| **Utilities** | | | | | |
| Electricity | 150 | 0.07 | \$/kWh | 10.1 | 1 |
| Steam | | | \$/t | | |
| Water | 5.33 | 0.25 | \$/t | 1.3 | 0.2 |
| Gypsum disposal | | | | 2.5 | 0.4 |
| Direct labor | 50 people | 50,000 | \$ | 7.6 | 1 |
| Maintenance | 3.0% capital cost | 3,000,000 | \$ | 9.1 | 1 |
| Administration | | | \$ | 2.4 | 0.4 |
| Depreciation | | | \$ | 30.3 | 4 |
| Total | | | | 684 | 100 |

[a] Phosphate rock of 32% $P_2O_5$ concentration, usage includes total losses (5%).

[b] 98% $H_2SO_4$ used, calculation based on 100% $H_2SO_4$.

Table 4.17 Purified phosphoric acid plant cost sheet (Gilmour, 2013).

| Phosphoric acid plant | | Capacity 1000 t/Day $P_2O_5$ | | 330 Days/Year | |
|---|---|---|---|---|---|
| | Usage/t $P_2O_5$ | Price | Unit | \$/t $P_2O_5$ | % |
| **Raw materials** | | | | | |
| Phosphoric acid[a] | 1.454 | 718 | \$/t | 1044.1 | 98 |
| Return acid credit[b] | -0.428 | 574 | \$/t | -254.9 | -23 |
| Solvent | 0.5 | 1.8 | \$/kg | 0.9 | 0.1 |
| Chemicals | | | | 50.0 | 5 |
| **Utilities** | | | | | |
| Electricity | 150 | 0.07 | \$/kWh | 10.1 | 1 |
| Steam | 3.5 | 10 | \$/t | 35.0 | 3 |
| Cooling water | 20 | 0.05 | \$/t | 1.0 | 0.1 |
| Process water | 1 | 0.9 | \$/t | 0.9 | 0.1 |
| Direct labor | 30 people | 50,000 | \$ | 18.2 | 2 |
| Maintenance | 2.5% capital cost | 2,250,000 | \$ | 27.3 | 3 |
| Administration | | | \$ | 9.6 | 0.9 |
| Depreciation | | | \$ | 109.1 | 10 |
| Total | | | | 1060 | 100 |

[a] Based on 59% $P_2O_5$ concentrated, low sulfate, acid feed, 2.5% losses.
[b] Return acid credit is negotiated and ranges and ranges 0% – 100% of the value of the feed acid, here it is 80%.

Table 4.18 Thermal phosphoric acid plant cost sheet (Gilmour, 2013).

| Thermal phosphoric acid plant | | Capacity 180 t/Day $P_2O_5$ | | 330 Days/Year | |
|---|---|---|---|---|---|
| | Usage/t $P_2O_5$ | Price | Unit | \$/t $P_2O_5$ | % |
| **Raw materials** | | | | | |
| Phosphorus | 0.437 | 2720 | \$/t | 1188.6 | 92 |
| Water | 0.4 | 0.9 | \$/t | 0.4 | 0 |
| Chemicals | | | | 20 | 2 |
| **Utilities** | | | | | |
| Electricity | 10 | 0.07 | \$/kWh | 0.7 | 0 |
| Water | 1 | 0.9 | \$/t | 0.9 | 0 |
| Direct labor | 20 people | 50,000 | \$ | 16.8 | 1 |
| Maintenance | 2.5% capital cost | 625,000 | \$ | 10.5 | 1 |
| Administration | | | \$ | 15 | 1 |
| Depreciation | | | \$ | 42.1 | 3 |
| Total | | | | 1295 | 100 |

As stated earlier, calcination is the only known method for the removal of cadmium from phosphates in the rock state. This technique was the subject of several research studies; the CERPHOS process (Kossir and Chik, 1996) reduced the cadmium content of Moroccan phosphate rock by 75 %, it consisted to heat in the range of 750 °C to 950 °C under controlled

pressure to decrease and volatilize cadmium, but the estimated cost was about 10 USD.ton$^{-1}$ of phosphate concentrate. Furthermore, before its dismantling, Nauru Phosphate Corporation had a calcination plant with a capacity of 75 tons.h$^{-1}$ and it decreased cadmium content in Nauru phosphate rock from about 600 to less than 120 mg.kg$^{-1}$ P (Syers, 2001). The uncalcined phosphate was sold at 50 USD.ton$^{-1}$, while the calcined phosphate was sold for about US$90 ton$^{-1}$ which appeared to be higher (Syers, 2001).

Calcination can reduce the phosphorite activity and lead to an atmospheric cadmium emission; in addition, it is seen as a costly method (Kauwenbergh, 2001). Actually, assuming that the heat capacity of phosphate ore is 0.8 kJ.kg$^{-1}$.°C$^{-1}$, the thermal efficiency of the process is about 70% and the energy cost is about 2 £.kWh$^{-1}$; then, a rough estimate of the increased cost of phosphate rock due to calcining would be about 6.7 USD.ton$^{-1}$ of ore. Since most phosphate ores contain about 33% $P_2O_5$, this figure results in an increased cost of about 20 USD.ton$^{-1}$ $P_2O_5$ (Booker, 1989).

Furthermore, the second possibility to decrease cadmium content in phosphate fertilizers is the purification of phosphoric acid. In his work, Davister (1996) reported that anhydrite co-crystallization is one of the most promising methods even if it is rarely used; the operating costs are still 20 % to 30 % of the wet process acid operating costs. Nevertheless, the other three processes exhibit an operating cost much higher, about 75 to 100 % of the wet process acid operating costs (Table 4.19). This difference is due to the high cost of the reagents (solvents the case of solvent extraction) and resins (in the case of ion exchange). Booker (1989) stated that the use of Duolite C264 resin to decrease Cd concentration of 1000 m$^3$.day$^{-1}$ of 28 % $P_2O_5$ WPA from 15 mg.L$^{-1}$ to less than 2 mg.L$^{-1}$ was estimated to increase the $P_2O_5$ price by about 13 %. However, the cost of phosphoric acid decadmiation by precipitation with sulfide ions (as in Tunisia) or by solvent extraction (as in Germany) is still higher compared to other processes.

As a result, the decadmiation of wet phosphoric acid remains essential in view of the harmful effects of cadmium on agricultural soils. However, this step leads to a rise in fertilizer prices in the range of 2 % − 15 % (Oosterhuis et al., 2000), which will ultimately affect farmers. Unfortunately, available data are relative and indicative, so that new data on implementation costs of purification technologies are needed.

Table 4.19 Estimated investment and operating cost (in millions of USD) of four processes used for the removal of cadmium from wet-process phosphoric acid in a plant with a capacity of approximately 200 tons day$^{-1}$ P located in Western Europe (Davister, 1996).

| Process | Conditions | Investment cost | Operating Cost (US$ ton$^{-1}$ of P) |
|---|---|---|---|
| Co-crystallization | Without residue treatment<br>With residue treatment | 7<br>8 | 14<br>14 – 21 |
| Precipitation | | 7 | 69 |
| Solvent extraction | With full acid pre-treatment | 9 | 73 |
| Ion exchange | With medium acid pre-treatment | 9 | 69 |
| Wet process phosphoric acid manufacture | | 25 | 69 – 92 |

## 4.6 Life cycle assessment of WPA manufacturing process

In light of the serious environmental problem and natural resources consumption caused by the production of phosphoric acid and phosphate fertilizers, it is necessary to assess the environmental impact generated by the manufacture of these products by the adoption of an effective approach, such as life cycle analysis (LCA).

LCA is a systematic method for evaluating the environmental impact of products, processes, or activities throughout their complete life cycle by identifying and quantifying the impact of materials and energy utilization, waste disposal, and direct emission (Huijbregts et al., 2016; Zhang et al., 2017). Within LCA, life cycle impact assessment models (LCIA) are used to estimate the environmental impact (Huijbregts et al., 2016). Goedkoop et al. (2009) developed an LCIA method called ReCiPe that harmonized the CML (Guinée, 2001) and Ecoindicator 99 (Pizzol et al., 2011) methods. There are two mainstream ways to derive characterization factors, i.e., at midpoint level and at endpoint level. The ReCiPe method includes 18 midpoint indicators (climate change, ozone depletion, terrestrial acidification, freshwater eutrophication, marine eutrophication, human toxicity, photochemical oxidant formation, particulate matter formation, terrestrial ecotoxicity, freshwater ecotoxicity, marine ecotoxicity, ionizing radiation, agricultural land occupation, urban land occupation, natural land transformation, water depletion, metal depletion, and fossil depletion). Midpoint indicators focus on single environmental problems, while endpoint indicators show the environmental impact on three higher aggregation levels, being the effect on human health, biodiversity, and resource scarcity ("LCIA: the ReCiPe model - RIVM,").

Several authors (da Silva and Kulay, 2005; Hong and Li, 2013; Ridoutt et al., 2013; Wu et al., 2015, 2014) used LCA to study the environmental impact of fertilizer consumption and manufacturing. All the above-mentioned fertilizer production studies focused on on-site cases, while they cannot represent regional information because of poor data representation.

Approximately 80 % of the total production of phosphate fertilizers in China is represented by diammonium phosphate (DAP) and monoammonium phosphate (MAP) fertilizers (Zhang et al., 2017), which appears problematic in terms of their damaging effects on the environment (heavy metal pollution, phosphogypsum, radioactivity). In addition, the phosphoric acid consumption in DAP and MAP fertilizer manufacturing was $7.15 \times 10^6$ tons per year in China. It is against this background that an LCA study was performed by Zhang et al. (2017) to evaluate the environmental impact generated from the DAP and MAP fertilizer industry in China to establish a database on DAP and MAP fertilizer production. Using the ReCiPe method (Goedkoop et al., 2009), they found that among the 18 categories, the key categories were terrestrial acidification, human toxicity, particulate matter formation, and marine toxicity. The most contributive substances were sulfur dioxide, nitrogen oxides, ammonia, particulates, copper, vanadium, nickel, cobalt, lead, mercury, and arsenic (Figure 4.15). By comparing the DAP and MAP scenarios, they noticed that the DAP scenario produced a large amount of emissions and consumed a substantial quantity of raw materials. Hence, the phosphogypsum produced by the phosphoric acid synthesis stage in the DAP scenario is low, and 42.86 % of phosphogypsum was reused by making bricks in the DAP scenario. At least 5.0 %, 0.2 %, 0.3 %, 0.3 %, 0.2 % environmental benefits of climate change, terrestrial acidification, human toxicity, particulate matter formation, and marine ecotoxicity categories could be respectively accomplished by reusing phosphogypsum. Besides, Zhang et al. (2017) reported that for both cases, the phosphoric acid stage was the major contributor to environmental impact due to the low-efficiency use of phosphate rock and the high amount of emitted pollutants from phosphate mining.

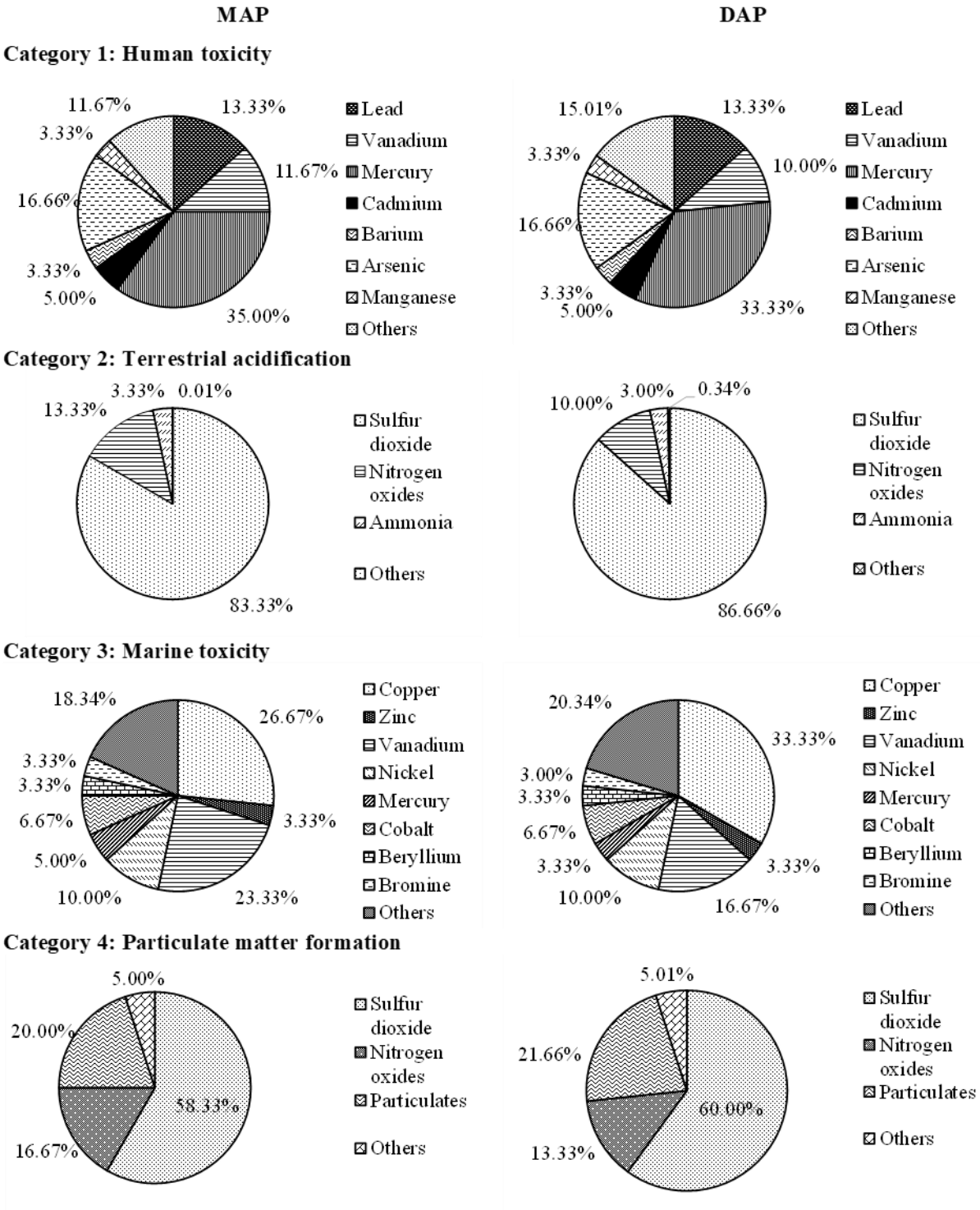


Figure 4.15 Contributions of substances in DAP and MAP to the key categories according to the work of (Zhang et al., 2017).

It is obvious that phosphoric acid production (it consumes large amounts of phosphate rock) has a detrimental effect on the environment, as well as it induces a depletion of natural resources. It is, therefore, necessary to focus on this intermediate step in the fertilizer industry to reduce the severity of its impact on the environment. However, in the literature, there are not many LCA studies on this product with the exception of a study that was conducted in 2015 on the environmental impact of Belgian phosphoric acid produced by the di-hemihydrate process (Belboom et al., 2015). In this study, environmental impacts of phosphoric acid production at both fertilizer and purified grades produced in the Belgian industrial plant of Prayon SA were assessed using the LCA methodology classified as Situation C from the ILCD handbook (European Commission, 2010) in accordance with the ISO standards 14040 (International Organization for Standardization (ISO), 2006a, p. 14040) and 14044 (International Organization for Standardization (ISO), 2006b, p. 14044). ILCD 2011 midpoint (European Commission, 2011) and ReCiPe 2008 (Goedkoop et al., 2009) were used to calculate the environmental impact of phosphoric acid. As a result, wet process purified phosphoric acid production induced specific environmental impacts approximately 1.5 times higher than the fertilizer grade for the 1 ton of $P_2O_5$ contained in the final product. Furthermore, fertilizer grade acid production allowed, depending on impact category, to reach 54% of the total impact of the purified acid. On the other hand, the manufacturing of purified phosphoric acid by thermal process, presumed to be produced in China and Kazakhstan, provided environmental impacts at least 7 times higher for climate change and fossil fuel consumption and 6 times higher for particle matter formation than the wet process. It is important to highlight that the production and consumption of electricity (Table 4.20) included in the thermal process were responsible for 90% of the total impact in all categories. In parallel, the wet process leads to higher emissions in the freshwater eutrophication category compared to the thermal process.

Table 4.20 Energy mix for electricity in China and Kazakhstan in 2011 (International Energy Agency, 2012).

| Fuel | China | Kazakhstan |
|---|---|---|
| Coal | 79.0% | 81.1% |
| Natural gas | 1.8% | 9.2% |
| Hydroelectricity | 14.8% | 9.1% |
| Nuclear energy | 1.8% | 0.0% |
| Wind | 1.5% | 0.0% |
| Waste | 0.2% | 0.0% |
| Biomass | 0.7% | 0.0% |
| Solar PV | 0.0% | 0.0% |
| Oil | 0.2% | 0.6% |

Based on the two studies cited below, it is clear that the two elements of wet phosphoric acid manufacturing, which severely affect the environment are the disposal of phosphogypsum and sulfuric acid production. For each ton of phosphoric acid produced, about four to five tons of phosphogypsum are produced (Belboom et al., 2015). Phosphogypsum is often stacked, landfilled, and dumped into surface water without any treatment (Contreras et al., 2015). Nevertheless, the phosphogypsum discharge leads to serious environmental impacts, such as heavy metal pollution, land use, and radioactive pollution (El-Didamony et al., 2013). The use of the di-hemihydrate process to produce phosphoric acid avoids the discharge of phosphogypsum and enables its use, in this case, in the plastering industry. Consequently, this allows a reduction of environmental impacts, *e.g.*, eutrophication through avoiding leachate or disposal into the sea, but also the minimization of the occupied land area, especially in countries where space is limited.

After phosphogypsum recovery, the production of sulfuric acid is the main parameter of the environmental impact of phosphoric acid production. In the case of di-hemihydrate process with double stage filtration, the setting up of a second modern sulfuric acid production plant with a cogeneration process reduced the impact of climate change by 80 %.

To sum up, WPA is the second most widely used acid in the world, and it is also linked to many products essential to our daily lives; so, it is important to obtain a precise value of the environmental impacts of its production. Hence, conducting an LCA that will emphasize the hotspots of this production and give indications of improvement from an environmental point of view is important. In addition, the LCA study conducted by Belboom et al. (2015) is very useful and could be extended for modeling other phosphoric acid facilities because 50 % of worldwide phosphoric acid is produced based on Prayon processes. It only needs to change specific data such as electricity mix, sulfuric acid production, and regulations depending on the location of industrial plants in the world.

## 4.7 Conclusions and perspectives

The implementation of WPA purification techniques will become increasingly mandatory, as the harmful effects of cadmium in agricultural soils have already led many countries to implement regulations to limit cadmium content in fertilizers. However, this action will affect several industrial sectors, as fertilizers are a pillar of food production and thus the quality of life. Indeed, the increase in the price of purified acid could raise fertilizer prices by 2 % to 15 %, which will affect end-users. Consequently, it is essential to think about developing advanced

and original cadmium abatement technologies from WPA that have not been progressed for years, whilst life cycle assessment of different phosphate industries must be achieved in order to evaluate the impact of this activity on the environment and living beings.

In this chapter, various processes have been reviewed for the removal of cadmium from phosphoric acid, such as solvent extraction, adsorption, ion exchange, precipitation, flotation, and membrane processes. These processes have been analyzed and compared on the basis of various criteria (technical, economic, environmental…). The following conclusions have been drawn:

- Solvent extraction is, nowadays, the most implemented at the industrial scale; $D_2EHDTPA$ and Kellex 100 extractants can be selected for the extraction and separation of cadmium from phosphoric acid under the different operating conditions. Even though this process presents many drawbacks, the lack of information in the literature, and the industrial applicability of alternative processes remains limited.
- Several alternative processes, such as adsorption, precipitation, and ion exchange, have shown high removal efficiencies: for example, under optimized conditions, cadmium removal achieved 80 % using $Na_2S$ as a precipitating agent, 90 % with impregnated resins, 68.6 % using Alamine 336 as an extractant, 99.2 % by nanofiltration, 98 % using carbon-sodium dodecylsulphonate, and 33 % using $(CH_3CH_2O)_2PS_2Na$, respectively. But these techniques present, however, various drawbacks, such as high energy input, environmental pollution due to by-products, high cost of reactants, organic solvents, and resins from an economic point of view. Thus, their industrial applicability still requires further investigation.
- Among the most recent liquid-liquid extraction techniques, ionic liquids seem to be very promising for an industrial-scale application of Cd(II) removal from phosphoric acid. They can be added to membrane materials or mixed in the liquid phase as an extractant enhancer. Liquid-liquid extraction can regain interest using ionic liquids because these latter exhibit extremely low vapor pressure, good thermal and chemical stabilities, wide liquid range, non-flammability, and great solvation ability for metal cations. Recently, the recovery of Cd(II) cations was enhanced using phosphonium/ammonium-based ionic liquids diluted in kerosene. While acidity is a key issue, some ionic liquids present the advantage of being compatible with concentrated acid media, for example, Aliquat 336 in PVC membranes. Their price may, however, be an issue.

- For economic reasons, a low-cost technique, *e.g.*, adsorption, could also be effective to remove low cadmium ions concentration from WPA; a wide range of natural low-cost adsorbents which have been developed or even waste products from industries can be tested to enhance the cadmium adsorption, but their variability (*e.g.*, for green adsorbents) and the competitive adsorption between impurities remain the main issues to solve.
- For other alternative techniques, such as ion exchange, flotation, precipitation in gas−liquid flow using $H_2S$ coupled to flotation, and membrane processes, the main reason for their limited availability is that they have not been deeply investigated up to now. For example, flotation could be used as an attractive alternative to filtration. So, it is important to stimulate studies in these fields to better assess their ability to remove cadmium from WPA solutions, which will determine whether they can be used at the industrial scale as a pretreatment and an upstream process.

# Chapter 5: A novel approach for removing cadmium from synthetic wet phosphoric acid using sulfide precipitation process operating in batch and continuous modes


## Abstract

The removal of heavy metals, especially cadmium, from wet phosphoric acid is still a challenging stage during the manufacturing of phosphate fertilizers. In this work, a novel approach was developed to improve the performance of the sulfide precipitation process as a purification technique. This is based on NaHS rather than $Na_2S$ as a precipitating agent in both batch and continuous modes for cadmium removal from synthetic wet phosphoric acid. First, the respective performance of $Na_2S$ and NaHS was compared in the batch mode. NaHS was shown to improve decadmiation in comparison to $Na_2S$ even though the same trends were observed for both precipitating agents as a function of operating conditions. An increase in Sulfur/$Cd^{2+}$ molar ratio improved cadmium sulfide precipitation. Conversely, increasing temperature and phosphoric acid concentration impaired the effectiveness of cadmium removal efficiency. An apparent kinetic model was developed taking into consideration the reaction mechanisms and supersaturation to predict the residual cadmium concentration in phosphoric acid solutions. The feasibility of the continuous process based on NaHS was also assessed. The results showed that a residence time of 40 min was needed to achieve 85.6 % of $Cd^{2+}$ elimination at 25 °C. As aggregation seemed to be the main mechanism governing particle size, this increased with the Sulfur/$Cd^{2+}$ ratio, which could improve downstream solid separation. Eventually, these findings of this study provide useful insights into the feasibility of chemical precipitation using NaHS as a technology of phosphoric acid decadmiation in the industry.



**Keywords:** Batch vs. Continuous modes; Cadmium removal; Kinetic modeling; Phosphoric acid purification; Precipitate characterization; Sulfide precipitation.

## 5.1 Introduction

Heavy metal ions as environmental pollutants have emerged as a worldwide preoccupation in the last years, due to their toxicity, persistence and non-biodegradability, which poses a serious detrimental impact on the ecological environment and human health (M. Li et al., 2022; Purkayastha et al., 2014). Particularly, their accumulation in soil constitutes a real concern for sustainable agriculture; thus, strict specifications are set for heavy metal concentrations in fertilizer products.

Recently, the focus of different institutions on the effect of heavy metals present in fertilizers has been noteworthy, and especially on cadmium (Ulrich, 2019). Cadmium is toxic and mutagenic element, and can cause kidney damage, anemia and bone diseases (Cichy et al., 2014; Owija et al., 2021). The primary sources of $Cd^{2+}$ can be partitioned into two categories: $Cd^{2+}$ is naturally present in the environment, including Earth's crust and oceans, and can be naturally brought to the soil (*e.g.*, by volcanic activity, weathering of Cd-containing rocks, sea spray), and through anthropogenic activities (such as mining and smelting of zinc-bearing ores, fossil fuel combustion, waste incineration, sewage sludge, irrigation waters, manure, and fertilizers derived from phosphate rock) (Roberts, 2014; Samrane et al., 2018). As regards the final cadmium content in phosphate fertilizers, the latter is related to the nature of the phosphate rock (sedimentary and igneous geological origins) as well as the manufacturing method (thermal and wet routes) (Cichy et al., 2014; Tjioe, 1987). Indeed, the majority of phosphate ores contain from 10 to 80 $g.ton^{-1}$ of cadmium depending on the deposit, and it can subsequently be found in wet phosphoric acid and also in phosphate fertilizers.

In the last decades, various technologies have been developed to remove heavy metals from industrial effluents, including solvent extraction (Abidli et al., 2022; Touati et al., 2009), chemical precipitation (Kumar et al., 2021; Lewis, 2017; Zieliński et al., 2019), adsorption (Cheng et al., 2022; Omri and Batis, 2013), ion exchange (Elzoghby, 2021; Taha et al., 2020), membrane processes (Elleuch et al., 2006; Khaless, 2006; Park and Kim, 2021; Xu et al., 2022), and flotation (Jdid et al., 1987; Salmani et al., 2013). In fact, the various tested techniques for the decadmiation of wet phosphoric acid have been thoroughly evaluated in a literature review presented in chapter 4. From among these processes, chemical precipitation (specifically by using soluble sulfide) is well known for its use in removing heavy metals from wastewaters under acidic conditions, such as acid mine drainage wastewater, mine tailing water, and metallurgical wastewaters (Kumar et al., 2021; Lewis, 2017, 2010; Ostermeyer et al., 2021). However, the precipitation performance is influenced by many operating and design

parameters, such as the type of precipitating agents, the nature and amount of heavy metal ions present in the solution, the coexistence of other ions that can inhibit the reaction, pH, hydraulic residence time, mixing and reactor designs (Estay et al., 2021; Pohl, 2020). The removal of heavy metals by the chemical precipitation process is achieved by using a large spectrum of inorganic salts as precipitating agents, including hydroxide, carbonate, sulfide, and phosphate salts, which foster the precipitation of metal ions to their solubility limits (Abidli et al., 2022).

Sulfide precipitation consists of effectively removing heavy metals from aqueous solutions by using different source of sulfide, namely $Na_2S$, NaHS, $Na_2S_2O_3$, $(NH_4)_2S$, CaS, FeS, BaS, and $H_2S$ (Deng et al., 2019; Gharabaghi et al., 2012; Jerroumi et al., 2020; Mokone et al., 2010; Ostermeyer et al., 2021). This is one of the most preferred technologies for the separation and recovery of heavy metals from wastewaters and hydrometallurgical solutions. For this purpose, it is frequently implemented in industry thanks to its multiple benefits, namely high removal/recovery effectiveness, low solubility of the resulting metal sulfide, moderate reaction rates, and, most interestingly, the potential for reuse of the sulfide precipitates (Jerroumi et al., 2020; Vemic et al., 2016). Metal sulfide precipitates can be formed as insoluble nano-powders, which favor their recycling and reuse for many industrial applications. These valuable nanoparticles are useful for several applications in different fields; for example, cadmium sulfide (CdS) is used in various catalytic and environmental applications, such as decolorization of azo-dyes, reduction of carbon dioxide hydrocarbons, hydrogen production, nitrate denitrification, and synthesis of acetic acid from carbon dioxide (Dong et al., 2020). However, it should be emphasized that this technique is highly sensitive to the types of precipitating agents and their concentrations (Veeken et al., 2003). In fact, an exhaustive literature review of recent studies on sulfide precipitation applied for the treatment of various aqueous matrices, with an emphasis on the overall process and its major unit operations, can be found in the review article by Estay et al. (2021).

As discussed above, the accumulation of cadmium in the soil is becoming a growing concern. Therefore, it is of interest to focus on reducing its concentration in wet-process phosphoric acid, the intermediate step in the manufacture of phosphate fertilizers, which ultimately will enhance the yield of agricultural production, as well as the quality of food and feed products. In this scope, sulfide precipitation can be also utilized for wet phosphoric acid purification since it has been used for the removal of metallic impurities from wastewaters under acidic conditions (Ye et al., 2017). Some investigations have been carried out on cadmium removal from wet phosphoric acid using mineral and organic sulfides (Ennaassia et al., 2002; Norwood and Tate,

1992; Samrane and Khouloud, 2017; Zieliński et al., 2019). For instance, through the study of Zieliński et al. (2019), it might be concluded that $Na_2S$ can be considered as an effective precipitating agent for eliminating cadmium from phosphoric acid, as the other precipitating agents, such as zinc ethylphenyldithiocarbamate (ZnEPDTC), sodium ethylphenyldithiocarbamate (NaEPDTC), and sodium cellulose xanthate (SCX) were not able to react with cadmium. Table 5.1 summarizes the major studies carried out on cadmium removal from phosphoric acid by sulfide precipitation.

Understanding the effects of Sulfur/$Cd^{2+}$ molar ratio, temperature, phosphoric acid concentration, and hydraulic residence time (HRT) during cadmium removal from wet phosphoric acid by using sulfide precipitation technology were important for controlling the quality improvement of phosphoric acid for its end uses in the fertilizers or the food industries, however, only a few databases were reported in the literature on this topic. Meanwhile, although the batch sulfide precipitation was studied for removing cadmium from wet phosphoric acid by sulfide precipitation, few attentions have been paid to the thermodynamic and kinetics modeling and continuous systems. In fact, the majority of these studies investigated the sulfide precipitation process in a small-scale batch system. Accordingly, the present work was conceived to shed light on the behavior of cadmium during sulfide precipitation in synthetic wet phosphoric acid (25 % $P_2O_5$) under various aspects. To this end, cadmium elimination from synthetic dilute phosphoric acid by precipitation, comparing NaHS and $Na_2S$ as the sulfide source, was investigated in a stirred tank reactor operating in both batch and continuous system by scaling up with a factor of around 50 compared to the existing studies. The effects of Sulfur/$Cd^{2+}$ molar ratio, acidity, temperature, hydraulic residence time (HRT), and the initial $Cd^{2+}$ concentration on the cadmium removal efficiency were explored. Furthermore, a kinetic model for cadmium removal from phosphoric acid solutions was developed taking the aforementioned parameters into account. Finally, the characterization of the recovered precipitate (CdS) was further discussed by means of the particle size measurement, semi-quantitative chemical, and morphological analyses.

Table 5.1 Studies performed on cadmium removal from phosphoric acid solutions by sulfide precipitation.

| Authors | Experimental conditions | | | | | Setup and scale development | Removal efficiency (%) | Highlights |
|---|---|---|---|---|---|---|---|---|
| | Precipitating agents (PA) | $H_3PO_4$ concentration ($\%P_2O_5$) | Initial Cd concentration ($mg.L^{-1}$) | Temperature (°C) | Residence time (a) or equilibrium time (b) (min) | | | |
| Zieliński et al. (2019) | ZnEPDTC | 25.11 | 101.95 | 20 | 60[(b)] | Small scale batch tests carried out in a thermostated water bath with a shaker model 357 | 12.43 | The precipitating agents were added in the proportion of 0.5 wt.% in reference to WPA, except sodium cellulose xanthate (1 wt.%), and sodium sulfide (0.2 wt.%). |
| | NaEPDTC | 25.11 | 81.85 | 20 | 60[(b)] | | 0.00 | |
| | SCX | 25.11 | 101.95 | 20 | 50[(b)] | | 37.76 | |
| | NaDBDTC | 25.11 | 81.85 | 20 | 50[(b)] | | 45.76 | |
| | $Na_2S$ | 25.11 | 101.95 | 20 | 60[(b)] | | 73.49 | |
| Samrane and Khouloud (2017) | NaHS | 42 | 61 | - | 3[(a)] | Continuous process in a tubular reactor operating under pressure | 86.80 | $N/P$ = 0.4, WPA mass-flow rate = 110 $g.min^{-1}$, NaHS mass-flow rate = 1.53 $g.min^{-1}$ |
| | | 38 | 55.9 | - | 3[(a)] | | 91.30 | $N/P$ = 0.4, WPA mass-flow rate = 102.52 $g.min^{-1}$, NaHS mass-flow rate = 1.30 $g.min^{-1}$ |
| | | 29 | 45.7 | - | 3[(a)] | | 86.10 | $N/P$ = 0.2, WPA mass-flow rate = 95.95 $g.min^{-1}$, NaHS mass-flow rate = 0.87 $g.min^{-1}$ |
| (Ennaassia et al., 2002) | $Na_2S$ | 10 | 56.2 | 20 | 60[(b)] | Small scale batch tests performed in thermostatic cell. Volume of solution 50 mL | 81.15 | Molar ratio $Na_2S/Cd^{2+}$= 2 |
| | | 10 | 56.2 | 70 | 60[(b)] | | 8.15 | Molar ratio $Na_2S/Cd^{2+}$= 2 |
| | | 10 | 56.2 | 40 | 60[(b)] | | 97.17 | Molar ratio $Na_2S/Cd^{2+}$= 10 |
| | | 10 | 56.2 | 70 | 60[(b)] | | 87.77 | Molar ratio $Na_2S/Cd^{2+}$= 10 |
| | | 20 | 56.2 | 20 | 60[(b)] | | 81.36 | Molar ratio $Na_2S/Cd^{2+}$= 4 |
| | | 20 | 56.2 | 60 | 60[(b)] | | 0.00 | Molar ratio $Na_2S/Cd^{2+}$= 4 |
| | | 30 | 56.2 | 20 | 60[(b)] | | 19.35 | Molar ratio $Na_2S/Cd^{2+}$= 10 |
| Norwood and Tate (1992) | $Na_2S$ | 30 | - | - | 30 | - | 5 | Molar ratio $Na_2S/P_2O_5$ = 0.0030 |
| | $Na_2S_{2.32}$ | 30 | - | - | 30 | | 0 | Molar ratio $Na_2S_{2.32}/P_2O_5$ = 0.0031 |
| | $Na_2S_{2.32}$ | 30 | - | - | 30 | | 5 | Molar ratio $Na_2S_{2.32}/P_2O_5$ = 0.0057 |

## 5.2 Materials and methods

### 5.2.1 Reagents

Cadmium sulfate ($CdSO_4 \geq 99.99$ %), sodium sulfide ($Na_2S \geq 60$ %), and phosphoric acid ($\geq 85$ wt.%) used in this investigation were purchased from Merck (Germany). Sodium hydrosulfide (NaHS) (purity 70 %) was provided by the OCP Group (Morocco). All reagents were used without further purification. Osmotic water was used to dissolve different quantities of NaHS or $Na_2S$ for preparing sulfide medium prior to precipitation assays, and to dilute phosphoric acid to obtain synthetic WPA solutions with mass concentrations ranged from 10 % to 30 % $P_2O_5$.

### 5.2.2 Precipitation experimental setup

The experimental setup for the cadmium sulfide precipitation included a 3.4 L double-jacket glass reactor (hermetically sealed with a stainless-steel cover) with an internal diameter of 150 mm and a depth of 300 mm. Stirring was accomplished by means of an overhead stirrer (Hei-TORQUE Precision 100, Heidolph; stirring rate range varying from 10 to 2000 rpm) equipped with a six-blade Rushton turbine, made of Teflon to withstand acidic media. The reactor outlet was coupled to a 10 L transparent PVC truncated cone settler compatible with acidic media. Temperature was controlled using a thermoregulator which provides 3 kW of heating power and a temperature up to 90 °C (TT–170 L, TOOL-TEMP AG). pH and ORP were monitored by means of pH and ORP electrodes (InPro 4260(i)/SG/120, Mettler Toledo Switzerland) connected to a transmitter (M200, Mettler Toledo, Switzerland). Moreover, the pilot unit included a $H_2S$ gas detector (Polytron 3000, Dräger, Germany) linked to a visual and audible alarm to guarantee safety during experiments.

The configuration of the batch system was altered to enable continuous operation, as depicted in Figure 5.1. Both phosphoric acid and sulfur species solutions were pumped from feed tanks to the reactor using two peristaltic pumps (PP 3300, VWR, USA). The feed pumps were calibrated to supply the liquid solution at a known flow rate. A schematic and a picture of the experimental setup are displayed in Figure 5.1.

(a)

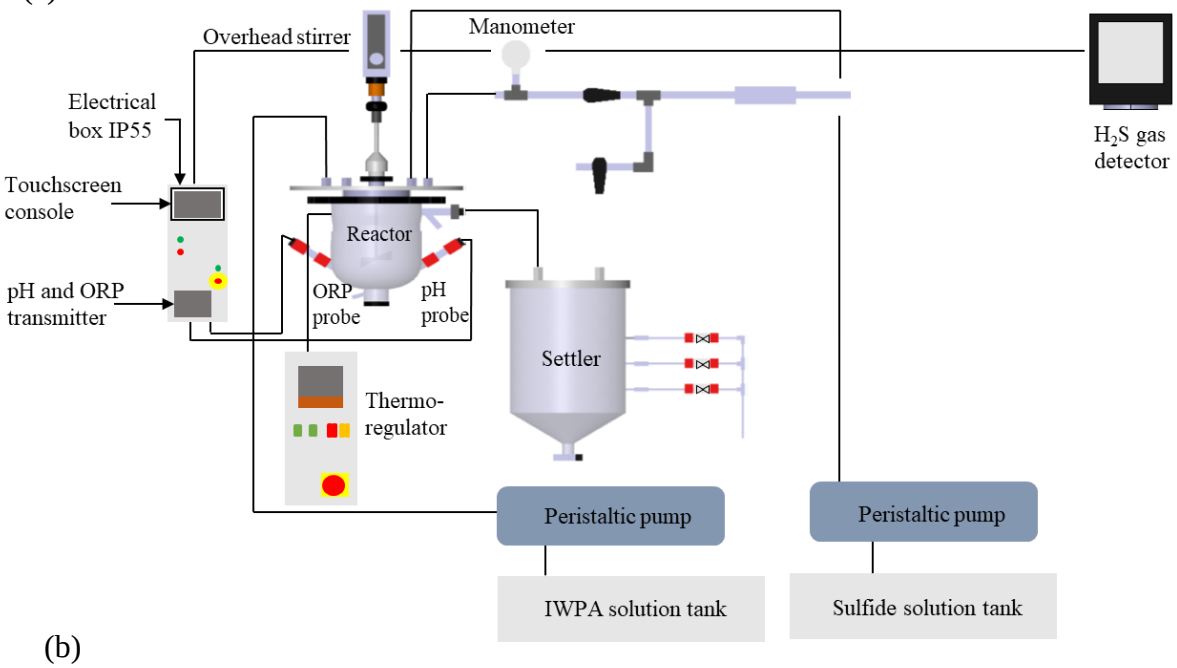


(b)


Figure 5.1 (a) Schematic and (b) photograph of the continuous pilot unit for cadmium sulfide precipitation from phosphoric acid effluent. ① Overheard stirrer, ② Electrical box IP55, ③ Touchscreen console, ④ Helium gas cylinder, ⑤ pH and ORP transmitter, ⑥ pH probe, ⑦ Peristaltic pump for $H_3PO_4$ solutions, ⑧ Thermoregulator, ⑨ $H_2S$ gas detector, ⑩ Six blade Rushton turbine, ⑪ ORP probe, ⑫ Settler, ⑬ Peristaltic pump for sulfide solutions, ⑭ Tank for discharging treated effluent.

### 5.2.3 Experimental procedure

In this study, experiments were performed with synthetic dilute phosphoric acid solutions that contained 20 $mg.L^{-1}$ of cadmium. It should be noted that the choice of these media was intended to simulate the Moroccan dilute wet phosphoric acid. Table 5.2 summarizes the characteristics of the phosphoric acid used in this study.

Table 5.2 Some characteristics of phosphoric acid solutions.

| Acid concentration (% $P_2O_5$) | Acid concentration (M) | Density at 25 °C ($g.mL^{-1}$) (Christensen and Reed, 1955) | Measured pH at 25 °C | Species concentration (M) (Dartiguelongue et al., 2016) | | | |
|---|---|---|---|---|---|---|---|
| | | | | $H^+$ | $H_3PO_4$ | $H_2PO_4^-$ | $H_5P_2O_8^-$ |
| 10 | 1.52 | 1.073 | 0.75 | 0.254 | 1.089 | 0.077 | 0.177 |
| 20 | 3.28 | 1.163 | 0.42 | 0.739 | 1.893 | 0.090 | 0.649 |
| 25 | 4.27 | 1.213 | 0.25 | 1.147 | 2.060 | 0.085 | 1.062 |
| 30 | 5.34 | 1.267 | 0.07 | 1.685 | 2.039 | 0.070 | 1.616 |

In batch experiments, the first objective was to examine the effect of the Sulfur/$Cd^{2+}$ molar ratio, ranging from 1/1 to 30/1, and that of the phosphoric acid concentration which varied from 10 % to 30 % $P_2O_5$ on the sulfide precipitation performance, while keeping a constant temperature at 25 °C. In the second part of this work, an investigation into the influence of temperature (from 25 °C to 70 °C), and that of the Sulfur/$Cd^{2+}$ molar ratio (from 1/1 to 30/1) on the cadmium removal kinetics from phosphoric acid (having a concentration of 25 % $P_2O_5$) by precipitation process was carried out. The initial cadmium ion concentration and reaction time were maintained at 20 $mg.L^{-1}$ and 60 min in all runs, respectively. As discussed during the description of the reagents, the sulfur source was either sodium disulfide ($Na_2S$) or sodium hydrosulfide (NaHS) solubilized in pure phosphoric acid solution. For this reason, the reactor was first filled with 1.5 L of phosphoric acid solution containing 20 $mg.L^{-1}$ of cadmium ion, and 0.5 L of concentrated sulfide solution (with a concentration that ranged from 22.83 to 684.91 $mg.L^{-1}$) was then entirely added to the mixture through an inlet point located on the top of the reactor. It should be noted that concentrated solutions of $Cd^{2+}$ and sulfide were prepared taking into account the dilution that occurred during the mixing of the solutions. The precipitation assays were conducted with a freshly prepared sulfide solution. During the experiments, the solution was mechanically stirred at 300 rpm. The temperature reaction was kept constant by means of a thermoregulator with an accuracy of ± 1 °C.

In continuous sulfide precipitation experiments, the reactor volume used was 2.75 L. To simulate the operational process in the industry, the reactor was first filled with diluted solution (25 % $P_2O_5$) having a volume of 2 L. Then, the sulfide solution with a volume of 0.75 L was added and the pumps were simultaneously started up which in turn provided the reactor with feed solutions. The impact of the HRT on the precipitation process was examined, by changing the latter from 20 to 40 min (where the flow rate of each reagent was equal to 68.75 and 34.38 $mL.min^{-1}$, respectively), under operating conditions of T = 25 °C, Sulfur/$Cd^{2+}$ = 10/1 – 30/1, and the initial $Cd^{2+}$ concentration 20 $mg.L^{-1}$. Moreover, the influence of the initial $Cd^{2+}$ concentration variation from 20 to 56 $mg.L^{-1}$ on the effectiveness of cadmium sulfide precipitation was examined under the operating conditions: Sulfur/$Cd^{2+}$ = 10/1 – 30/1, T = 25 °C, and HRT = 40 min. All continuous experiments were conducted in a phosphoric acid medium with a concentration of 25 % $P_2O_5$. Batch and continuous experiments were run in duplicate.

### 5.2.4 Analytical methods

During experiments, 15 mL phosphoric acid solution samples were collected as a function of time. Each sample was filtered through a 0.45 µm syringe filter and analyzed for determining the residual cadmium concentration in phosphoric acid solutions. The initial and residual concentrations of cadmium ions were analyzed using calibrated atomic absorption spectrophotometer (PinAAcle 900Z, Perkin Elmer, USA).

The removal yield of cadmium ions from phosphoric acid medium was determined using the equation below:

$$\eta = \frac{C_{ini} - C_{resid}}{C_{ini}} \quad (5.1)$$

where $C_{ini}$ ($mg.L^{-1}$) and $C_{resid}$ ($mg.L^{-1}$) represent the initial cadmium concentration and that remaining after the precipitation reaction at a given time, respectively.

At the end of each continuous experiment, the solution in the reactor was filtered and the obtained sulfide precipitates were collected, rinsed with deionized water, and dried at 40 °C for further characterization. X-ray diffraction mineralogical analyzes were carried out on a Bruker D8 Discover diffractometer ($Cu - K\alpha$ radiation, $\lambda$ = 1.5406 Å, 30 kV and 10 mA). The instrument was configured for scanning in the range of 5° to 80° at $2\theta$. The software "X'PertHigh score" was used for data processing. Morphological analysis for the precipitate

was also carried out by HiROX SH 4000M Scanning Electron Microscope (SEM) equipped with Bruker SCU Energy Dispersive X-ray Spectrometer (EDS) for qualitative elemental analysis of the precipitate. Before being placed under the microscope, the samples were metallized by applying a thin layer of carbon for enhancing the quality of the subsequent SEM images. The sample surface was scanned over randomly selected areas at magnifications of 3500×, 4000×, 5000×, 5500×. The particle size distribution of the fine particles was performed using a Malvern Mastersizer 2000 laser granulometer in the range of 0.020 – 2000 μm. The scattering model applied to determine the particle size in the software is the Mie theory.

## 5.3 Results and discussion

In an attempt to achieve a thorough insight into the precipitation cadmium sulfide from synthetic wet phosphoric acid solutions, an investigation was undertaken on the effects of the Sulfur/$Cd^{2+}$ molar ratio, the temperature, the phosphoric acid concentration, and the initial cadmium concentration; both in batch and continuous modes. Furthermore, the effect of the molar ratio on the composition and the particle size of the precipitate has been examined.

### 5.3.1 Batch operation

#### *5.3.1.1 The effect of molar ratio, phosphoric acid concentration, and temperature on cadmium sulfide precipitation*

Figure 5.2 depicts the effect of $Sulfur/Cd^{2+}$ molar ratio on the cadmium removal efficiency using NaHS and $Na_2S$. The results indicate that the removal yield of cadmium from diluted phosphoric acid solutions increased with the dosage of sulfur. Indeed, the $Cd^{2+}$ removal yield has gone up from 0.16 % to 90.34 % and 0.32 % to 74.80 % by increasing the Sulfur/$Cd^{2+}$ molar ratio from 1/1 to 30/1, for NaHS and $Na_2S$, respectively. In addition, for a Sulfur/$Cd^{2+}$ of 30/1, the removal efficiency of cadmium by NaHS (90 %) was superior to the one achieved by $Na_2S$ (75 %). These experimental results exhibited a good reproducibility. Several reasons can explain the differences between these two precipitating agents which correspond to the acid/base equilibrium of sulfide anions. The first reason could be a slight change in pH: NaHS provides solutions a bit more acidic than $Na_2S$, but the difference vanishes in concentrated phosphoric acid. The second one, more convincing, is the effect of ionic strength and especially of cations. In terms of ionic strength, 1 mmol/L NaHS adds only 1 mmol ionic strength and $Na^+$ cations, whereas $Na_2S$ adds 3 mmol ionic strength and 2 mmol cations; this affects activity coefficient and, thus, chemical equilibria, so that a slight salting-in effect of CdS is possible for

cations with $Na_2S$ in comparison to NaHS. In addition, high ionic strength reduces gas solubility, while $H_2S$ is the main species of soluble sulfur (Foucher et al., 1999). As the values of activity coefficient are not known in such concentrated media, only precipitation data is available, but the analysis of NaHS solubility and speciation in phosphoric acid deserves further research in the future.

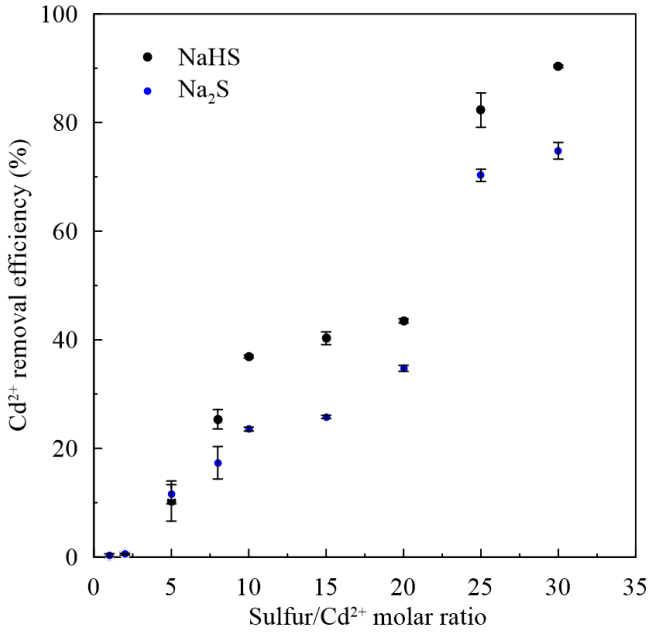


Figure 5.2 Effect of Sulfur/$Cd^{2+}$ molar ratio on the cadmium precipitation using NaHS and $Na_2S$ at T = 25 °C and [$H_3PO_4$] = 25 % $P_2O_5$.

For the sake of conciseness, only the results using NaHS as a precipitating agent will be presented in the following figures, as both agents induce the same trends as a function of temperature or acid concentration with an enhanced Cd removal using NaHS.

Moreover, it is a well-known fact that the concentration of sulfur species is a strong function of pH (Lewis, 2010), and following the reaction (Eq. (5.2) and (5.3)), the addition of NaHS or $Na_2S$ to a phosphoric acid medium provided $H_2S$ in aqueous form, which decreased the number of species involved in the sulfide precipitation reaction ($HS^-$and $S^{2-}$). In the beginning of the reaction, some of the $H_2S$ was lost from the system as a gas, and the other proportion of the gaseous hydrogen sulfide was dissolved into the phosphoric acid solutions to undergo a deprotonation reaction (Eqs. (4.19) and (4.20)). Thereby, excess sulfide is required to drive the precipitation of cadmium sulfides in acidic complex media, such as phosphoric acid solution. Indeed, the acquired findings on the effect of the Sulfur/$Cd^{2+}$ molar ratio on the efficiency of cadmium sulfide precipitation showed that the removal yield of $Cd^{2+}$ ions increased

progressively with the increment of sulfur/$Cd^{2+}$ up to 20/1. Then, the $Cd^{2+}$ elimination efficiency improved remarkably to reach 82.23 % for Sulfur/$Cd^{2+}$ = 25/1, which brings to the conclusion that the removal of $Cd^{2+}$ ions by sulfide precipitation is highly sensitive to the sulfide dosage. These findings are in line with those earlier found in literature for cadmium sulfide precipitation from phosphoric acid solutions of varying concentrations.

$$NaHS + H_3PO_4 \rightarrow H_2S + Na^+ + H_2PO_4^- \quad (5.2)$$

$$Na_2S + H_3PO_4 \rightarrow H_2S + 2Na^+ + HPO_4^{2-} \quad (5.3)$$

During the experimental tests, it was observed that when the sulfide solution (Sulfur/$Cd^{2+}$ = 15/1) was added to the phosphoric acid solution with a concentration of 10 % $P_2O_5$, a precipitate was quickly formed in the appearance of orange-colored particles, which typified the cadmium sulfide precipitate (CdS). However, as the acidity level gradually increased, the mixture of reagents became turbid, and this time the precipitate was in colloidal form. Furthermore, similar observations were made when studying the molar ratio effect on the effectiveness of cadmium sulfide precipitation in phosphoric acid solution of 25 % $P_2O_5$ concentration.

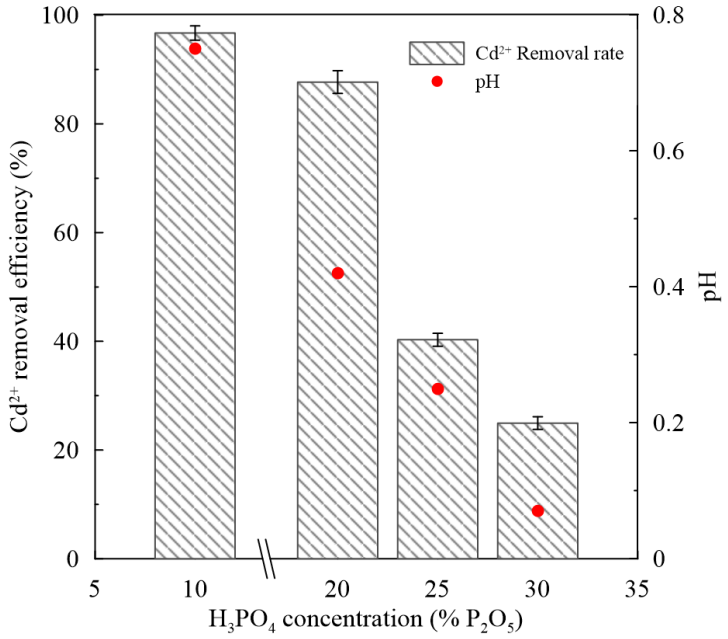


Figure 5.3 Influence of $H_3PO_4$ concentration on decadmiation effectiveness at T = 25 °C and Sulfur/$Cd^{2+}$ = 15/1.

Figure 5.3 shows the cadmium removal yield against acid phosphoric concentration. The value achieved after 60 min of precipitation reaction was 96.0 % and 24.4 % in the case of phosphoric acid solutions with a concentration of 10 % and 30 % $P_2O_5$, respectively. Hence,

the higher concentration of phosphoric acid, the lower decadmiation efficiency. This can be explained by the fact that when phosphoric acid concentration increased, the presence of $H^+$ ions augmented, and the latter mop up $S^{2-}$ ions, and subsequently the efficiency of sulfide precipitation fell.

Figure 5.4 displays the effect of temperature on the yield of $Cd^{2+}$ removed from 25 % $P_2O_5$. Based on this Figure, cadmium sulfide precipitation efficiency decreased with increasing acid temperature from 25 °C to 70 °C. For instance, for a molar ratio of Sulfur/$Cd^{2+}$ = 20/1, the $Cd^{2+}$ removal efficiency was found to decrease from 43 % to 24 % as the temperature increased from 25 °C to 70 °C. This can be attributed to the decline in $H_2S$ solubility and thereafter the lack of available sulfide. This statement is corroborated by the work of Xuan Hai et al. (2012) wherein they measured the $H_2S$ solubility in phosphoric acid solutions. The authors found that for a phosphoric acid solution (47.2 % $P_2O_5$), $H_2S$ solubility decreased by increasing the temperature from 40 °C to 80 °C.

Parallelly, Figure 5.4a-c also illustrates the $Cd^{2+}$ removal from phosphoric acid solutions (25 % $P_2O_5$) as a function of reaction time, and exhibit that $Cd^{2+}$ removal efficiency significantly increased from 0 to approximately 15 min, and then continued to slightly augment until a reaction time of 30 min to reach an equilibrium value over a period of 60 min. This finding is consistent with those of Ennaassia et al. (2002) and Zieliński et al. (2019) who studied the precipitation of cadmium sulfides in phosphoric acid under a reaction time of 60 min. This indicates that to reach high removal efficiency, 45 min to 60 min can be a good range for continuous operation.

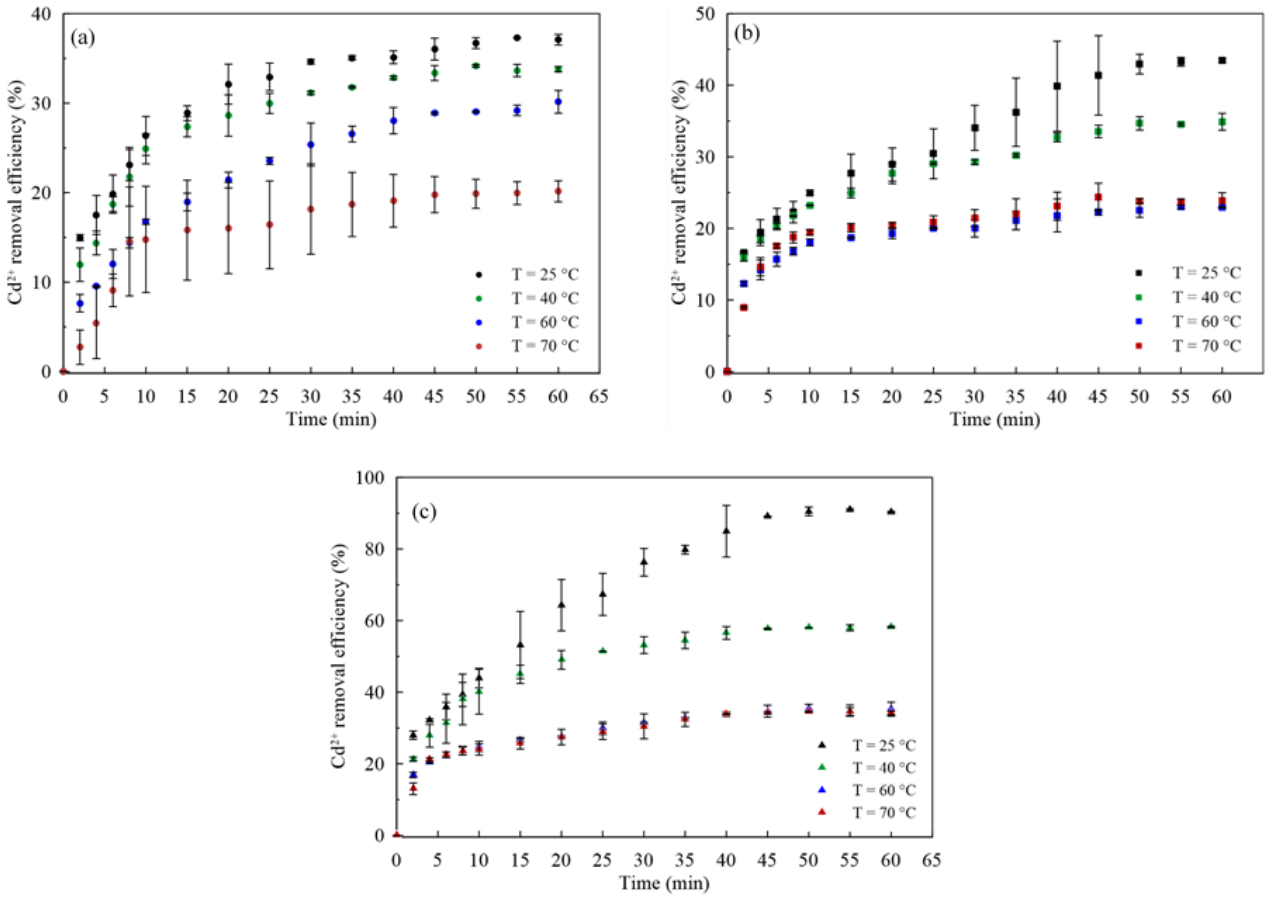


Figure 5.4 Effect of operating temperature on the cadmium removal yield from phosphoric acid solution of 25 % $P_2O_5$. (a) Sulfur/$Cd^{2+}$ = 10/1, (b) Sulfur/$Cd^{2+}$ = 20/1, and (c) Sulfur/$Cd^{2+}$ = 30/1.

### *5.3.1.2 Thermodynamic and kinetic modeling*

#### *5.3.1.2.1 Thermodynamic modeling*

At first one could consider the different chemical equilibria existing in concentrated phosphoric acid. For that purpose, it is possible to use the latest information available in this field given by Dartiguelongue (2014) and Dartiguelongue et al. (2016), based on theoretical and experimental studies (in particular using the data of Elmore et al. (1965)). Only two chemical equilibria (Eqs. (5.4) and (5.5)) are taken into account in concentrated phosphoric acid solution (the values of the equilibrium constants are given for a 25 °C temperature). In these equations, $(X) = \gamma_X \cdot [X]$ corresponds to the activity of species X, while $\gamma_X$ and [X] are the activity coefficient and the concentration of this species, respectively. With the help of the authors, it has been possible to get the values of the concentrations and activity coefficients of

the different species according to nominal phosphoric acid concentration, which corresponds to the total concentration of the species derived from the equilibria (Table 5.2). Meanwhile, the aqueous $Cd^{2+}$ – $H_3PO_4$ system can be characterized by the equilibria given in Powell et al. (2011). Compared to this complete set of data, the reactions considered were the ones implementing the phosphoric acid species appearing in Eqs. (5.4) and (5.5) (*i.e.*, $H_2PO_4^-$) and complexing cadmium ion (Eqs. (5.6) and (5.7)). Thus, considering the usual cadmium concentrations in WPA solutions (20 $mg.L^{-1}$), it is possible to estimate its speciation via a mass balance. For example, in a 25 % $P_2O_5$ solution, the species distribution is as follow, indicating a majority of free cadmium: $Cd^{2+}$ (68.6 %), $CdH_2PO_4^+$ (27.8 %), $Cd(H_2PO_4)_{2(aq)}$ (3.6 %).

In cadmium precipitation using sulfide ion, the reaction for cadmium sulfide formation is described by Eq. (5.8). Nevertheless, in a solution of phosphoric acid, which is an acidic medium, it is well-known that sulfur is predominantly in the form of $H_2S$ (Eqs. (4.19) and (4.20)). Hence, the expected reaction for $CdS$ precipitation can be considered as in Eq. (5.9). Basically, the thermodynamic equilibrium that takes place in the precipitation of metal sulfides can be stated as given below. Considering the constants $K_1$, $K_2$ and $K_s$, Eq. (5.9) is then rewritten as given by Eq. (5.10). Besides, it should be pointed out that $H_2S$ is partitioned between the aqueous solution and the gaseous phase above it, following Henry's law (Eq. (5.11)).

According to Dalas et al. (1991) and Wang and Tessier (1999), $Cd(II)$ is also able to react with $HS^-$ to form a range of soluble complexes. The main reactions can be schematically represented by Eqs. (5.12)-(5.15), where $\beta_j$ indicates the thermodynamic formation constant and $j = 1$ to 4. These values are given in this reference as concentration constants. Moreover, considering the acidity constant $K_1^0$ value and the phosphoric acid solution pH, one could consider that $HS^-$ ion concentration as very weak (less than $4.10^{-10}$ M). In addition, the $\beta_3$ and $\beta_4$ constants are low, enabling to neglect $Cd(HS)_4^{2-}$ and $Cd(HS)_3^-$ in the cadmium speciation.

Table 5.3 The primary reactions involved in the cadmium/sulfide/phosphoric acid system.

| Chemical equilibria | | | | Ref. |
|---|---|---|---|---|
| $H_3PO_4 \rightleftarrows H^+ + H_2PO_4^-$ | $K_1^* = \frac{(H^+)(H_2PO_4^-)}{(H_3PO_4)}$ | $\log K_1^* = -2.126$ | (5.4) | Dartiguelongue (2014) |
| $H_3PO_4 + H_2PO_4^- \rightleftarrows H_5P_2O_8^-$ | $K_2^* = \frac{(H_5P_2O_8^-)}{(H_2PO_4^-)(H_3PO_4)}$ | $\log K_2^* = 0.15$ | (5.5) | |
| $Cd^{2+} + H_2PO_4^- \rightleftarrows CdH_2PO_4^+$ | $\beta_1^* = \frac{[CdH_2PO_4^+]}{[Cd^{2+}][H_2PO_4^-]}$ | $\log \beta_1^* = 0.7 \pm 0.2$ | (5.6) | Powell et al. (2011) |
| $Cd^{2+} + 2H_2PO_4^- \rightleftarrows Cd(H_2PO_4)_2$ | $\beta_2^* = \frac{[Cd(H_2PO_4)_2]}{[Cd^{2+}][H_2PO_4^-]^2}$ | $\log \beta_2^* = 0.9 \pm 0.2$ | (5.7) | |
| $Cd^{2+} + S^{2-} \rightleftarrows CdS(s)$ | $K_s = (Cd^{2+})(S^{2-})$ | | (5.8) | (Ennaassia et al., 2002; Lewis, 2010) |
| $Cd^{2+} + H_2S \rightleftarrows CdS(s) + 2H^+$ | $K_s' = \frac{(H^+)^2}{(Cd^{2+})(H_2S)}$ | | (5.9) | |
| $Cd^{2+} + H_2S \rightleftarrows CdS(s) + 2H^+$ | $K_s' = \frac{K_2 K_1}{K_s}$ | $\log K_s' = 7.2$ | (5.10) | |
| $H_2S_{(g)} \rightleftarrows H_2S$ | $K_{H_2S} = \frac{(H_2S)}{P_{H_2S}}$ | $\log K_{H_2S} = -1.17$ | (5.11) | |
| $Cd^{2+} + HS^- \rightleftarrows Cd(HS)^+$ | $\beta_1 = \frac{[Cd(HS)^+]}{[Cd^{2+}][HS^-]}$ | $\log \beta_1 = 7.6$ at 25 °C | (5.12) | Dalas et al. (1991); Wang and Tessier (1999) |
| $Cd^{2+} + 2HS^- \rightleftarrows Cd(HS)_2^0$ | $\beta_2 = \frac{[Cd(HS)_2^0]}{[Cd^{2+}][HS^-]^2}$ | $\log \beta_2 = 14.6$ at 25 °C | (5.13) | |
| $Cd^{2+} + 3HS^- \rightleftarrows Cd(HS)_3^-$ | $\beta_3 = \frac{[Cd(HS)_3^-]}{[Cd^{2+}][HS^-]^3}$ | $\log \beta_3 = 16.5$ at 25 °C | (5.14) | |
| $Cd^{2+} + 4HS^- \rightleftarrows Cd(HS)_4^{2-}$ | $\beta_4 = \frac{[Cd(HS)_4^{2-}]}{[Cd^{2+}][HS^-]^4}$ | $\log \beta_4 = 18.9$ at 25 °C | (5.15) | |

$K_s$ refers to the solubility product of cadmium sulfide.
$K_1$ and $K_2$ refer to the acidic dissociation constants of $H_2S$.
$K_{H_2S}$ and $P_{H_2S}$ are the Henry's constant and the pressure of $H_2S$, respectively.
$\beta_1$ - $\beta_4$ are the thermodynamic formation constants.

After having listed the main reactions occurring in the cadmium/sulfide/phosphoric acid system (Table 5.3), it is now possible to establish mass balance on the elements. We first formulate the hypothesis that the speciation of phosphoric acid is not modified by the presence of cadmium and sulfur: their concentrations are weak (few ppm, *i.e.,* less than $2.10^{-3}$ M) compared to phosphoric acid species (whose data can be found in Table 5.2). A mass balance on sulfur will establish the following equation (Eq. (5.16)):

$$[\mathrm{Cd(II)}]_0(y-1)[\mathrm{H_2S}] + \frac{[\mathrm{H^+}]^2}{\mathrm{K'_S}}(1 + \beta_1^*[\mathrm{H_2PO_4^{2-}}] + \beta_2^*[\mathrm{H_2PO_4^{2-}}]^2) = [\mathrm{H_2S}]^2\left(1 + \frac{\mathrm{K_1K_2}}{[\mathrm{H^+}]^2} + \frac{\mathrm{K_2}}{[\mathrm{H^+}]} + \frac{{\mathrm{K_2}}^2\beta_2}{\mathrm{K'_S}} + \frac{\mathrm{V_G P_{atm}}}{\mathrm{RTK_{H_2S}}}\right) \quad (5.16)$$

where y is the Sulfur/$Cd^{2+}$ molar ratio, $[\mathrm{Cd^{2+}}]_0$ the initial $Cd^{2+}$ concentration. The resolution to this equation will determine the value of $[\mathrm{H_2S}]$ that will be injected in the equation on cadmium:

$$[\mathrm{Cd(II)}]_{\mathrm{sol}} = \frac{[\mathrm{H^+}]^2}{\mathrm{K'_S}[\mathrm{H_2S}]}\left(1 + \frac{\mathrm{K_2}[\mathrm{H_2S}]}{[\mathrm{H^+}]}\beta_1 + \frac{{\mathrm{K_2}}^2[\mathrm{H_2S}]^2\beta_2}{[\mathrm{H^+}]^2} + \beta_1^*[\mathrm{H_2PO_4^{2-}}] + \beta_2^*[\mathrm{H_2PO_4^{2-}}]^2\right) \quad (5.17)$$

*5.3.1.2.2 Kinetic modeling*

In precipitation processes, supersaturation is the thermodynamic driving force. Indeed, the supersaturation magnitude in the precipitation system controls the particle rate processes including nucleation, crystal growth, aggregation, and breakup.

The supersaturation ratio, S, of CdS can be defined as:

$$\mathrm{S} = \frac{(\mathrm{Cd^{2+}}) \times (\mathrm{H_2S})}{\mathrm{K'_s}} \quad (5.18)$$

and the relative supersaturation $\sigma$ can be written as:

$$\sigma = \mathrm{S}^{1/2} - 1 \quad (5.19)$$

The apparent kinetics of the main processes, *i.e.* nucleation and growth, can be expressed as an apparent reaction rate, $r_{\mathrm{precipitation}}$, that can depend on either S or σ, via a semi-empirical relation (Eq. (5.20)) (Dalas et al., 1991).

$$r_{\mathrm{precipitation}}(\mathrm{t}) = \frac{\mathrm{d[Cd(II)]_{sol}}}{\mathrm{dt}} = \mathrm{k}\sigma^{\mathrm{n}} = \mathrm{k}\left(\mathrm{S}^{1/2} - 1\right)^{\mathrm{n}} \quad (5.20)$$

Neglecting Cd and sulfur complexes, Eq. (16) can be simplified and provide a rough approximation of $H_2S$ content, so that Eq. (5.20) can be rewritten as:

$$r_{\text{precipitation}} = \frac{d[Cd(II)]_{sol}}{dt} = k\sigma^{n} = k\left(S^{1/2} - 1\right)^{n}$$
$$= k\left(\left(\frac{(Cd^{2+}) \times (H_2S)}{K_s'}\right)^{1/2} - 1\right)^{n} \quad (5.21)$$
$$\approx k\left(\left(\frac{[Cd^{2+}] \times ([Cd^{2+}]_0(y-1) \mp [Cd^{2+}])}{K_s'}\right)^{1/2} - 1\right)^{n}$$

where $(Cd^{2+})_0$ and $[Cd^{2+}]_0$ denote the $Cd^{2+}$ initial activity and initial concentration.

Basically, the kinetic model equation (Eq. (5.21)) includes two parameters that are required to be calculated: k and n, which are the apparent rate constant and the reaction order, respectively. They were determined by the parametric identification methodology by finding the optimal value of parameters through minimizing the sum of the squared error (SSE) between the model's predicted $Cd^{2+}$ residual concentration and the measured one.

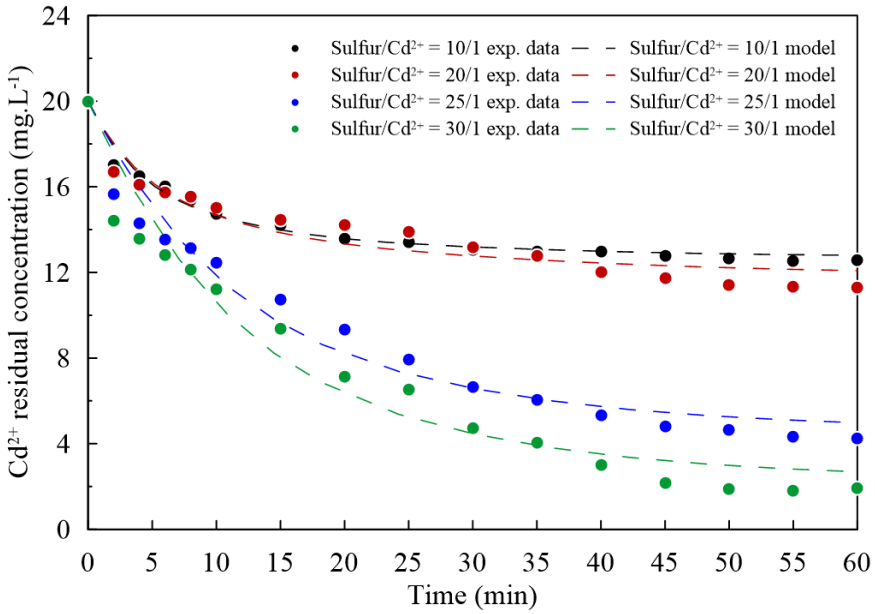


Figure 5.5 Comparison between the experimental and computed $Cd^{2+}$ residual concentration (Sulfur/$Cd^{2+}$ = 10/1 – 30/1, $[H_3PO_4]$ = 25 % $P_2O_5$, and T = 25 °C).

Figure 5.5 presents the evolution of the $Cd^{2+}$ residual concentration in phosphoric acid (25 % $P_2O_5$) measured and calculated by Eq. (5.17) with time for different $Sulfur/Cd^{2+}$ molar ratios, and at a temperature of 25 °C. Through Figure 5.5, it is clear that the experimental and predicted results are in good agreement for the Sulfur/$Cd^{2+}$ = 10/1, and then a slight discrepancy

can be seen between the experimental and calculated $Cd^{2+}$ residual concentration for the Sulfur/$Cd^{2+}$ = 20/1 to 30/1. However, this model is currently unable to predict the amount of cadmium removed from a phosphoric acid medium with a temperature above 25 °C due to the lack of thermodynamic data for this system at different temperatures. This is also indicated in Table 5.4, which gives the apparent rate constant and the reaction order as a function of temperature from 25 °C to 70 °C, where it can be noticed that there is not a clear evolution of these two parameters with temperature.

Table 5.4 Derived pseudo-kinetic parameters values for cadmium removal by sulfide precipitation using parametric identification method.

| T (°C) | Sulfur/$Cd^{2+}$ = 10/1 | | Sulfur/$Cd^{2+}$ = 20/1 | | Sulfur/$Cd^{2+}$ = 25/1 | | Sulfur/$Cd^{2+}$ = 30/1 | |
|---|---|---|---|---|---|---|---|---|
| | k ($L.mol^{-1}.s^{-1}$) | n | k ($L.mol^{-1}.s^{-1}$) | n | k ($L.mol^{-1}.s^{-1}$) | n | k ($L.mol^{-1}.s^{-1}$) | n |
| 20 | $2.338 \times 10^{-6}$ | 1.683 | $2.198 \times 10^{-6}$ | 2.102 | $1.506 \times 10^{-7}$ | 1.533 | $5.747 \times 10^{-8}$ | 1.649 |
| 40 | $1.967 \times 10^{-6}$ | 1.509 | $7.898 \times 10^{-6}$ | 2.258 | - | - | $9.132 \times 10^{-7}$ | 1.740 |
| 60 | $9.314 \times 10^{-7}$ | 1.409 | $3.594 \times 10^{-5}$ | 2.320 | - | - | $8.268 \times 10^{-6}$ | 2.211 |
| 70 | $1.401 \times 10^{-6}$ | 1.319 | $8.772 \times 10^{-6}$ | 1.845 | - | - | $5.437 \times 10^{-6}$ | 1.984 |

### 5.3.2 Continuous operation

After examining the precipitation performance of $Cd^{2+}$ by sodium hydrosulfide in the batch mode, interest was paid to the continuous cadmium sulfide precipitation experiments which closely reflect the industrial applications. For this reason, it is necessary to calculate the required flow rates of the feed solutions to precipitate the cadmium sulfides from the phosphoric acid solutions. To do so, a reaction time of 30 min was determined and it is known that the HRT must be greater than the reaction time; thus, the HRT was set at 40 min and the total flow rate ($Q_T = Q_{H_3PO_4} + Q_{Sulfur}$) was subsequently calculated. Only precipitation by NaHS was investigated.

#### *5.3.2.1 Effect of molar ratio and temperature on cadmium sulfide precipitation*

The influence of Sulfur/$Cd^{2+}$ molar ratio on cadmium elimination was investigated. Figure 5.6a hence illustrates the $Cd^{2+}$ removal efficiency profile as a function of molar ratio $Sulfur/Cd^{2+}$. Considering a hydraulic residence time of 40 min, cadmium removal efficiency increased from 29 % to 83 % when the $Sulfur/Cd^{2+}$ augmented from 10/1 to 30/1, respectively.

Under optimal conditions, *i.e.*, Sulfur/$Cd^{2+}$ = 25/1 and a temperature of 25 °C, more than 79 % of $Cd^{2+}$ in a 25 % $P_2O_5$ phosphoric acid solution could be precipitated by NaHS. Consequently, the influence of temperature on the amount of cadmium removed in the

continuous process was evaluated on the basis of these conditions. Figure 5.6b depicts the evolution of $Cd^{2+}$ removal efficiency with increasing temperature from 25 °C to 70 °C. As it was noted in batch process, the effectiveness of cadmium removal yield by sulfide precipitation showed a downward trend with increasing temperature. According to Figure 5.6b, the $Cd^{2+}$ removal efficiency decreased from 83% to 39% with the increase in temperature from 25 to 70 °C, respectively.

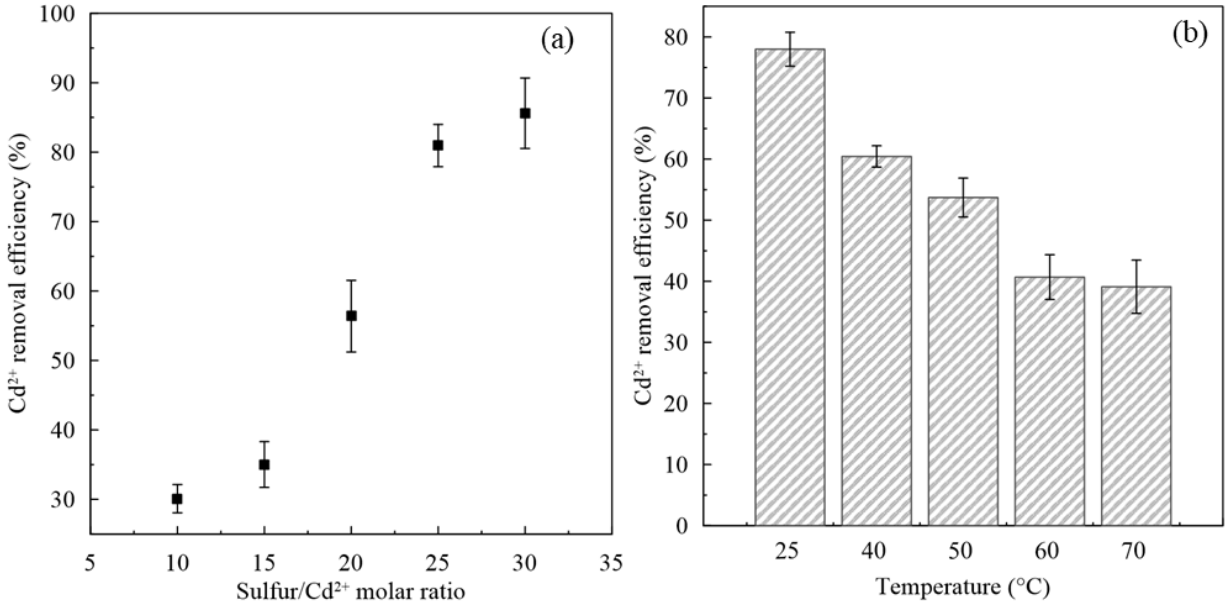


Figure 5.6 Cadmium removal efficiency versus (a) Sulfur/$Cd^{2+}$ molar ratio in continuous mode (HRT = 40 min, and temperature = 25 °C), and (b) temperature in continuous mode (HRT = 40 min, and Sulfur/$Cd^{2+}$ = 25/1).

### *5.3.2.2 Effect of hydraulic residence time on cadmium sulfide precipitation*

Cadmium removal efficiency by sulfide precipitation as a function of flow rate at the optimum temperature and different Sulfur/$Cd^{2+}$ molar ratios from 10/1 to 30/1 is depicted in Figure 5.7a. The results exhibited that the efficient $Cd^{2+}$ removal efficiency was reached with the total volumetric flow rate of 68.76 mL.min$^{-1}$ (HRT = 40 min). As apparent in Figure 5.7a, once the total flow rate increased from 68.76 to 137.52 mL.min$^{-1}$, which means that HRT decreased from 40 to 20 min, the yield of cadmium removed decreased from 33 % to 25 % for Sulfur/$Cd^{2+}$ = 15/1, and from 83 % to 65 % for Sulfur/$Cd^{2+}$ = 30/1, respectively. The drop in $Cd^{2+}$ removal efficiency with increasing flow rate was relatively obvious since the HRT is greater when the flow rate is low. This implied that the untreated phosphoric acid solutions remained longer in the reactor, allowing more time for the precipitation reaction to progress.

Thus, high HRT enhanced the cadmium sulfide precipitation yield by promoting contact and mixing between cadmium and sulfide species.

Besides, it is worthy of note that the results obtained are in line with those of (Ukeles et al. (1994), who found the removal efficiency of $Cu^{2+}$ and $Cd^{2+}$ ions using dithiophosphinate from phosphoric acid solution (27 % $P_2O_5$) increased with the increment of the HRT from 5 to 60 min. In fact, an HRT of 60 min and high temperature were beneficial for accelerating the decomposition of the dithiophosphinate reagent. Additionally, Sampaio et al. (2010) and (2009) conducted investigations on the removal of $Cu^{2+}$, $Ni^{2+}$ and $Zn^{2+}$ ions by continuous sulfide precipitation using $Na_2S$ with a residence time of 30 min. Nevertheless, it is relatively difficult to compare the results considering that the operating conditions, the nature of the aqueous matrix, as well as the sulfide source used are not entirely similar. Also, it should be mentioned that generally, the HRT did not exceed 60 min for some metal impurities such as Cu, Ni, Zn, Cd (Menzel et al., 2021; Reis et al., 2013; Sampaio et al., 2010; Veeken et al., 2003) which may lead to avoiding the dissolution of the formed metal sulfide precipitate after longer reaction times due to the presence of atmospheric $O_2$ (Estay et al., 2021).

#### *5.3.2.3 Effect of initial $Cd^{2+}$ concentration on cadmium sulfide precipitation*

The effect of initial $Cd^{2+}$ concentration on the cadmium removal effectiveness under different Sulfur/$Cd^{2+}$ molar ratio is illustrated in Figure 5.7b. At higher molar ratio, a relatively high removal yield was achieved by raising the initial $Cd^{2+}$ concentration from 20 to 56 $mg.L^{-1}$. Otherwise, for a molar ratio Sulfur/$Cd^{2+}$ = 15/1, the $Cd^{2+}$ removal yield values were 49.51 % and 35.02 % with residual concentrations of 28.57 $mg.L^{-1}$ and 13.05 $mg.L^{-1}$, for a phosphoric acid solution containing 56 and 20 $mg.L^{-1}$, respectively. This can be justified by the fact that increasing the initial $Cd^{2+}$ ions concentration and, of course, the sulfide ions concentration resulted in an enhancement of the formation of CdS following the reaction (Eq. (5.10)), and eventually to an improvement of the $Cd^{2+}$ removal efficiency. Actually, this can be explained by the fact that $Cd^{2+}$ is dominated by its high affinity for sulfur in contrast to oxygen donor ligands to which cadmium has a weak affinity (Powell et al., 2011). Thus, the formation of complexes such as $CdH_2PO_4^+$ (Eq. (5.6)) and $Cd(HPO_4)_2^{2-}$ (Eq. (5.7)) decreased since the concentration ratio $[Cd^{2+}]/[H_2PO_4^-]$ was diminished.

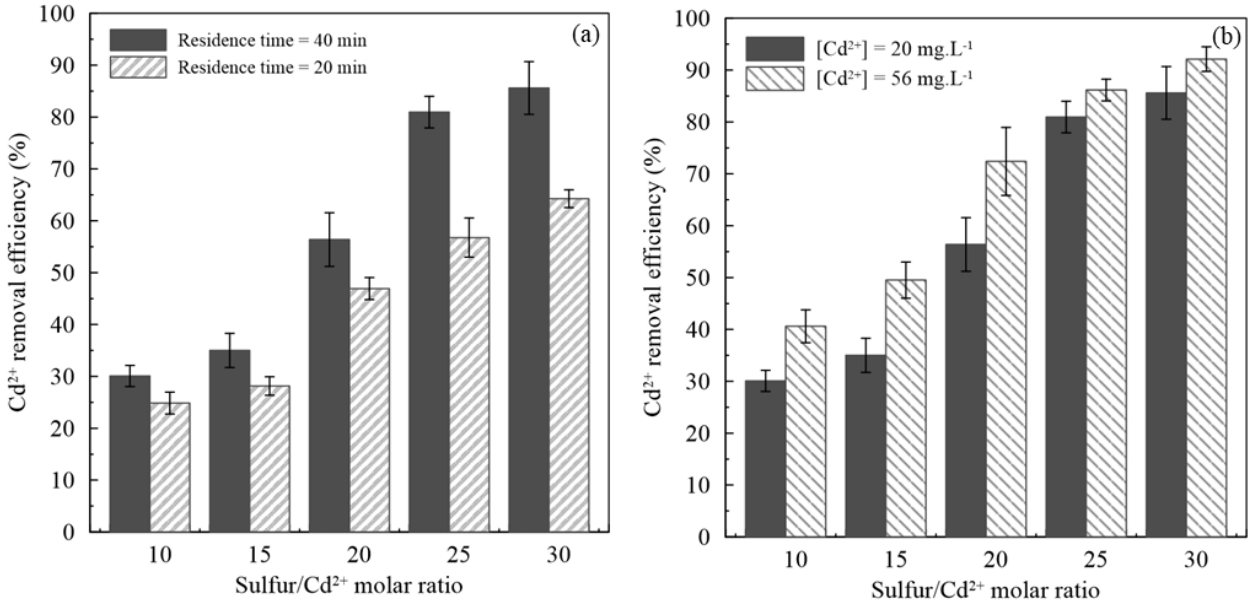


Figure 5.7 (a) Effect of HRT on cadmium sulfide precipitation (Sulfur/$Cd^{2+}$ from 10/1 to 30/1, T = 25 °C, [$H_3PO_4$] = 25 % $P_2O_5$), and (b) Effect of initial $Cd^{2+}$ concentration on cadmium removal yield (HRT = 40 min, and T = 25 °C).

### 5.3.3 Batch vs. Continuous system

As outlined earlier, the hydraulic residence time was well chosen by respecting the reaction time that served to reach a high cadmium ion removal yield in batch system. Actually, when comparing the results obtained in the batch mode with those in the continuous system, it can be noticed that at the same time, similar cadmium removal yields were approximately achieved. For instance, for a Sulfur/$Cd^{2+}$ molar ratio of 30/1, the cadmium removal yield was 90.34 % and 85.61 % in the batch and the continuous system, respectively (Table 5.5). Therefore, this indicated that the behavior of sulfur species and cadmium ions in a phosphoric acid medium was identical in both operation modes, which implied that the kinetic model was still appropriate. Accordingly, the results in batch mode can be extrapolated, which can be of some benefit for the wet phosphoric acid purification by sulfide precipitation, and mainly on the industrial scale.

Table 5.5 Comparison between the cadmium removal efficiency achieved by sulfide precipitation in batch and continuous operation at 25 °C.

| Sulfur/$Cd^{2+}$ | $Cd^{2+}$ removal yield (%) | |
|---|---|---|
| | Batch | Continuous |
| 10/1 | 36.91 ± 0.24 | 30.09 ± 2.04 |
| 15/1 | 40.26 ± 1.18 | 35.01 ± 3.29 |
| 20/1 | 43.50 ± 0.38 | 56.38 ± 5.16 |
| 25/1 | 82.29 ± 3.16 | 80.96 ± 3.05 |
| 30/1 | 90.34 ± 0.23 | 85.61 ± 5.07 |

On the whole, the obtained findings indicate that the removal of $Cd^{2+}$ cadmium ions present in synthetic phosphoric acid solutions by precipitation using sulfide-based precipitants, such as NaHS is achievable. Meanwhile, the few studies (Norwood and Tate, 1992; Zieliński et al., 2019) carried out on phosphoric acid decadmiation by sulfide precipitation have mostly focused on the effects of the operating parameters on the process efficiency, and on the kinetics of cadmium sulfide precipitation, while neglecting the effect of the processing conditions on the generated precipitate. Hence, the following section emphasizes the precipitate formed in the continuous precipitation process by providing morphological, and elemental characterization as well as a particle size analysis.

### 5.3.4 Precipitated particles characterization

The orange precipitate obtained from the precipitation of cadmium ions by NaHS was subjected to further chemical analyses and this section presents the main findings. As previously quoted, in a precipitation system, the supersaturation level is defined by the activity of the species involved and the solubility product $K_s$ of the precipitate. Since metal sulfides are sparingly soluble ($K_s < 10^{-15}$), metal sulfide precipitation process is generally characterized by high levels of supersaturation (Table 5.6), even at reagent concentrations below 0.1 mM (Mokone et al., 2012). Therefore, primary nucleation is the prominent mechanism in charge of particle formation and very small particles are usually formed. Figure 5.8 shows that the availability of excess sulfide has a large effect on the particle size. In Figure 5.8, it is noticed that by increasing the Sulfur/$Cd^{2+}$ molar ratio, the size of CdS solid particles increased, which enables an easier solid separation process to extract CdS from phosphoric acid. The median diameter ($D_{50}$) increased from 28.5 to 260.75 μm, for a Sulfur/$Cd^{2+}$ molar ratio of 10/1 to 30/1, respectively. Nonetheless, Mokone et al. (2010) investigated the effect of metal to sulfide molar ratio on the particle size of the metal sulfides ZnS and CuS, and they found that an excess sulfide led to the reduction of the particle size of copper sulfide, in contrast, it had a relatively

negligible effect on the particle size of ZnS. Actually, this discrepancy in the results may be related to the difference in the effluent pH, which was equal to 6 in the study of Mokone et al. (2010) while 25 % $P_2O_5$ phosphoric acid solution has a pH <1. More interesting, crystal agglomeration might be the primary mechanism controlling the particle size increase of CdS precipitate.

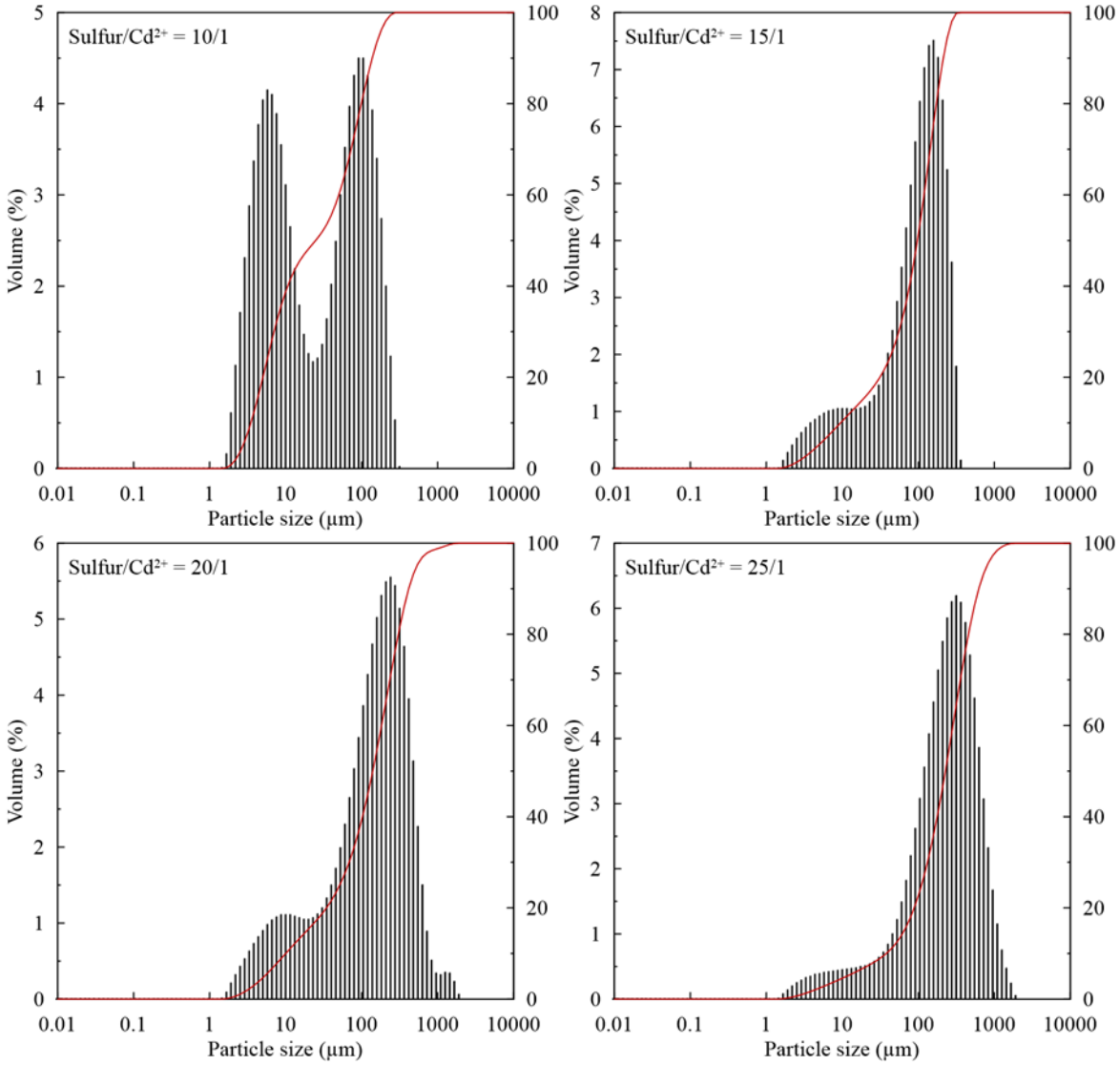


Figure 5.8 Particle size distribution in volume of the obtained CdS precipitate: Sulfur/$Cd^{2+}$ = 10/1 ($D_{50}$ = 28.50 μm), Sulfur/$Cd^{2+}$ = 15/1 ($D_{50}$ = 111.57 μm), Sulfur/$Cd^{2+}$ = 20/1 ($D_{50}$ = 160.74 μm), Sulfur/$Cd^{2+}$ = 25/1 ($D_{50}$ = 260.75 μm).

Table 5.6 Cadmium sulfide solubility product and supersaturation levels used under different sulfur/metal molar flux in continuous mode.

| $Cd^{2+}$ concentration ($mg.L^{-1}$) | $Cd^{2+}$ concentration ($mol.L^{-1}$) | Solubility product | Molar flux Sulfur/$Cd^{2+}$ | Supersaturation ($mol.L^{-1}$) |
|---|---|---|---|---|
| 20 | $1.78 \times 10^{-4}$ | $1 \times 10^{-27}$[a] | 10/1 | $3.56 \times 10^{25}$ |
| | | | 15/1 | $5.34 \times 10^{25}$ |
| | | | 20/1 | $7.12 \times 10^{25}$ |
| | | | 25/1 | $8.90 \times 10^{25}$ |
| | | | 30/1 | $1.07 \times 10^{26}$ |
| 56 | $4.98 \times 10^{-4}$ | | 10/1 | $2.79 \times 10^{26}$ |
| | | | 15/1 | $4.18 \times 10^{26}$ |
| | | | 20/1 | $5.58 \times 10^{26}$ |
| | | | 25/1 | $6.97 \times 10^{26}$ |
| | | | 30/1 | $8.37 \times 10^{26}$ |

[a] data from Haynes (2015).

Furthermore, Kind (2002) ensured that the particles that are currently viewed throughout precipitation process are secondary particles, resulting from the aggregation of primary particles. Additionally, owing to the electrical charge on the surface of the particles, the stability and the primary particles aggregation in aqueous solution are set by the balance between attractive van der Waals forces and electrostatic forces of repulsion. The electrical charge on the surface of the particles can be induced by surface chemical reactions and surface adsorption, and in particular, metal sulfides are known for their adsorption of sulfur species $H_2S$, $HS^-$ and $S^{2-}$ (Bryson and Bijsterveld, 1991; Kolthoff and Moltzau, 1935). As such, particles generated in the presence of excess sulfide are of greater susceptibility to bearing a significant surface charge and thus to stabilize in suspension by virtue of electrical repulsion forces. However, the ability of metal sulfides to adsorb sulfide ions present in solution is linked to the operating pH. Obviously, by decreasing the operating pH of the precipitation system, the relative content of $H_2S_{(aq)}$ increases and that of available $HS^-$ and $S^{2-}$ decreases. In other words, the amount of $HS^-$ and $S^{2-}$ ions that are going to adsorb on the particles surface will be reduced. It remains possible for $H_2S_{(aq)}$ ions to adsorb, their neutral charge does not alter the surface charge of the particles. As a result, the aggregation of the initially formed primary particles becomes more conducive, which leads to the increase in particle size of cadmium sulfide. Thereafter, the settling characteristics of the formed precipitates were further enhanced. SEM images exhibit that the aggregation mechanism became significantly more apparent while increasing the Sulfur/$Cd^{2+}$ molar ratio (Figure 5.9). For instance, taking the case of the molar ratio Sulfur/$Cd^{2+}$ = 30/1, when zooming in on a single entity, it was noticed that it is an aggregate formed of a plurality of nanoparticles. Thus, the speciation of aqueous sulfides as a function of pH is shown

to be the most critical factor that significantly affects the cadmium ion removal efficiency, the solid particle formation mechanisms, as well as the solid-liquid separation characteristics of the precipitate. Identical findings were reported by Gim-Krumm et al. (2019) and Mokone et al. (2010) who found that a high number of CuS particles with small average size, strongly negative surface charge, and poor sedimentation characteristics were resulted when the CuS precipitation process was performed in the presence of excess sulfide at pH 6. Conversely, when the process was carried out at an operational pH of 2, with excess sulfide present in the solution, the zeta potential became less negative and the deletion of aggregation was diminished, the particle size was enlarged more 20-fold, and the settling characteristics of the formed precipitates improved.

Besides the particle zeta potentials, authors (Estay et al., 2021; Gim-Krumm et al., 2019; Xia et al., 2021) revealed that the hydrophilicity/hydrophobicity of metal sulfides affect the interactions between these particles and subsequently the aggregation performance in wastewater. Actually, it was found that the aggregation of hydrophobic copper sulfide precipitates was mainly reliant on hydrophobic interactions, which were largely affected by mechanical forces induced by stirring and pumping. While the aggregation of hydrophilic zinc sulfide precipitates was shown to be primarily impacted by the zeta potentials of the precipitate, which in turn were controlled by the solution pH and sulfide reagent dosage as also discussed above for the case of cadmium sulfide precipitation in phosphoric acid solutions (Gim-Krumm et al., 2019). Recently, Xia et al. (2021) reported that the particle size of CdS in acidic wastewater was higher and it increased by augmenting the $H_2SO_4$ concentration. Also, they indicated that CdS were hydrophilic particles that preferably bind to $H_2O$ molecules to provide stable dispersions in aqueous media. Furthermore, they found that by decreasing the pH solution, the hydrophilicity of CdS was reduced and the zeta potential was less negative. Nevertheless, the formation of cadmium sulfide under different operating conditions can lead to different hydrophilic/hydrophobic properties, which will subsequently alter the particle aggregation performance. Thus, it will further be of considerable interest to analyze the aggregation performance of CdS particles in a phosphoric acid medium (25 % $P_2O_5$) by studying the effect of the Sulfur/$Cd^{2+}$ molar ratio on the zeta potential as well as the hydrophobic and hydrophilic properties. This will eventually contribute to improving the solid-liquid separation efficiency.

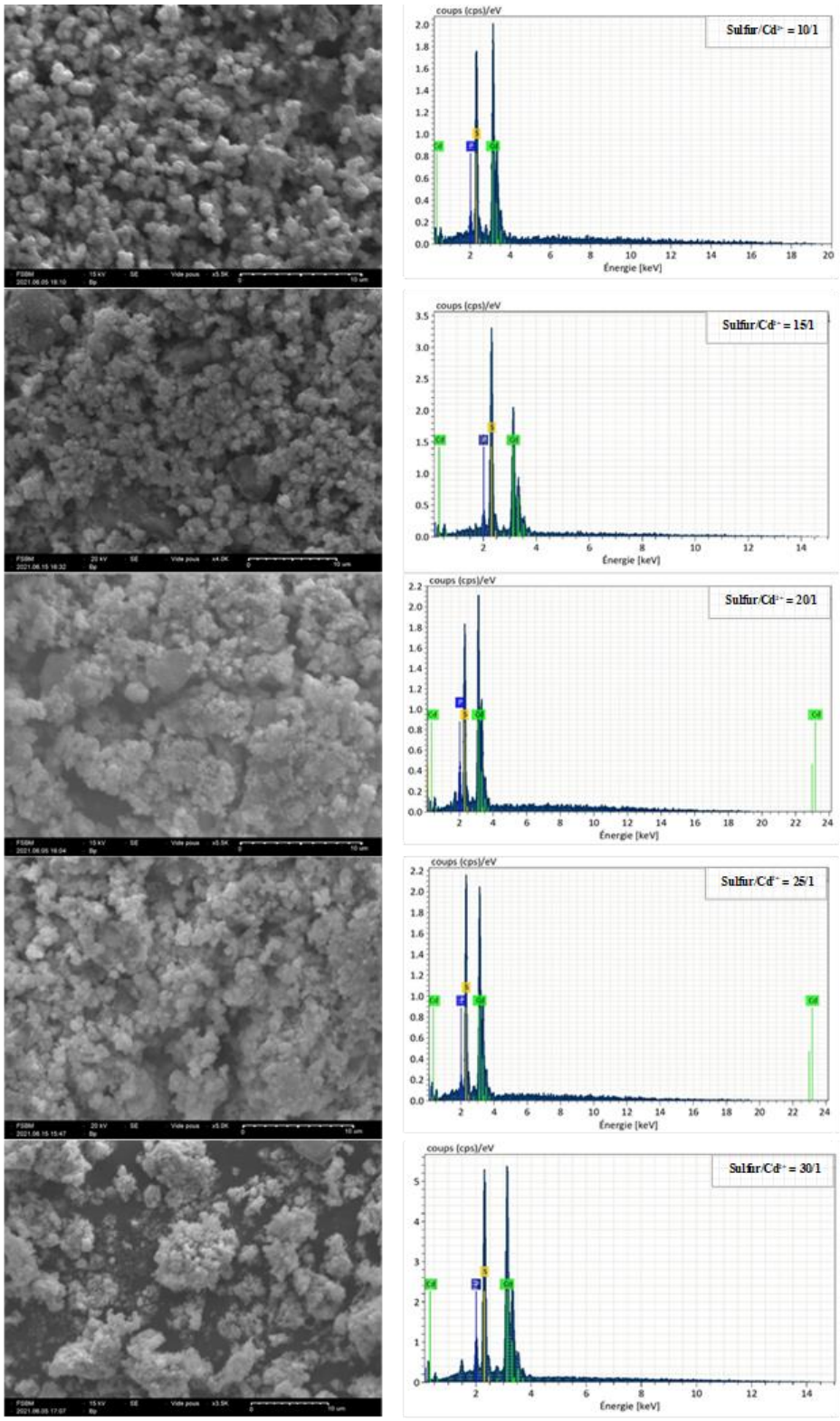


Figure 5.9 SEM and EDS analysis performed on cadmium sulfide produced in the precipitation process at different Sulfur/$Cd^{2+}$ = 10/1 – 30/1.

The XRD diffractograms in Figure 5.10 reveal firstly that the orange precipitate was mainly composed of cadmium sulfide (CdS). The diffractions at around d = 3.5915 Å implied a hexagonal CdS crystal structure. These findings are in accordance with those provided by the study of Milligan (2002), wherein it was reported that hexagonal CdS was formed in the presence of sulfur vapor. Besides, Milligan (2002) found that yellow-colored CdS is generally obtained by precipitation of $Cd^{2+}$ ions from alkaline or cold solutions, while orange or red-colored CdS from acidic or hot solutions. Secondly, the precipitates exhibited high crystallinity, except for the solid resulting from the $Sulfur/Cd^{2+}$ molar ratio of 30/1. Overall, the peak intensity decreased with increasing $Sulfur/Cd^{2+}$ molar ratio starting from 10/1 to 30/1. The EDS maps (Figure 5.9) and the results summarized in Table 5.7 indicate that the precipitate formed from the precipitation of cadmium sulfide from a phosphoric acid solution with a concentration of 25 % $P_2O_5$ consist of a large quantity of Cd, S and a minor amount of P, which agrees with the XRD results.

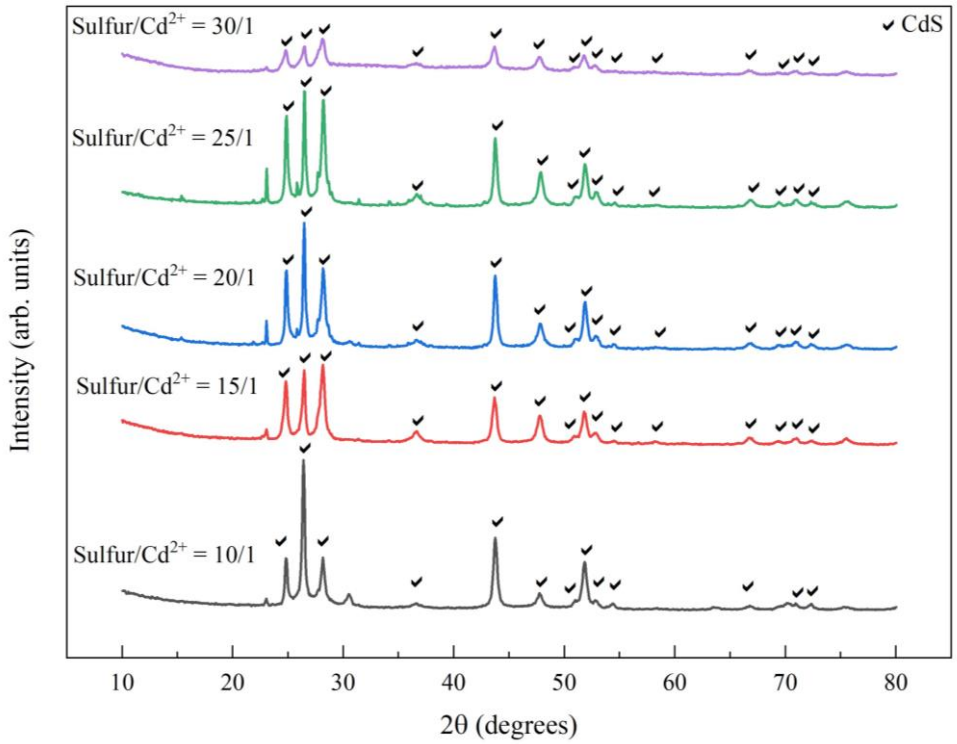


Figure 5.10 XRD patterns of CdS precipitate for different $Sulfur/Cd^{2+}$ molar ratio.

Ultimately, it can be said that sulfide precipitation performance and the properties of the formed solid phase are extremely dependent on several parameters which are mainly supersaturation, concentration of reactive sulfide species, pH, and temperature (Figure 5.11).

Table 5.7 EDS results of the produced CdS precipitate.

| Precipitate | Sulfur/$Cd^{2+}$ molar ratio | Element | Mass (weight %) | Mass (atomic %) |
|---|---|---|---|---|
| Cadmium sulfide (CdS) | 10/1 | Cd | 47.79 | 48.34 |
| | | S | 13.10 | 46.45 |
| | | P | 1.42 | 5.22 |
| | 15/1 | Cd | 51.77 | 38.09 |
| | | S | 21.92 | 56.54 |
| | | P | 2.01 | 5.37 |
| | 20/1 | Cd | 55.53 | 44.70 |
| | | S | 15.85 | 44.71 |
| | | P | 3.63 | 10.59 |
| | 25/1 | Cd | 61.13 | 43.52 |
| | | S | 20.93 | 52.22 |
| | | P | 1.65 | 4.26 |
| | 30/1 | Cd | 63.63 | 46.05 |
| | | S | 18.10 | 45.91 |
| | | P | 3.06 | 8.04 |

## 5.4 Conclusions

In this investigation, the removal of cadmium ion from phosphoric acid solutions by sulfide precipitation in mechanically stirred tank in both batch and continuous modes using sodium hydrosulfide (NaHS) was evaluated. The achieved results revealed that operating parameters such as sulfide to cadmium molar ratio, temperature, phosphoric acid concentration, as well as hydraulic residence time strongly influenced the cadmium removal efficiency. The main findings of this work are as follows:

(1) The performance of cadmium sulfide precipitation from synthetic dilute phosphoric acid solution (25 % $P_2O_5$) achieved by NaHS was superior to that obtained by $Na_2S$ because of the ionic strength. In addition, the purification of synthetic dilute phosphoric acid using NaHS as a precipitating agent is more cost-effective because its price is considerably lower than that of $Na_2S$, so that it is more attractive at industrial scale.

(2) In the continuous process, a residence time of 40 min was sufficient to achieve similar cadmium removal yields as in the batch process. Meanwhile, an increase in the initial $Cd^{2+}$

concentration led to an improvement of the cadmium removal effectiveness as the sulfide content augmented.

(3) An increase in either temperature or phosphoric acid concentration had an adverse impact on the sulfide precipitation efficiency both in the batch and continuous processes, which is due to the lower solubility of $H_2S$ and the decrease in sulfide content.

(4) The residual $Cd^{2+}$ concentrations calculated by the proposed kinetic model for cadmium sulfide precipitation were in agreement with those measured, but only at a temperature of 25 °C because of the lack of thermodynamic data on this system as a function of temperature.

(5) An increase in supersaturation level resulting from a higher sulfide concentration had a significant effect on the particle size distribution. Actually, the mean particle size of CdS increased by rising the sulfide to metal molar ratio, enabling an easier solid-liquid downstream separation process. Therefore, crystal agglomeration was the prevailing mechanism governing the particle size of CdS precipitate which was hexagonal CdS with high purity.

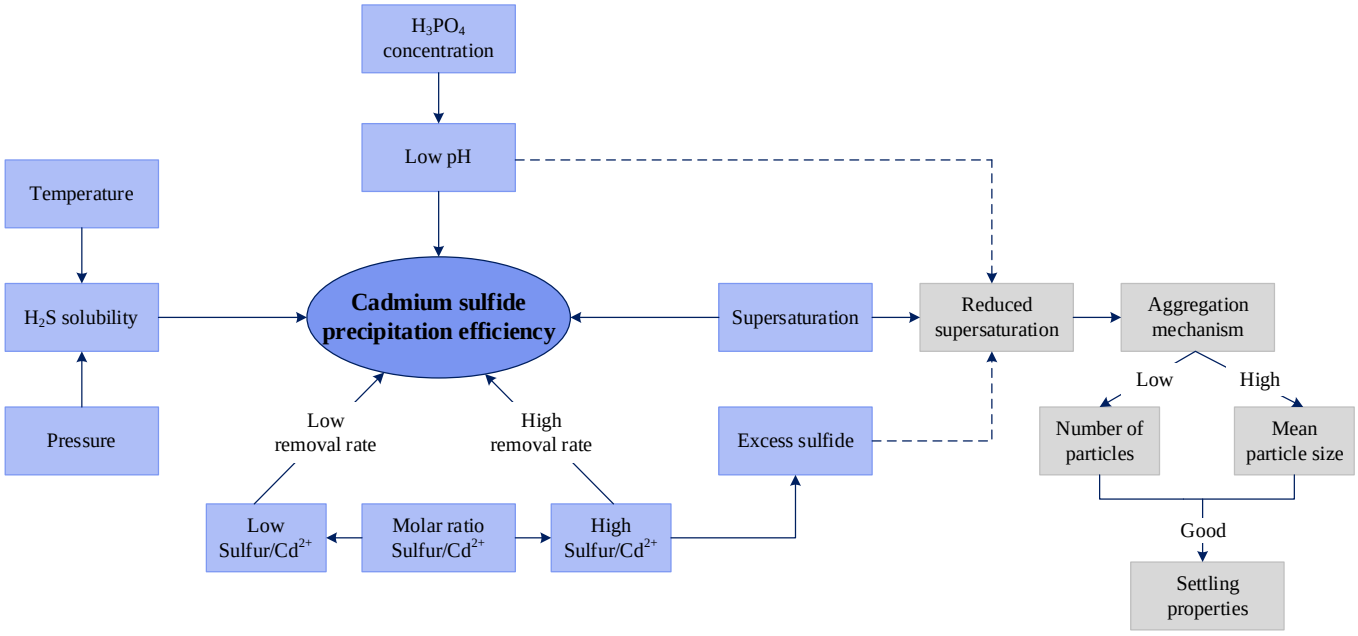


Figure 5.11 Parameters influencing cadmium sulfide precipitation in phosphoric acid solutions.

# Chapter 6: Purification of industrial wet phosphoric acid solution by sulfide precipitation in batch and continuous modes: performance analysis, kinetic modeling, and precipitate characterization


## Abstract

The purification of wet-process phosphoric acid has always been a challenge for both academic and industrial researchers. A treatment unit was developed to mitigate metallic impurities, such as cadmium, from industrial dilute wet phosphoric acid solution (25 % $P_2O_5$) by NaHS precipitation in batch and continuous modes. The effects of operating parameters on the purification performance were evaluated: namely Sulfur/$Cd^{2+}$ molar ratio, the presence of other metallic ions besides $Cd^{2+}$, temperature, and hydraulic residence time. In the batch mode, equilibrium was attained in less than 20 min; augmenting Sulfur/$Cd^{2+}$ molar ratio increased the CdS precipitation effectiveness up to 86 %, but temperature increment had an adverse effect. In the continuous mode, a hydraulic residence time of 40 min was necessary to reach the same yield as in the batch mode at 25 °C. Sulfidation was found to eliminate simultaneously other metallic impurities (especially Cu and As) originally present in the wet-produced phosphoric acid. Finally, NaHS precipitation was able to reduce the concentration of cadmium from 65.95 mg Cd/kg $P_2O_5$ to 11.15 mg Cd/kg $P_2O_5$ from untreated WPA solution (25 % $P_2O_5$) at 25 °C, which outperforms most of the published data based on alternative treatment processes.



**Keywords:** Industrial wet phosphoric acid; Metallic ions; Sulfide precipitation; Batch and continuous operations; Kinetic modeling; Precipitate characterization.

## 6.1 Introduction

Phosphoric acid is a vital staple chemical raw material, which is abundantly solicited in many industrial sectors such as phosphate fertilizers, detergents, food additives, electronics, medicine, and beverages, etc. (Schorr and Valdez, 2017; Zhuang et al., 2020). In particular, the phosphate fertilizer industry consumes a large share of the industrial phosphoric acid produced on a global scale. In turn, phosphate fertilizers play a pivotal role in the food security system, and they cannot be substituted. As the world's demography continues to climb, so does the demand for food, which is reflected in an expanding global need for phosphate fertilizers (Elzoghby, 2021). According to the United Nations, world food production is foreseen to increase up to 70 % by 2050, leading to an increment in the world population of over 9 billion people, and thereby an increase in the global market demand for phosphate fertilizers, and obviously for industrial phosphoric acid as well (Daneshgar et al., 2018; Kernebeek et al., 2018). As of today, phosphoric acid is manufactured in two main ways, namely thermal and wet processes (Gilmour, 2013). The first one, the thermal route, has the merit of reducing the amount of metallic impurities, but this technique is very expensive due to its high energy consumption (Becker, 1989). Alternatively, the wet route is the most commonly used on an industrial scale owing to its affordability and it is also more eco-friendly than the earlier process. Nevertheless, its main inconvenience lies in the occurrence of relatively high concentrations of organic (*i.e.*, humic acid) (Zhou et al., 2022), and inorganic impurities (*i.e.*, sulfate, uranium, arsenic, cadmium, copper, etc.) (Roberts, 2014). Table 6.1 provides the complex chemical composition of wet phosphoric acid (WPA) obtained from different phosphate rocks in several regions.

Indeed, the specifications and regulations regarding the quality of industrial phosphoric acid, to reduce heavy metals content and precisely cadmium, are increasingly numerous and stringent when the intended application is in fertilizers, food, pharmaceuticals, and electronics (Taha et al., 2020; Ulrich, 2019), with the ultimate goal of improving the quality of human life and preserving the natural environment. This challenge has been the focus of several lines of research to develop technologies for the purification of wet-process industrial phosphoric acid. In this regard, solvent extraction, chemical precipitation, co-crystallization, adsorption using activated carbon or biosorbents, ion exchange, and membrane processes have been investigated to eliminate inorganic impurities including cadmium (Qamouche et al., 2021; Xu et al., 2022).

Among the techniques mentioned above, membrane processes and ion exchange are not implemented at an industrial scale; they could offer an emerging solution if intensive

investigations are carried out in this trend, so as to find new materials and develop rigorous membranes with high selectivity to metal impurities enclosed cadmium, and which are able to withstand in a highly acidic medium. For solvent extraction process, although it is industrially deployed on a large scale, it presents several weaknesses, such as secondary pollution, solvent exorbitant-cost, and it requires pre- and post-treatment for an effective cadmium extraction; in addition, large amounts of solvent are used which could have a severe impact on the environment (Taha et al., 2020). Sulfide precipitation seems to be more suitable, as it can be effectually incorporated into existing installations at a competitive cost. It shows various benefits like high selectivity for metal removal and can be successfully integrated into existing facilities at a low cost. It exhibits a number of positive aspects, including the potential for selective metal removal, poor solubility of metal sulfide precipitates, rapid reaction rates, and the possibility for valorizing of metal sulfide precipitates, which may present an opening for the recovery of valued and strategic metals (Gharabaghi et al., 2012; Lewis, 2017; Mokone et al., 2010); furthermore, the sulfides in excess can be effectively removed as volatile hydrogen sulfide. A few research reports were performed on cadmium removal from industrial WPA by sulfide precipitation process using mineral sulfides. Indeed, Zieliński et al. (2019) reported that $Na_2S$ can be considered as an effective precipitating agent for eliminating cadmium from WPA solution (25 % $P_2O_5$), compared to other precipitant, such as (ZnEPDTC), (NaEPDTC), and (SCX) that were not able to react with cadmium. Norwood and Tate (1992) compared the performance of organic (5 % $Na_2CS_3$, Thio-Red II, and TMT-15) and inorganic ($Na_2S$, $Na_2S_n$) sulfide precipitants to remove mercury, copper, lead, chromium, cadmium, manganese, and zinc from 30 % $P_2O_5$WPA solution. According to the removal yield obtained, it was found that 5 % $Na_2CS_3$ was able to remove in the following order copper> mercury> lead> chromium> cadmium> manganese> zinc. Conversely, Thio-Red II did not significantly react with cadmium (<8%), manganese (<2 %), chromium (<1 %), and zinc (<1 %). Also, the use of TMT-15 did not lead to a separation of the heavy metals since the addition of this reagent to phosphoric acid resulted in the precipitation of trithiocyanuric acid. Other patent applications, such as (Berglund, 1981; Plessen et al., 1983), suggested a neutralization before the addition of a sulfide solution, with sodium hydroxide and/or ammonia. However, the above-proposed option could induce an important dilution or a medium change by the introduction of additional components due to potassium hydroxide or sodium hydroxide uses, which in turn can alter the phosphates fertilizers production. Thus, the patent application WO 2017/023153 A2 (Samrane and Khouloud, 2017) proposed an approach to remove cadmium by precipitation using NaHS during the manufacture of ammonium phosphate fertilizers.

Table 6.1 Chemical composition of WPA from various regions.

| | WPA (Morocco) (Khaless, 2006) | Crude WPA (Abu Zaabal, Egypt) (Taha et al., 2020) | WPA (Florida, United States) (Beltrami et al., 2014) | WPA (Homs, Syria) (Beltrami et al., 2014) | Filter WPA (Abu Tartur, Egypt) (Abdel-Ghafar et al., 2019) | WPA (Taiwan) (Beltrami et al., 2014) | WPA (Iran) (Beltrami et al., 2014) | WPA (Jorf Lasfar, El Jadida, Morocco) (Hakkar et al., 2021) | Merchant-grade PA (Morocco) (Qamouche et al., 2021) |
|---|---|---|---|---|---|---|---|---|---|
| (wt. %) | | | | | | | | | |
| $P_2O_5$ | 23 | 23.2 | 30 | 28 | 25.92 | 30 | 29 | 26.16 | 30 |
| $H_3PO_4$ | 31.76 | 32.04 | 41.43 | 38.67 | 35.80 | 41.43 | 40.05 | 36.13 | 41.43 |
| $Fe_2O_3$ | 0.12 | - | - | - | 2.77 | - | - | 0.47 | 0.27 |
| CaO | 0.17 | n.d. | - | - | 0.07 | - | - | 0.48 | 0.31 |
| $Al_2O_3$ | 0.07 | n.d. | - | - | 0.35 | - | - | 0.21 | 0.06 |
| MgO | 0.63 | n.d. | n.d. | - | 0.75 | - | n.d. | 0.72 | 0.54 |
| F | 0.82 | - | - | 1.8 | n.d. | - | - | 1.07 | n.d. |
| $SO_3$ | 2.66 | n.d. | n.d. | n.d. | n.d. | n.d. | n.d. | n.d. | n.d. |
| $Na_2O$ | 0.08 | n.d. | n.d. | n.d. | n.d. | n.d. | n.d. | n.d. | n.d. |
| $K_2O$ | 0.03 | n.d. | n.d. | n.d. | n.d. | n.d. | n.d. | n.d. | 0.38 |
| $SiO_2$ | 0.35 | n.d. | - | n.d. | n.d. | - | n.d. | 0.4 | n.d. |
| Cl | - | n.d. | n.d. | 0.125 | n.d. | - | n.d. | n.d. | n.d. |
| $SO_4$ | n.d. | n.d. | - | 2 | n.d. | - | - | n.d. | n.d. |
| (ppm) | | | | | | | | | |
| $SO_4$ | n.d. | n.d. | 14,996 | - | n.d. | 4,262 | 23,885 | n.d. | n.d. |
| Fe | - | 7,956 | 7,103 | 1,044 | - | 963 | 5,255 | - | - |
| F | - | 7,203 | 1,342 | - | n.d. | 18,627 | 1,035 | - | n.d. |
| Ca | - | n.d. | 631 | 683 | - | 3,599 | 1,194 | - | - |
| Mg | - | n.d. | n.d. | 4,016 | - | 979 | n.d. | - | - |
| Al | - | n.d. | 1,894 | 610 | - | 600 | 796 | - | - |
| Cl | 413 | n.d. | n.d. | - | n.d. | 324 | n.d. | n.d. | n.d. |
| Si | - | n.d. | <79 | n.d. | n.d. | 4,459 | n.d. | - | n.d. |
| Co | n.d. | n.d. | n.d. | n.d. | 6 | n.d. | n.d. | n.d. | n.d. |
| Mn | 7 | 482 | n.d. | n.d. | 220 | n.d. | n.d. | n.d. | n.d. |
| Cr | 219 | 101 | n.d. | n.d. | 40 | n.d. | n.d. | n.d. | 117 |
| Zn | 333 | 227 | n.d. | n.d. | 160 | n.d. | n.d. | n.d. | 118 |
| Cu | 14 | n.d. | n.d. | n.d. | 24 | n.d. | n.d. | n.d. | 14 |
| Cd | 11 | 14 | n.d. | n.d. | n.d. | n.d. | n.d. | n.d. | 6 |
| Pb | n.d. | 46 | n.d. | n.d. | n.d. | n.d. | n.d. | n.d. | n.d. |
| As | 4 | n.d. | n.d. | n.d. | n.d. | n.d. | n.d. | n.d. | 7 |
| Ba | n.d. | n.d. | n.d. | n.d. | 6 | n.d. | n.d. | n.d. | n.d. |
| Ni | n.d. | n.d. | n.d. | n.d. | 40 | n.d. | n.d. | n.d. | 16 |
| V | 142 | n.d. | 158 | n.d. | 47 | 51 | n.d. | n.d. | 80 |
| U | n.d. | n.d. | 130 | 48 | n.d. | 53 | 66 | n.d. | 87 |

(n.d.: not determined)

In light of the above, only one study was conducted on cadmium sulfide precipitation in industrial WPA solutions, intended for phosphate fertilizer production, using NaHS. The present paper provides an extensive study on evaluating the performance of sulfide precipitation as a purification technique for WPA, which is a well-known complex medium. To this end, this

investigation focused on the sulfide precipitation of metallic impurities, such as cadmium from industrial solutions of WPA in a mechanically stirred reactor functioning in the batch and the continuous modes. With this aim in mind, this study examined in detail the effects of operational parameters, such as Sulfur/$Cd^{2+}$ molar ratio, temperature, the presence of other metallic impurities, and hydraulic residence time on cadmium removal efficiency using sodium hydrosulfide (NaHS) as the sulfide source. Additionally, a kinetic model for removing cadmium from industrial WPA solutions was developed by considering the effects of Sulfur/$Cd^{2+}$ molar ratio and temperature variation on the main precipitation mechanisms. Moreover, to assess the sulfide precipitation among the other purification techniques, a comparison with the literature was carried out, focusing on operating conditions close to those of this work. Eventually, the characterization of the resulting precipitate was carefully conducted with the help of semi-quantitative chemical and morphological analyses to propose a mechanism of cadmium removal using NaHS.

## 6.2 Materials and methods

The present section is intended to describe the reagents used, including the chemical composition of the industrial phosphoric acid (25 % $P_2O_5$) involved the experimental set-up and the procedure followed, as well as the analytical methods adopted to successfully carry out this investigation aiming at removing the metallic impurities and particularly cadmium from the WPA solutions.

### 6.2.1 Reagents

Sodium hydrosulfide (NaHS, 70 % purity) and the untreated industrial wet phosphoric (WPA) acid used in this research study were provided by Jorf Lasfar El-Jadida industrial complex (OCP group S.A, Morocco). Indeed, the WPA involved was manufactured by processing Khouribga phosphate rocks. The industrial WPA chemical composition is reported in Table 6.2. All reagents were utilized without further purification. The sulfide solutions were prepared to the desired concentrations using osmotic water before every precipitation assay. It should be underlined that the WPA of this study was collected only after $H_2SO_4$ attack and filtration, and before undergoing any other treatment.

Table 6.2 Specifications of the WPA (25 % $P_2O_5$, d = 1.213 g.mL$^{-1}$) used in this study.

| Constituent | Concentration (wt%) | Constituent | Concentration (mg.L$^{-1}$) | Concentration (ppm) |
|---|---|---|---|---|
| $P_2O_5$ | 25 | Cr | 98.28 | 81.02 |
| $SiO_2$ (T) | 0.139 | As | 6.74 | 5.56 |
| Al | 0.106 | Cd | 20.00 | 16.49 |
| Fe | 0.111 | Mn | 14.04 | 11.58 |
| K | 0.065 | Co | 1.12 | 0.93 |
| F | 0.185 | Ni | 25.27 | 20.83 |
| | | Cu | 29.20 | 24.07 |
| | | Ba | 0.56 | 0.46 |
| | | V | 129.16 | 106.48 |

### 6.2.2 Experimental setup

The experimental tests on the removal of cadmium ions from dilute industrial wet phosphoric acid (25 % $P_2O_5$) were carried out in a mechanically stirred tank operating in batch and continuous flow systems. A detailed description of the experimental setup and its schematic diagram are available in section 5.2 of chapter 5.

### 6.2.3 Experimental procedure

#### *6.2.3.1 Batch experiments*

Regarding the batch experiments, the work consisted first in investigating the effect of the Sulfur/$Cd^{2+}$ molar ratio, ranging from 25/1 to 70/1 on the precipitation efficiency, keeping a constant temperature at 25 °C. Indeed, this molar ratio range was defined from preliminary experiments, which highlighted a good $Cd^{2+}$ removal efficiency from synthetic PA solution using 25/1 molar ratio.

The second part focused on the study of the effect of temperature (from 25 °C to 70 °C), and that of the Sulfur/$Cd^{2+}$ molar ratio (from 25/1 to 70/1) on the kinetics of cadmium separation from WPA (25 % $P_2O_5$) by sulfide precipitation process. An additional consideration is that the initial $Cd^{2+}$ concentration after dilution and reaction time were set at 20 mg.L$^{-1}$ and 60 min, respectively, in all experiments.

The reactor was first fed with 1.5 L of industrial WPA solution containing 26.67 mg.L$^{-1}$ of cadmium ion, and 0.5 L of concentrated sulfide solution (with a concentration ranging from 0.713 to 1.996 g.L$^{-1}$) was then fully added to the medium via an inlet located on top of the reactor. It should be noted that concentrated solutions of $Cd^{2+}$ and sulfide were prepared considering the dilution that occurred during the mixing of the solutions. The liquid volume in

use for the batch experiments was 2 L. A freshly prepared sulfide solution was employed for conducting the precipitation tests. During the experiments, the solution was mechanically agitated with the aid of a vertical stirrer at 300 rpm. The temperature was maintained constant through a thermoregulator with an accuracy of ± 1 °C. Batch experiments were run in duplicate.

#### *6.2.3.2 Continuous experiments*

In continuous mode, the reactor volume used was 2.75 L. To simulate the operational process in the industry, the reactor was first filled with dilute industrial WPA solution (25 % $P_2O_5$) having a volume of 2 L. Then, the sulfide solution with a volume of 0.75 L was added and the pumps were simultaneously started up, which in turn provided the reactor with feed solutions. The influences of Sulfur/$Cd^{2+}$ molar ratio varying from 25/1 to 70/1, and temperature in a range of 25 °C to 70 °C were examined while keeping the flow rate of each reagent constant and equal to 34.38 mL.min$^{-1}$, and the total flow rate was 68.75 mL.min$^{-1}$ for an HRT equal to 40 min. Similarly, the effect of flow rate on the precipitation process was investigated by varying the flow rate of each pump from 34.38 mL.min$^{-1}$ to 137.50 mL.min$^{-1}$, under the following experimental conditions: T = 25 °C, Sulfur/$Cd^{2+}$ = 40/1 and 60/1), and the initial $Cd^{2+}$ concentration was invariably 20 mg.L$^{-1}$. Continuous experiments were performed in duplicate.

### 6.2.4 Sample collection and analytical methods

In the batch mode, 15 mL samples of phosphoric acid solution were collected at 1 min intervals during the first 10 min and at 5 min intervals between 10 min and 60 min, whereas in the continuous system, samples were collected in the steady-state regime. Then, each sample was directly filtered and analyzed, to determine the residual concentration of cadmium in the phosphoric acid solutions.

The initial ($C_{ini}$) and residual ($C_{resid}$) contents of $Cd^{2+}$ were determined by calibrated atomic absorption spectrophotometer (PinAAcle 900Z, Perkin Elmer, USA). The removal efficiency $Cd^{2+}$ from WPA solution was calculated using the equation (Eq. (5.1)).

After each experiment on the effect of Sulfur/$Cd^{2+}$ molar ratio in the batch mode was completed, the solution in the reactor was filtered and the resulting precipitates were collected, rinsed with deionized water, and dried for further analysis. The elemental composition of the formed precipitate for the different Sulfur/$Cd^{2+}$ molar ratios was determined by X-ray fluorescence (XRF) spectrometry (Epsilon 4, Malvern Panalytical, UK).

Morphological analysis for the precipitate was additionally performed by HiROX SH 4000M Scanning Electron Microscope (SEM) equipped with Bruker SCU Energy Dispersive X-ray Spectrometer (EDS) to provide a qualitative elemental analysis of the precipitate. The scans were run at an accelerating voltage of 10 kV in high vacuum mode. The powder samples were fixed on a ribbon with carbon. This operation was carried out using a vacuum system, with a deposition time of about 60 s to form a thin film. The sample surface was scanned on arbitrarily chosen areas at 60×, 200×, 400×, 500×, 900×, and 1500× magnification ratios.

## 6.3 Results and discussion

This section is devoted to reporting and discussing the obtained finding in order to elucidate the mechanisms involved in the removal of metallic contaminants, such as cadmium by NaHS from untreated WPA with a concentration of 25 % $P_2O_5$.

### 6.3.1 Batch sulfide precipitation process

#### *6.3.1.1 Effect of molar ratio, other metallic impurities presence, and temperature*

Figure 6.1 illustrates the evolution of $Cd^{2+}$ removal efficiency with the Sulfur/$Cd^{2+}$ molar ratio variation. This shows that the increment of Sulfur/$Cd^{2+}$ molar ratio from 25/1 to 70/1 generated an increase in the elimination of cadmium ions present in diluted WPA (25 % $P_2O_5$) solution from 21.48 % to 86.31 %, respectively. Sulfide concentration is significantly affected by low pH value ($H_2S$ is the major element at low pH) and an excess is necessary to promote Cd precipitation. Besides, the occurrence of sulfates in phosphoric acid (resulting from the attack of phosphates with sulfuric acid) negatively impacted the performance of WPA purification by sulfides since it caused a decrease in the $H_2S$ solubility in phosphoric acid, which subsequently led to a decrease in the efficiency of decadmiation (Gilmour, 2013).

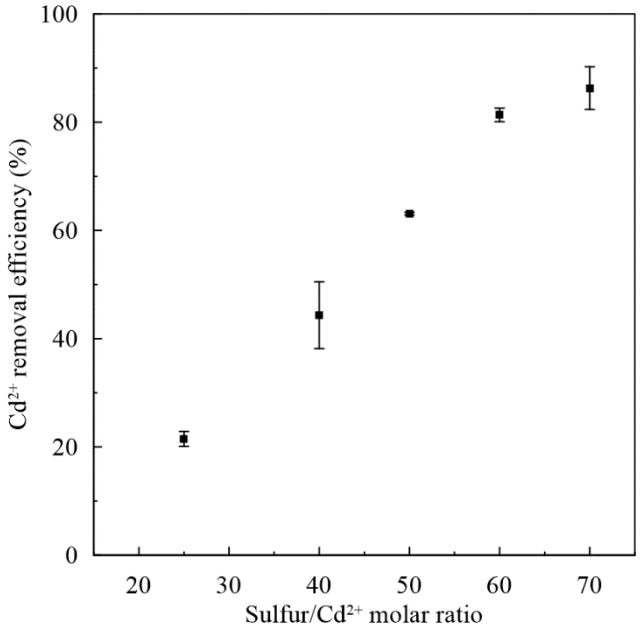


Figure 6.1 Effect of Sulfur/$Cd^{2+}$ molar ratio on the cadmium precipitation in WPA (25 % $P_2O_5$) at T = 25 °C.

By comparing the results obtained in synthetic phosphoric acid (results presented in chapter 5) and those obtained in the case of industrial WPA, it can be clearly stated that for a Sulfur/$Cd^{2+}$ molar ratio equal to 25/1 the yield of decadmiation was 82.3 %. Whereas in industrial WPA, the $Cd^{2+}$ removal effectiveness strongly dropped until it reached 21.5 %. The reason behind the separation efficiency diminution is mainly due to the occurrence of several metallic impurities such as copper, and arsenic which in turn can react with sulfides (see sub-section 6.3.3). Therefore, this is one of the explanations for the large amount of NaHS consumed to precipitate cadmium. Table 6.3 exhibits the XRF analysis of the dark-brown precipitate obtained after the filtration of the treated WPA solutions (25 % $P_2O_5$) for different Sulfur/$Cd^{2+}$ molar ratios. This table proves that sulfides reacted mostly with metals like copper as well as metalloids, such as arsenic.

Table 6.3 XRF analysis of the dark-brown precipitate obtained for different Sulfur/$Cd^{2+}$ molar ratios and at a temperature of 25 °C.

| Component | Concentration (wt. %) | | | | |
|---|---|---|---|---|---|
| | Sulfur/$Cd^{2+}$ = 25/1 | Sulfur/$Cd^{2+}$ = 40/1 | Sulfur/$Cd^{2+}$ = 50/1 | Sulfur/$Cd^{2+}$ = 60/1 | Sulfur/$Cd^{2+}$ = 70/1 |
| S | 41.426 | 60.138 | 50.141 | 28.971 | 38.101 |
| Cu | 28.887 | 20.903 | 23.414 | 28.981 | 23.654 |
| As | 10.722 | 6.883 | 8.644 | 12.129 | 8.791 |
| Cd | 0.039 | 3.052 | 9.854 | 17.082 | 21.093 |
| Zn | 0.000 | 0.175 | 0.267 | 0.539 | 0.440 |
| Ni | 0.030 | 0.000 | 0.000 | 0.027 | 0.000 |
| Mn | 0.002 | 0.000 | 0.002 | 0.000 | 0.000 |
| Cr | 0.036 | 0.025 | 0.019 | 0.030 | 0.022 |
| Fe | 0.338 | 0.219 | 0.216 | 0.350 | 0.182 |
| Mo | 1.098 | 1.162 | 2.505 | 3.048 | 3.056 |
| Ti | 0.011 | 0.005 | 0.006 | 0.015 | 0.002 |
| V | 0.020 | 0.010 | 0.000 | 0.020 | 0.000 |
| U | 0.086 | 0.033 | 0.044 | 0.079 | 0.049 |

These results are in good agreement with those published in the literature (Gharabaghi et al., 2012; Ye et al., 2017). Gharabaghi et al. (2012) observed that during the sulfide precipitation of metals, copper was precipitated first, and then cadmium. While zinc began to precipitate when the concentration of cadmium remained at lower levels. Thereby, they concluded that Cd, Zn, and Ni were not noticeably precipitated during copper separation. Similarly, Ye et al. (2017) pointed out that copper was firstly precipitated as a consequence of copper sulfide being the most insoluble metal sulfide (solubility product equal to $6 \times 10^{-36}$), followed sequentially by lead, zinc, and finally iron utilizing sulfide precipitation in the bioleach leachate (pH 1.25). Regarding phosphoric acid solutions, Ukeles et al. (1994) used DTPN agent to remove copper and cadmium from either diluted and concentrated WPA solutions, and they also found that cadmium started to precipitate only after total copper consumption. That is why they used iron powder for the cementation of the $Cu^{2+}$ to copper metal to prevent $Cu^{2+}$ from reacting with DTPN.

WPA is well known to be produced at temperatures between 60 °C and 70 °C, so it is worthwhile to investigate the effect of temperature on the performance of the sulfide precipitation process as a means of purifying WPA. Figure 6.2 displays the effect of temperature on the $Cd^{2+}$ removal from 25 % of $P_2O_5$. The yield of cadmium sulfide precipitation diminished with increasing acid temperature from 25 °C to 70 °C at atmospheric pressure. For instance, for

a molar ratio of Sulfur/$Cd^{2+}$ = 50/1, the removal efficiency of $Cd^{2+}$ was seen to decrease from 63.09 % to 28.66 % as the temperature augmented from 25°C to 70°C. This is due to the drop in the $H_2S$ solubility and, subsequently, the shortage of available sulfide. This is confirmed by Xuan Hai et al. (2012) who observed that a temperature increment induced a decrease in $H_2S$ solubility in a synthetic phosphoric acid solution of 47.2 % $P_2O_5$. Moreover, it is relevant to indicate that the $H_2S$ solubility is strongly influenced on both sides by the WPA concentration and also by the presence of impurities in the WPA medium.

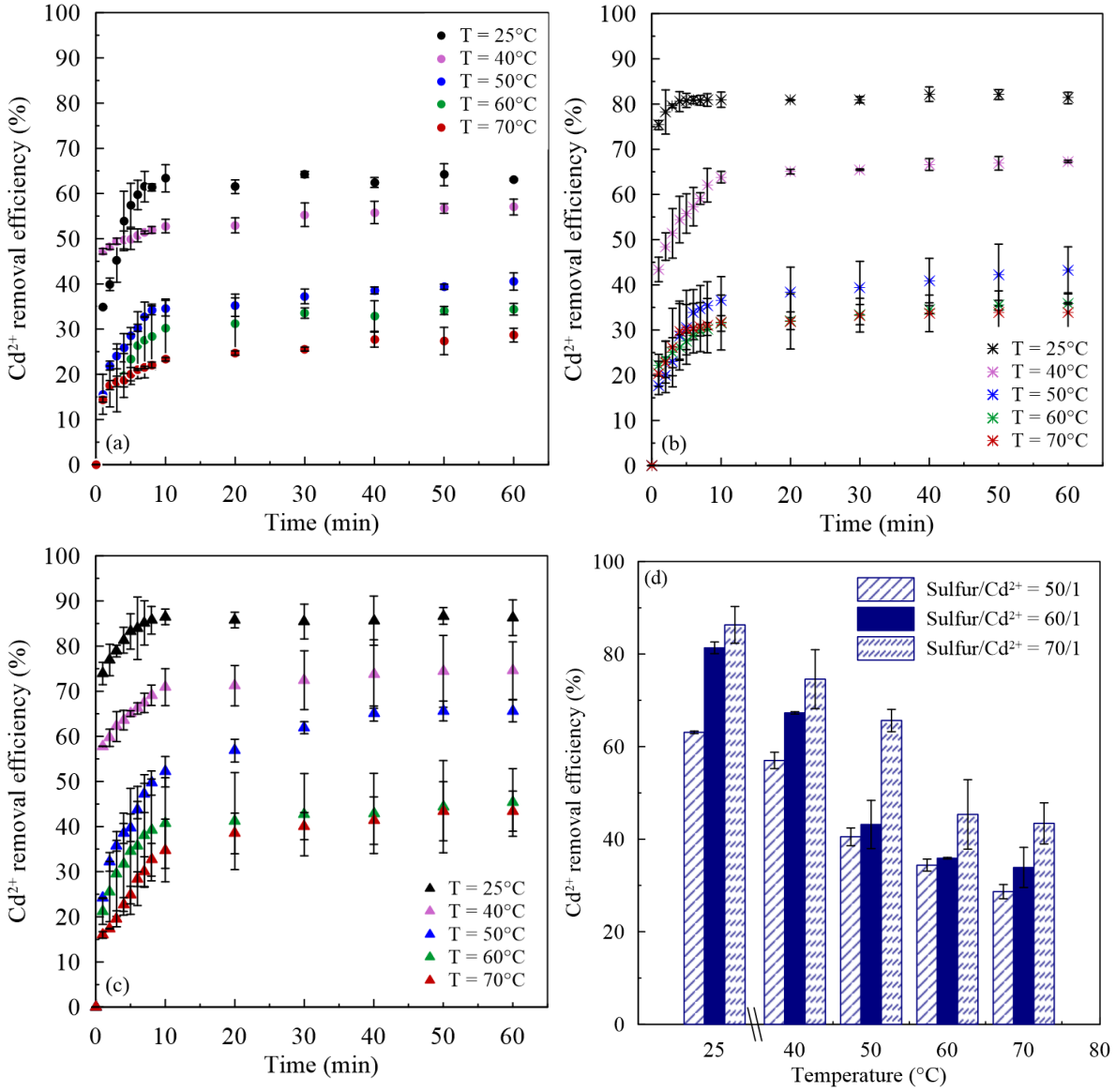


Figure 6.2 Cadmium removal efficiency versus time with a temperature variation from 25 °C to 70 °C and (a) Sulfur/$Cd^{2+}$ = 50/1, (b) Sulfur/$Cd^{2+}$ = 60/1, and (c) Sulfur/$Cd^{2+}$ = 70/1. (d) Effect of temperature in $Cd^{2+}$ removal efficiency from WPA solution of 25 % $P_2O_5$ in batch conditions (reaction time = 60 min).

#### *6.3.1.2 Thermodynamic and kinetic modeling of CdS precipitation*

Kinetic study is an important way to get an understanding of the mechanism of any process. In the case of cadmium sulfide precipitation, the sulfur to metal ratio and temperature play an important role in the removal of cadmium from WPA solution (25 % $P_2O_5$) and the effect of these parameters on the cadmium removal rate can be assessed by a kinetic study. As illustrated in Figure 6.3, the higher the Sulfur/$Cd^{2+}$ molar ratio, the easier is the cadmium elimination. Moreover, it can be noticed that the cadmium concentration decreases rapidly until the first 30 minutes of the reaction time, after which it is nearly stable.

The kinetic model proposed in Chapter 5 (sub-section 5.3.1.2) was used to predict the residual $Cd^{2+}$ concentrations for different Sulfur/$Cd^{2+}$ molar ratios in the case of dilute WPA medium. Indeed, Eq. (5.21) is an expression of the apparent rate constant (k) and the order of reaction (n) which need to be determined. The optimal values of these parameters were determined via the parametric identification method by reducing the sum of squared errors (SSE) between the $Cd^{2+}$ residual concentration predicted by the model and that obtained experimentally. MATLAB® 2017 software (The MathWorks, USA) was used to implement this method.

Figure 6.3 shows the time-dependent evolution of the $Cd^{2+}$ residual concentration measured and calculated by Eq. (5.17), for Sulfur/$Cd^{2+}$ molar ratio varying from 25/1 to 70/1 and at a temperature of 25 °C. From Figure 6.3a, it can be deduced that the predicted and experimentally obtained results are in excellent accordance, and this is valid for all the studied Sulfur/$Cd^{2+}$ molar ratios. This was further proven by the parity plot illustrated in Figure 6.3b and the SSE, which was low and equal to 0.95, 3.44, 3.76, 0.16, and 1.08 for Sulfur/$Cd^{2+}$ molar ratios being equal to 25/1, 40/1, 50/1, 60/1, and 70/1, which correspond to correlation coefficients $R^2$ of 0.954, 0.963, 0.078, 0.999, 0.999, and 0.996, respectively. In contrast, this model is at this stage unsuitable for predicting the amount of cadmium separated from a phosphoric acid medium with a temperature exceeding 25 °C, due to the paucity of thermodynamic data for this system at different high temperatures. Table 6.4 provides a summary of the apparent rate constant and reaction order obtained as a function of temperature from 25 °C to 70 °C and for different Sulfur/$Cd^{2+}$ molar ratios. The k and n data highlights that Eq. (5.21) corresponds to an apparent kinetics that encompasses complex mechanisms that involve coprecipitation with other species, homogeneous and heterogeneous nucleation, and growth.

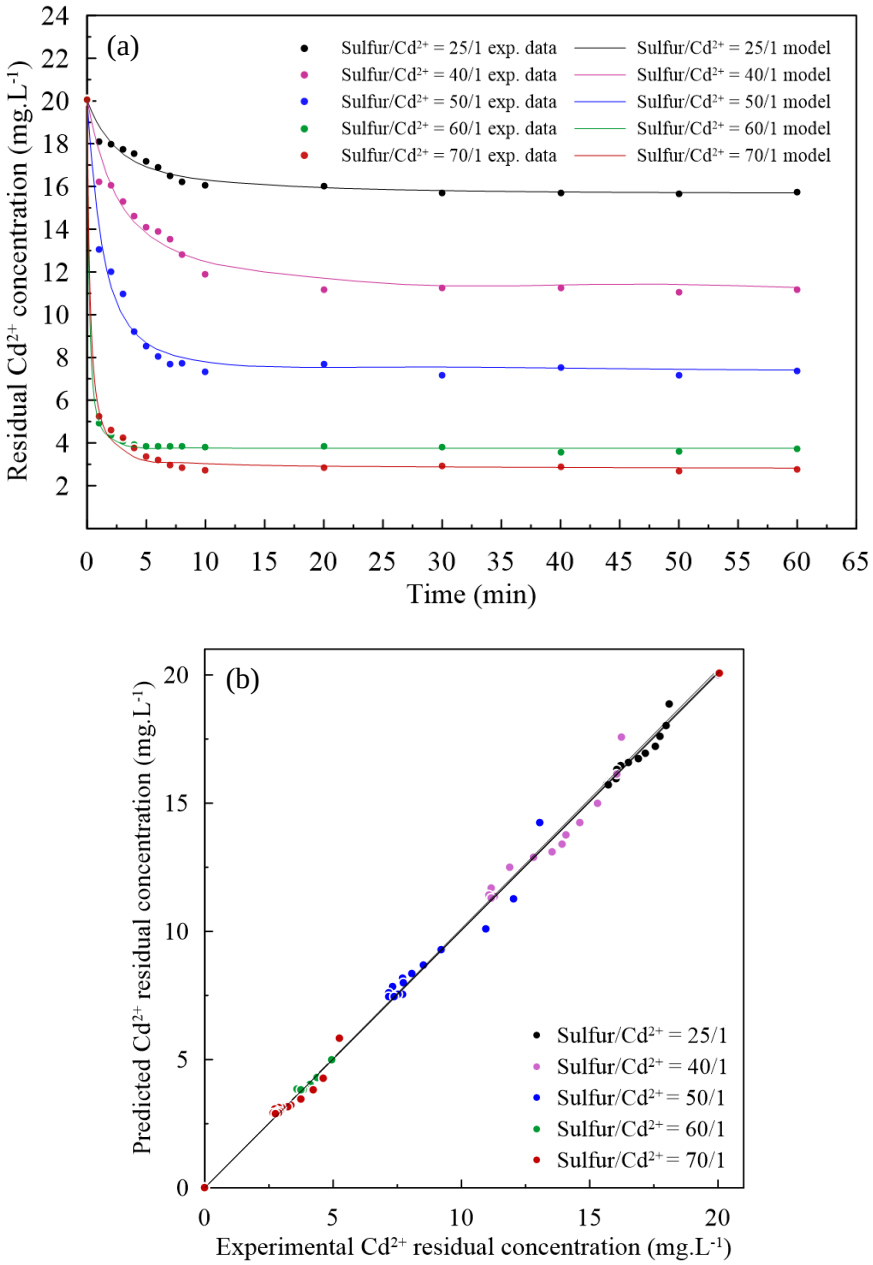


Figure 6.3 (a) Comparison between the experimentally measured and calculated residual $Cd^{2+}$ concentration using Eq. (16) in WPA solution (25 % $P_2O_5$) for Sulfur/$Cd^{2+}$ = 25/1 – 70/1 and at T = 25 °C. (b) Calculated versus experimental $Cd^{2+}$ residual concentration in WPA (25 % $P_2O_5$).

Table 6.4 Derived pseudo-kinetic parameters values for cadmium removal by sulfide precipitation using parametric identification method.

| Temperature (°C) | Sulfur/$Cd^{2+}$ = 25/1 | | Sulfur/$Cd^{2+}$ = 40/1 | | Sulfur/$Cd^{2+}$ = 50/1 | | Sulfur/$Cd^{2+}$ = 60/1 | | Sulfur/$Cd^{2+}$ = 70/1 | |
|---|---|---|---|---|---|---|---|---|---|---|
| | k ($L.mol^{-1}.s^{-1}$) | n | k ($L.mol^{-1}.s^{-1}$) | n | k ($L.mol^{-1}.s^{-1}$) | n | k ($L.mol^{-1}.s^{-1}$) | n | k ($L.mol^{-1}.s^{-1}$) | n |
| 25 | $7.358 \times 10^{-6}$ | 1.637 | $3.175 \times 10^{-6}$ | 1.742 | $2.570 \times 10^{-6}$ | 1.533 | $7.804 \times 10^{-6}$ | 1.877 | $2.969 \times 10^{-6}$ | 2.369 |
| 40 | - | - | - | - | $2.318 \times 10^{-4}$ | 3.523 | $6.992 \times 10^{-6}$ | 2.594 | $1.000 \times 10^{-5}$ | 3.084 |
| 50 | - | - | - | - | $1.036 \times 10^{-5}$ | 2.232 | $7.185 \times 10^{-6}$ | 2.138 | $1.754 \times 10^{-6}$ | 2.348 |
| 60 | - | - | - | - | $7.835 \times 10^{-6}$ | 1.951 | $1.074 \times 10^{-4}$ | 2.906 | $1.078 \times 10^{-5}$ | 2.271 |
| 70 | - | - | - | - | $1.352 \times 10^{-4}$ | 2.920 | $2.552 \times 10^{-5}$ | 2.039 | $3.333 \times 10^{-6}$ | 1.943 |

Table 6.5 Comparison between the cadmium removal efficiency achieved by sulfide precipitation in batch and continuous mode (HRT: 40 min) under different operating conditions.

| Sulfur/ $Cd^{2+}$ | Cadmium removal efficiency (%) | | | | | | | | | |
|---|---|---|---|---|---|---|---|---|---|---|
| | T = 25 °C | | T = 40 °C | | T = 50 °C | | T = 60 °C | | T = 70 °C | |
| | Batch | Continuous | Batch | Continuous | Batch | Continuous | Batch | Continuous | Batch mode | Continuous |
| 25/1 | 21±2 | 27±2 | - | - | - | - | - | - | - | - |
| 40/1 | 44±6 | 46±6 | - | - | - | - | - | - | - | - |
| 50/1 | 63.1±0.3 | 67±2 | - | - | - | - | - | - | - | - |
| 60/1 | 81±2 | 82.7±0.9 | 67.3±0.3 | 70.43±2 | 43±5 | 44.86±2 | 35.9±0.1 | 36.3±0.2 | 34±4 | 33±3 |
| 70/1 | 86±4 | 89±3 | - | - | - | - | - | - | - | - |

### 6.3.2 Continuous sulfide precipitation process

Sulfide precipitation in the continuous mode was also examined, as this operation mode is encountered at the industrial scale. Thus, the flow rates of the necessary feed solutions, *i.e.*, WPA and sulfide solutions, to precipitate cadmium sulfides were calculated. It is common knowledge that the HRT must be higher than the reaction time, which is equal to 30 min in our case. The chosen HRT was 40 min, and therefore the total flow rate ($Q_T = Q_{H3PO4} + Q_{Sulfur}$) was equal to the ratio of the reaction volume ($V_R$ = 2.75 L) to the HRT.

#### *6.3.2.1 Effect of molar ratio and temperature on cadmium sulfide precipitation*

The investigation of the Sulfur/$Cd^{2+}$ molar ratio and temperature effects on $Cd^{2+}$ separation from WPA solutions (25 % $P_2O_5$) by continuous sulfide precipitation process was also investigated. Figure 6.4 displays the plot of $Cd^{2+}$ removal efficiency achieved for an HRT of 40 min as a function of the Sulfur/$Cd^{2+}$ molar ratio at 25 °C. Clearly, the cadmium elimination efficiency rose from 27.38 % to 89.38 % by increasing the Sulfur/$Cd^{2+}$ from 25/1 to 70/1. As an example, for a Sulfur/$Cd^{2+}$ molar ratio equal to 60/1 and a temperature of 25 °C, a $Cd^{2+}$ removal yield of 82.73 % was reached, which means that the $Cd^{2+}$ concentration in WPA solution (25 % $P_2O_5$) decreased from 20 mg.$L^{-1}$ (65.95 mg Cd/kg $P_2O_5$) to 3.38 mg.$L^{-1}$ (11.15 mg Cd/kg $P_2O_5$).

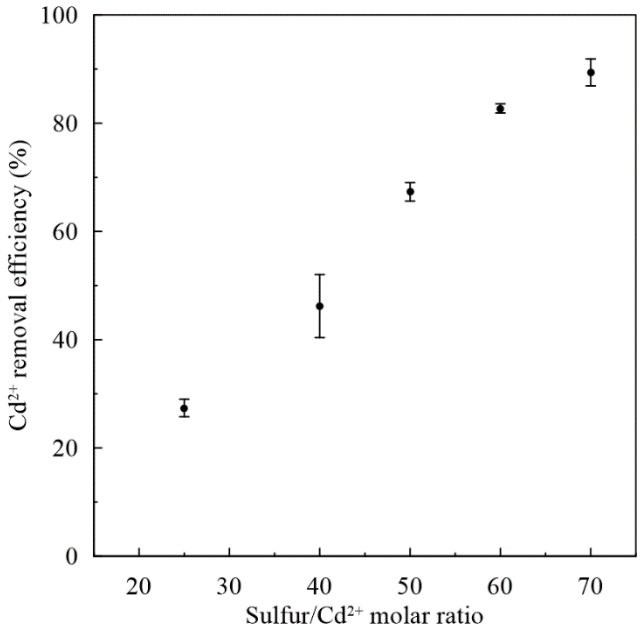


Figure 6.4 Cadmium removal efficiency versus Sulfur/$Cd^{2+}$ molar ratio in continuous mode (volumetric flow rate $Q_{Sulfur} = Q_{H3PO4}$ = 34.38 mL.$min^{-1}$, and T = 25 °C).

The impact of temperature on the cadmium removal yield by the sulfide precipitation process in continuous mode was also examined for the molar ratio (Sulfur/$Cd^{2+}$ = 60/1), and while varying the temperature from 25 °C to 70 °C. Figure 6.5a depicts the trend of $Cd^{2+}$ removal efficiency with rising temperature from 25 °C to 70 °C. As it was foreseen in the batch mode, the amount of cadmium removed diminished by increasing the temperature up to 70 °C. The $Cd^{2+}$ ion removal yield was reduced from 82.73 % to 33.18 % as the temperature was increased from 25 °C to 70 °C (Figure 6.5a) due to the $H_2S$ solubility decline. These findings are in line with those of (Ennaassia et al., 2002), who concluded that the efficiency of cadmium removal from synthetic phosphoric acid by sulfide precipitation was negatively influenced by increasing temperature from 20 °C to 70 °C.

#### *6.3.2.2 Effect of hydraulic residence time on cadmium sulfide precipitation*

The effectiveness of cadmium removal by sulfide precipitation as a function of flow rate; for Sulfur/$Cd^{2+}$ molar ratios of 40/1 and 60/1 and at a temperature of 25 °C; is displayed in Figure 6.5b. When raising the total flow rate from 68.75 to 275 mL.$min^{-1}$, the yield of cadmium removal was reduced from 46.21 % to 17.13 % for Sulfur/$Cd^{2+}$ = 40/1, and from 82.73 % to 19.90 % for Sulfur/$Cd^{2+}$ = 60/1. The decrease in $Cd^{2+}$ removal efficiency with increasing flow rate was evidenced by the fact that the HRT is inversely proportional to flow rate. For instance, the HRT corresponding to the total flow rate of 68.75 mL.$min^{-1}$ and 275 mL.$min^{-1}$ is 40 min and 10 min, respectively. This can be explained as the untreated WPA solutions were in the reactor for much longer at low flow rates, which subsequently gave more time for the sulfide precipitation reaction to proceed. On the other hand, the low flow rate improved the precipitation efficiency of cadmium sulfide and other metallic impurities by actually fostering contact and mixing between heavy metals and sulfide species. Therefore, an average HRT between 30 and 40 min is required to reach an optimal cadmium removal efficiency, and more specifically in the presence of other impurities that also possess an affinity for sulfur.

#### *6.3.2.3 Comparison of batch and continuous sulfide precipitation process*

Comparing data related to the $Cd^{2+}$ removal efficiency from WPA solutions in the batch and continuous modes, it can be underlined that the carrying out of the precipitation in continuous system reached the same yield of $Cd^{2+}$ separation effectiveness at 25 °C when the HRT was 40 min, as shown by Table 6.5. Therefore, continuous process can be applied for the WPA purification by sulfide precipitation and mainly on the industrial scale.

The comparison between Figure 6.3 and Figure 6.5b also highlights that in the batch mode, cadmium sulfidation is completed within 10 – 20 min for Sulfur/$Cd^{2+}$ ratio equal to 40/1 and 60/1. Conversely, the cadmium removal yield still increases for the same ratios when HRT rises up to 40 min in the continuous mode. This confirms the non-linear behavior of the precipitation process in the batch mode and the high sensitivity of these mechanisms to mixing and micromixing conditions, which implies that the switch from batch to continuous mode is not straightforward.

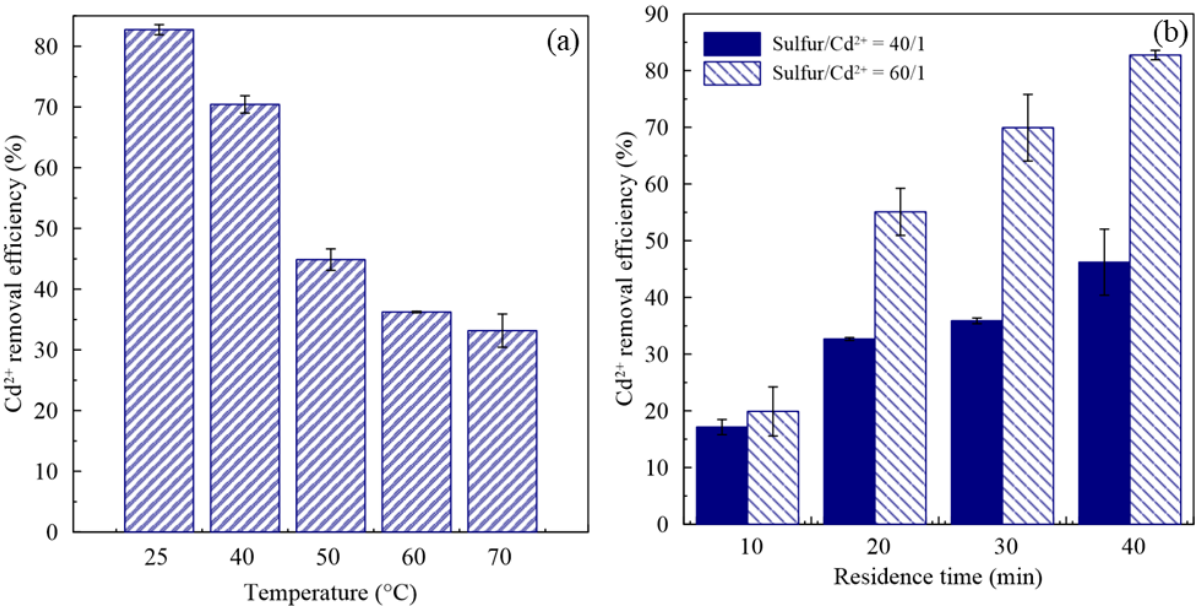


Figure 6.5 Effect of (a) temperature in continuous mode (volumetric flow rate $Q_{Sulfur} = Q_{H3PO4}$ = 34.38 mL.$min^{-1}$, Sulfur/$Cd^{2+}$ = 60/1) and (b) HRT on cadmium sulfide precipitation (Sulfur/$Cd^{2+}$ = 40/1 and 60/1, T = 25 °C, [$H_3PO_4$] = 25 % $P_2O_5$).

### 6.3.3 Solid phase characterization

Once the precipitation reaction was completed, a dark-brown colored precipitate was obtained (Figure 6.6). The EDS maps (Figure 6.7) and data presented in Table 6.6 revealed that the precipitate formed from the cadmium sulfide precipitation from diluted WPA solution (25 % $P_2O_5$) was composed of metal impurities mixture (such as Cu, Zn, Cd, As), as well as S, and a small amount of P, which was in line with the XRF results.

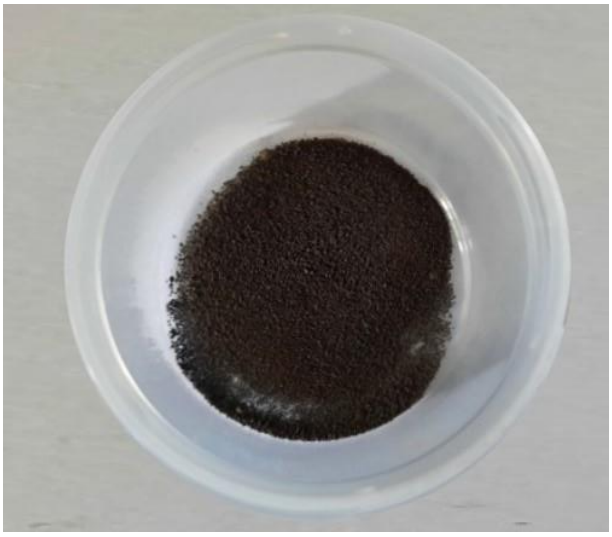

Figure 6.6 Resulting precipitate after one hour of formation at T = 25°C, $[H_3PO_4]$ = 25 % $P_2O_5$, and Sulfur/$Cd^{2+}$ = 60/1.

Table 6.6 EDS results of the obtained precipitate for different Sulfur/$Cd^{2+}$ molar ratios.

| | Sulfur/$Cd^{2+}$ molar ratio | Element | Mass (weight %) | Mass (atomic %) |
|---|---|---|---|---|
| Dark-brown precipitate | 25/1 | O | 32.78 | 54.00 |
| | | P | 8.24 | 7.01 |
| | | S | 37.69 | 30.98 |
| | | Cu | 14.44 | 5.99 |
| | | Zn | 1.65 | 0.66 |
| | | As | 3.85 | 1.35 |
| | | Cd | 0.04 | 0.01 |
| | 40/1 | O | 23.03 | 49.76 |
| | | P | 4.97 | 5.55 |
| | | S | 32.64 | 35.18 |
| | | Cu | 12.55 | 6.83 |
| | | Zn | 1.18 | 0.63 |
| | | As | 2.67 | 1.23 |
| | | Cd | 2.70 | 0.83 |
| | 60/1 | O | 23.44 | 49.85 |
| | | P | 5.30 | 5.82 |
| | | S | 33.77 | 35.83 |
| | | Cu | 10.32 | 5.52 |
| | | Zn | 1.00 | 0.52 |
| | | As | 2.80 | 1.27 |
| | | Cd | 3.92 | 1.19 |
| | 70/1 | O | 13.31 | 35.59 |
| | | P | 0.81 | 1.11 |
| | | S | 33.12 | 41.18 |
| | | Cu | 20.71 | 13.94 |
| | | Zn | 2.45 | 1.60 |
| | | As | 6.16 | 3.52 |
| | | Cd | 5.96 | 3.06 |

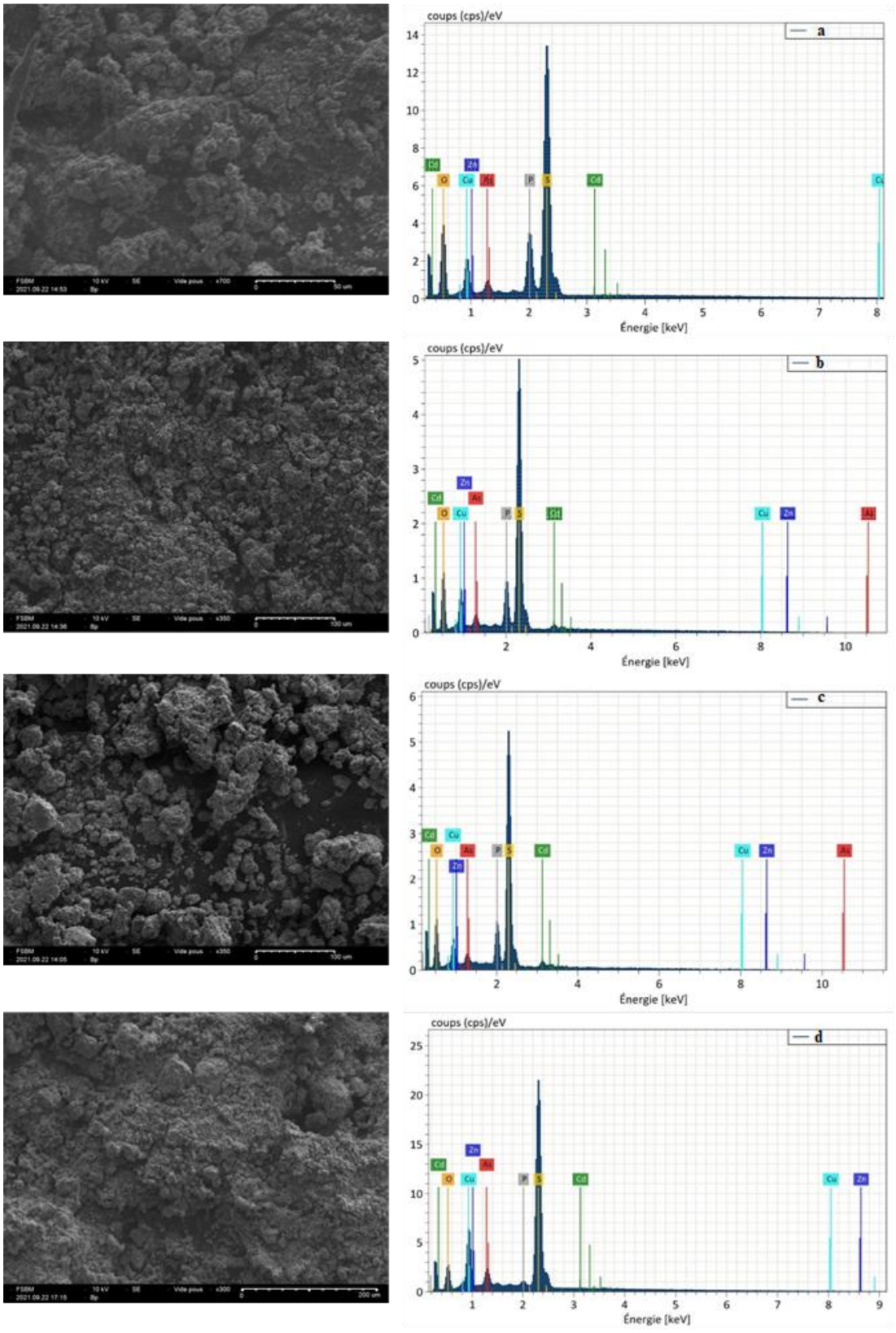


Figure 6.7 SEM and EDS analysis carried out on the resulting precipitate by the precipitation process at different Sulfur/$Cd^{2+}$ (a) 25/1, (b) 40/1, (c) 60/1, and (d) 70/1.

In parallel, Figure 6.8 illustrates the precipitate particle size distribution in volume for Sulfur/$Cd^{2+}$ from 25/1 and 60/1. It was found that by augmenting the Sulfur/$Cd^{2+}$ molar ratio, the size of CdS solid particles increased. The median diameter ($D_{50}$) augmented from 42.13 µm to 213.81 µm, for a Sulfur/$Cd^{2+}$ molar ratio varying from 25/1 to 70/1. In fact, Kind (2002) demonstrated that the particles seen along the precipitation process are secondary particles, resulting from the aggregation of primary particles. Therefore, the stability and aggregation of primary particles in an aqueous solution are controlled by the balance between van der Waals forces of attraction and electrostatic repulsion forces because of the electrical charge on the surface of the particles. Additionally, metal sulfides are known to adsorb the sulfur species $H_2S$, $HS^-$, and $S^{2-}$ (Bryson and Bijsterveld, 1991; Kolthoff and Moltzau, 1935), which can induce an electrical charge on the particles surface. Thus, particles generated in the presence of sulfide excess are more likely to carry an important surface charge, and thus stabilize in suspension under electrical repulsion forces. However, the potential of metal sulfides to adsorb sulfide ions present in solution is linked to the operating pH. Consequently, the aggregation of the initially formed primary particles becomes more favorable, which in turn resulted in the solid particles growth. Subsequently, the sedimentation characteristics of the formed precipitates are further improved (Figure 6.9a). SEM images show that the aggregation mechanism became noticeably more apparent by raising the Sulfur/$Cd^{2+}$ molar ratio (Figure 6.7). For example, considering the case of Sulfur/$Cd^{2+}$ molar ratio = 60/1 (Figure 6.9b), when focusing on a single particle, it can be observed that it is an aggregate formed by a multitude of nanoparticles.

While the feasibility of the batch and the continuous decadmiation process based on sulfide precipitation had already been proved in the previous sections, these final results highlight the feasibility of the downstream solid-liquid separation process to recover CdS particles.

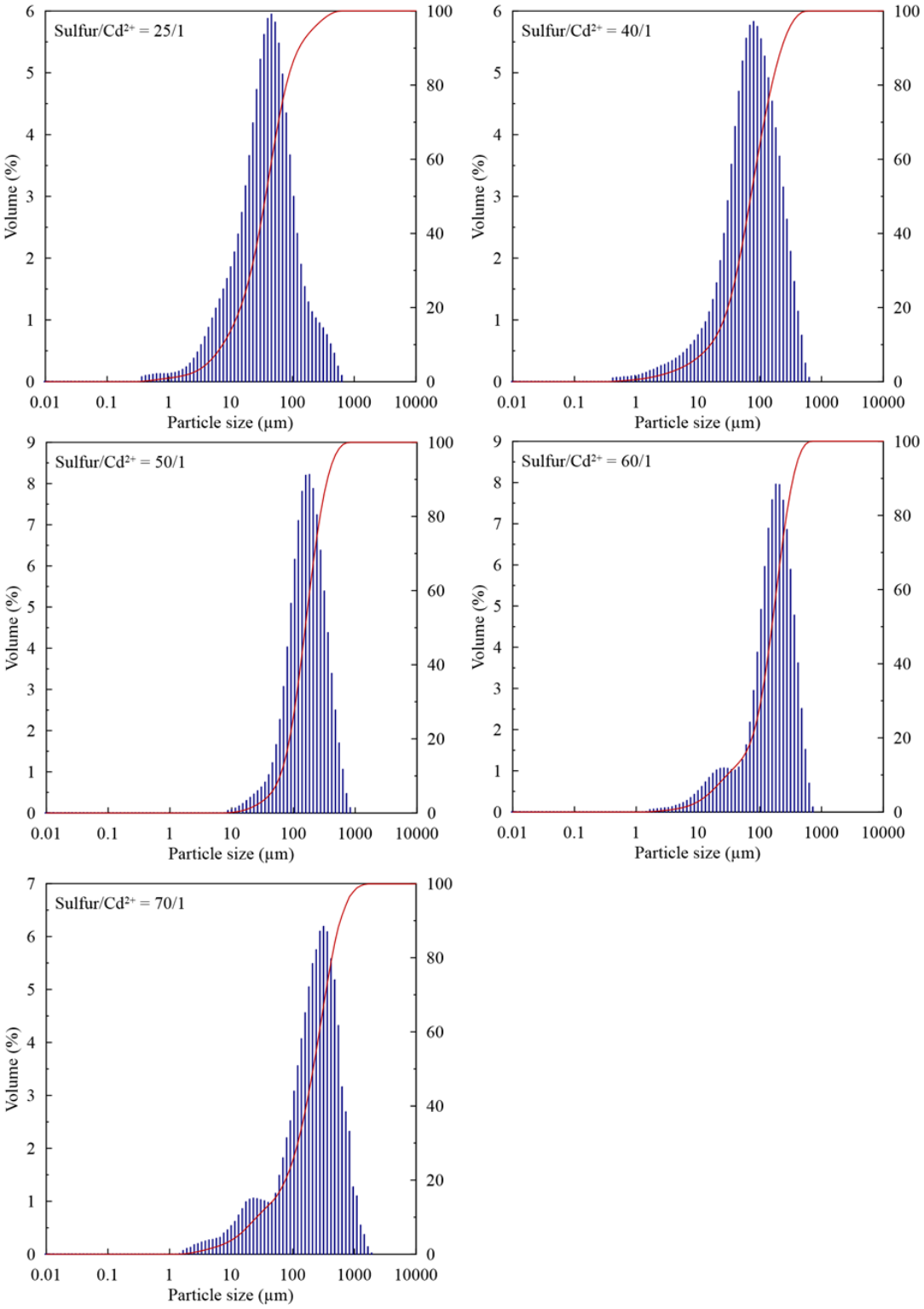


Figure 6.8 Particle size distribution in volume of the resulting precipitate for Sulfur/$Cd^{2+}$ = 25/1 ($D_{50}$ = 42.13 μm), Sulfur/$Cd^{2+}$ = 40/1 ($D_{50}$ = 82.08 μm), Sulfur/$Cd^{2+}$ = 50/1 ($D_{50}$ = 178.17 μm), Sulfur/$Cd^{2+}$ = 60/1 ($D_{50}$ = 180.28 μm), and Sulfur/$Cd^{2+}$ = 70/1 ($D_{50}$ = 213.81 μm).

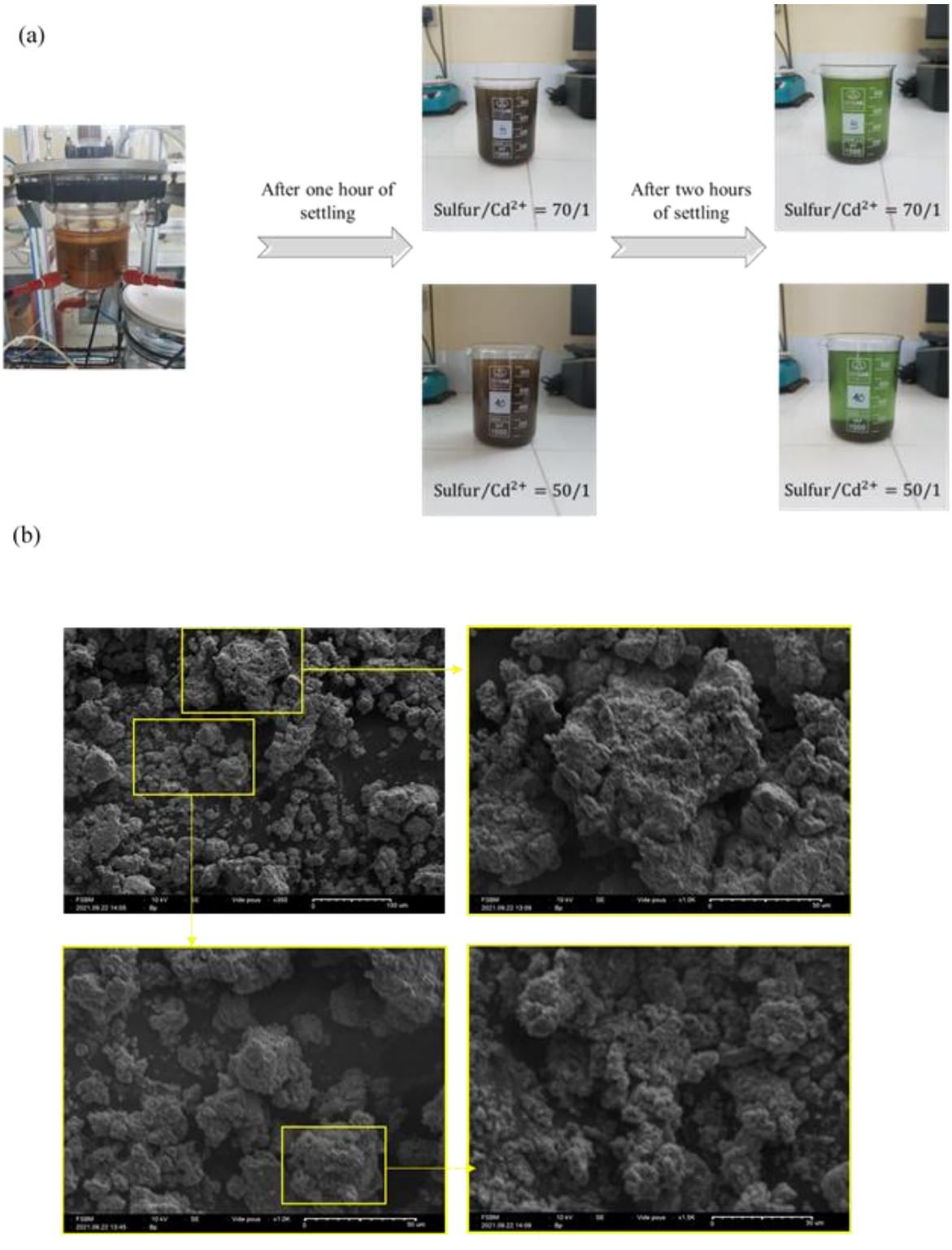


Figure 6.9 (a) Original photographs of WPA solution (25 % $P_2O_5$) collected after treatment using NaHS (Sulfur/$Cd^{2+}$ = 50/1 and 70/1) and settled for a time period of 1h and 2 h. (b) SEM micrographs of precipitate obtained at Sulfur/$Cd^{2+}$ = 60/1 and 25 °C.

### 6.3.4 Comparison of different purification processes applied for WPA decadmiation

The purification of wet-produced phosphoric acid started as a feasible route to furnish a cheaper alternative to thermal acid for manufacturing bulk technical industrial phosphates (mainly STPP) (Gilmour, 2013). The occurrence of metallic cations (such as cadmium, copper, zinc, arsenic, and lead) negatively impairs the final quality of phosphoric acid, as well as they lead to a detrimental impact on the environment and human health. However, the separation of metallic impurities at very low concentrations remains a paramount challenge for the phosphate industry. For this purpose, several separation processes have been proposed for purifying the WPA (Khaless, 2006; Nazari et al., 2005; Taha et al., 2020). Table 6.7 provides a comparison of several purification technologies to separate cadmium from diluted WPA with similar $P_2O_5$ content. This table highlights that sulfide precipitation using NaHS outperforms most of the published data based on alternative processes, in particular ion exchange, the performance of which is limited to low sulfur content and requires long HRT. NaHS is also cheap in comparison to alternative chemicals proposed for precipitation. Despite the abundant literature on solvent extraction, this requires chemicals and does not exhibit better performance as well. Finally, sulfide precipitation using NaHS appears to be a promising technique for the decadmiation of WPA at an industrial scale as the treated WPA solutions (with a content of 11 mg Cd/kg $P_2O_5$) become appropriate for manufacturing phosphate fertilizers in compliance with the standards set by the European Union institutions (Regulation (EU) 2019/1009) which restrict the Cd content in phosphate fertilizers at 60 mg Cd/kg $P_2O_5$, as well as by some countries (Finland, Poland, Slovakia, Sweden, Netherlands, etc.) that limit the concentration of cadmium in phosphate fertilizers at 20 – 50 mg Cd/kg $P_2O_5$ (Ulrich, 2019).

Table 6.7 Comparison of several purification technologies to separate cadmium form diluted WPA.

| Purification process | $H_3PO_4$ concentration (w% $P_2O_5$) | $Cd^{2+}$ initial concentration | | $Cd^{2+}$ residual concentration | | Temperature (°C) | Reaction time (min) | $Cd^{2+}$ removal yield (%) | Comments | Reference |
|---|---|---|---|---|---|---|---|---|---|---|
| | | ($mg.L^{-1}$) | mg Cd /kg $P_2O_5$ | ($mg.L^{-1}$) | mg Cd /kg $P_2O_5$ | | | | | |
| Solvent extraction | 27 | 26 | 78.04 | 17.42 | 52.28 | Ambient temperature | 5 | 33 | The used organic phase was 1% (vol) Alamine 336 + 1.5% (vol) iso-dodecanol in B-65 kerosene. | Nazari et al. (2005) |
| Nanofiltration | ≤ 29 | 13.11 | 47.82 | 3.80[a]<br>4.59[b]<br>11.58[c] | 13.86[a]<br>16.74[b]<br>42.24[c] | 20±5 | - | 71[a]<br>65[b]<br>11.67[c] | - Dead-end filtration was the flow configuration adopted.<br>- $Cd^{2+}$ removal efficiency reached by using the three organic membranes: Desal5-DL [a], Desal KH [b], and MPF-36 [c]. | Khaless (2006) |
| Solvent extraction | 30 | 45.61 | 120 | 12.31 | 32.39 | 20 | - | 73 | The extractant in question was Cyanex 302 with a concentration of 1400 ppm. | Boussen (2007) |
| Chemical precipitation | 25 | 101.95[d]<br>81.85[e]<br>101.95[f]<br>81.85[g] | 336.20[d]<br>269.92[e]<br>336.20[f]<br>269.92[g] | 89.28[d]<br>81.85[e]<br>63.45[f]<br>44.40[g] | 294.41[d]<br>269.91[e]<br>209.23[f]<br>146.41[g] | 20 | 60 | 12.43[d]<br>0.00[e]<br>37.76[f]<br>45.76[g] | $Cd^{2+}$ abatement yield obtained when using ZnEPDTC [d], NaEPDTC [e], CSX [f], and NaDBDTC [g]. | Zieliński et al. (2019) |
| Ion exchange | 23.2 | 16.7 | 60.29 | 2.2[h]<br>14.7[i]<br>9.9[j] | 7.94[h]<br>53.07[i]<br>35.74[j] | 20±1 | 1440 | 86.83[h]<br>11.98[i]<br>40.72[j] | - $Cd^{2+}$ removal efficiency achieved when using MTC1600H (sulfonic resin) [h], MTS9500 (aminophosphonic resin) [i], and MTS9570 (phosphonic/sulfonic resin) [j] were used for the purification of crude WPA.<br>- Resin dose was 2.5 $g.L^{-1}$ | Taha et al. (2020) |
| Sulfide precipitation | 25 | 20 | 65.95 | 3.38 | 11.15 | 25 | 20 (batch)<br>40 (continuous) | 83 ± 1 | - Sulfur/$Cd^{2+}$ = 60/1<br>- Continuous sulfide precipitation using NaHS | Present study |

## 6.4 Conclusions

In this work, the separation of cadmium from industrial WPA solutions (25 % $P_2O_5$) by batch and continuous sulfide precipitation process was investigated. The major findings revealed that the crucial factors which significantly influence the decrease in cadmium content from WPA solutions are the Sulfur/$Cd^{2+}$ molar ratio, the presence of other heavy metals, and the temperature, as well as the HRT. For a Sulfur/$Cd^{2+}$ = 25/1, the cadmium removal yield was low due to the occurrence of other heavy metals, such as copper which can react with sulfides prior to cadmium, owing to the low product solubility of copper sulfide; that is why an augmentation of Sulfur/$Cd^{2+}$ ratio was required to reach 86 % of cadmium removal from crude WPA. An increase in operating temperature from 25 °C to 70 °C led to a decrease in the cadmium removal efficiency by sulfide precipitation, due to the drop in the solubility of $H_2S$. Moreover, the proposed kinetic model based on the results obtained from the batch study, was able to calculate the $Cd^{2+}$ residual concentrations for different Sulfur/$Cd^{2+}$ molar ratios. Thus, the calculated and measured $Cd^{2+}$ residual concentrations were in good agreement. Regarding the continuous operation, an HRT equal to 40 min was required to reach the maximum cadmium removal efficiency, and more specifically in the presence of other metallic impurities that also possess an affinity for sulfides. Furthermore, the dark-brown precipitate chemical characterization indicated that sulfidation was beneficial in removing cadmium as well as other metallic impurities, such as copper and arsenic. The increase in sulfur to metal ratio had a strong effect on the particle size distribution.

Eventually, compared to other purification processes, sulfide precipitation was able to reduce the concentration of cadmium from 65.95 mg Cd/kg $P_2O_5$ to 11.15 mg Cd/kg $P_2O_5$ from untreated WPA solution (25 % $P_2O_5$) at 25 °C.

# CONCLUSIONS AND PERSPECTIVES

In this work, a study of the manganese ions removal from drinking water by gas−liquid oxidation in multiphase reactors, such as bubble columns and airlifts, was conducted. Meanwhile, the investigation of the cadmium elimination from synthetic and industrial wet phosphoric acid solutions using sulfide precipitation in batch and continuous modes was also evaluated. The most interesting findings are summarized below.

As mentioned before, groundwater is an unavoidable source of drinking water for populations. However, it is also very common for groundwater to contain dissolved manganese, which must be reduced for both public health and aesthetic purposes. To deal with this issue, oxidation of dissolved manganese using strong oxidizing agents such as ozone, $KMnO_4$, and chlorine has been largely implemented at the industrial scale. However, the use of these chemicals is impeded by producing secondary pollution which is not acceptable in drinking water production. For this reason, the removal of manganese by oxidation using atmospheric oxygen can be achieved in different types of multiphase reactors such as bubble column and airlift and appears to be more simple, appropriate, and cost-effective.

The first objective of the present work was to investigate the feasibility of manganese mitigation from drinking using an oxidation process based on aeration in square bubble columns and split-rectangular airlift reactors. Firstly, an overview of hydrodynamics and mass transfer characteristics of these pneumatic reactors, as well as detailed knowledge about manganese chemistry and involved mechanisms in Mn(II) oxidation process were discussed. Regarding the obtained experimental findings, the oxygen mass transfer was not a limiting step for Mn(II) removal by oxidation. In contrast, the increment of pH (9.2 – 10) and initial dissolved manganese concentration (5 $mg.L^{-1}$ – 20 $mg.L^{-1}$) resulted in an improvement in Mn(II) remediation and a decrease in the required treatment time. Moreover, experimental data indicated that the Mn(II) oxidation kinetics was highly-dependent on pH and that it showed an autocatalytic behavior. Thus, the kinetic of manganese oxidation by aeration was shown to be pseudo-first order in Mn(II). With respect to the performance of the two reactors, it should be emphasized that the aeration in the airlift reactor allowed achieving an Mn(II) removal efficiency of 90 % for a treatment time of 25 min and an energy requirement of 0.029 $kWh.m^{-3}$ as opposed to the BC reactor which needed a

time of 60 min and energy consumption of 0.072 kWh.m$^{-3}$. Thus, airlift reactors seem to be suitable for Mn(II) oxidation by atmospheric air owing to their internal liquid recirculation between compartments, and good mixing time that ensure a good homogeneity of $MnO_2$ particles inside the reactor, which then fosters the Mn(II) oxidation. Ultimately, the prospects of this work are that the aeration process will be performed in multiphase reactors operating in a continuous system, a fact that is similar to the industrial situation. In addition, the assessment of the aeration performance as a demanganization technique of simulated and real groundwater that are known for their abundance of different co-contaminants.

Meanwhile, the second objective was to explore in depth the purification of phosphoric acid solutions. In fact, wet phosphoric acid has a vital role in the manufacture of phosphate fertilizers. Yet, it includes a mixture of impurities that are naturally present in the raw materials involved in the production process. Heavy metals, among them cadmium, are considered the Achilles heel of wet phosphoric acid manufacturing, therefore, it is important to restrict the levels of cadmium to alleviate the serious environmental impact. In this framework, cadmium removal from synthetic and industrial phosphoric acid solutions with batch and continuous sulfide precipitation using sodium hydrosulfide (NaHS) was evaluated.

Before undertaking our experimental study, sulfide precipitation and other WPA purification techniques have to be understood from a theoretical and technical view, hence, a comprehensive literature review on the industrial processes of WPA decadmiation was performed. The main mechanisms involved in the cadmium and other impurities removal were unveiled, operating key parameters were identified and their effects on the process efficiency were deeply discussed. Besides, the cost and environmental impacts of manufacturing and purifying phosphoric acid were evaluated.

As for the investigation on the decadmiation of synthetic phosphoric acid, the achieved outcomes revealed that operating parameters enclosed sulfide to cadmium molar ratio, temperature, phosphoric acid concentration, as well as hydraulic residence time importantly impacted the cadmium removal effectiveness. Additionally, the efficiency of cadmium sulfide precipitation from synthetic dilute phosphoric acid solution (25 % $P_2O_5$) reached by NaHS was higher than that obtained by $Na_2S$ because of the ionic strength. an increase in either temperature or phosphoric acid concentration exhibited a negative effect on the sulfide precipitation efficiency

both in the batch and continuous processes, which is due to the lower solubility of $H_2S$ and subsequently the drop in sulfide content. In the continuous process, a residence time of 40 min was sufficient to achieve similar cadmium removal yields as in the batch process. Meanwhile, augmenting the initial $Cd^{2+}$ concentration induced an enhancement of the cadmium removal yield as the sulfide content increased. The residual $Cd^{2+}$ concentrations computed by the proposed kinetic model for cadmium sulfide precipitation were in line with those measured, but only at a temperature equal to 25 °C due to the lack of thermodynamic data describing $H_3PO_4/H_2S/Cd^{2+}$ system as a function of temperature. Besides, an increase in supersaturation level resulting from a higher sulfide concentration had an important effect on the particle size distribution. Indeed, the mean particle size of CdS augmented by rising the sulfur to metal molar ratio. Consequently, the crystal agglomeration was the mechanism governing the particle size of CdS precipitate which was hexagonal CdS with high purity.

Concerning the mitigation of cadmium from industrial WPA solutions (25 % $P_2O_5$) by batch and continuous sulfide precipitation process. The major results indicated that for a Sulfur/$Cd^{2+}$ = 25/1, the cadmium removal efficiency was poor due to the presence of other heavy metals, such as copper. Therefore, an increase in Sulfur/$Cd^{2+}$ ratio was needed to attain 86 % of cadmium removal from crude industrial WPA. An increase in operating temperature from 25 °C to 70 °C also induced a decrease in the cadmium removal efficiency by sulfide precipitation. Moreover, a hydraulic residence time equal to 40 min was required to reach the maximum cadmium removal yield, specifically in the occurrence of other metallic impurities that also have an affinity for sulfides. Eventually, further chemical characterization of the dark brown precipitate demonstrated that sulfidation was conducive to the removal of cadmium as well as other metal impurities, such as copper and arsenic. With the increase in the sulfur to metal ratio, a notable effect on the particle size distribution was also observed.

To conclude, the performance of sulfide precipitation in removing cadmium from an untreated dilute industrial WPA solution (25 % $P_2O_5$) using NaHS was assessed and the proof of concept of both batch and continuous processes was established. On the one hand, it was observed that sulfidation beneficially removed other metal contaminants. On the other hand, compared to other purification processes, sulfide precipitation was able to reduce the concentration of cadmium from

65.95 mg Cd/kg $P_2O_5$ to 11.15 mg Cd/kg $P_2O_5$ from untreated industrial WPA solution (25 % $P_2O_5$) at 25 °C.

Therefore, to expand on this study, future work should be undertaken on the effectiveness of sulfide precipitation as a purification technique of concentrated WPA solutions (52 % $P_2O_5$ – 54 % $P_2O_5$) by using and comparing the performance of other precipitating agents as well. Nevertheless, as WPA solutions are a complex matrix with high acidity levels, it will be interesting to test the feasibility of coupling sulfide precipitation with pre-treatment techniques to intensify the separation of metallic impurities from dilute and concentrated WPA solutions to meet and sustain the standards established by institutions. Moreover, the properties of the precipitate (*i.e.*, Zeta potential and particle size) resulting from the decadmiation of the wet phosphoric acid solutions by sulfide precipitation process should be examined to determine the reliable liquid-separation technique for separating the metallic precipitate and the treated phosphoric acid solutions. Furthermore, the resulting precipitate is rich in metals that could be recovered in a variety of industries. That is why potential avenues for the recovery of these metal precipitates from phosphoric acid solutions, their sustainability, and their economic viability should be evaluated.

# REFERENCES


Abashar, M.E., Narsingh, U., Rouillard, A.E., Judd, R., 1998. Hydrodynamic Flow Regimes, Gas Holdup, and Liquid Circulation in Airlift Reactors. Ind. Eng. Chem. Res. 37, 1251–1259. https://doi.org/10.1021/ie9704612

Abdel-Ghafar, H.M., Abdel-Aal, E.A., Ibrahim, M.A.M., El-Shall, H., Ismail, A.K., 2019. Purification of high iron wet-process phosphoric acid via oxalate precipitation method. Hydrometallurgy 184, 1–8. https://doi.org/10.1016/j.hydromet.2018.12.011

Abdennebi, N., Bagane, M., Chtara, C., 2013. Removal of Copper from Phosphoric Acid by Adsorption on Tunisian Bentonite. Journal of Chemical Engineering & Process Technology 04, 1–4. https://doi.org/10.4172/2157-7048.1000166

Abdulkadir, M., Kajero, O.T., Zhao, D., Al–Sarkhi, A., Hunt, A., 2021. Experimental investigation of liquid viscosity's effect on the flow behaviour and void fraction in a small diameter bubble column: How much do we know? Journal of Petroleum Science and Engineering 207, 109182. https://doi.org/10.1016/j.petrol.2021.109182

Abidli, A., Huang, Y., Ben Rejeb, Z., Zaoui, A., Park, C.B., 2022. Sustainable and efficient technologies for removal and recovery of toxic and valuable metals from wastewater: Recent progress, challenges, and future perspectives. Chemosphere 292, 133102. https://doi.org/10.1016/j.chemosphere.2021.133102

Akita, K., Yoshida, F., 1973. Gas Holdup and Volumetric Mass Transfer Coefficient in Bubble Columns. Effects of Liquid Properties. Ind. Eng. Chem. Proc. Des. Dev. 12, 76–80. https://doi.org/10.1021/i260045a015

Albijanić, B., Havran, V., Petrović, D.Lj., Đurić, M., Tekić, M.N., 2007. Hydrodynamics and mass transfer in a draft tube airlift reactor with dilute alcohol solutions. AIChE Journal 53, 2897–2904. https://doi.org/10.1002/aic.11306

Almela, A., Elizalde, M.P., 1995. Solvent extraction of cadmium (II) from acidic media by Cyanex 302. Hydrometallurgy 37, 47–57. https://doi.org/10.1016/0304-386X(94)00012-R

Almela, A., Elizalde, M.P., Gómez, J.M., 1998. Cadmium(II) extraction from phosphoric media by bis(2,4,4-trimethylpentyl) thiophosphinic acid (Cyanex 302). Fluid Phase Equilibria 145, 301–310. https://doi.org/10.1016/S0378-3812(97)00332-4

Alonso, A.I., Urtiaga, A.M., Zamacona, S., Irabien, A., Ortiz, I., 1997. Kinetic modelling of cadmium removal from phosphoric acid by non-dispersive solvent extraction. Journal of Membrane Science 130, 193–203. https://doi.org/10.1016/S0376-7388(97)00028-8

Al-Rashdi, B., Somerfield, C., Hilal, N., 2011. Heavy Metals Removal Using Adsorption and Nanofiltration Techniques. Separation & Purification Reviews 40, 209–259. https://doi.org/10.1080/15422119.2011.558165

Al-Shahrani, S.S., Nosier, S.A., El-Shazly, A.H., Abdel-Aziz, M.H., 2020. Effect of surfactants on mass transfer in a bubble column equipped with a horizontal tube bundles. International Communications in Heat and Mass Transfer 113, 104548. https://doi.org/10.1016/j.icheatmasstransfer.2020.104548

Al-Tarazi, M., Bert M. Heesink, A., Versteeg, G.F., 2004. Precipitation of metal sulphides using gaseous hydrogen sulphide: mathematical modelling. Chemical Engineering Science 59, 567–579. https://doi.org/10.1016/j.ces.2003.11.006

Al-Tarazi, M., Heesink, A.B.M., Versteeg, G.F., Azzam, M.O.J., Azzam, K., 2005. Precipitation of CuS and ZnS in a bubble column reactor. AIChE Journal 51, 235–246. https://doi.org/10.1002/aic.10310

Alves, S.S., Orvalho, S.P., Vasconcelos, J.M.T., 2005. Effect of bubble contamination on rise velocity and mass transfer. Chemical Engineering Science 60, 1–9. https://doi.org/10.1016/j.ces.2004.07.053

Al-Wakeel, K.Z., Abd El Monem, H., Khalil, M.M.H., 2015. Removal of divalent manganese from aqueous solution using glycine modified chitosan resin. Journal of Environmental Chemical Engineering 3, 179–186. https://doi.org/10.1016/j.jece.2014.11.022

Alyüz, B., Veli, S., 2009. Kinetics and equilibrium studies for the removal of nickel and zinc from aqueous solutions by ion exchange resins. Journal of Hazardous Materials 167, 482–488. https://doi.org/10.1016/j.jhazmat.2009.01.006

Al-Zoubi, H.S., Al-Thyabat, S.S., 2012. Treatment of a Jordanian Phosphate Mine Wastewater by Hybrid Dissolved Air Flotation and Nanofiltration. Mine Water Environ 31, 214–224. https://doi.org/10.1007/s10230-012-0197-1

Ammar, S.H., Akbar, A.S., 2018. Oilfield produced water treatment in internal-loop airlift reactor using electrocoagulation/flotation technique. Chinese Journal of Chemical Engineering 26, 879–885. https://doi.org/10.1016/j.cjche.2017.07.020

Ammar, S.H., Ibrahim Elaibi, A., Sh. Mohammed, I., 2020. Core/shell Fe3O4@Al2O3-PMo magnetic nanocatalyst for photocatalytic degradation of organic pollutants in an internal

loop airlift reactor. Journal of Water Process Engineering 37, 101240. https://doi.org/10.1016/j.jwpe.2020.101240

Ammar, S.H., Ismail, N.N., Ali, A.D., Abbas, W.M., 2019. Electrocoagulation technique for refinery wastewater treatment in an internal loop split-plate airlift reactor. Journal of Environmental Chemical Engineering 7, 103489. https://doi.org/10.1016/j.jece.2019.103489

Anastasiou, A.D., Passos, A.D., Mouza, A.A., 2013. Bubble columns with fine pore sparger and non-Newtonian liquid phase: Prediction of gas holdup. Chemical Engineering Science 98, 331–338. https://doi.org/10.1016/j.ces.2013.05.006

Anbia, M., Amirmahmoodi, S., 2016. Removal of Hg (II) and Mn (II) from aqueous solution using nanoporous carbon impregnated with surfactants. Arabian Journal of Chemistry 9, S319–S325. https://doi.org/10.1016/j.arabjc.2011.04.004

Ates, A., 2014. Role of modification of natural zeolite in removal of manganese from aqueous solutions. Powder Technology 264, 86–95. https://doi.org/10.1016/j.powtec.2014.05.023

Ates, A., Akgül, G., 2016. Modification of natural zeolite with NaOH for removal of manganese in drinking water. Powder Technology 287, 285–291. https://doi.org/10.1016/j.powtec.2015.10.021

Augier, F., Raimundo, P.M., 2021. Effect of rheology on mass transfer and bubble sizes in a bubble column operated in the heterogeneous regime. The Canadian Journal of Chemical Engineering 99, 1177–1185. https://doi.org/10.1002/cjce.23903

Awwad, N.S., El-Nadi, Y.A., Hamed, M.M., 2013. Successive processes for purification and extraction of phosphoric acid produced by wet process. Chemical Engineering and Processing: Process Intensification 74, 69–74. https://doi.org/10.1016/j.cep.2012.11.009

Aydin, S., Tufekci, N., Arayici, S., Ozturk, I., 2000. Catalytic effects of high Mn(IV) concentrations on Mn(II) oxidation. Water Science and Technology 42, 387–392. https://doi.org/10.2166/wst.2000.0343

Babić, B.M., Milonjić, S.K., Polovina, M.J., Čupić, S., Kaludjerović, B.V., 2002. Adsorption of zinc, cadmium and mercury ions from aqueous solutions on an activated carbon cloth. Carbon 40, 1109–1115. https://doi.org/10.1016/S0008-6223(01)00256-1

Barahoei, M., Hatamipour, M.S., Afsharzadeh, S., 2020. CO2 capturing by chlorella vulgaris in a bubble column photo-bioreactor; Effect of bubble size on CO2 removal and growth rate. Journal of CO2 Utilization 37, 9–19. https://doi.org/10.1016/j.jcou.2019.11.023

Barlak, M.S., Değermenci, N., Cengiz, İ., Ucun Özel, H., Yildiz, E., 2020. Comparison of phenol removal with ozonation in jet loop reactor and bubble column. Journal of Environmental Chemical Engineering 8, 104402. https://doi.org/10.1016/j.jece.2020.104402

Barrera-Díaz, C.E., Balderas-Hernández, P., Bilyeu, B., 2018. Chapter 3 - Electrocoagulation: Fundamentals and Prospectives, in: Martínez-Huitle, C.A., Rodrigo, M.A., Scialdone, O. (Eds.), Electrochemical Water and Wastewater Treatment. Butterworth-Heinemann, pp. 61–76. https://doi.org/10.1016/B978-0-12-813160-2.00003-1

Barta, L., Bradley, D.J., 1983. Interaction model for the volumetric properties of weak electrolytes with application to H3PO4. Journal of Solution Chemistry 12, 631–643. https://doi.org/10.1007/BF00648667

Bavandi, R., Emtyazjoo, M., Saravi, H.N., Yazdian, F., Sheikhpour, M., 2019. Study of capability of nanostructured zero-valent iron and graphene oxide for bioremoval of trinitrophenol from wastewater in a bubble column bioreactor. Electronic Journal of Biotechnology 39, 8–14. https://doi.org/10.1016/j.ejbt.2019.02.003

Becker, P., 1989. Phosphates and phosphoric acid: raw materials, technology, and economics of the wet process. Marcel Dekker, Inc., New York.

Belboom, S., Szöcs, C., Léonard, A., 2015. Environmental impacts of phosphoric acid production using di-hemihydrate process: a Belgian case study. Journal of Cleaner Production 108, 978–986. https://doi.org/10.1016/j.jclepro.2015.06.141

Beltrami, D., Cote, G., Mokhtari, H., Courtaud, B., Moyer, B.A., Chagnes, A., 2014. Recovery of Uranium from Wet Phosphoric Acid by Solvent Extraction Processes. Chem. Rev. 114, 12002–12023. https://doi.org/10.1021/cr5001546

Bendada, A., Meniai, A.-H., Bencheikh, L.M., 2001. Modeling of Phosphoric Acid Purification by Liquid-Liquid Extraction. Chemical Engineering & Technology 24, 1273–1280. https://doi.org/10.1002/1521-4125(200112)24:12<1273::AID-CEAT1273>3.0.CO;2-J

Benredjem, Z., Delimi, R., 2009. Use of extracting agent for decadmiation of phosphate rock. Physics Procedia 2, 1455–1460. https://doi.org/10.1016/j.phpro.2009.11.116

Benredjem, Z., Delimi, R., Khelalfa, A., 2016. Cadmium extraction from phosphate ore. Effect of microwave. Arabian Journal of Chemistry 9, S446–S450. https://doi.org/10.1016/j.arabjc.2011.05.016

Berglund, H.A.L., 1981. A method of purifying phosphoric acid of heavy metal. EP0023195A3.

Besagni, G., Di Pasquali, A., Gallazzini, L., Gottardi, E., Colombo, L.P.M., Inzoli, F., 2017a. The effect of aspect ratio in counter-current gas-liquid bubble columns: Experimental

results and gas holdup correlations. International Journal of Multiphase Flow 94, 53–78. https://doi.org/10.1016/j.ijmultiphaseflow.2017.04.015

Besagni, G., Gallazzini, L., Inzoli, F., 2019. On the scale-up criteria for bubble columns. Petroleum, SI: Experimental & Numerical Study of Multiphase Flow Phenomena and Models in Oil & Gas Industry 5, 114–122. https://doi.org/10.1016/j.petlm.2017.12.005

Besagni, G., Inzoli, F., 2017. The effect of liquid phase properties on bubble column fluid dynamics: Gas holdup, flow regime transition, bubble size distributions and shapes, interfacial areas and foaming phenomena. Chemical Engineering Science 170, 270–296. https://doi.org/10.1016/j.ces.2017.03.043

Besagni, G., Inzoli, F., 2016. Influence of internals on counter-current bubble column hydrodynamics: Holdup, flow regime transition and local flow properties. Chemical Engineering Science 145, 162–180. https://doi.org/10.1016/j.ces.2016.02.019

Besagni, G., Inzoli, F., De Guido, G., Pellegrini, L.A., 2017b. The dual effect of viscosity on bubble column hydrodynamics. Chemical Engineering Science 158, 509–538. https://doi.org/10.1016/j.ces.2016.11.003

Besagni, G., Inzoli, F., De Guido, G., Pellegrini, L.A., 2016. Experimental investigation on the influence of ethanol on bubble column hydrodynamics. Chemical Engineering Research and Design 112, 1–15. https://doi.org/10.1016/j.cherd.2016.06.009

Besagni, G., Inzoli, F., Ziegenhein, T., 2018. Two-Phase Bubble Columns: A Comprehensive Review. Chem. Engineering 2, 13. https://doi.org/10.3390/chemengineering2020013

Bessiere, J., Bruant, M., Jdid, E.A., Blazy, P., 1986. Flottation ionique du cadmium et de l'arsenic par un dithiophosphate dans les solutions concentrées en acide phosphorique. International Journal of Mineral Processing 16, 63–74. https://doi.org/10.1016/0301-7516(86)90075-X

Bhattacharyya, D., Jumawan, A.B., Grieves, R.B., 1979. Separation of Toxic Heavy Metals by Sulfide Precipitation. Separation Science and Technology 14, 441–452. https://doi.org/10.1080/01496397908058096

Bishnoi, N.R., Bajaj, M., Sharma, N., Gupta, A., 2004. Adsorption of Cr(VI) on activated rice husk carbon and activated alumina. Bioresource Technology 91, 305–307. https://doi.org/10.1016/S0960-8524(03)00204-9

Blažej, M., Kiša, M., Markoš, J., 2004. Scale influence on the hydrodynamics of an internal loop airlift reactor. Chemical Engineering and Processing: Process Intensification 43, 1519–1527. https://doi.org/10.1016/j.cep.2004.02.003

Blazy, P., Jdid, E.-A., 2000. Flottation - Mécanismes et réactifs. Techniques de l'Ingénieur J3350 V1, 1–25.

Bolton, J.R., Bircher, K.G., Tumas, W., Tolman, C.A., 2001. Figures-of-merit for the technical development and application of advanced oxidation technologies for both electric- and solar-driven systems (IUPAC Technical Report). Pure and Applied Chemistry 73, 627–637. https://doi.org/10.1351/pac200173040627

Bolton, J.R., Bircher, K.G., Tumas, W., Tolman, C.A., 1996. Figures-of-Merit for the Technical Development and Application of Advanced Oxidation Processes. Journal of Advanced Oxidation Technologies 1, 13–17. https://doi.org/10.1515/jaots-1996-0104

Booker Nicholas Anthony, 1989. Removal of Cadmium from Wet-Process Phosphoric Acid by Cation Exchange. Imperial College of Science and Technology, London.

Bose, A., O'Shea, R., Lin, R., Murphy, J.D., 2022. Optimisation and performance prediction of photosynthetic biogas upgrading using a bubble column. Chemical Engineering Journal 437, 134988. https://doi.org/10.1016/j.cej.2022.134988

Bouaifi, M., Hebrard, G., Bastoul, D., Roustan, M., 2001. A comparative study of gas hold-up, bubble size, interfacial area and mass transfer coefficients in stirred gas–liquid reactors and bubble columns. Chemical Engineering and Processing: Process Intensification 40, 97–111. https://doi.org/10.1016/S0255-2701(00)00129-X

Boulkroune, N., Meniai, A.H., 2012. Modeling Purification of Phosphoric Acid Contaminated with Cadmium by Liquid-liquid Extraction. Energy Procedia 18, 1189–1198. https://doi.org/10.1016/j.egypro.2012.05.134

Boussen, R., 2007. Valorisation de l'acide phosphorique par précipitation du cadmium et pertraction de l'uranium. Université Mohammed V - Agdal Faculté des Sciences, Rabat, Maroc.

Bromley, L.A., 1973. Thermodynamic properties of strong electrolytes in aqueous solutions. AIChE Journal 19, 313–320. https://doi.org/10.1002/aic.690190216

Bryson, A.W., Bijsterveld, C.H., 1991. Kinetics of the precipitation of manganese and cobalt sulphides in the purification of a manganese sulphate electrolyte. Hydrometallurgy 27, 75–84. https://doi.org/10.1016/0304-386X(91)90079-2

Bulatovic, S.M., 2007. Handbook of flotation reagents: chemistry, theory and practice, 1st ed. ed. Elsevier, Amsterdam ; Boston.

Camarasa, E., Vial, C., Poncin, S., Wild, G., Midoux, N., Bouillard, J., 1999. Influence of coalescence behaviour of the liquid and of gas sparging on hydrodynamics and bubble

characteristics in a bubble column. Chemical Engineering and Processing: Process Intensification 38, 329–344. https://doi.org/10.1016/S0255-2701(99)00024-0

Cappelli, D., Glennon, B., Donnellan, P., 2022. Feasibility analysis of using a bubble column evaporator as a solvent swap device. Chemical Thermodynamics and Thermal Analysis 6, 100050. https://doi.org/10.1016/j.ctta.2022.100050

Cerri, M.O., Futiwaki, L., Jesus, C.D.F., Cruz, A.J.G., Badino, A.C., 2008. Average shear rate for non-Newtonian fluids in a concentric-tube airlift bioreactor. Biochemical Engineering Journal 39, 51–57. https://doi.org/10.1016/j.bej.2007.08.009

Chalupa, J., Pocik, O., Halecky, M., Kozliak, E., 2020. Thermophilic waste air treatment of an airborne ethyl acetate/toluene mixture in a bubble column reactor: Stability towards temperature changes. Journal of Hazardous Materials 384, 120744. https://doi.org/10.1016/j.jhazmat.2019.120744

Charerntanyarak, L., 1999. Heavy metals removal by chemical coagulation and precipitation. Water Science and Technology, Chemical process industries and environmental management 39, 135–138. https://doi.org/10.1016/S0273-1223(99)00304-2

Chaumat, H., Billet, A.M., Delmas, H., 2007. Hydrodynamics and mass transfer in bubble column: Influence of liquid phase surface tension. Chemical Engineering Science, 8th International Conference on Gas-Liquid and Gas-Liquid-Solid Reactor Engineering 62, 7378–7390. https://doi.org/10.1016/j.ces.2007.08.077

Chegukrishnamurthi, M., Shahabazuddin, M., Sreevathsan, S., Sarada, R., Mudliar, S.N., 2020. Ozonation as non-thermal option for bacterial load reduction of Chlorella biomass cultivated in airlift photobioreactor. Journal of Cleaner Production 276, 123029. https://doi.org/10.1016/j.jclepro.2020.123029

Chen, J., Ruan, J.-W., Ye, J.-X., Cheng, Z.-W., Chen, D.-Z., 2020. Removal of gaseous tetrahydrofuran via a three-phase airlift bioreactor loaded with immobilized cells of GFP-tagged Pseudomonas oleovorans GDT4. Chemosphere 258, 127148. https://doi.org/10.1016/j.chemosphere.2020.127148

Chen, S., Gong, W., Mei, G., Zhou, Q., Bai, C., Xu, N., 2011. Primary biodegradation of sulfide mineral flotation collectors. Minerals Engineering 24, 953–955. https://doi.org/10.1016/j.mineng.2011.01.003

Chen, W., Tsutsumi, A., Otawara, K., Shigaki, Y., 2003. Local Bubble Dynamics and Macroscopic Flow Structure in Bubble Columns with Different Scales. The Canadian Journal of Chemical Engineering 81, 1139–1148. https://doi.org/10.1002/cjce.5450810603

Chen, Z., Min, H., Hu, D., Wang, H., Zhao, Y., Cui, Y., Zou, X., Wu, P., Ge, H., Luo, K., Zhang, L., Liu, W., 2020. Performance of a novel multiple draft tubes airlift loop membrane bioreactor to treat ampicillin pharmaceutical wastewater under different temperatures. Chemical Engineering Journal 380, 122521. https://doi.org/10.1016/j.cej.2019.122521

Cheng, S., Zhao, S., Guo, H., Xing, B., Liu, Y., Zhang, C., Ma, M., 2022. High-efficiency removal of lead/cadmium from wastewater by MgO modified biochar derived from crofton weed. Bioresource Technology 343, 126081. https://doi.org/10.1016/j.biortech.2021.126081

Cherif, M., Mgaidi, A., Ammar, M.N., Abderrabba, M., Fürst, W., 2000a. Modelling of the equilibrium properties of the system H3PO4–H2O: representation of VLE and liquid phase composition. Fluid Phase Equilibria 175, 197–212. https://doi.org/10.1016/S0378-3812(00)00458-1

Cherif, M., Mgaidi, A., Ammar, N., Vallee, G., Fürst, W., 2000b. A New Investigation of Aqueous Orthophosphoric Acid Speciation Using Raman Spectroscopy. Journal of Solution Chemistry 29, 15.

Chilekar, V.P., van der Schaaf, J., Kuster, B.F.M., Tinge, J.T., Schouten, J.C., 2010. Influence of elevated pressure and particle lyophobicity on hydrodynamics and gas–liquid mass transfer in slurry bubble columns. AIChE Journal 56, 584–596. https://doi.org/10.1002/aic.11987

Chilekar, V.P., Warnier, M.J.F., van der Schaaf, J., Kuster, B.F.M., Schouten, J.C., van Ommen, J.R., 2005. Bubble size estimation in slurry bubble columns from pressure fluctuations. AIChE Journal 51, 1924–1937. https://doi.org/10.1002/aic.10427

Chisti, M.Y., 1989. Airlift bioreactors. Elsevier Applied Science, London; New York.

Chisti, M.Y., Moo-Young, M., 1987. Airlift Reactors: Characteristics, Applications and Design Considerations. Chemical Engineering Communications 60, 195–242. https://doi.org/10.1080/00986448708912017

Chockalingam, E., Subramanian, S., Natarajan, K.A., 2003. Studies on biodegradation of organic flotation collectors using Bacillus polymyxa. Hydrometallurgy 71, 249–256. https://doi.org/10.1016/S0304-386X(03)00163-4

Choi, K.H., Chisti, Y., Moo-Young, M., 1996. Comparative evaluation of hydrodynamic and gas—liquid mass transfer characteristics in bubble column and airlift slurry reactors. The Chemical Engineering Journal and the Biochemical Engineering Journal 62, 223–229. https://doi.org/10.1016/0923-0467(96)03085-0

Choi, K.H., Lee, W.K., 1993. Circulation liquid velocity, gas holdup and volumetric oxygen transfer coefficient in external-loop airlift reactors. Journal of Chemical Technology & Biotechnology 56, 51–58. https://doi.org/10.1002/jctb.280560110

Christensen, J.H., Reed, R.B., 1955. Density of Aqueous Solutions of Phosphoric Acid. INDUSTRIAL AND ENGINEERING CHEMISTRY 47, 1277–1280.

Christensen, S.G., Thomsen, K., 2003. Modeling of Vapor−Liquid−Solid Equilibria in Acidic Aqueous Solutions. Industrial & Engineering Chemistry Research 42, 4260–4268. https://doi.org/10.1021/ie030227d

Cichy, B., Jaroszek, H., Paszek, A., 2014. Cadmium in phosphate fertilizers; ecological and economical aspects. CHEMIK 68, 837–842.

Considine, G.D., 2005. Van Nostrand's encyclopedia of chemistry, 5th ed. John Wiley & Sons, Hoboken, New Jersey.

Contreras, A., García, F., Molinaa, E., Merchuk, J.C., 1999. Influence of sparger on energy dissipation, shear rate, and mass transfer to sea water in a concentric-tube airlift bioreactor. Enzyme and Microbial Technology 25, 820–830. https://doi.org/10.1016/S0141-0229(99)00119-2

Contreras, M., Pérez-López, R., Gázquez, M.J., Morales-Flórez, V., Santos, A., Esquivias, L., Bolívar, J.P., 2015. Fractionation and fluxes of metals and radionuclides during the recycling process of phosphogypsum wastes applied to mineral CO2 sequestration. Waste Management, Urban Mining 45, 412–419. https://doi.org/10.1016/j.wasman.2015.06.046

Cooper, C.M., Fernstrom, G.A., Miller, S.A., 1944. Performance of Agitated Gas-Liquid Contactors. Ind. Eng. Chem 36, 504–509. https://doi.org/10.1021/ie50414a005

Cortina, J.L., Miralles, N., Aguilar, M., Sastre, A.M., 1996. Distribution studies of Zn(II), Cu(II) and Cd(II) with Levextrel resins containing di(2,4,4-trimethylpentyl)phosphonic acid (Lewatit TP807'84). Hydrometallurgy 40, 195–206. https://doi.org/10.1016/0304-386X(94)00078-H

Couvert, A., Bastoul, D., Roustan, M., Chatellier, P., 2004. Hydrodynamic and mass transfer study in a rectangular three-phase air-lift loop reactor. Chemical Engineering and Processing: Process Intensification, Special Issue on Gas-Liquid and Gas-Liquid-Solid Reactor Engineering 43, 1381–1387. https://doi.org/10.1016/j.cep.2003.06.001

Couvert, A., Roustan, M., Chatellier, P., 1999. Two-phase hydrodynamic study of a rectangular air-lift loop reactor with an internal baffle. Chemical Engineering Science 54, 5245–5252. https://doi.org/10.1016/S0009-2509(99)00246-8

Crini, G., Lichtfouse, E., 2019. Advantages and disadvantages of techniques used for wastewater treatment. Environ Chem Lett 17, 145–155. https://doi.org/10.1007/s10311-018-0785-9

Cruz, J.-L., Renon, H., 1978. A new thermodynamic representation of binary electrolyte solutions nonideality in the whole range of concentrations. AIChE Journal 24, 817–830. https://doi.org/10.1002/aic.690240508

da Silva, G.A., Kulay, L.A., 2005. Environmental performance comparison of wet and thermal routes for phosphate fertilizer production using LCA – A Brazilian experience. Journal of Cleaner Production, Life Cycle Assessment 13, 1321–1325. https://doi.org/10.1016/j.jclepro.2005.05.004

Dalas, E., Kallitsis, J., Sakkopoulos, S., Vitoratos, E., Koutsoukos, P.G., 1991. Cadmium sulfide precipitation in aqueous media: Spontaneous precipitation and controlled overgrowth on polyaniline. Journal of Colloid and Interface Science 141, 137–145. https://doi.org/10.1016/0021-9797(91)90309-V

Daneshgar, S., Callegari, A., Capodaglio, A.G., Vaccari, D., 2018. The Potential Phosphorus Crisis: Resource Conservation and Possible Escape Technologies: A Review. Resources 7, 37. https://doi.org/10.3390/resources7020037

Dartiguelongue, A., 2014. Etude de la spéciation de l'uranium(VI) dans les solutions d'acide phosphorique et de sa récupération par extraction liquide-liquide (Theses). ENSTA ParisTech, France.

Dartiguelongue, A., Provost, E., Chagnes, A., Cote, G., Fürst, W., 2016. Experimental Determination and Modeling of the Speciation of Uranium(VI) in Phosphoric Acid Medium. Solvent Extraction and Ion Exchange 34, 241–259. https://doi.org/10.1080/07366299.2016.1169145

Das, S., Mahalingam, H., 2020. Novel immobilized ternary photocatalytic polymer film based airlift reactor for efficient degradation of complex phthalocyanine dye wastewater. Journal of Hazardous Materials 383, 121219. https://doi.org/10.1016/j.jhazmat.2019.121219

Dashtban Kenari, S.L., Barbeau, B., 2016. Size and Zeta Potential of Oxidized Iron and Manganese in Water Treatment: Influence of pH, Ionic Strength, and Hardness. Journal of Environmental Engineering 142, 04016010. https://doi.org/10.1061/(ASCE)EE.1943-7870.0001101

Davies, S.H.R., Morgan, J.J., 1989. Manganese(II) oxidation kinetics on metal oxide surfaces. Journal of Colloid and Interface Science 129, 63–77. https://doi.org/10.1016/0021-9797(89)90416-5

Davister, A., 1996. Studies and research on processes for the elimination of cadmium from phosphoric acid. OECD Proceedings, Paris, Saltsjobaden, Sweden, pp. 21–30.

de Jesus, S.S., Moreira Neto, J., Santana, A., Maciel Filho, R., 2015. Influence of impeller type on hydrodynamics and gas-liquid mass-transfer in stirred airlift bioreactor. AIChE Journal 61, 3159–3171. https://doi.org/10.1002/aic.14871

De Ridder, M., De Jong, S., Polchar, J., Lingemann, S., 2012. Risks and Opportunities in the Global Phosphate Rock Market: Robust Strategies in Times of Uncertainty (No. 17/12/12). The Hague Centre for Strategic Studies, Netherlands.

Deborde, M., von Gunten, U., 2008. Reactions of chlorine with inorganic and organic compounds during water treatment—Kinetics and mechanisms: A critical review. Water Research 42, 13–51. https://doi.org/10.1016/j.watres.2007.07.025

Deckwer, W.D., Hallensleben, J., Popovic, M., 1980a. Exclusion of gas sparger influence on mass transfer in bubble columns. The Canadian Journal of Chemical Engineering 58, 190–197. https://doi.org/10.1002/cjce.5450580209

Deckwer, W.D., Louisi, Y., Zaidi, A., Ralek, M., 1980b. Hydrodynamic Properties of the Fischer-Tropsch Slurry Process. Ind. Eng. Chem. Proc. Des. Dev. 19, 699–708. https://doi.org/10.1021/i260076a032

Deckwer, W.D., Schumpe, A., 1993. Improved tools for bubble column reactor design and scale-up. Chemical Engineering Science 48, 889–911. https://doi.org/10.1016/0009-2509(93)80328-N

Deckwer, W.D., Serpemen, Y., Ralek, M., Schmidt, B., 1981. On the relevance of mass transfer limitations in the Fischer-Tropsch slurry process. Chemical Engineering Science 36, 773–774. https://doi.org/10.1016/0009-2509(81)85092-0

Delnoij, E., Kuipers, J.A.M., 2000. Measurement of gas-liquid two-phase flow in bubble columns using ensemble correlation PIV. Chemical Engineering Science 55, 3385–3395.

Deng, Z., Oraby, E.A., Eksteen, J.J., 2019. The sulfide precipitation behaviour of Cu and Au from their aqueous alkaline glycinate and cyanide complexes. Separation and Purification Technology 218, 181–190. https://doi.org/10.1016/j.seppur.2019.02.056

Deng, Z., Wang, T., Zhang, N., Wang, Z., 2010. Gas holdup, bubble behavior and mass transfer in a 5m high internal-loop airlift reactor with non-Newtonian fluid. Chemical Engineering Journal 160, 729–737. https://doi.org/10.1016/j.cej.2010.03.078

Deo, N., Natarajan, K.A., 1998. Biological removal of some flotation collector reagents from aqueous solutions and mineral surfaces. Minerals Engineering 11, 717–738. https://doi.org/10.1016/S0892-6875(98)00058-2

Direction des études et des prévisions financières, 2018. Note conjoncture (No. 258). Ministère de l'économie et des finances, Morocco.

Dong, G., Wang, H., Yan, Z., Zhang, J., Ji, X., Lin, M., Dahlgren, R.A., Shang, X., Zhang, M., Chen, Z., 2020. Cadmium sulfide nanoparticles-assisted intimate coupling of microbial and photoelectrochemical processes: Mechanisms and environmental applications. Science of The Total Environment 740, 140080. https://doi.org/10.1016/j.scitotenv.2020.140080

Dong, X., Liu, Z., Liu, F., Li, Z., Wei, W., Wang, X., Xu, X., 2019. Effect of liquid phase rheology and gas–liquid interface property on mass transfer characteristics in bubble columns. Chemical Engineering Research and Design 142, 25–33. https://doi.org/10.1016/j.cherd.2018.11.035

Dong, Y., Lin, H., Liu, Q., Huo, H., 2014. Treatment of flotation wastewater using biological activated carbon. J. Cent. South Univ. 21, 3580–3587. https://doi.org/10.1007/s11771-014-2339-z

Drahoš, J., Zahradník, J., Punčochář, M., Fialová, M., Bradka, F., 1991. Effect of operating conditions on the characteristics of pressure fluctuations in a bubble column. Chemical Engineering and Processing: Process Intensification 29, 107–115. https://doi.org/10.1016/0255-2701(91)87019-Y

Drandev, S., Penev, K.I., Karamanev, D., 2016. Study of the hydrodynamics and mass transfer in a rectangular airlift bioreactor. Chemical Engineering Science 146, 180–188. https://doi.org/10.1016/j.ces.2016.02.041

Duan, X., Wang, C., Wang, T., Xie, X., Zhou, X., Ye, Y., 2018. A polysulfone-based anion exchange membrane for phosphoric acid concentration and purification by electro-electrodialysis. Journal of Membrane Science 552, 86–94. https://doi.org/10.1016/j.memsci.2018.02.004

El Araby, R., Hawash, S., El Diwani, G., 2009. Treatment of iron and manganese in simulated groundwater via ozone technology. Desalination 249, 1345–1349. https://doi.org/10.1016/j.desal.2009.05.006

El Azher, N., Gourich, B., Vial, C., Bellhaj, M.S., Bouzidi, A., Barkaoui, M., Ziyad, M., 2005. Influence of alcohol addition on gas hold-up, liquid circulation velocity and mass transfer coefficient in a split-rectangular airlift bioreactor. Biochemical Engineering Journal 23, 161–167. https://doi.org/10.1016/j.bej.2004.12.003

El Azher, N., Gourich, B., Vial, C., Soulami, M.B., Ziyad, M., 2008. Study of ferrous iron oxidation in Morocco drinking water in an airlift reactor. Chemical Engineering and Processing: Process Intensification 47, 1877–1886. https://doi.org/10.1016/j.cep.2007.10.013

El-Didamony, H., Gado, H.S., Awwad, N.S., Fawzy, M.M., Attallah, M.F., 2013. Treatment of phosphogypsum waste produced from phosphate ore processing. Journal of Hazardous Materials 244–245, 596–602. https://doi.org/10.1016/j.jhazmat.2012.10.053

Elleuch, M.B.C., Amor, M.B., Pourcelly, G., 2006. Phosphoric acid purification by a membrane process: Electrodeionization on ion-exchange textiles. Separation and Purification Technology 51, 285–290. https://doi.org/10.1016/j.seppur.2006.02.009

Ellis, D., Bouchard, C., Lantagne, G., 2000. Removal of iron and manganese from groundwater by oxidation and microfiltration. Desalination 130, 255–264. https://doi.org/10.1016/S0011-9164(00)00090-4

Elmore, K.L., Hatfield, J.D., Dunn, R.L., Jones, A.D., 1965. Dissociation of Phosphoric Acid Solutions at 25°C. The Journal of Physical Chemistry 69, 3520–3525. https://doi.org/10.1021/j100894a045

Elmore, K.L., Mason, C.M., Christensen, J.H., 1946. Activity of Orthophosphoric Acid in Aqueous Solution at 25°C from Vapor Pressure Measurements. Journal of the American Chemical Society 68, 2528–2532. https://doi.org/10.1021/ja01216a029

Elyahyaoui, A., Bouhlassa, S., 2001. Extraction of cadmium and iodocadmat species by di(2-ethylhexyl) phosphoric acid from perchloric and phosphoric media. Applied Radiation and Isotopes 54, 921–926. https://doi.org/10.1016/S0969-8043(00)00341-9

Elzoghby, A.A., 2021. Kinetic and equilibrium studies for U(VI) and Cd(II) sorption from commercial phosphoric acid using C100H resin. J Radioanal Nucl Chem 329, 899–911. https://doi.org/10.1007/s10967-021-07832-7

Ennaassia, Et., El Kacemi, K., Kossir, A., Cote, G., 2002. Study of the removal of Cd(II) from phosphoric acid solutions by precipitation of CdS with Na2S. Hydrometallurgy 64, 101–109. https://doi.org/10.1016/S0304-386X(02)00009-9

Esmaeili, A., Guy, C., Chaouki, J., 2015. The effects of liquid phase rheology on the hydrodynamics of a gas–liquid bubble column reactor. Chemical Engineering Science 129, 193–207. https://doi.org/10.1016/j.ces.2015.01.071

Estay, H., Barros, L., Troncoso, E., 2021. Metal Sulfide Precipitation: Recent Breakthroughs and Future Outlooks. Minerals 11, 1385. https://doi.org/10.3390/min11121385

European Commission, 2007. Reference document on Best Available Techniques for the Manufacture of Large Volume Inorganic Chemicals - Ammonia, Acids and Fertilizers. Sevilla, Spain.

European Commission, Joint Research Centre, Institute for Environment and Sustainability, 2011. International reference life cycle data system (ILCD) handbook general guide for life cycle assessment: provisions and action steps. Publications Office, Luxembourg.

European Commission, Joint Research Centre, Institute for Environment and Sustainability, 2010. International Reference Life Cycle Data System (ILCD) Handbook - General guide for Life Cycle Assessment - Detailed guidance, First edition. ed. Publications Office of the European Union, Luxembourg.

European Fertilizer Manufacturer's Association, 2000. Booklet No. 4 of 8: Production of phosphoric acid. EFMA, Belgium.

Fard, M.G., 2020. CFD Modeling of Multiphase Turbulent Flows in a Bubble Column Reactor. Universitat Rovira i Virgili I, Spain.

Feki, M., Fourati, M., Chaabouni, M.M., Ayedi, H.F., 1994. Purification of wet process phosphoric acid by solvent extraction liquid-liquid equilibrium at 25 and 40°C of the system water-phosphoric acid-methylisobutylketone. The Canadian Journal of Chemical Engineering 72, 939–944. https://doi.org/10.1002/cjce.5450720523

Ferreira, A., Rocha, F., Mota, A., Teixeira, J.A., 2017. 8 - Nonmechanically Agitated Bioreactors, in: Larroche, C., Sanromán, M.Á., Du, G., Pandey, A. (Eds.), Current Developments in Biotechnology and Bioengineering. Elsevier, pp. 217–233. https://doi.org/10.1016/B978-0-444-63663-8.00008-2

Food and Agriculture Organization of the United Nations, 2015. World fertilizer trends and outlook to 2018. Rome.

Foucher, S., Battaglia-Brunet, F., Ignatiadis, I., Morin, D., Richalet, G., 1999. Etude de la précipitation de certains métaux, contenus dans des solutions complexes, par l'hydrogène sulfuré (No. BRGM R 40554). Service minier national, France.

Fu, F., Wang, Q., 2011. Removal of heavy metal ions from wastewaters: A review. Journal of Environmental Management 92, 407–418. https://doi.org/10.1016/j.jenvman.2010.11.011

Galera Martínez, M., Pham Minh, D., Nzihou, A., Sharrock, P., 2020. Valorization of calcium carbonate-based solid wastes for the treatment of hydrogen sulfide in a semi-continuous reactor: Part II – Slurry bubble column pilot. Chemical Engineering Journal 390, 124576. https://doi.org/10.1016/j.cej.2020.124576

Gallucci, F., Pacheco Tanaka, A., van Sint Annaland, M., 2019. Ethanol Reforming in Thermally Coupled, Fluidized-Bed, Bubble Column, and Membrane Reactors, in: Ethanol. Elsevier, pp. 355–382. https://doi.org/10.1016/B978-0-12-811458-2.00014-6

Ganesan, P., Lakshmi, J., Sozhan, G., Vasudevan, S., 2013. Removal of manganese from water by electrocoagulation: Adsorption, kinetics and thermodynamic studies. The Canadian Journal of Chemical Engineering 91, 448–458. https://doi.org/10.1002/cjce.21709

Gao, K., Xue, C., Yang, M., Li, L., Qian, P., Gao, Zheng, Gao, Zhigang, Deng, X., 2022. Optimization of light intensity and photoperiod for growing Chlorella sorokiniana on cooking cocoon wastewater in a bubble-column bioreactor. Algal Research 62, 102612. https://doi.org/10.1016/j.algal.2021.102612

García-Abuín, A., Gómez-Díaz, D., Navaza, J.M., Sanjurjo, B., 2010. Effect of surfactant nature upon absorption in a bubble column. Chemical Engineering Science 65, 4484–4490. https://doi.org/10.1016/j.ces.2010.04.009

Garcia-Ochoa, F., Gomez, E., 2009. Bioreactor scale-up and oxygen transfer rate in microbial processes: An overview. Biotechnology Advances 27, 153–176. https://doi.org/10.1016/j.biotechadv.2008.10.006

Garcia-Ochoa, F., Gomez, E., Santos, V.E., Merchuk, J.C., 2010. Oxygen uptake rate in microbial processes: An overview. Biochemical Engineering Journal 49, 289–307. https://doi.org/10.1016/j.bej.2010.01.011

García-Pérez, T., López, J.C., Passos, F., Lebrero, R., Revah, S., Muñoz, R., 2018. Simultaneous methane abatement and PHB production by Methylocystis hirsuta in a novel gas-recycling bubble column bioreactor. Chemical Engineering Journal 334, 691–697. https://doi.org/10.1016/j.cej.2017.10.106

Garrido, A., Pashley, R.M., Ninham, B.W., 2018. Water sterilisation using different hot gases in a bubble column reactor. Journal of Environmental Chemical Engineering 6, 2651–2659. https://doi.org/10.1016/j.jece.2018.04.004

Gemello, L., Plais, C., Augier, F., Cloupet, A., Marchisio, D.L., 2018. Hydrodynamics and bubble size in bubble columns: Effects of contaminants and spargers. Chemical Engineering Science 184, 93–102. https://doi.org/10.1016/j.ces.2018.03.043

Geng, S., Li, Z., Liu, H., Yang, C., Gao, F., He, T., Huang, Q., 2020. Hydrodynamics and mass transfer in a slurry external airlift loop reactor integrating mixing and separation. Chemical Engineering Science 211, 115294. https://doi.org/10.1016/j.ces.2019.115294

Gerke, T.L., Little, B.J., Barry Maynard, J., 2016. Manganese deposition in drinking water distribution systems. Science of The Total Environment 541, 184–193. https://doi.org/10.1016/j.scitotenv.2015.09.054

Gharabaghi, M., Irannajad, M., Azadmehr, A.R., 2012. Selective Sulphide Precipitation of Heavy Metals from Acidic Polymetallic Aqueous Solution by Thioacetamide. Ind. Eng. Chem. Res. 51, 954–963. https://doi.org/10.1021/ie201832x

Gharib, J., Keshavarz Moraveji, M., Davarnejad, R., Malool, M.E., 2013. Hydrodynamics and mass transfer study of aliphatic alcohols in airlift reactors. Chemical Engineering Research and Design 91, 925–932. https://doi.org/10.1016/j.cherd.2012.08.021

Ghofrani, I., Moosavi, A., 2020. Brine elimination by hybridization of a novel brine-recycle bubble-column humidification-dehumidification system with a multiple-effect distillation system. Energy Conversion and Management 217, 113004. https://doi.org/10.1016/j.enconman.2020.113004

Gholami, F., Zinatizadeh, A.A., Zinadini, S., McKay, T., Sibali, L., 2020. An innovative jet loop-airlift bioreactor for simultaneous removal of carbon and nitrogen from soft drink industrial wastewater: Process performance and kinetic evaluation. Environmental Technology & Innovation 19, 100772. https://doi.org/10.1016/j.eti.2020.100772

Gilmour, R., 2013. Phosphoric Acid: Purification, Uses, Technology, and Economics. CRC Press. https://doi.org/10.1201/b16187

Gim-Krumm, M., Quilaqueo, M., Rojas, V., Seriche, G., Ruby-Figueroa, R., Cortés-Arriagada, D., Romero, J., Troncoso, E., Estay, H., 2019. Impact of precipitate characteristics and precipitation conditions on the settling performance of a sulfide precipitation process: An exhaustive characterization of the aggregation behavior. Hydrometallurgy 189, 105150. https://doi.org/10.1016/j.hydromet.2019.105150

Godbole, S.P., Honath, M.F., Shah, Y.T., 1982. Holdup structure in highly viscous Newtonian and non-Newtonian liquids in bubble columns. Chemical Engineering Communications 16, 119–134. https://doi.org/10.1080/00986448208911090

Godbole, S.P., Schumpe, A., Shah, Y.T., Carr, N.L., 1984. Hydrodynamics and mass transfer in non-Newtonian solutions in a bubble column. AIChE Journal 30, 213–220. https://doi.org/10.1002/aic.690300207

Goedkoop, M., Heijungs, R., Huijbregts, M., 2009. A life cycle impact assessment method which comprises harmonized category indicators at the midpoint and the endpoint level -ReCiPe 2008- Report I: Characterisation. Ministry of Housing, Spatial Planning and Environment (VROM), Netherlands.

Gong, C.-K., Xu, X., Yang, Q., 2022. Gas holdup at dynamic equilibrium region of a bubble column: Effect of bubble generator performance. Chemical Engineering Journal 443, 136382. https://doi.org/10.1016/j.cej.2022.136382

González, M.P., Navarro, R., Saucedo, I., Avila, M., Revilla, J., Bouchard, Ch., 2002. Purification of phosphoric acid solutions by reverse osmosis and nanofiltration. Desalination 147, 315–320. https://doi.org/10.1016/S0011-9164(02)00558-1

Gorain, P.C., Paul, I., Bhadoria, P.S., Pal, R., 2019. An integrated approach towards agricultural wastewater remediation with fatty acid production by two cyanobacteria in bubble column photobioreactors. Algal Research 42, 101594. https://doi.org/10.1016/j.algal.2019.101594

Gotfryd, L., Cox, M., 2006. The selective recovery of cadmium(II) from sulfate solutions by a counter-current extraction–stripping process using a mixture of diisopropylsalicylic acid and Cyanex® 471X. Hydrometallurgy 81, 226–233. https://doi.org/10.1016/j.hydromet.2006.01.001

Gourich, B., EL Azher, N., Soulami Bellhaj, M., Delmas, H., Bouzidi, A., Ziyad, M., 2005. Contribution to the study of hydrodynamics and gas–liquid mass transfer in a two- and three-phase split-rectangular airlift reactor. Chemical Engineering and Processing: Process Intensification 44, 1047–1053. https://doi.org/10.1016/j.cep.2004.12.002

Gourich, B., El Azher, N., Vial, C., Soulami, M.B., Ziyad, M., 2006a. Study of Hydrodynamics, Mixing and Gas-Liquid Mass Transfer in a Split-Rectangular Airlift Reactor. The Canadian Journal of Chemical Engineering 84, 539–547. https://doi.org/10.1002/cjce.5450840505

Gourich, B., Vial, C., Essadki, A.H., Allam, F., Belhaj Soulami, M., Ziyad, M., 2006b. Identification of flow regimes and transition points in a bubble column through analysis of differential pressure signal—Influence of the coalescence behavior of the liquid phase. Chemical Engineering and Processing: Process Intensification 45, 214–223. https://doi.org/10.1016/j.cep.2005.09.002

Gourich, B., Vial, Ch., El Azher, N., Belhaj Soulami, M., Ziyad, M., 2008. Influence of hydrodynamics and probe response on oxygen mass transfer measurements in a high aspect ratio bubble column reactor: Effect of the coalescence behaviour of the liquid phase. Biochemical Engineering Journal 39, 1–14. https://doi.org/10.1016/j.bej.2007.08.011

Gregory, D., Carlson, K.H., 2001. Ozonation Of Dissolved Manganese In The Presence Of Natural Organic Matter. Ozone: Science & Engineering 23, 149–159. https://doi.org/10.1080/01919510108961997

Gregory, O.J., Barnett, S.M., Deluise, F.J., 1980. Manganese Removal from Water by a Precipitate Flotation Technique. Separation Science and Technology 15, 1499–1512. https://doi.org/10.1080/01496398008055602

Guinée, J., 2001. Handbook on life cycle assessment — operational guide to the ISO standards. Int J LCA 6, 255–255. https://doi.org/10.1007/BF02978784

Haghtalab, A., Nosrati, M., 1998. Nonrandom factor model for the excess Gibbs free energy of weak electrolytes including phosphoric acid. Fluid Phase Equilibria 152, 43–55. https://doi.org/10.1016/S0378-3812(98)00386-0

Hakkar, M., Ezzahra Arhouni, F., Mahrou, A., Bilal, E., Bertau, M., Roy, A., Steiner, G., Haneklaus, N., Mazouz, H., Boukhair, A., Benjelloun, M., 2021. Enhancing rare earth element transfer from phosphate rock to phosphoric acid using an inexpensive fly ash additive. Minerals Engineering 172, 107166. https://doi.org/10.1016/j.mineng.2021.107166

Hamza, W., Chtara, C., Benzina, M., 2016. Purification of industrial phosphoric acid (54 %) using Fe-pillared bentonite. Environmental Science and Pollution Research 23, 15820–15831. https://doi.org/10.1007/s11356-015-5557-5

Han, M., González, G., Vauhkonen, M., Laari, A., Koiranen, T., 2017. Local gas distribution and mass transfer characteristics in an annulus-rising airlift reactor with non-Newtonian fluid. Chemical Engineering Journal 308, 929–939. https://doi.org/10.1016/j.cej.2016.09.102

Hanna, A.A., Ali, A.F., 2007. Removal of organic matter from crude wet-process phosphoric acid. Journal of Chemical Technology & Biotechnology 55, 205–208. https://doi.org/10.1002/jctb.280550302

Hannachi, A., Habaili, D., Chtara, C., Ratel, A., 2007. Purification of wet process phosphoric acid by solvent extraction with TBP and MIBK mixtures. Separation and Purification Technology 55, 212–216. https://doi.org/10.1016/j.seppur.2006.12.014

Hao, O.J., Davis, A.P., Chang, P.H., 1991. Kinetics of Manganese(II) Oxidation with Chlorine. Journal of Environmental Engineering 117, 359–374. https://doi.org/10.1061/(ASCE)0733-9372(1991)117:3(359)

Hasanen, A., Orivuori, P., Aittamaa, J., 2006. Measurements of local bubble size distributions from various flexible membrane diffusers. Chemical Engineering and Processing: Process Intensification 45, 291–302. https://doi.org/10.1016/j.cep.2005.09.003

Hashemi, S., Macchi, A., Servio, P., 2009. Gas–liquid mass transfer in a slurry bubble column operated at gas hydrate forming conditions. Chemical Engineering Science 64, 3709–3716. https://doi.org/10.1016/j.ces.2009.05.023

Haynes, W.M., 2015. CRC Handbook of Chemistry and Physics, 96th Edition, 96th ed. CRC Press.

Hébrard, G., Zeng, J., Loubière, K., 2009. Effect of surfactants on liquid side mass transfer coefficients: A new insight. Chemical Engineering Journal 148, 132–138. https://doi.org/10.1016/j.cej.2008.08.027

Hegely, L., Roesler, J., Alix, P., Rouzineau, D., Meyer, M., 2017. Absorption methods for the determination of mass transfer parameters of packing internals: A literature review. AIChE Journal 63, 3246–3275. https://doi.org/10.1002/aic.15737

Hikita, H., Asai, S., Tanigawa, K., Segawa, K., Kitao, M., 1981. The volumetric liquid-phase mass transfer coefficient in bubble columns. The Chemical Engineering Journal, An International Journal of Research and Development 22, 61–69. https://doi.org/10.1016/0300-9467(81)85006-X

Hikita, H., Kikukawa, H., 1974. Liquid-phase mixing in bubble columns: Effect of liquid properties. The Chemical Engineering Journal 8, 191–197. https://doi.org/10.1016/0300-9467(74)85024-0

Hinojosa Reyes, L., Saucedo Medina, I., Navarro Mendoza, R., Revilla Vázquez, J., Avila Rodríguez, M., Guibal, E., 2001. Extraction of Cadmium from Phosphoric Acid Using Resins Impregnated with Organophosphorus Extractants. Industrial & Engineering Chemistry Research 40, 1422–1433. https://doi.org/10.1021/ie0005349

Hong, J., Li, X., 2013. Speeding up cleaner production in China through the improvement of cleaner production audit. Journal of Cleaner Production, Special Volume: Sustainable consumption and production for Asia: Sustainability through green design and practice 40, 129–135. https://doi.org/10.1016/j.jclepro.2012.09.024

Hu, D., Zhao, Y., Wang, H., Min, H., Cui, Y., Luo, K., Zhang, L., Liu, W., Zhang, Y., 2020. Multiple draft tubes airlift loop membrane bioreactor as an efficient system for acidic

7-amino cephalosporanic acid (7-ACA) wastewater treatment. Bioresource Technology 304, 123014. https://doi.org/10.1016/j.biortech.2020.123014

Huang, C. P., 1978. Chemical interactions between inorganic and activated carbon, in: Carbon Adsorption Handbook. pp. 281–325.

Huang, C.P., 1978. Chemical interactions between inorganic and activated carbon, in: Carbon Adsorption Handbook. Paul N. Cheremisinoff, Fred Ellerbusch, pp. 281–325.

Huang, S.-D., Wilson, D.J., 1976. Foam Separation of Mercury(II) and Cadmium(II) from Aqueous Systems. Separation Science 11, 215–222. https://doi.org/10.1080/01496397608085316

Hughmark, G.A., 1967. Holdup and Mass Transfer in Bubble Columns. Ind. Eng. Chem. Proc. Des. Dev. 6, 218–220. https://doi.org/10.1021/i260022a011

Huijbregts, M.A.J., Steinmann, Z.J.N., Elshout, P.M.F., Stam, G., Verones, F., Vieira, M.D.M., Hollander, A., Zijp, M., Van Zelm, R., 2016. ReCiPe 2016 A harmonized life cycle impact assessment method at midpoint and endpoint level Report I: Characterization (No. 2016– 0401). National Institute for Public Health and the Environment, Netherlands.

International Energy Agency, 2012. Statistics: electricity and heat for 2011.

International Organization for Standardization (ISO), 2006a. ISO 14040: Environmental Management - Life Cycle Assessment - Principles and Framework.

International Organization for Standardization (ISO), 2006b. ISO 14044: Environmental Management e Life Cycle Assessment e Requirements and Guidelines.

Islam, Md.S., Rahaman, Md.S., Yeum, J.H., 2015. Phosphine-functionalized electrospun poly(vinyl alcohol)/silica nanofibers as highly effective adsorbent for removal of aqueous manganese and nickel ions. Colloids and Surfaces A: Physicochemical and Engineering Aspects 484, 9–18. https://doi.org/10.1016/j.colsurfa.2015.07.023

Jabbar, L.R., Al-Farraji, A., 2022. S-scheme ZIF-8/Ag2S heterojunction photocatalyst for degradation of organic pollutant using batch and external loop airlift reactors. Environmental Nanotechnology, Monitoring & Management 18, 100701. https://doi.org/10.1016/j.enmm.2022.100701

Jaganyi, D., Altaf, M., Wekesa, I., 2013. Synthesis and characterization of whisker-shaped MnO2 nanostructure at room temperature. Appl Nanosci 3, 329–333. https://doi.org/10.1007/s13204-012-0135-3

Jamnongwong, M., Loubière, K., Dietrich, N., Hébrard, G., 2010. Experimental study of oxygen diffusion coefficients in clean water containing salt, glucose or surfactant:

Consequences on the liquid-side mass transfer coefficients. Chemical Engineering Journal 165, 758–768. https://doi.org/10.1016/j.cej.2010.09.040

Jdid, E., Blazy, P., Bessiere, J., 1982. Flotattion ionique de l'uranium contenu dans l'acide phosphorique industriel. Documents B.R.G.M. 61, 317–334.

Jdid, E.A., Blazy, P., Bessiere, J., Floreancig, A., 1987. Process for the purification of wet-process phosphoric acid by removal of cadmium. US4634580A.

Jerroumi, S., Amarine, M., Nour, H., Lekhlif, B., Jamal, J.E., 2020. Removal of nickel through sulfide precipitation and characterization of electroplating wastewater sludge. Water Quality Research Journal 55, 345–357. https://doi.org/10.2166/wqrj.2020.116

Jia, X., Hu, W., Yuan, X., Yu, K., 2015. Effect of surfactant type on interfacial area and liquid mass transfer for CO2 absorption in a bubble column. Chinese Journal of Chemical Engineering 23, 476–481. https://doi.org/10.1016/j.cjche.2014.11.027

Jiang, C., 1996. Thermodynamics of aqueous phosphoric acid solution at 25°C. Chemical Engineering Science 51, 689–693.

Jiang, X., Wu, J., Jin, Z., Yang, S., Shen, L., 2020. Enhancing the removal of H2S from biogas through refluxing of outlet gas in biological bubble-column. Bioresource Technology 299, 122621. https://doi.org/10.1016/j.biortech.2019.122621

Jiao, W., Chen, W., Chang, A.C., Page, A.L., 2012. Environmental risks of trace elements associated with long-term phosphate fertilizers applications: A review. Environmental Pollution 168, 44–53. https://doi.org/10.1016/j.envpol.2012.03.052

Jin, B., Lant, P., 2004. Flow regime, hydrodynamics, floc size distribution and sludge properties in activated sludge bubble column, air-lift and aerated stirred reactors. Chemical Engineering Science 59, 2379–2388. https://doi.org/10.1016/j.ces.2004.01.061

Jin, H., Liu, D., Yang, S., He, G., Guo, Z., Tong, Z., 2004. Experimental Study of Oxygen Mass Transfer Coefficient in Bubble Column with High Temperature and High Pressure. Chemical Engineering & Technology 27, 1267–1272. https://doi.org/10.1002/ceat.200402111

Jin, H., Yang, S., He, G., Liu, D., Tong, Z., Zhu, J., 2014. Gas–Liquid Mass Transfer Characteristics in a Gas–Liquid–Solid Bubble Column under Elevated Pressure and Temperature. Chinese Journal of Chemical Engineering 22, 955–961. https://doi.org/10.1016/j.cjche.2014.06.019

Jin, H., Yang, S., Wang, M., Williams, R.A., 2007. Measurement of Gas Holdup Profiles in A Gas Liquid Cocurrent Bubble Column Using Electrical Resistance Tomography. AIP Conference Proceedings 914, 869–876. https://doi.org/10.1063/1.2747525

Jr, J.F.Z., Clark, D.M., Rafal, M., Scrivner, N.C., 2010. Handbook of Aqueous Electrolyte Thermodynamics: Theory & Application. John Wiley & Sons.

Jusoh, A., Su Shiung, L., Ali, N., Noor, M.J.M.M., 2007. A simulation study of the removal efficiency of granular activated carbon on cadmium and lead. Desalination 206, 9–16. https://doi.org/10.1016/j.desal.2006.04.048

Kabay, N., Demircioğlu, M., Ekinci, H., Yüksel, M., Sağlam, M., Akçay, M., Streat, M., 1998a. Removal of Metal Pollutants (Cd(II) and Cr(III)) from Phosphoric Acid Solutions by Chelating Resins Containing Phosphonic or Diphosphonic Groups†. Ind. Eng. Chem. Res. 37, 2541–2547.

Kabay, N., Demircioğlu, M., Ekinci, H., Yüksel, M., Sağlam, M., Streat, M., 1998b. Extraction of Cd(II) and Cu(II) from phosphoric acid solutions by solvent-impregnated resins (SIR) containing cyanex 302. Reactive and Functional Polymers 38, 219–226. https://doi.org/10.1016/S1381-5148(98)00034-0

Kang, K.C., Kim, S.S., Choi, J.W., Kwon, S.H., 2008. Sorption of $Cu^{2+}$ and $Cd^{2+}$ onto acid- and base-pretreated granular activated carbon and activated carbon fiber samples. Journal of Industrial and Engineering Chemistry 14, 131–135. https://doi.org/10.1016/j.jiec.2007.08.007

Kang, S.-Y., Lee, J.-U., Moon, S.-H., Kim, K.-W., 2004. Competitive adsorption characteristics of $Co^{2+}$, $Ni^{2+}$, and $Cr^{3+}$ by IRN-77 cation exchange resin in synthesized wastewater. Chemosphere 56, 141–147. https://doi.org/10.1016/j.chemosphere.2004.02.004

Kang, Y., Cho, Y.J., Woo, K.J., Kim, S.D., 1999. Diagnosis of bubble distribution and mass transfer in pressurized bubble columns with viscous liquid medium. Chemical Engineering Science 54, 4887–4893. https://doi.org/10.1016/S0009-2509(99)00209-2

Kantarci, N., Borak, F., Ulgen, K.O., 2005. Bubble column reactors. Process Biochemistry 40, 2263–2283. https://doi.org/10.1016/j.procbio.2004.10.004

Katsoyiannis, I.A., Zouboulis, A.I., 2004. Application of biological processes for the removal of arsenic from groundwaters. Water Research 38, 17–26. https://doi.org/10.1016/j.watres.2003.09.011

Kauwenbergh, S.J.V., 1997. Cadmium and other minor elements in world resources of phosphate rock. Proceedings - Fertiliser Society (United Kingdom) 1–40.

Kauwenbergh, V., 2001. Cadmium and other potential hazards. Fertilizer International 51–69.

Kawase, Y., Moo-Young, M., 1987. Theoretical prediction of gas hold-up in bubble columns with Newtonian and non-Newtonian fluids. Ind. Eng. Chem. Res. 26, 933–937. https://doi.org/10.1021/ie00065a014

Kawase, Y., Umeno, S., Kumagai, T., 1992. The prediction of gas hold-up in bubble column reactors: Newtonian and non-Newtonian fluids. The Chemical Engineering Journal 50, 1–7. https://doi.org/10.1016/0300-9467(92)80001-Q

Kaya, A., Ören, A.H., 2005. Adsorption of zinc from aqueous solutions to bentonite. Journal of Hazardous Materials 125, 183–189. https://doi.org/10.1016/j.jhazmat.2005.05.027

Kelkar, B.G., Godbole, S.P., Honath, M.F., Shah, Y.T., Carr, N.L., Deckwer, W.-D., 1983. Effect of addition of alcohols on gas holdup and backmixing in bubble columns. AIChE J. 29, 361–369. https://doi.org/10.1002/aic.690290303

Kernebeek, H.R.J. van, Oosting, S.J., Ittersum, M.K. van, Ripoll-Bosch, R., Boer, I.J.M. de, 2018. Closing the phosphorus cycle in a food system: insights from a modelling exercise. animal 12, 1755–1765. https://doi.org/10.1017/S1751731118001039

Kessick, M.A., Morgan, J.J., 1975. Mechanism of autoxidation of manganese in aqueous solution. Environ. Sci. Technol. 9, 157–159. https://doi.org/10.1021/es60100a008

Khaless, K., 2006. Procédé de purification de l'acide phosphorique industriel avec introduction d'opération à membrane pour éliminer les impuretés contaminantes. Université de Rennes 1, Université Mohammed V Rabat.

Khobragade, M.U., Pal, A., 2014. Investigation on the adsorption of Mn(II) on surfactant-modified alumina: Batch and column studies. Journal of Environmental Chemical Engineering 2, 2295–2305. https://doi.org/10.1016/j.jece.2014.10.008

Kilonzo, P.M., Margaritis, A., Bergougnou, M.A., 2010. Hydrodynamics and mass transfer characteristics in an inverse internal loop airlift-driven fibrous-bed bioreactor. Chemical Engineering Journal 157, 146–160. https://doi.org/10.1016/j.cej.2009.11.023

Kilonzo, P.M., Margaritis, A., Bergougnou, M.A., Yu, J., Ye, Q., 2007. Effects of geometrical design on hydrodynamic and mass transfer characteristics of a rectangular-column airlift bioreactor. Biochemical Engineering Journal 34, 279–288. https://doi.org/10.1016/j.bej.2006.12.014

Kind, M., 2002. Colloidal aspects of precipitation processes. Chemical Engineering Science, Particulate Processes 57, 4287–4293. https://doi.org/10.1016/S0009-2509(02)00345-7

Kirkpatrick, R.D., Lockett, M.J., 1974. The influence of approach velocity on bubble coalescence. Chemical Engineering Science 29, 2363–2373. https://doi.org/10.1016/0009-2509(74)80013-8

Koide, K., Yamazoe, S., Harada, S., 1985. Effects of surface-active substances on gas holdup and gas-liquid mass transfer in bubble column. J. Chem. Eng. Japan / JCEJ 18, 287–292. https://doi.org/10.1252/jcej.18.287

Kojić, P.S., Tokić, M.S., Šijački, I.M., Lukić, N.Lj., Petrović, D.Lj., Jovičević, D.Z., Popović, S.S., 2015. Influence of the Sparger Type and Added Alcohol on the Gas Holdup of an External-Loop Airlift Reactor. Chemical Engineering & Technology 38, 701–708. https://doi.org/10.1002/ceat.201400578

Kolthoff, I.M., Moltzau, D.R., 1935. Induced Precipitation and Properties of Metal Sulfides. Chemical reviews 17, 293–325. https://doi.org/10.1021/cr60058a001

Kononova, O.N., Bryuzgina, G.L., Apchitaeva, O.V., Kononov, Y.S., 2019. Ion exchange recovery of chromium (VI) and manganese (II) from aqueous solutions. Arabian Journal of Chemistry 12, 2713–2720. https://doi.org/10.1016/j.arabjc.2015.05.021

Kononova, O.N., Bryuzgina, G.L., Apchitaeva, O.V., Kononov, Y.S., 2015. Ion exchange recovery of chromium (VI) and manganese (II) from aqueous solutions. Arabian Journal of Chemistry 12, 2713–2720. https://doi.org/10.1016/j.arabjc.2015.05.021

Kontogeorgis, G.M., Folas, G.K., 2010. Thermodynamic Models for Industrial Applications. John Wiley & Sons, Ltd, Chichester, UK. https://doi.org/10.1002/9780470747537

Korpijarvi, J., Oinas, P., Reunanen, J., 1999. Hydrodynamics and mass transfer in an airlift reactor. Chemical Engineering Science 54, 2255–2262. https://doi.org/10.1016/S0009-2509(98)00439-4

Kossir, A., Chik, A., 1996. Promoting the development and semi-industrial application of a potentially high performing process for cadmium removal from phosphate rock. OECD Proceedings, Paris, Saltsjobaden, Sweden, pp. 41–44.

Kouzbour, S., Gourich, B., Gros, F., Vial, C., Allam, F., Stiriba, Y., 2019. Comparative analysis of industrial processes for cadmium removal from phosphoric acid: A review. Hydrometallurgy 188, 222–247. https://doi.org/10.1016/j.hydromet.2019.06.014

Kováts, P., Thévenin, D., Zähringer, K., 2020. Influence of viscosity and surface tension on bubble dynamics and mass transfer in a model bubble column. International Journal of Multiphase Flow 123, 103174. https://doi.org/10.1016/j.ijmultiphaseflow.2019.103174

Krishna, R., Urseanu, M.I., Dreher, A.J., 2000. Gas hold-up in bubble columns: influence of alcohol addition versus operation at elevated pressures. Chemical Engineering and Processing: Process Intensification 39, 371–378. https://doi.org/10.1016/S0255-2701(00)00093-3

Krishna, R., Wilkinson, P.M., Van Dierendonck, L.L., 1991. A model for gas holdup in bubble columns incorporating the influence of gas density on flow regime transitions. Chemical Engineering Science 46, 2491–2496. https://doi.org/10.1016/0009-2509(91)80042-W

Kumar, A., Degaleesan, T.E., Laddha, G.S., Hoelscher, H.E., 1976. Bubble swarm characteristics in bubble columns. Can. J. Chem. Eng. 54, 503–508. https://doi.org/10.1002/cjce.5450540525

Kumar, K., Das, D., 2012. Growth characteristics of Chlorella sorokiniana in airlift and bubble column photobioreactors. Bioresource Technology 116, 307–313. https://doi.org/10.1016/j.biortech.2012.03.074

Kumar, M., Nandi, M., Pakshirajan, K., 2021. Recent advances in heavy metal recovery from wastewater by biogenic sulfide precipitation. Journal of Environmental Management 278, 111555. https://doi.org/10.1016/j.jenvman.2020.111555

Kumar, N., Bansal, A., Gupta, R., 2018. Shear rate and mass transfer coefficient in internal loop airlift reactors involving non-Newtonian fluids. Chemical Engineering Research and Design 136, 315–323. https://doi.org/10.1016/j.cherd.2018.05.042

Kurniawan, T.A., Chan, G.Y.S., Lo, W., Babel, S., 2006. Comparisons of low-cost adsorbents for treating wastewaters laden with heavy metals. Science of The Total Environment 366, 409–426. https://doi.org/10.1016/j.scitotenv.2005.10.001

Lakhdissi, E.M., 2020. Hydrodynamics and Mass Transfer of Two-Phase and Three-Phase Bubble Column Reactors (phd). Polytechnique Montréal.

Lakhdissi, E.M., Fallahi, A., Guy, C., Chaouki, J., 2020. Effect of solid particles on the volumetric gas liquid mass transfer coefficient in slurry bubble column reactors. Chemical Engineering Science 227, 115912. https://doi.org/10.1016/j.ces.2020.115912

Lanson, B., Drits, V.A., Silvester, E., Manceau, A., 2000. Structure of H-exchanged hexagonal birnessite and its mechanism of formation from Na-rich monoclinic buserite at low pH. American Mineralogist 85, 826–838. https://doi.org/10.2138/am-2000-5-625

Lau, R., Peng, W., Velazquez-Vargas, L.G., Yang, G.Q., Fan, L.-S., 2004. Gas−Liquid Mass Transfer in High-Pressure Bubble Columns. Ind. Eng. Chem. Res. 43, 1302–1311. https://doi.org/10.1021/ie030416w

LCIA: the ReCiPe model - RIVM [WWW Document], n.d. URL https://www.rivm.nl/en/Topics/L/Life_Cycle_Assessment_LCA/ReCiPe (accessed 7.17.18).

Leal Pérez, B.J., Medrano Jiménez, J.A., Bhardwaj, R., Goetheer, E., van Sint Annaland, M., Gallucci, F., 2021. Methane pyrolysis in a molten gallium bubble column reactor for sustainable hydrogen production: Proof of concept & techno-economic assessment. International Journal of Hydrogen Energy 46, 4917–4935. https://doi.org/10.1016/j.ijhydene.2020.11.079

Leonard, C., Ferrasse, J.-H., Boutin, O., Lefevre, S., Viand, A., 2015. Bubble column reactors for high pressures and high temperatures operation. Chemical Engineering Research and Design 100, 391–421. https://doi.org/10.1016/j.cherd.2015.05.013

Leonard, C., Ferrasse, J.-H., Lefevre, S., Viand, A., Boutin, O., 2021. Bubble rising velocity and bubble size distribution in columns at high pressure and temperature: From lab scale experiments to design parameters. Chemical Engineering Research and Design 173, 108–118. https://doi.org/10.1016/j.cherd.2021.07.003

Leonard, C., Ferrasse, J.-H., Lefevre, S., Viand, A., Boutin, O., 2019. Gas hold up in bubble column at high pressure and high temperature. Chemical Engineering Science 200, 186–202. https://doi.org/10.1016/j.ces.2019.01.055

Letzel, H.M., Schouten, J.C., Krishna, R., van den Bleek, C.M., 1999. Gas holdup and mass transfer in bubble column reactors operated at elevated pressure. Chemical Engineering Science 54, 2237–2246. https://doi.org/10.1016/S0009-2509(98)00418-7

Lewis, A., 2017. Precipitation of Heavy Metals, in: Rene, E.R., Sahinkaya, E., Lewis, A., Lens, P.N.L. (Eds.), Sustainable Heavy Metal Remediation: Volume 1: Principles and Processes, Environmental Chemistry for a Sustainable World. Springer International Publishing, Cham, pp. 101–120. https://doi.org/10.1007/978-3-319-58622-9_4

Lewis, A.E., 2010. Review of metal sulphide precipitation. Hydrometallurgy 104, 222–234. https://doi.org/10.1016/j.hydromet.2010.06.010

Li, C., 2018. Modeling and optimization of industrial Fischer–Tropsch synthesis with the slurry bubble column reactor and iron-based catalyst. Chinese Journal of Chemical Engineering 26, 1102–1109. https://doi.org/10.1016/j.cjche.2018.01.002

Li, M., Kuang, S., Kang, Y., Ma, H., Dong, J., Guo, Z., 2022. Recent advances in application of iron-manganese oxide nanomaterials for removal of heavy metals in the aquatic environment. Science of The Total Environment 819, 153157. https://doi.org/10.1016/j.scitotenv.2022.153157

Li, M., Zhou, M., Tan, C., Tian, X., 2019. Enhancement of CO2 biofixation and bioenergy generation using a novel airlift type photosynthetic microbial fuel cell. Bioresource Technology 272, 501–509. https://doi.org/10.1016/j.biortech.2018.10.078

Li, M., Zhou, M., Tian, X., Tan, C., Gu, T., 2021. Enhanced bioenergy recovery and nutrient removal from swine wastewater using an airlift-type photosynthetic microbial fuel cell. Energy 226, 120422. https://doi.org/10.1016/j.energy.2021.120422

Li, Y., Feng, K., Wu, C., Mei, J., Zhang, S., Ye, J., Chen, Jianmeng, Zhao, J., Chen, Jianrong, 2022. Mass transfer and reaction simultaneously enhanced airlift microbial electrolytic

cell system with high gaseous o-xylene removal capacity. Chemosphere 291, 132888. https://doi.org/10.1016/j.chemosphere.2021.132888

Lin, J., Han, M., Wang, T., Zhang, T., Wang, J., Jin, Y., 2004. Influence of the gas distributor on the local hydrodynamic behavior of an external loop airlift reactor. Chemical Engineering Journal 102, 51–59. https://doi.org/10.1016/j.cej.2004.01.023

Lin, S., 2002. Heavy metal removal from water by sorption using surfactant-modified montmorillonite. Journal of Hazardous Materials 92, 315–326. https://doi.org/10.1016/S0304-3894(02)00026-2

Lin, T.-J., Juang, R.-C., Chen, Y.-C., Chen, C.-C., 2001. Predictions of flow transitions in a bubble column by chaotic time series analysis of pressure fluctuation signals. Chemical Engineering Science, 16th International Conference on Chemical Reactor Engineering 56, 1057–1065. https://doi.org/10.1016/S0009-2509(00)00322-5

Lin, T.-J., Tsuchiya, K., Fan, L.-S., 1998. Bubble flow characteristics in bubble columns at elevated pressure and temperature. AIChE Journal 44, 545–560. https://doi.org/10.1002/aic.690440306

Liu, G., Yang, X., Zhong, H., 2017. Molecular design of flotation collectors: A recent progress. Advances in Colloid and Interface Science 246, 181–195. https://doi.org/10.1016/j.cis.2017.05.008

Liu, Y., Li, Y., Xu, H., Xu, J., 2019. Oxidation removal of gaseous Hg0 using enhanced-Fenton system in a bubble column reactor. Fuel 246, 358–364. https://doi.org/10.1016/j.fuel.2019.03.018

Liu, Z., Yang, X., Demeestere, K., Van Hulle, S., 2021. Insights into a packed bubble column for removal of several ozone-persistent TrOCs by ozonation: removal kinetics, energy efficiency and elimination prediction. Separation and Purification Technology 275, 119170. https://doi.org/10.1016/j.seppur.2021.119170

Lizon, T.G., Ortiz, E.S.P. de, 1997. Separation of cadmium from phosphoric acid containing $Cu^{2+}$ and $Cd^{2+}$ using surfactant liquid membranes. Begel House Inc., Turkey, pp. 1–10. https://doi.org/10.1615/ICHMT.1997.IntSymLiqTwoPhaseFlowTranspPhen.290

Loubière, K., Hébrard, G., 2004. Influence of liquid surface tension (surfactants) on bubble formation at rigid and flexible orifices. Chemical Engineering and Processing: Process Intensification, Special Issue on Gas-Liquid and Gas-Liquid-Solid Reactor Engineering 43, 1361–1369. https://doi.org/10.1016/j.cep.2004.03.009

Lu, J., Corvalan, C.M., Chew, Y.M.J., Huang, J.-Y., 2019. Coalescence of small bubbles with surfactants. Chemical Engineering Science 196, 493–500. https://doi.org/10.1016/j.ces.2018.11.002

Lu, X., Ding, J., Wang, Y., Shi, J., 2000. Comparison of the hydrodynamics and mass transfer characteristics of a modified square airlift reactor with common airlift reactors. Chemical Engineering Science 55, 2257–2263. https://doi.org/10.1016/S0009-2509(99)00473-X

Luo, L., Liu, F., Xu, Y., Yuan, J., 2011. Hydrodynamics and mass transfer characteristics in an internal loop airlift reactor with different spargers. Chemical Engineering Journal 175, 494–504. https://doi.org/10.1016/j.cej.2011.09.078

Luo, L., Yan, Y., Xie, P., Sun, J., Xu, Y., Yuan, J., 2012. Hilbert–Huang transform, Hurst and chaotic analysis based flow regime identification methods for an airlift reactor. Chemical Engineering Journal 181–182, 570–580. https://doi.org/10.1016/j.cej.2011.11.093

Maalej, S., Benadda, B., Otterbein, M., 2003. Interfacial area and volumetric mass transfer coefficient in a bubble reactor at elevated pressures. Chemical Engineering Science 58, 2365–2376. https://doi.org/10.1016/S0009-2509(03)00085-X

Magalhães, I.B., Ferreira, J., Castro, J. de S., Assis, L.R. de, Calijuri, M.L., 2022. Agro-industrial wastewater-grown microalgae: A techno-environmental assessment of open and closed systems. Science of The Total Environment 834, 155282. https://doi.org/10.1016/j.scitotenv.2022.155282

Manjrekar, O.N., Dudukovic, M.P., 2019. Identification of flow regime in a bubble column reactor with a combination of optical probe data and machine learning technique. Chemical Engineering Science: X 2, 100023. https://doi.org/10.1016/j.cesx.2019.100023

Manjrekar, O.N., Hamed, M., Dudukovic, M.P., 2018. Gas hold-up and mass transfer in a pilot scale bubble column with and without internals. Chemical Engineering Research and Design 135, 166–174. https://doi.org/10.1016/j.cherd.2018.05.008

Martín, M., Montes, F.J., Galán, M.A., 2008. Mass Transfer Rates from Oscillating Bubbles in Bubble Columns Operating with Viscous Fluids. Ind. Eng. Chem. Res. 47, 9527–9536. https://doi.org/10.1021/ie801077s

Matis, K.A., Mavros, P., 1991. Recovery of Metals by Ion Flotation from Dilute Aqueous Solutions. Separation and Purification Methods 20, 1–48. https://doi.org/10.1080/03602549108021407

McLaughlin, M.J., Singh, B.R., 1999. Cadmium in Soils and Plants. Springer Netherlands, Dordrecht.

Mecibah, W., 2013. Elimination des métaux lourds de l'acide phosphorique par un procédé membranaire. Université de Badji Mokhtar Annaba, Algérie.

Mecibah, W., Delimi, R., Gabli, M., 2012. Elimination du cadmium de l'acide phosphorique par électrodialyse 7.

Melesse, A.G., Velmurugan, N., Shanmugham Venkatachalam, S., Pothanamkandathil Chacko, S., Demissie, B.A., 2020. Startup of granulation of sludge in sequencing batch airlift reactor for simultaneous removal of nitrogen and organic carbon from tannery wastewater. Journal of Water Process Engineering 38, 101605. https://doi.org/10.1016/j.jwpe.2020.101605

Mellah, A., Bauer, D., 1995. The extraction of titanium, chromium and cadmium from phosphoric acid solutions by p- (1 ,1, 3, 3-tetramethyl butyl) phenyl phosphoric acid in kerosene diluent. Hydrometallurgy 37, 117–121. https://doi.org/10.1016/0304-386X(93)E0081-X

Mellah, A., Benachour, D., 2007a. The solvent extraction of zinc, cadmium and chromium from phosphoric acid solutions by tri-n butyl phosphate in kerosene diluent. Separation and Purification Technology 56, 220–224. https://doi.org/10.1016/j.seppur.2007.01.037

Mellah, A., Benachour, D., 2007b. Adsorption of heavy metals from industrial phosphoric acid by Algerian activated bentonlte. Modeling, in: Annales de Chimie Science Des Matériaux. Lavoisier, France, pp. 487–504.

Mellah, A., Benachour, D., 2006a. Solvent extraction of heavy metals contained in phosphoric acid solutions by 7-(4-ethyl-1-methyloctyl)-8-hydroxyquinoline in kerosene diluent. Hydrometallurgy 81, 100–103. https://doi.org/10.1016/j.hydromet.2005.10.005

Mellah, A., Benachour, D., 2006b. The solvent extraction of zinc and cadmium from phosphoric acid solution by di-2-ethyl hexyl phosphoric acid in kerosene diluent. Chemical Engineering and Processing: Process Intensification 45, 684–690. https://doi.org/10.1016/j.cep.2006.02.004

Mendes, C.E., Badino, A.C., 2016. Hydrodynamics of Newtonian and non-Newtonian liquids in internal-loop airlift reactors. Biochemical Engineering Journal 109, 137–152. https://doi.org/10.1016/j.bej.2016.01.007

Mendes, C.E., Badino, A.C., 2015. Oxygen transfer in different pneumatic bioreactors containing viscous Newtonian fluids. Chemical Engineering Research and Design 94, 456–465. https://doi.org/10.1016/j.cherd.2014.09.002

Menoyo, B., Elizalde, M.P., Almela, A., 2001. Extraction of lead by Cyanex 302 from acid phosphoric media. Solvent Extraction and Ion Exchange 19, 677–698. https://doi.org/10.1081/SEI-100103815

Menzel, K., Barros, L., García, A., Ruby-Figueroa, R., Estay, H., 2021. Metal sulfide precipitation coupled with membrane filtration process for recovering copper from acid mine drainage. Separation and Purification Technology 270, 118721. https://doi.org/10.1016/j.seppur.2021.118721

Merchuk, J. c., Gluz, M., 2002. Bioreactors, Air-lift Reactors, in: Encyclopedia of Bioprocess Technology. John Wiley & Sons, Ltd. https://doi.org/10.1002/0471250589.ebt029

Merchuk, J.C., 2003. Airlift Bioreactors: Review of Recent Advances. The Canadian Journal of Chemical Engineering 81, 324–337. https://doi.org/10.1002/cjce.5450810301

Messnaoui, B., Bounahmidi, T., 2005. Modeling of excess properties and vapor–liquid equilibrium of the system H3PO4–H2O. Fluid Phase Equilibria 237, 77–85. https://doi.org/10.1016/j.fluid.2005.08.002

Milligan, W.O., 2002. The Color and Crystal Structure of Precipitated Cadmium Sulfide. The Journal of Physical Chemistry. https://doi.org/10.1021/j150357a009

Mirón, A.S., Camacho, F.G., Gómez, A.C., Grima, E.M., Chisti, Y., 2000. Bubble-column and airlift photobioreactors for algal culture. AIChE Journal 46, 1872–1887. https://doi.org/10.1002/aic.690460915

Mohamadnia, S., Tavakoli, O., Faramarzi, M.A., 2022. Production of fucoxanthin from the microalga Tisochrysis lutea in the bubble column photobioreactor applying mass transfer coefficient. Journal of Biotechnology 348, 47–54. https://doi.org/10.1016/j.jbiotec.2022.03.009

Mohammadzade Fard, S., Farsi, M., Rahimpour, M.R., 2021. Optimization of ethylene dimerization in a bubble column reactor based on coupling kinetic and equilibrium models. Chemical Engineering Research and Design 174, 357–364. https://doi.org/10.1016/j.cherd.2021.07.030

Mokhtari, M., Chaouki, J., 2021. Effect of solid loading and particle size on the phase holdup distribution and bubble behaviour in a pilot-scale slurry bubble column. Chemical Engineering Science 243, 116732. https://doi.org/10.1016/j.ces.2021.116732

Mokone, T.P., van Hille, R.P., Lewis, A.E., 2012. Metal sulphides from wastewater: Assessing the impact of supersaturation control strategies. Water Research 46, 2088–2100. https://doi.org/10.1016/j.watres.2012.01.027

Mokone, T.P., van Hille, R.P., Lewis, A.E., 2010. Effect of solution chemistry on particle characteristics during metal sulfide precipitation. Journal of Colloid and Interface Science 351, 10–18. https://doi.org/10.1016/j.jcis.2010.06.027

Monser, L., Ben Amor, M., Ksibi, M., 1999. Purification of wet phosphoric acid using modified activated carbon. Chemical Engineering and Processing: Process Intensification 38, 267–271. https://doi.org/10.1016/S0255-2701(99)00008-2

Montoya, G., Lucas, D., Baglietto, E., Liao, Y., 2016. A review on mechanisms and models for the churn-turbulent flow regime. Chemical Engineering Science 141, 86–103. https://doi.org/10.1016/j.ces.2015.09.011

Moraveji, M.K., Mohsenzadeh, E., Fakhari, M.E., Davarnejad, R., 2012a. Effects of surface active agents on hydrodynamics and mass transfer characteristics in a split-cylinder airlift bioreactor with packed bed. Chemical Engineering Research and Design 90, 899–905. https://doi.org/10.1016/j.cherd.2011.10.008

Moraveji, M.K., Pasand, M.M., Davarnejad, R., Chisti, Y., 2012b. Effects of surfactants on hydrodynamics and mass transfer in a split-cylinder airlift reactor. The Canadian Journal of Chemical Engineering 90, 93–99. https://doi.org/10.1002/cjce.20516

Moraveji, M.K., Sajjadi, B., Davarnejad, R., 2011. Gas-Liquid Hydrodynamics and Mass Transfer in Aqueous Alcohol Solutions in a Split-Cylinder Airlift Reactor. Chemical Engineering & Technology 34, 465–474. https://doi.org/10.1002/ceat.201000373

Morgan, J.J., Stumm, W., 1964. Colloid-chemical properties of manganese dioxide. Journal of Colloid Science 19, 347–359. https://doi.org/10.1016/0095-8522(64)90036-4

Mouza, A.A., Dalakoglou, G.K., Paras, S.V., 2005. Effect of liquid properties on the performance of bubble column reactors with fine pore spargers. Chemical Engineering Science 60, 1465–1475. https://doi.org/10.1016/j.ces.2004.10.013

Mthombeni, N.H., Mbakop, S., Onyango, M.S., 2016. Adsorptive Removal of Manganese from Industrial and Mining Wastewater. Proceedings of the Sustainable Research and Innovation Conference 36–45.

Mudde, R.F., 2005. Gravity-driven bubbly flows. Annu. Rev. Fluid Mech. 37, 393–423. https://doi.org/10.1146/annurev.fluid.37.061903.175803

Mudde, R.F., Harteveld, W.K., van den Akker, H.E.A., 2009. Uniform Flow in Bubble Columns. Ind. Eng. Chem. Res. 48, 148–158. https://doi.org/10.1021/ie8000748

Mukhopadhyay, A., Duttagupta, S., Mukherjee, A., 2022. Emerging organic contaminants in global community drinking water sources and supply: A review of occurrence,

processes and remediation. Journal of Environmental Chemical Engineering 10, 107560. https://doi.org/10.1016/j.jece.2022.107560

Mulder, M., 1998. Basic principles of membrane technology, 2nd edition. ed. Springer, Kluwer Academic, Netherlands.

Mylarappa, M., Lakshmi, V.V., Mahesh, K.R.V., Nagaswarupa, H.P., Raghavendra, N., 2016. A facile hydrothermal recovery of nano sealed MnO2 particle from waste batteries: An advanced material for electrochemical and environmental applications. IOP Conf. Ser.: Mater. Sci. Eng. 149, 012178. https://doi.org/10.1088/1757-899X/149/1/012178

Naidoo, N., Pauck, W.J., Carsky, M., 2021. Effects of sparger design on the gas holdup and mass transfer in a pilot scale external loop airlift reactor. South African Journal of Chemical Engineering 37, 127–134. https://doi.org/10.1016/j.sajce.2021.05.009

Nakanoh, M., Yoshida, F., 1980. Gas Absorption by Newtonian and Non-Newtonian Liquids in a Bubble Column. Ind. Eng. Chem. Process Des. Dev. 19, 190–195. https://doi.org/10.1021/i260073a033

Nandi, S., Jaju, S.J., 2015. Hydrodynamics of Pilot Plant Scale Airlift Reactor in Presence of Alcohols. Polish Journal of Chemical Technology 118–123. https://doi.org/10.1515/pjct-2015-0059

Nazari, K., Ghadiri, A., Babaie, H., 2005. Elimination of cadmium from wet process phosphoric acid with Alamine 336. Minerals Engineering 18, 1233–1238. https://doi.org/10.1016/j.mineng.2005.07.008

Niglio, S., Procentese, A., Russo, M.E., Piscitelli, A., Marzocchella, A., 2019. Integrated enzymatic pretreatment and hydrolysis of apple pomace in a bubble column bioreactor. Biochemical Engineering Journal 150, 107306. https://doi.org/10.1016/j.bej.2019.107306

Nikakhtari, H., Hill, G.A., 2005. Hydrodynamic and oxygen mass transfer in an external loop airlift bioreactor with a packed bed. Biochemical Engineering Journal 27, 138–145. https://doi.org/10.1016/j.bej.2005.08.014

Nili, S., Arshadi, M., Yaghmaei, S., 2022. Fungal bioleaching of e-waste utilizing molasses as the carbon source in a bubble column bioreactor. Journal of Environmental Management 307, 114524. https://doi.org/10.1016/j.jenvman.2022.114524

Nkele, K., Mpenyana-Monyatsi, L., Masindi, V., 2022. Challenges, advances and sustainabilities on the removal and recovery of manganese from wastewater: A review. Journal of Cleaner Production 134152. https://doi.org/10.1016/j.jclepro.2022.134152

Nock, W.J., Heaven, S., Banks, C.J., 2016. Mass transfer and gas–liquid interface properties of single CO2 bubbles rising in tap water. Chemical Engineering Science 140, 171–178. https://doi.org/10.1016/j.ces.2015.10.001

Noh, Y.-G., Lee, Y.J., Kim, J., Kim, Y.K., Ha, J., Kalanur, S.S., Seo, H., 2022. Enhanced efficiency in CO2-free hydrogen production from methane in a molten liquid alloy bubble column reactor with zirconia beads. Chemical Engineering Journal 428, 131095. https://doi.org/10.1016/j.cej.2021.131095

Norwood, V.M., Kohler, J.J., 1990. Organic reagents for removing heavy metals from a 10-34-0 (N-P2O5-K2O) grade fertilizer solution and wet-process phosphoric acid. Fertilizer Research 26, 113–117. https://doi.org/10.1007/BF01048749

Norwood, V.M., Tate, L.R., 1992. Removing Heavy Metals from Phosphoric Acid and Phosphate Fluid Fertilizers: Organic and Inorganic Reagents, in: Vandegrift, G.F., Reed, D.T., Tasker, I.R. (Eds.), Environmental Remediation. American Chemical Society, Washington, DC, pp. 147–160. https://doi.org/10.1021/bk-1992-0509.ch011

Novák, M., Klekner, V., 1988. Comparison of various methods of KLa estimation in cultures of filamentous microorganisms. Biotechnol Tech 2, 243–248. https://doi.org/10.1007/BF01875536

Olmos, E., Gentric, C., Poncin, S., Midoux, N., 2003. Description of flow regime transitions in bubble columns via laser Doppler anemometry signals processing. Chemical Engineering Science 58, 1731–1742. https://doi.org/10.1016/S0009-2509(03)00002-2

Omri, H., Batis, N.H., 2013. Removal of Cd(II) from Phosphoric Acid Solution by Adsorbents: Equilibrium and Kinetic Studies. Chemical Science Transactions 2, 357–366. https://doi.org/10.7598/cst2013.285

Oosterhuis, F.H., Brouwer, F.M., Wijnants, H.J., 2000. A possible EU wide charge on cadmium in phosphate fertilizers: Economics and environmental implications Final Report to the European Commission. Institute for Environmental Studies, Amsterdam.

Ortiz, I., Alonso, A.I., Urtiaga, A.M., Demircioglu, M., Kocacik, N., Kabay, N., 1999. An Integrated Process for the Removal of Cd and U from Wet Phosphoric Acid. Industrial & Engineering Chemistry Research 38, 2450–2459. https://doi.org/10.1021/ie980686s

Ostermeyer, P., Bonin, L., Folens, K., Verbruggen, F., García-Timermans, C., Verbeken, K., Rabaey, K., Hennebel, T., 2021. Effect of speciation and composition on the kinetics and precipitation of arsenic sulfide from industrial metallurgical wastewater. Journal of Hazardous Materials 409, 124418. https://doi.org/10.1016/j.jhazmat.2020.124418

Owija, N.Y., Kosa, S.A., Abdel Salam, M., 2021. Removal of cadmium ions from aqueous solution by zero valent iron nanoparticles: Equilibrium and thermodynamic studies. Journal of Molecular Liquids 342, 117462. https://doi.org/10.1016/j.molliq.2021.117462

Öztürk, S.S., Schumpe, A., Deckwer, W.-D., 1987. Organic liquids in a bubble column: Holdups and mass transfer coefficients. AIChE Journal 33, 1473–1480. https://doi.org/10.1002/aic.690330907

Painmanakul, P., Hébrard, G., 2008. Effect of different contaminants on the α-factor: Local experimental method and modeling. Chemical Engineering Research and Design 86, 1207–1215. https://doi.org/10.1016/j.cherd.2008.06.009

Painmanakul, P., Loubière, K., Hébrard, G., Mietton-Peuchot, M., Roustan, M., 2005. Effect of surfactants on liquid-side mass transfer coefficients. Chemical Engineering Science 60, 6480–6491. https://doi.org/10.1016/j.ces.2005.04.053

Pankow, J.F., Morgan, J.J., 1981. Kinetics for the aquatic environment. Environ. Sci. Technol. 15, 1306–1313. https://doi.org/10.1021/es00093a003

Park, Y.-G., Kim, K.-T., 2021. Selective separation of various heavy metals from synthesized phosphoric acid solutions. Journal of Industrial and Engineering Chemistry 95, 267–276. https://doi.org/10.1016/j.jiec.2020.12.032

Patel, P., Raju, N.J., Reddy, B.C.S.R., Suresh, U., Gossel, W., Wycisk, P., 2016. Geochemical processes and multivariate statistical analysis for the assessment of groundwater quality in the Swarnamukhi River basin, Andhra Pradesh, India. Environ Earth Sci 75, 611. https://doi.org/10.1007/s12665-015-5108-x

Patel, S., Majumder, S.K., Ghosh, P., 2021. Ozonation of diclofenac in a laboratory scale bubble column: Intermediates, mechanism, and mass transfer study. Journal of Water Process Engineering 44, 102325. https://doi.org/10.1016/j.jwpe.2021.102325

Paul, T., Sinharoy, A., Pakshirajan, K., Pugazhenthi, G., 2020. Lipid-rich bacterial biomass production using refinery wastewater in a bubble column bioreactor for bio-oil conversion by hydrothermal liquefaction. Journal of Water Process Engineering 37, 101462. https://doi.org/10.1016/j.jwpe.2020.101462

Pereira, F.M., Loures, C.C.A., Amaral, M.S., Gomes, F.M., Pedro, G.A., Machado, M.A.G., Reis, C.E.R., Silva, M.B., 2018. Evaluation of fatty acids production by Chlorella minutissima in batch bubble-column photobioreactor. Fuel 230, 155–162. https://doi.org/10.1016/j.fuel.2018.04.170

Pereira, T.C., Zanoelo, E.F., Passig, F.H., Benincá, C., de Carvalho, K.Q., 2021. Reduction of p-nitrophenol in an airlift electrochemical reactor with iron electrodes. Journal of Environmental Chemical Engineering 9, 105223. https://doi.org/10.1016/j.jece.2021.105223

Petersen, E.E., Margaritis, A., 2001. Hydrodynamic and Mass Transfer Characteristics of Three-Phase Gaslift Bioreactor Systems. Critical Reviews in Biotechnology 21, 233–294. https://doi.org/10.1080/07388550108984172

Piazza, A., Ciancio Casalini, L., Pacini, V.A., Sanguinetti, G., Ottado, J., Gottig, N., 2019. Environmental Bacteria Involved in Manganese(II) Oxidation and Removal From Groundwater. Frontiers in Microbiology 10.

Pitzer, K.S., 1973. Thermodytriarnics of Electrolytes. I. Theoretical Basis and General Equation. The Journal of Physical Chemistry 77, 268–277.

Pitzer, K.S., Silvester, L.F., 1976. Thermodynamics of Electrolytes. VI. Weak Electrolytes Including H3PO4. Journal of Solution Chemistry 5, 269–278.

Pizzol, M., Christensen, P., Schmidt, J., Thomsen, M., 2011. Impacts of "metals" on human health: a comparison between nine different methodologies for Life Cycle Impact Assessment (LCIA). Journal of Cleaner Production 19, 646–656. https://doi.org/10.1016/j.jclepro.2010.05.007

Platford, R.F., 1975. Thermodynamics of Aqueous Solutions of Orthophosphoric Acid from the Freezing Point to 298.15°K. Journal of Solution Chemistry 4, 591–598.

Plengsakul, J., Powtongsook, S., Nootong, K., 2021. Plastic media reduced algal wall-growth of Chlorococcum humicola for the cultivation in internal-loop airlift photobioreactor. Algal Research 53, 102131. https://doi.org/10.1016/j.algal.2020.102131

Plessen, H.V.D., Bodenbenner, K.D., Baechle, H.T.D., 1983. Procedure for recovery of cadmium-free crude phosphoric acid. DE3134847A1.

Pohl, A., 2020. Removal of Heavy Metal Ions from Water and Wastewaters by Sulfur-Containing Precipitation Agents. Water Air Soil Pollut 231, 503. https://doi.org/10.1007/s11270-020-04863-w

Pohorecki, R., Moniuk, W., Zdrójkowski, A., 1999. Hydrodynamics of a bubble column under elevated pressure. Chemical Engineering Science 54, 5187–5193. https://doi.org/10.1016/S0009-2509(99)00238-9

Polli, M., Stanislao, M.D., Bagatin, R., Bakr, E.A., Masi, M., 2002. Bubble size distribution in the sparger region of bubble columns. Chemical Engineering Science 57, 197–205. https://doi.org/10.1016/S0009-2509(01)00301-3

Powell, K.J., Brown, P.L., Byrne, R.H., Gajda, T., Hefter, G., Leuz, A.-K., Sjöberg, S., Wanner, H., 2011. Chemical speciation of environmentally significant metals with inorganic ligands. Part 4: The Cd2+ + OH–, Cl–, CO32–, SO42–, and PO43– systems (IUPAC Technical Report). Pure and Applied Chemistry 83, 1163–1214. https://doi.org/10.1351/PAC-REP-10-08-09

Preston, C.M., Adams, W.A., 1977. A laser Raman spectroscopy study of aqueous phosphoric acid. Canadian Journal of Applied Spectroscopy 22, 125–136.

Preston, J.S., Preez, A.C. du, 1994. The solvent extraction of cadmium and zinc by mixtures of carboxylic acids and alkanethiols. Solvent Extraction and Ion Exchange 12, 667–685. https://doi.org/10.1080/07366299408918231

Purkayastha, D., Mishra, U., Biswas, S., 2014. A comprehensive review on Cd(II) removal from aqueous solution. Journal of Water Process Engineering 2, 105–128. https://doi.org/10.1016/j.jwpe.2014.05.009

Qamouche, K., Chetaine, A., El Yahyaoui, A., Moussaif, A., Fröhlich, P., Bertau, M., Haneklaus, N., 2021. Uranium and other heavy metal sorption from Moroccan phosphoric acid with argan nutshell sawdust. Minerals Engineering 171, 107085. https://doi.org/10.1016/j.mineng.2021.107085

Reddy, B.R., Priya, D.N., Park, K.H., 2006. Separation and recovery of cadmium(II), cobalt(II) and nickel(II) from sulphate leach liquors of spent Ni–Cd batteries using phosphorus based extractants. Separation and Purification Technology 50, 161–166. https://doi.org/10.1016/j.seppur.2005.11.020

Reilly, I.G., Scott, D.S., De Bruijn, T., Jain, A., Piskorz, J., 1986. A correlation for gas holdup in turbulent coalescing bubble columns. Can. J. Chem. Eng. 64, 705–717. https://doi.org/10.1002/cjce.5450640501

Reis, F.D., Silva, A.M., Cunha, E.C., Leão, V.A., 2013. Application of sodium- and biogenic sulfide to the precipitation of nickel in a continuous reactor. Separation and Purification Technology 120, 346–353. https://doi.org/10.1016/j.seppur.2013.09.023

Ridoutt, B.G., Wang, E., Sanguansri, P., Luo, Z., 2013. Life cycle assessment of phosphorus use efficient wheat grown in Australia. Agricultural Systems 120, 2–9. https://doi.org/10.1016/j.agsy.2013.04.007

Riet, K.V., 1979. Review of Measuring Methods and Results in Nonviscous Gas-Liquid Mass Transfer in Stirred Vessels. Ind. Eng. Chem. Process Des. Dev. 18, 357–364. https://doi.org/10.1021/i260071a001

Roberts, T.L., 2014. Cadmium and Phosphorous Fertilizers: The Issues and the Science. Procedia Engineering, SYMPHOS 2013 - 2nd International Symposium on Innovation and Technology in the Phosphate Industry 83, 52–59. https://doi.org/10.1016/j.proeng.2014.09.012

Robinson, R.A., Stokes, R.H., 2002. Electrolyte solutions, 2., rev. ed. ed. Dover Publ, Mineola, NY.

Roccaro, P., Barone, C., Mancini, G., Vagliasindi, F.G.A., 2007. Removal of manganese from water supplies intended for human consumption: a case study. Desalination, Ninth Environmental Science and Technology Symposium 210, 205–214. https://doi.org/10.1016/j.desal.2006.05.045

Rodrigues, C.S.D., Borges, R.A.C., Lima, V.N., Madeira, L.M., 2018. p-Nitrophenol degradation by Fenton's oxidation in a bubble column reactor. Journal of Environmental Management 206, 774–785. https://doi.org/10.1016/j.jenvman.2017.11.032

Rodríguez, Y., Firmino, P.I.M., Pérez, V., Lebrero, R., Muñoz, R., 2020. Biogas valorization via continuous polyhydroxybutyrate production by Methylocystis hirsuta in a bubble column bioreactor. Waste Management 113, 395–403. https://doi.org/10.1016/j.wasman.2020.06.009

Rollbusch, P., Bothe, M., Becker, M., Ludwig, M., Grünewald, M., Schlüter, M., Franke, R., 2015. Bubble columns operated under industrially relevant conditions – Current understanding of design parameters. Chemical Engineering Science 126, 660–678. https://doi.org/10.1016/j.ces.2014.11.061

Ruan, Y., He, D., Chi, R., 2019. Review on Beneficiation Techniques and Reagents Used for Phosphate Ores. Minerals 9, 1–18. https://doi.org/10.3390/min9040253

Ruiz-Beviá, F., Fernández-Sempere, J., Boluda-Botella, N., 1995. Variation of phosphoric acid diffusion coefficient with concentration. AIChE Journal 41, 185–189. https://doi.org/10.1002/aic.690410118

Rujiruttanakul, Y., Pavasant, P., 2011. Influence of configuration on the performance of external loop airlift contactors. Chemical Engineering Research and Design 89, 2254–2261. https://doi.org/10.1016/j.cherd.2011.02.017

Rumpf, B., Maurer, G., 1994. Solubility of ammonia in aqueous solutions of phosphoric acid: Model development and application. Journal of Solution Chemistry 23, 37–51. https://doi.org/10.1007/BF00972606

Ruzicka, M.C., Drahoš, J., Mena, P.C., Teixeira, J.A., 2003. Effect of viscosity on homogeneous–heterogeneous flow regime transition in bubble columns. Chemical

Engineering Journal, Festschrift Prof. Cor M. van den Bleek 96, 15–22. https://doi.org/10.1016/j.cej.2003.08.009

Ruzicka, M.C., Zahradník, J., Drahoš, J., Thomas, N.H., 2001. Homogeneous–heterogeneous regime transition in bubble columns. Chemical Engineering Science 56, 4609–4626. https://doi.org/10.1016/S0009-2509(01)00116-6

Sadeghizadeh, A., Rahimi, R., Farhad Dad, F., 2018. Computational fluid dynamics modeling of carbon dioxide capture from air using biocatalyst in an airlift reactor. Bioresource Technology 253, 154–164. https://doi.org/10.1016/j.biortech.2018.01.025

Şal, S., Gül, Ö.F., Özdemir, M., 2013. The effect of sparger geometry on gas holdup and regime transition points in a bubble column equipped with perforated plate spargers. Chemical Engineering and Processing: Process Intensification 70, 259–266. https://doi.org/10.1016/j.cep.2013.03.012

Sallanko, J., Lakso, E., Lehmikangas, M., 2005. The Effect of Ozonation on the Size Fractions of Manganese. Ozone: Science & Engineering 27, 147–151. https://doi.org/10.1080/01919510590925266

Salmani, M.H., Davoodi, M., Ehrampoush, M.H., Ghaneian, M.T., Fallahzadah, M.H., 2013. Removal of cadmium (II) from simulated wastewater by ion flotation technique. J Environ Health Sci Engineer 10, 16. https://doi.org/10.1186/1735-2746-10-16

Sampaio, R.M.M., Timmers, R.A., Kocks, N., André, V., Duarte, M.T., van Hullebusch, E.D., Farges, F., Lens, P.N.L., 2010. Zn–Ni sulfide selective precipitation: The role of supersaturation. Separation and Purification Technology 74, 108–118. https://doi.org/10.1016/j.seppur.2010.05.013

Sampaio, R.M.M., Timmers, R.A., Xu, Y., Keesman, K.J., Lens, P.N.L., 2009. Selective precipitation of Cu from Zn in a pS controlled continuously stirred tank reactor. Journal of Hazardous Materials 165, 256–265. https://doi.org/10.1016/j.jhazmat.2008.09.117

Samrane, K., Boulif, R., Dhiba, D., Bouhaouss, A., 2018. Improvements and intesification of industrial co-crystallization process for cadmium removal from wet phosphoric. Int. J. Eng. Sci. Res. Technol. 7, 152–163. https://doi.org/10.5281/zenodo. 1476369

Samrane, K., Khouloud, M., 2017. Procédé de fabrication d'un engrais à base de phosphate d'ammonium présentant une teneur réduite en cadmium. WO2017023153A2.

Sánchez Mirón, A., Cerón García, M.-C., García Camacho, F., Molina Grima, E., Chisti, Y., 2004. Mixing in Bubble Column and Airlift Reactors. Chemical Engineering Research and Design 82, 1367–1374. https://doi.org/10.1205/cerd.82.10.1367.46742

Sánchez-Vázquez, V., Shirai, K., González, I., Gutiérrez-Rojas, M., 2018. Polycyclic aromatic hydrocarbon-emulsifier protein produced by Aspergillus brasiliensis (niger) in an airlift bioreactor following an electrochemical pretreatment. Bioresource Technology 256, 408–413. https://doi.org/10.1016/j.biortech.2018.02.043

Sardeing, R., Painmanakul, P., Hébrard, G., 2006. Effect of surfactants on liquid-side mass transfer coefficients in gas–liquid systems: A first step to modeling. Chemical Engineering Science 61, 6249–6260. https://doi.org/10.1016/j.ces.2006.05.051

Sarhan, A.R., Naser, J., Brooks, G., 2018. CFD model simulation of bubble surface area flux in flotation column reactor in presence of minerals. International Journal of Mining Science and Technology 28, 999–1007. https://doi.org/10.1016/j.ijmst.2018.05.004

Sarrafi, A., Müller-Steinhagen, H., Smith, J.M., Jamialahmadi, M., 1999. Gas holdup in homogeneous and heterogeneous gas—liquid bubble column reactors. The Canadian Journal of Chemical Engineering 77, 11–21. https://doi.org/10.1002/cjce.5450770104

Sasaki, S., Hayashi, K., Tomiyama, A., 2016. Effects of liquid height on gas holdup in air–water bubble column. Experimental Thermal and Fluid Science 72, 67–74. https://doi.org/10.1016/j.expthermflusci.2015.10.027

Schäfer, R., Merten, C., Eigenberger, G., 2002. Bubble size distributions in a bubble column reactor under industrial conditions. Experimental Thermal and Fluid Science 26, 595–604. https://doi.org/10.1016/S0894-1777(02)00189-9

Schorr, M., Valdez, B., 2017. Phosphoric Acid Industry: Problems and Solutions. BoD – Books on Demand.

Schröder, J.J., Cordell, D., Smit, A.L., Rosemarin, A., 2010. Sustainable Use of Phosphorus (No. 375). Wageningen University and Research Centre, Netherlands.

Schumpe, A., Deckwer, W.D., 1987. Viscous media in tower bioreactors: Hydrodynamic characteristics and mass transfer properties. Bioprocess Engineering 2, 79–94. https://doi.org/10.1007/BF00369528

Sebba, F., 1959. Concentration by Ion Flotation. Nature 184, 1062–1063.

Selvaratnam, M., Spiro, M., 1965. Transference numbers of orthophosphoric acid and the limiting equivalent conductance of the H2PO–4 ion in water at 25°C. Trans. Faraday Soc. 61, 360–373. https://doi.org/10.1039/TF9656100360

Shafaei, A., Rezayee, M., Arami, M., Nikazar, M., 2010. Removal of Mn2+ ions from synthetic wastewater by electrocoagulation process. Desalination 260, 23–28. https://doi.org/10.1016/j.desal.2010.05.006

Shah, M., Kiss, A.A., Zondervan, E., van der Schaaf, J., de Haan, A.B., 2012. Gas Holdup, Axial Dispersion, and Mass Transfer Studies in Bubble Columns. Ind. Eng. Chem. Res. 51, 14268–14278. https://doi.org/10.1021/ie301227t

Shah, Y.T., Kelkar, B.G., Godbole, S.P., Deckwer, W.-D., 1982. Design parameters estimations for bubble column reactors. AIChE Journal 28, 353–379. https://doi.org/10.1002/aic.690280302

Shaikh, A., Al-Dahhan, M.H., 2007. A Review on Flow Regime Transition in Bubble Columns 70.

Shan, C., Xu, Y., Hua, M., Gu, M., Yang, Z., Wang, P., Lu, Z., Zhang, W., Pan, B., 2018. Mesoporous Ce-Ti-Zr ternary oxide millispheres for efficient catalytic ozonation in bubble column. Chemical Engineering Journal 338, 261–270. https://doi.org/10.1016/j.cej.2018.01.046

Sheikhi, A., Sotudeh-Gharebagh, R., Zarghami, R., Mostoufi, N., Alfi, M., 2013. Understanding bubble hydrodynamics in bubble columns. Experimental Thermal and Fluid Science 45, 63–74. https://doi.org/10.1016/j.expthermflusci.2012.10.008

Shi, Y., Wu, S., Ren, H., Jin, M., Wang, L., Qiao, N., Yu, D., 2020. Computational fluid dynamics and factor analysis of a novel swirling demulsified airlift loop reactor for the treatment of refined soybean oil wastewater. Bioresource Technology 296, 122316. https://doi.org/10.1016/j.biortech.2019.122316

Shiea, M., Mostoufi, N., Sotudeh-Gharebagh, R., 2013. Comprehensive study of regime transitions throughout a bubble column using resistivity probe. Chemical Engineering Science 100, 15–22. https://doi.org/10.1016/j.ces.2013.01.047

Shioya, S., Dunn, I.J., 1978. A Dynamic oxygen transfer coefficient measurement method for column reactors. Chemical Engineering Science 33, 1529–1534. https://doi.org/10.1016/0009-2509(78)85203-8

Siegel, M.H., Robinson, C.W., 1992. Application of airlift gas-liquid-solid reactors in biotechnology. Chemical Engineering Science 47, 3215–3229. https://doi.org/10.1016/0009-2509(92)85030-F

Singh Thakur, L., Parmar, H., Kumar Varma, A., Kumar Chaurasia, A., Mondal, P., 2022. Removal of manganese from synthetic wastewater by Vetiveria zizanioides. Materials Today: Proceedings. https://doi.org/10.1016/j.matpr.2022.08.395

Sirohi, R., Kumar Pandey, A., Ranganathan, P., Singh, S., Udayan, A., Kumar Awasthi, M., Hoang, A.T., Chilakamarry, C.R., Kim, S.H., Sim, S.J., 2022. Design and applications

of photobioreactors- a review. Bioresource Technology 349, 126858. https://doi.org/10.1016/j.biortech.2022.126858

Sis, H., Chander, S., 2003. Reagents used in the flotation of phosphate ores: a critical review. Minerals Engineering 16, 577–585. https://doi.org/10.1016/S0892-6875(03)00131-6

Skidmore, H.J., Hutter, K.J., 1999. Methods of purifying phosphoric acid. US5945000A.

Skorovarov, J.I., Ruzin, L.I., Lomonosov, A.V., Tselitschev, G.K., 1998. Solvent extraction for cleaning phosphoric acid in fertilizer production. Journal of Radioanalytical and Nuclear Chemistry 229, 111–117. https://doi.org/10.1007/BF02389457

Sluyter, G., Kleber, J., Perz, F., Grund, B., Leuchs, S., Sieberz, S., Bubenheim, P., Thum, O., Liese, A., 2020. Fermentative oxidation of butane in bubble column reactors. Biochemical Engineering Journal 155, 107486. https://doi.org/10.1016/j.bej.2020.107486

Sobhanardakani, S., Parvizimosaed, H., Olyaie, E., 2013. Heavy metals removal from wastewaters using organic solid waste—rice husk. Environmental Science and Pollution Research 20, 5265–5271. https://doi.org/10.1007/s11356-013-1516-1

Sobhi, M., Gaballah, M.S., Han, T., Cui, X., Li, B., Sun, H., Guo, J., Dong, R., 2021. Nutrients recovery from fresh liquid manure through an airlift reactor to mitigate the greenhouse gas emissions of open anaerobic lagoons. Journal of Environmental Management 294, 112956. https://doi.org/10.1016/j.jenvman.2021.112956

Sole, K.C., Hiskey, J.B., 1995. Solvent extraction of copper by Cyanex 272, Cyanex 302 and Cyanex 301. Hydrometallurgy 37, 129–147. https://doi.org/10.1016/0304-386X(94)00023-V

Sorlini, S., Gialdini, F., Biasibetti, M., Collivignarelli, C., 2014. Influence of drinking water treatments on chlorine dioxide consumption and chlorite/chlorate formation. Water Research 54, 44–52. https://doi.org/10.1016/j.watres.2014.01.038

Stenström, S., Aly, G., 1985. Extraction of cadmium from phosphoric acid solutions with amines Part I. Extractant selection, stripping, scrubbing and effects of other components. Hydrometallurgy 14, 231–255. https://doi.org/10.1016/0304-386X(85)90035-0

Stumm, W., Morgan, J.J., 2012. Aquatic Chemistry: Chemical Equilibria and Rates in Natural Waters. John Wiley & Sons.

Sultanbayeva, G.Sh., Holze, R., Chernyakova, R.M., Jussipbekov, U.Zh., 2013. Removal of $Fe^{2+}$-, $Cu^{2+}$-, $Al^{3+}$- and $Pb^{2+}$-ions from phosphoric acid by sorption on carbonate-

modified natural zeolite and its mixture with bentonite. Microporous and Mesoporous Materials 170, 173–180. https://doi.org/10.1016/j.micromeso.2012.11.022

Suriya Narayanan, G., kumar, G., Seepana, S., Elankovan, R., Arumugan, S., Premalatha, M., 2018. Isolation, identification and outdoor cultivation of thermophilic freshwater microalgae Coelastrella sp . FI69 in bubble column reactor for the application of biofuel production. Biocatalysis and Agricultural Biotechnology 14, 357–365. https://doi.org/10.1016/j.bcab.2018.03.022

Sutton, S., Pott, R.W.M., Du Toit, W., 2022. Desorption of oxygen from wine and model wine solutions in a bubble column. Chemical Engineering Science 255, 117648. https://doi.org/10.1016/j.ces.2022.117648

Syers, J.K., 2001. Progress in the development of decadmiation of phosphorus fertilizers. Australia, pp. 101–106.

Taha, M.H., Masoud, A.M., Khawassek, Y.M., Hussein, A.E.M., Aly, H.F., Guibal, E., 2020. Cadmium and iron removal from phosphoric acid using commercial resins for purification purpose. Environ Sci Pollut Res. https://doi.org/10.1007/s11356-020-09342-7

Tait, B.K., 1992. The extraction of some base metal ions by Cyanex 301 Cyanex 302 and their binary extractant mixtures with Aliquat 336. Solvent Extraction and Ion Exchange 10, 799–809. https://doi.org/10.1080/07366299208918136

Takagi, S., Matsumoto, Y., 2011. Surfactant Effects on Bubble Motion and Bubbly Flows. Annu. Rev. Fluid Mech. 43, 615–636. https://doi.org/10.1146/annurev-fluid-122109-160756

Talvy, S., 2003. Airlift et colonne à bulles en écoulement gaz-liquide et gaz-liquide-solide (These de doctorat). Toulouse, INSA.

Tang, X., Wang, J., Zhang, H., Yu, M., Guo, Y., Li, G., Liang, H., 2021. Respective role of iron and manganese in direct ultrafiltration: from membrane fouling to flux improvements. Separation and Purification Technology 259, 118174. https://doi.org/10.1016/j.seppur.2020.118174

Tao, J., Huang, J., Geng, S., Gao, F., He, T., Huang, Q., 2020. Experimental investigation of hydrodynamics and mass transfer in a slurry multistage internal airlift loop reactor. Chemical Engineering Journal 386, 122769. https://doi.org/10.1016/j.cej.2019.122769

Tarento, T.D.C., McClure, D.D., Dehghani, F., Kavanagh, J.M., 2019. Pilot-scale production of phylloquinone (vitamin K1) using a bubble column photo-bioreactor. Biochemical Engineering Journal 150, 107243. https://doi.org/10.1016/j.bej.2019.107243

Taubert, R.D., Boehm, U., 1975. Cadmium sulphide prodn. from contaminated phosphoric acid - by treating with gaseous hydrogen sulphide. DE2422902A1.

Tchowa Medjiade, W., Rosenbaum Alvaro, A., Schumpe, A., 2017. Flow regime transitions in a bubble column. Chemical Engineering Science 170, 263–269. https://doi.org/10.1016/j.ces.2017.04.010

Teng, Z., Yuan Huang, J., Fujita, K., Takizawa, S., 2001. Manganese removal by hollow fiber micro-filter. Membrane separation for drinking water. Desalination 139, 411–418. https://doi.org/10.1016/S0011-9164(01)00342-3

Thomsen, K., 2009. Electrolyte Solutions: Thermodynamics, Crystallization, Separation methods. Technical University of Denmark, Denmark.

Thorat, B.N., Joshi, J.B., 2004. Regime transition in bubble columns: experimental and predictions. Experimental Thermal and Fluid Science 28, 423–430. https://doi.org/10.1016/j.expthermflusci.2003.06.002

Tjioe, T.T., 1987. Reduction of the cadmium content of phosphoric acid and calcium sulfate. Delft University of Technology, Netherlands.

Toama, H.Z., 2017. World phosphate industry. Iraqi Bulletin of Geology and Mining 7, 5–23.

Tobiason, J.E., Bazilio, A., Goodwill, J., Mai, X., Nguyen, C., 2016. Manganese Removal from Drinking Water Sources. Curr Pollution Rep 2, 168–177. https://doi.org/10.1007/s40726-016-0036-2

Touati, M., Benna-Zayani, M., Kbir-Ariguib, N., Trabelsi-Ayadi, M., Buch, A., Grossiord, J.L., Pareau, D., Stambouli, M., 2009. Extraction of cadmium (II) from phosphoric acid media using the di(2-ethylhexyl)dithiophosphoric acid (D2EHDTPA): Feasibility of a continuous extraction-stripping process. Hydrometallurgy 95, 135–140. https://doi.org/10.1016/j.hydromet.2008.05.012

Toye, D., Fransolet, E., Simon, D., Crine, M., L'Homme, G., Marchot, P., 2008. Possibilities and Limits of Application of Electrical Resistance Tomography in Hydrodynamics of Bubble Columns. The Canadian Journal of Chemical Engineering 83, 4–10. https://doi.org/10.1002/cjce.5450830103

Ukeles, S.D., Ben-Yoseph, E., Finkelstein, N.P., 1994. Cadmium removal from phosphoric acid—Israeli experience, in: Hydrometallurgy '94. Springer Netherlands, Dordrecht, pp. 683–699. https://doi.org/10.1007/978-94-011-1214-7_45

Ulrich, A.E., 2019. Cadmium governance in Europe's phosphate fertilizers: Not so fast? Science of The Total Environment 650, 541–545. https://doi.org/10.1016/j.scitotenv.2018.09.014

United Nations Environment Programme, Internation Fertilizer Industry Association, 2001. Enviromental Aspects of phosphate and potash mining. UNEP and IFA, Paris.

Urseanu, M.I., Guit, R.P.M., Stankiewicz, A., van Kranenburg, G., Lommen, J.H.G.M., 2003. Influence of operating pressure on the gas hold-up in bubble columns for high viscous media. Chemical Engineering Science, 17th International Symposium of Chemical Reaction Engineering (IS CRE 17) 58, 697–704. https://doi.org/10.1016/S0009-2509(02)00597-3

Urtiaga, A.M., Alonso, A., Ortiz, I., Daoud, J.A., El-Reefy, S.A., Pérez de Ortiz, S., Gallego, T., 2000. Comparison of liquid membrane processes for the removal of cadmium from wet phosphoric acid. Journal of Membrane Science 164, 229–240. https://doi.org/10.1016/S0376-7388(99)00197-0

U.S. Geological Survey, 2012. Mineral Commodity Summaries 2012: U.S. Geological Survey. U.S. Department of the Interior, Virginia.

Van Tran, B., Ich Ngo, S., Lim, Y.-I., Hung Pham, H., Lim, S.-H., Go, K.-S., Nho, N.-S., 2021. Estimation of physical properties and hydrodynamics of slurry bubble column reactor for catalytic hydrocracking of vacuum residue. Chemical Engineering Journal 418, 129378. https://doi.org/10.1016/j.cej.2021.129378

Vandu, C.O., Krishna, R., 2004. Influence of scale on the volumetric mass transfer coefficients in bubble columns. Chemical Engineering and Processing: Process Intensification 43, 575–579. https://doi.org/10.1016/S0255-2701(03)00015-1

Vanraes, P., Ghodbane, H., Davister, D., Wardenier, N., Nikiforov, A., Verheust, Y.P., Van Hulle, S.W.H., Hamdaoui, O., Vandamme, J., Van Durme, J., Surmont, P., Lynen, F., Leys, C., 2017. Removal of several pesticides in a falling water film DBD reactor with activated carbon textile: Energy efficiency. Water Research 116, 1–12. https://doi.org/10.1016/j.watres.2017.03.004

Vasconcelos, J.M.T., Orvalho, S.P., Alves, S.S., 2002. Gas–liquid mass transfer to single bubbles: Effect of surface contamination. AIChE Journal 48, 1145–1154. https://doi.org/10.1002/aic.690480603

Vasconcelos, J.M.T., Rodrigues, J.M.L., Orvalho, S.C.P., Alves, S.S., Mendes, R.L., Reis, A., 2003. Effect of contaminants on mass transfer coefficients in bubble column and airlift contactors. Chemical Engineering Science 58, 1431–1440. https://doi.org/10.1016/S0009-2509(02)00675-9

Veeken, A.H.M., de Vries, S., Rulkens, W.H., 2003. Selective Precipitation of Heavy Metals as Controlled by a Sulfide-Selective Electrode. Separation Science and Technology 38, 1–19. https://doi.org/10.1081/ SS-120016695

Vemic, M., Bordas, F., Comte, S., Guibaud, G., Lens, P.N.L., van Hullebusch, E.D., 2016. Recovery of molybdenum, nickel and cobalt by precipitation from the acidic leachate of a mineral sludge. Environmental Technology 37, 2231–2242. https://doi.org/10.1080/09593330.2016.1146341

Vial, C., Camarasa, E., Poncin, S., Wild, G., Midoux, N., Bouillard, J., 2000. Study of hydrodynamic behaviour in bubble columns and external loop airlift reactors through analysis of pressure fluctuations. Chemical Engineering Science 55, 2957–2973. https://doi.org/10.1016/S0009-2509(99)00551-5

Vial, C., Poncin, S., Wild, G., Midoux, N., 2001. A simple method for regime identification and flow characterisation in bubble columns and airlift reactors. Chemical Engineering and Processing: Process Intensification 40, 135–151. https://doi.org/10.1016/S0255-2701(00)00133-1

Virta, R.L., 2002. Mineral commodity summaries 2002: U.S. geological survey. U.S. Department of the Interior, Washington, DC.

von Gunten, U., 2003. Ozonation of drinking water: Part I. Oxidation kinetics and product formation. Water Research 37, 1443–1467. https://doi.org/10.1016/S0043-1354(02)00457-8

Wallis, G.B., 1969. One-dimensional two-phase flow. McGraw-Hill, New York, NY.

Wan, S., Ma, M., Lv, L., Qian, L., Xu, S., Xue, Y., Ma, Z., 2014. Selective capture of thallium(I) ion from aqueous solutions by amorphous hydrous manganese dioxide. Chemical Engineering Journal 239, 200–206. https://doi.org/10.1016/j.cej.2013.11.010

Wang, F., Tessier, A., 1999. Cadmium Complexation with Bisulfide. Environ. Sci. Technol. 33, 4270–4277. https://doi.org/10.1021/es990283z

Wang, H., Lu, Z., Qian, D., Li, Y., Zhang, W., 2007. Single-crystal α-MnO2 nanorods: synthesis and electrochemical properties. Nanotechnology 18, 115616. https://doi.org/10.1088/0957-4484/18/11/115616

Wei, C., Wu, B., Li, G., Chen, K., Jiang, M., Ouyang, P., 2014. Comparison of the hydrodynamics and mass transfer characteristics in internal-loop airlift bioreactors utilizing either a novel membrane-tube sparger or perforated plate sparger. Bioprocess Biosyst Eng 37, 2289–2304. https://doi.org/10.1007/s00449-014-1207-4

Wei, M., Chen, J., Wang, X., 2016. Removal of arsenic and cadmium with sequential soil washing techniques using Na 2 EDTA, oxalic and phosphoric acid: Optimization conditions, removal effectiveness and ecological risks. Chemosphere 156, 252–261. https://doi.org/10.1016/j.chemosphere.2016.04.106

Wei, R., Pashley, R.M., 2020. An improved evaporation process with helium inlet in a bubble column evaporator for seawater desalination. Desalination 479, 114329. https://doi.org/10.1016/j.desal.2020.114329

Weissenborn, P.K., Pugh, R.J., 1996. Surface Tension of Aqueous Solutions of Electrolytes: Relationship with Ion Hydration, Oxygen Solubility, and Bubble Coalescence. Journal of Colloid and Interface Science 184, 550–563. https://doi.org/10.1006/jcis.1996.0651

Whitman, W.G., 1962. The two film theory of gas absorption. International Journal of Heat and Mass Transfer 5, 429–433. https://doi.org/10.1016/0017-9310(62)90032-7

WHO, 2017. Guidelines for Drinking-Water Quality: Fourth Edition Incorporating the First Addendum, WHO Guidelines Approved by the Guidelines Review Committee. World Health Organization, Geneva.

Wolstein, F.D., Baechle, H.-T.D., Von, P.H.D., Orth, A.F.D., 1983. Process for the reduction of the heavy metal content in raw phosphate. EP0087065A1.

Wong, J.M., 1984. Chlorination-Filtration for Iron and Manganese Removal. Journal AWWA 76, 76–79. https://doi.org/10.1002/j.1551-8833.1984.tb05265.x

Wu, H., Yuan, Z., Gao, L., Zhang, L., Zhang, Y., 2015. Life-cycle phosphorus management of the crop production–consumption system in China, 1980–2012. Science of The Total Environment 502, 706–721. https://doi.org/10.1016/j.scitotenv.2014.09.056

Wu, H., Yuan, Z., Zhang, Y., Gao, L., Liu, S., 2014. Life-cycle phosphorus use efficiency of the farming system in Anhui Province, Central China. Resources, Conservation and Recycling 83, 1–14. https://doi.org/10.1016/j.resconrec.2013.12.002

Xia, Z., Peng, X., Kong, L., Hu, X., 2021. Hydrophilicity/hydrophobicity of metal sulfide particles as a determinator of aggregation performance in wastewater. Journal of Water Process Engineering 40, 101900. https://doi.org/10.1016/j.jwpe.2020.101900

Xing, L., Pullin, H., Bullock, L., Renforth, P., Darton, R.C., Yang, A., 2022. Potential of enhanced weathering of calcite in packed bubble columns with seawater for carbon dioxide removal. Chemical Engineering Journal 431, 134096. https://doi.org/10.1016/j.cej.2021.134096

Xu, P., Wei, Y., Cheng, N., Li, S., Li, W., Guo, T., Wang, X., 2019. Evaluation on the removal performance of dichloromethane and toluene from waste gases using an airlift packing

reactor. Journal of Hazardous Materials 366, 105–113. https://doi.org/10.1016/j.jhazmat.2018.11.081

Xu, P., Wei, Y., Ma, C., Li, S., Guo, T., Wang, X., Li, W., 2020. Multi-factorial analysis of the removal of dichloromethane and toluene in an airlift packing bioreactor. Journal of Environmental Management 261, 109665. https://doi.org/10.1016/j.jenvman.2019.109665

Xu, S., He, R., Dong, C., Sun, N., Zhao, S., He, H., Yu, H., Zhang, Y.-B., He, T., 2022. Acid stable layer-by-layer nanofiltration membranes for phosphoric acid purification. Journal of Membrane Science 644, 120090. https://doi.org/10.1016/j.memsci.2021.120090

Xuan Hai, L., Yu Wen, L., Yanjuan, Z., Yan Xuan, W., 2012. Experimental study on the solubility of hydrogen sulfide in phosphoric acid solution. Inorganic Salt Industry 44, 30–32.

Yagi, H., Yoshida, F., 1974. Oxygen absorption in fermenters: Effects of surfactants, antifoaming agents, and sterilized cells 52, 905–916.

Yang, W., Wang, J., Jin, Y., 2001. Mass Transfer Characteristics of Syngas Components in Slurry System at Industrial Conditions. Chemical Engineering & Technology 24, 651–657. https://doi.org/10.1002/1521-4125(200106)24:6<651::AID-CEAT651>3.0.CO;2-X

Yang, X., De Buyck, P.-J., Zhang, R., Manhaeghe, D., Wang, H., Chen, L., Zhao, Y., Demeestere, K., Van Hulle, S.W.H., 2022. Enhanced removal of refractory humic- and fulvic-like organics from biotreated landfill leachate by ozonation in packed bubble columns. Science of The Total Environment 807, 150762. https://doi.org/10.1016/j.scitotenv.2021.150762

Yang, X., Liu, Z., Manhaeghe, D., Yang, Y., Hogie, J., Demeestere, K., Van Hulle, S.W.H., 2021. Intensified ozonation in packed bubble columns for water treatment: Focus on mass transfer and humic acids removal. Chemosphere 283, 131217. https://doi.org/10.1016/j.chemosphere.2021.131217

Yazdian, F., Shojaosadati, S.A., Nosrati, M., Pesaran Hajiabbas, M., Vasheghani-Farahani, E., 2009. Investigation of gas properties, design, and operational parameters on hydrodynamic characteristics, mass transfer, and biomass production from natural gas in an external airlift loop bioreactor. Chemical Engineering Science 64, 2455–2465. https://doi.org/10.1016/j.ces.2009.02.023

Ye, M., Li, G., Yan, P., Ren, J., Zheng, L., Han, D., Sun, S., Huang, S., Zhong, Y., 2017. Removal of metals from lead-zinc mine tailings using bioleaching and followed by

sulfide precipitation. Chemosphere 185, 1189–1196. https://doi.org/10.1016/j.chemosphere.2017.07.124

Yuan, A., Wang, X., Wang, Y., Hu, J., 2009. Textural and capacitive characteristics of MnO2 nanocrystals derived from a novel solid-reaction route. Electrochimica Acta 54, 1021–1026. https://doi.org/10.1016/j.electacta.2008.08.057

Zahradník, J., Fialová, M., Ru˚žička, M., Drahosˇ, J., Kasˇtánek, F., Thomas, N.H., 1997. Duality of the gas-liquid flow regimes in bubble column reactors. Chemical Engineering Science 52, 3811–3826. https://doi.org/10.1016/S0009-2509(97)00226-1

Zedníková, M., Orvalho, S., Fialová, M., Ruzicka, M., 2018. Measurement of Volumetric Mass Transfer Coefficient in Bubble Columns. ChemEngineering 2, 19. https://doi.org/10.3390/chemengineering2020019

Zermane, S., Meniai, A.H., 2012. Experimental Study of Competitive Adsorption of Heavy Metals and Organic Matter for the Phosphoric Acid Purification. Energy Procedia 18, 888–895. https://doi.org/10.1016/j.egypro.2012.05.103

Zevenhoven, R., Legendre, D., Said, A., Järvinen, M., 2019. Carbon dioxide dissolution and ammonia losses in bubble columns for precipitated calcium carbonate (PCC) production. Energy 175, 1121–1129. https://doi.org/10.1016/j.energy.2019.03.112

Zhang, F., Wang, Q., Hong, J., Chen, W., Qi, C., Ye, L., 2017. Life cycle assessment of diammonium- and monoammonium-phosphate fertilizer production in China. Journal of Cleaner Production 141, 1087–1094. https://doi.org/10.1016/j.jclepro.2016.09.107

Zhang, T., Wei, C., Feng, C., Ren, Y., Wu, H., Preis, S., 2019. Advances in characteristics analysis, measurement methods and modelling of flow dynamics in airlift reactors. Chemical Engineering and Processing - Process Intensification 144, 107633. https://doi.org/10.1016/j.cep.2019.107633

Zhang, W., Cheng, C.Y., Pranolo, Y., 2010. Investigation of methods for removal and recovery of manganese in hydrometallurgical processes. Hydrometallurgy 101, 58–63. https://doi.org/10.1016/j.hydromet.2009.11.018

Zhao, F.-W., Li, X., Yang, Y.-L., 2009. Study on the Effect of Manganese(II) Removal with Oxidation and Coagulation Aid of Potassium Manganate, in: 2009 3rd International Conference on Bioinformatics and Biomedical Engineering. Presented at the 2009 3rd International Conference on Bioinformatics and Biomedical Engineering, Beijing, China, pp. 1–4. https://doi.org/10.1109/ICBBE.2009.5163512

Zhou, Y., Zheng, G., Long, Y., Liu, Z., Tao, C., Liu, R., 2022. Advanced oxidation processes for wet-process phosphoric acid: Enhanced phosphorus recovery and removal of

organic matters. Hydrometallurgy 210, 105842. https://doi.org/10.1016/j.hydromet.2022.105842

Zhuang, H., Zhong, Y., Yang, L., 2020. Adsorption equilibrium and kinetics studies of divalent manganese from phosphoric acid solution by using cationic exchange resin. Chinese Journal of Chemical Engineering 28, 2758–2770. https://doi.org/10.1016/j.cjche.2020.07.029

Zhuk, A.Z., Borzenko, V.I., Buzoverov, E.A., Ivanov, P.P., Shkolnikov, E.I., 2022. Comparative analysis of hydrogen production technologies: Hydrothermal oxidation of the “carbonless” aluminum and water electrolysis. Renewable Energy 197, 1244–1250. https://doi.org/10.1016/j.renene.2022.08.023

Zieliński, J., Huculak-Mączka, M., Kaniewski, M., Nieweś, D., Hoffmann, K., Hoffmann, J., 2019. Kinetic modelling of cadmium removal from wet phosphoric acid by precipitation method. Hydrometallurgy 190, 105157. https://doi.org/10.1016/j.hydromet.2019.105157

Zuber, N., Findlay, J.A., 1965. Average Volumetric Concentration in Two-Phase Flow Systems. J. Heat Transfer 87, 453–468. https://doi.org/10.1115/1.3689137

**Abstract:** Metal and heavy metal pollution has a detrimental impact on the ecological environment and human health due to their toxicity, persistence, and non-biodegradability, even in trace amounts. Therefore, it has become necessary in order to preserve the environment while maintaining natural, health, and economic balances (within a sustainable development approach) to adapt and implement treatment and purification techniques available from process engineering. To this end, hydrometallurgical processes constitute a promising technology for the recovery and removal of metals and potentially toxic heavy metals from aqueous solutions such as water and phosphoric acid solutions. In this context, this work was devoted:

- On the one hand, the study of the manganese ions removal from drinking water by aeration process in pneumatically agitated reactors such as bubble columns and airlifts. The objective was also to compare their performances according to the specific energy consumed to carry out this reaction. However, the study of the hydrodynamic and mass transfer characteristics of these reactors is essential before proceeding to the manganese removal.
- On the other hand, to the investigation of the cadmium elimination from synthetic and industrial wet phosphoric acid solutions using batch and continuous sulfide precipitation in a conceived and manufactured unit for acidic effluent treatment.

**Keywords:** Pneumatically agitated reactors; Drinking water; Phosphoric acid; Precipitation; Demanganization; Decadmiation.

**Résumé :** La pollution par les métaux et les métaux lourds a des répercussions néfastes considérables sur l'environnement écologique et la santé humaine en raison de leur toxicité, de leur persistance et de leur caractère non biodégradable, et ce même à l'état de traces. Il est ainsi devenu nécessaire afin de préserver l'environnement tout en maintenant les équilibres naturel, sanitaire et économique (dans une démarche de développement durable) d'adapter et de mettre en œuvre des techniques de traitement et d'épuration disponibles et adaptées du génie des procédés. A cet effet, les procédés hydrométallurgiques se présentent comme une technologie prometteuse pour la récupération et l'élimination des métaux et des métaux lourds contenus dans des solutions aqueuses telles que l'eau et l'acide phosphorique. A cet égard, ce travail est consacré :

- D'une part à l'étude de l'élimination des ions manganèse de l'eau potable par un procédé d'aération dans des réacteurs à agitation pneumatique tels que les colonnes à bulles et les airlifts. L'objectif final est également de comparer leurs performances en fonction de l'énergie consommée pour mener à bien cette réaction.
- D'autre part à la séparation du cadmium des solutions d'acide phosphorique produit par voie humide (synthétique et industriel) par la précipitation par des sulfures, en mode discontinu et continu, dans une unité conçue et fabriquée pour le traitement des effluents acides.

**Mots-clés :** Réacteurs à agitation pneumatique ; Eaux potables ; Acide phosphorique ; Précipitation ; Démanganisation ; Décadmiation.